

INVESTIGATION INTO THE PERFORMANCE OF STUDY BY FRACTIONAL ORDER CONTROL SYSTEM ON UNSTABLE PROCESS

Thesis

Submitted by

Deep Mukherjee

Doctor of Philosophy (Engineering)

**Department of Electrical Engineering
Faculty Council of Engineering & Technology
Jadavpur University
Kolkata, India**

2024

1. Title of the thesis: INVESTIGATION INTO THE PERFORMANCE OF STUDY BY FRACTIONAL ORDER CONTROL SYSTEM ON UNSTABLE PROCESS

2. Name, Designation: **Dr. Palash Kumar Kundu**
& Institution of Professor
Supervisor/s Department of Electrical Engineering
Jadavpur University, Kolkata-700032, India

Dr. Apurba Kumar Ghosh
Associate Professor & HOD
Department of Applied Electronics &
Instrumentation Engineering
University Institute of Technology,
Burdwan University, Burdwan-713104,
India

3. List of Publication:

Journal Publications:

- [1] **Deep Mukherjee**, G.Lloyds Raja, and Palash Kundu, “Optimal Fractional Order IMC-Based Series Cascade Control Strategy with Dead-Time Compensator for Unstable Processes”, **Journal of Control Automation and Electrical Systems**, Vol. 32, pp. 30-41, 2021.
- [2] **Deep Mukherjee**, G.Lloyds Raja, Palash Kundu, and Apurba Ghosh, “Modified Augmented Fractional Order Control Schemes for Cart Inverted pendulum Using Constrained Luus-Jaakola Optimisation”, **International Journal of Modelling, Identification and Control**, Vol. 38, no. 3/4, pp. 367-379, 2022.
- [3] **Deep Mukherjee**, G.Lloyds Raja, Palash Kundu, and Apurba Ghosh, “Design of Optimal Fractional Order Lyapunov Based Model Reference Adaptive Control Scheme for CSTR”, **IFAC-PapersOnLine**, Vol. 55, no. 1, pp. 436-441, 2022.
- [4] **Deep Mukherjee**, G.Lloyds Raja, Palash Kundu, and Apurba Ghosh, “Improved Fractional Augmented Control Strategies for Continuously Stirred Tank Reactors”, **Asian Journal of Control**, Vol. 25, pp. 2165-2182, 2023.

- [5] **Deep Mukherjee**, G.Lloyds Raja, Palash Kundu, and Apurba Ghosh, “Analysis of Improved Fractional Backstepping and Lyapunov Strategies for Stabilization of Inverted Pendulum”, *Sādhana*, Vol. 49, 2024.
- [6] **Deep Mukherjee**, Palash Kumar Kundu, Apurba Ghosh, “A performance analysis of fractional order based MARC controller over optimal fractional order PID controller on inverted pendulum”, *International Journal of Engineering & Technology*, Vol. 7, no. 2.21, pp. 29–33, 2018.
- [7] **Deep Mukherjee**, G. L. Raja, Palash Kundu, and Apurba Ghosh, “Fractional Standalone Backstepping control approach for continuous stirred tank reactors”, *International Journal of Robust and Nonlinear Control*, Under – Review.

Conference Publication:

- [1] **Deep Mukherjee**, Palash Kundu, and Apurba Ghosh, “PID controller design for an interacting tank level process with time delay using MATLAB FOMCON toolbox”, 2016, 2nd International Conference on Control, Instrumentation, Energy & Communication (CIEC), Kolkata, India, 2016.

Book Chapters:

- [1] **Deep Mukherjee**, Palash Kundu, and Apurba Ghosh, “A stability analysis of inverted pendulum system using fractional-order MIT rule of MARC controller”, In: Satapathy, S., Tavares, J., Bhateja, V., Mohanty, J. (eds) Information and Decision Sciences. Advances in Intelligent Systems and Computing, Vol. 701. Springer, Singapore, 2018.
- [2] **Deep Mukherjee**, Palash Kundu, and Apurba Ghosh, “Analysis of Conventional and Fractional-Order Controllers for Nonlinear CSTR System”, In: Sherpa, K.S., Bhoi, A.K., Kalam, A., Mishra, M.K. (eds) Advances in Smart Grid and Renewable Energy. ETAEERE 2020. Lecture Notes in Electrical Engineering, Vol. 691. Springer, Singapore, 2020.

4. List of Patent :

- [1] **Deep Mukherjee**, G.Lloyds Raja, and Palash Kundu, “A System for Advanced Dead-time Compensator-Based Series Cascade Control Structure for Unstable Processes”, PATENT No: 2021102343, Australian Innovation Patent, 2021.

5. List of Presentations in National/ International/Conferences/Workshops:

- [1] **Deep Mukherjee**, Palash Kundu, and Apurba Ghosh, “PID controller design for an interacting tank level process with time delay using MATLAB FOMCON toolbox”, 2016, 2nd International Conference on Control, Instrumentation, Energy & Communication (CIEC) , Kolkata, India, 2016.
- [2] **Deep Mukherjee**, Palash Kundu, and Apurba Ghosh, “A stability analysis of inverted pendulum system using fractional-order MIT rule of MARC controller”, 2017, 6th International Conference on Frontiers in Intelligent Computing: Theory and Applications (FICTA), Bhubaneswar, India, 2017.
- [3] **Deep Mukherjee**, Palash Kundu, and Apurba Ghosh, “A performance analysis of fractional order based MARC controller over optimal fractional order PID controller on inverted pendulum”, XIV Control Instrumentation System Conference CISCON-2017, Manipal Institute of Technology, Manipal, India, 2017.
- [4] **Deep Mukherjee**, Palash Kundu, and Apurba Ghosh, “Analysis of Conventional and Fractional-Order Controllers for Nonlinear CSTR System”, 2nd International Conference on Emerging Trends and Advances in Electrical Engineering and Renewable Energy (ETAEEERE-2020), Bhubaneswar, India, 2020.

"Statement of Originality"

I Deep Mukherjee registered on 31st May 2019, do hereby declare that this thesis entitled "INVESTIGATION INTO THE PERFORMANCE OF STUDY BY FRACTIONAL ORDER CONTROL SYSTEM ON UNSTABLE PROCESS" contains literature survey and original research work done by the undersigned candidate as part of Doctoral studies.

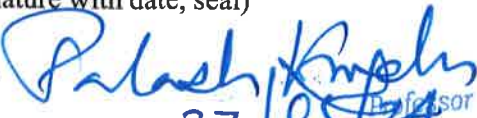
All information in this thesis have been obtained and presented in accordance with existing academic rules and ethical conduct. I declare that, as required by these rules and conduct, I have fully cited and referred all materials and results that are not original to this work.

I also declare that I have checked this thesis as per the "Policy on Anti Plagiarism, Jadavpur University, 2019", and the level of similarity as checked by iThenticate software is 7 %.

Signature of Candidate: Deep Mukherjee

Date: 27/5/2024

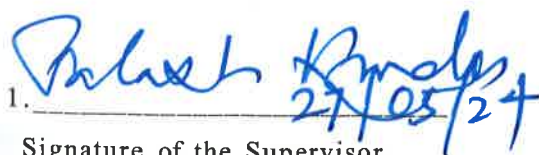
Certified by Supervisor(s):
(Signature with date, seal)

1. 
27/05/24
Professor
Electrical Engineering Department
JADAVPUR UNIVERSITY
Kolkata - 700 032

2. 
27/05/24
Dr. Apurba Kr. Ghosh
Associate Professor & In-Charge, AEE Dept.
University Institute of Technology
Burdwan University Burdwan-713104

CERTIFICATE FROM THE SUPERVISORS

This is to certify that, the thesis entitled **"INVESTIGATION INTO THE PERFORMANCE OF STUDY BY FRACTIONAL ORDER CONTROL SYSTEM ON UNSTABLE PROCESS"** submitted by **Shri Deep Mukherjee**, who got his name registered on **31st May 2019**, for the award of Ph.D. (Engg.) degree of Jadavpur University is absolutely based upon his own work under the supervision of Dr. Palash Kumar Kundu, and Dr. Apurba Kumar Ghosh and that neither his thesis nor any part of the thesis has been submitted for any degree / diploma or any other academic award anywhere before.

1.  27/05/24

Signature of the Supervisor
and date with Office Seal

Professor
Electrical Engineering Department
JADAVPUR UNIVERSITY
Kolkata - 700 032

2.  27/05/24

Signature of the Supervisor
and date with Office Seal

Dr. Apurba Kr. Ghosh
Associate Professor & In-Charge, ABE Dept.
University Institute of Technology
Burdwan University Burdwan-713104

Acknowledgement

First, it is a moment for me to express immense respect to my supervisors, Dr. Palash Kumar Kundu of Electrical Engineering Department, Jadavpur University and Dr. Apurba Kumar Ghosh of Applied Electronics and Instrumentation Engineering Department, University Institute of Technology, Burdwan University for their advice and guidance offered throughout this research journey. The kind of support, encouragement, constructive ideas, and criticism by supervisors enriched me with skill and assist to reach at this stage.

I am grateful to the Head of Electrical Engineering Department, Jadavpur University, for giving this research opportunity. I would also like to thank the Dean of my current organization, School of Electronics Engineering, KIIT Deemed to be University, for offering support to complete my research work.

I want to express my heartfelt gratitude also to Dr. G. Lloyds Raja, Assistant Professor, NIT Patna, for his kind cooperation and valuable guidance in improving composing and technicality of research manuscripts.

The work would not been possible without tireless motivation and constant support of my parents Mr. Tapan Kumar Mukherjee and Mrs. Mandira Mukherjee who are the inspirations of my life. I would like to express my sincere respect to my elder brother Mr. Manik Bandyopadhaya for his active support. I would like to express my sincere respect to my elder sister Mrs. Moumita Bhattacharya for her active support. I would like to express my heartfelt gratitude to my wife Mrs. Minakshi Mukherjee for her constant encouragement to complete my Ph.D.

I also thank the almighty for providing me mental strength to complete the research work.

Finally, I would like to thank everyone who has encouraged to complete this work.

Jadavpur University, Kolkata, India

Deep Mukherjee
Deep Mukherjee

***Dedicated to
my Parents,
Elder sister,
Wife and
Daughter***

PREFACE

A very new and developing area of control theory that has attracted a lot of attention recently is fractional order control. Compared to standard integer-order (IO) controllers, fractional order (FO) control can employ more degrees of freedom to achieve better performance and resilience. Despite a number of difficulties, fractional order control has the capability to reshape control theory and improve efficiency and reliability across a wide range of applications. In this thesis, two distinct benchmark unstable processes as single input-multi output (SIMO) inverted pendulum and continuous stirred tank reactor are taken into considerations to test the efficiencies of various control strategies. One of the most difficult systems to control in the field of control engineering is the linear inverted pendulum (IP), which is based on the use of segway transportation as a real-time application. It is challenging to control the system towards its desired upright position. Apart from application on mechanical nonlinear under actuated system, nonlinear Continuous stirred tank reactor (CSTR) is adopted to be another challenging application in chemical engineering and controlling concentration and temperature smoothly in presence of disturbance is a difficult task. Despite efforts to provide a necessary speed of action, current standalone and augmented traditional control schemes are unable to achieve a smooth performance on set-point tracking and noise rejection, which are crucial factors for investigating control actions on unstable processes. These schemes reported higher integral errors with a significant degree of overshoot. Due to its limitation to real numbers, the traditional scheme basically fails to accurately depict the behavior of the system. So, to address this major issue a beneficial control feature with fractional order is proposed to deliver more detailed information about the functioning of the system using extra degree of freedom. It might be possible to attain a better balance between stability and robustness by allowing the order to be a fraction between zero and one for fractional derivative or integral function. This trait emphasizes the positive aspects of using fractional order calculus in control engineering. Thus, this thesis proposes various novel standalone, and augmented fractional order control strategies, taking into account MRAC, IMC, smith predictor, proportional-integral-derivative (PID), and backstepping schemes. This thesis aims to investigate the significant impact of fractional order control schemes over traditional schemes using nominal condition, model uncertainties, dead time, noise, load disturbances, and nonlinear effects. It also aims to investigate the most effective and trustworthy fractional order control strategy among various proposed topologies for controlling the nonlinear systems. Lower integral errors, total variation (TV) of control efforts, overshoot, and settling time are preferable. To retain a fair level of accuracy, the major critical task is to convert the FO model into an appropriate estimated IO model in the designed rules. The indirect fractional order

approximation technique is preferred over direct method as it offers approximation of fractional order Laplace operator solely unlike direct method. A novel improved biquadratic exact phase approximation method is explored as the most efficient alternative method over the popular Oustaloup and continued fraction expansion (CFE) methods offering more steady, flat, and ripple-free approximated result. In order to attain global stability, proposed fractional order Lyapunov (FOLY) rule of MRAC is found to be more effective than proposed fractional order Massachusetts institute of technology (FOMIT) rule by choosing an appropriate Lyapunov function and controls inverted pendulum more swiftly and gracefully compared to integer order (IO) MIT, and other traditional schemes. Additionally, a variety of novel fractional order augmented schemes are proposed for the inverted pendulum in order to investigate their significant impact over the standalone traditional scheme. The speed of action is comparatively improved with lower error metrics and TV by the augmented FOLY-FO-proportional-integral (PI) and 2 degree of freedom (DOF) FOPI rules. Furthermore, 2 DOF FOPI augmented FOLY and FOMIT techniques produce robust noise rejection. Disturbance rejection is the most critical task for industrial unstable process as well. Consequently, various novel FOIMC-series cascaded control structure (SCCS) with dead-time compensator, dual-loop FOLY-FOPID, FOLY-IMC FOPID, and FOIMC-FOPD predictor strategies are proposed for CSTR in order to explore each of their noteworthy impacts individually. The robust servo-regulatory action and noise rejection are attained by FOIMC-SCCS dead time compensator over reported traditional cascaded schemes and the substantial benefit of proposed dual-loop strategies is also addressed over proposed standalone FOLY scheme to better handle set-point and noise rejection. While all of the aforementioned dual-loop techniques produce promising outcomes, the FOIMC-FOPD predictor produces a fairly decent outcome in terms of stability under noise and disturbance. To fine-tune the control parameters, a combination of in-depth simulation studies and optimization techniques are used. Despite offering lower error metrics, overshoot, and TV by the different proposed standalone and augmented fractional order control strategies, still there is a major scope of improvement on producing a more trustworthy control action by offering fastest speed of action, zero overshoot, lowest integral errors, and smoothest control efforts amid noise and disturbance. Finally, standalone fractional order backstepping (FOB) strategy is proposed as a productive alternate to reported augmented conventional backstepping schemes and the aforementioned proposed fractional order strategies to control the nonlinear systems using strict-feedback recursive technique. The global stability of the unstable systems is attained by FOB using proper Lyapunov function. The proposed simple and straightforward FOB rule is explored as the most trustworthy strategy by offering lowest error metrics without needless overshoot, and fastest speed of action on inverted pendulum and CSTR systems.

Contents

| | Page No. |
|--|----------|
| Preface | i |
| Contents | iii |
| List of Symbols and Abbreviations | vii |
| List of Figures | x |
| List of Tables | xiv |
| CHAPTER 1: Introduction | 1 |
| 1.1 Introduction | 1 |
| 1.2 Overview of Unstable Process | 2 |
| 1.2.1 Required Model of Inverted Pendulum | 2 |
| 1.2.2 Required Model of Continuous Stirred Tank Reactor (CSTR) | 4 |
| 1.3 Role of Controller | 6 |
| 1.3.1 Design Objectives and Specifications of Basic Control Schemes | 6 |
| 1.4 Salient Features and Flaws of Traditional Schemes | 8 |
| 1.5 Issues on Implementing of Fractional Order Model | 9 |
| 1.5.1 Existing Solution Technique | 9 |
| 1.6 Motivation | 10 |
| 1.7 Objective | 10 |
| 1.8 Scope of Work | 10 |
| 1.9 Thesis Outline | 11 |
| References | 14 |
| CHAPTER 2: A Brief Review on Various Control Methodologies and Its Applications on Unstable Systems | 18 |
| 2.1 Introduction | 18 |
| 2.2 Inverted Pendulum | 20 |
| 2.2.1 Classification and Structures | 20 |
| 2.2.2 Comparisons and Limitations between Three Types of Structures | 21 |
| 2.2.3 Mathematical Modeling | 21 |
| 2.2.3.1 Lagrange Method | 21 |
| 2.2.3.2 Newton-Euler Method | 23 |
| 2.2.3.3 State Space Model Representation | 26 |
| 2.3 Continuous Stirred Tank Reactor (CSTR) | 28 |
| 2.3.1 Classification and Characteristic of Chemical Reactors | 28 |
| 2.3.2 Characteristics and Limitation of Continuous Stirred Tank Reactor | 29 |
| 2.3.2.1 Ideal Version | 30 |
| 2.3.2.2 Non-Ideal Version | 32 |
| 2.3.3 Physical Modeling of Ideal CSTR | 33 |
| 2.3.3.1 Mathematical approach for mass balance | 33 |
| 2.3.3.2 Mathematical modelling for Temperatures | 34 |
| 2.3.3.3 State variable form | 35 |

| | |
|--|-----|
| 2.3.3.4 Linearization | 35 |
| 2.4 A Brief Survey on Different Control Algorithms for Unstable Processes | 36 |
| 2.4.1 PID (Proportional-Integral-Derivative) Controller | 36 |
| 2.4.2 MRAC (Model Reference Adaptive Control) | 40 |
| 2.4.3 IMC (Internal Model Control) | 47 |
| 2.4.4 Backstepping Controller | 51 |
| 2.5 Summary | 56 |
| References | 56 |
| CHAPTER 3: Brief Overview on Fractional Order Mathematics and Its Implementation in Controlling Processes | 64 |
| 3.1 Introduction | 64 |
| 3.2 Preliminaries of Fractional Calculus | 66 |
| 3.2.1 Gamma Function | 66 |
| 3.2.2 Beta Function | 67 |
| 3.2.3 Mittag-Leffler Function | 67 |
| 3.3 Overview of Fractional Derivatives and Integrals | 67 |
| 3.3.1 Application of Fractional Order Derivative | 68 |
| 3.3.2 Grunwald-Letnikov (G-L) Construction | 70 |
| 3.3.3 Riemann-Liouville (R-L) Construction | 71 |
| 3.3.3.1 Application of R-L Fractional Integral | 73 |
| 3.3.4 Caputo Construction | 74 |
| 3.4 Theoretical Background of Implementation of Fractional Calculus | 75 |
| 3.4.1 FOMCON Toolkit | 77 |
| 3.4.1.1 Toolkit Features | 77 |
| 3.4.1.2 Computation of Fractional Order Model | 79 |
| 3.4.1.3 Application of FOMCON Toolkit | 81 |
| 3.4.1.4. Stability Solution of FOTF | 88 |
| 3.4.1.5 Limitation of FOMCON Toolkit | 90 |
| 3.4.2 Investigation on Direct Continuous Laplace Analytical Solution | 91 |
| 3.4.2.1 R-L Based Linear Homogeneous Fractional Model Solution | 91 |
| 3.4.2.2 Caputo Based Linear Homogeneous Fractional Model Solution | 92 |
| 3.4.2.3 Caputo Based Non-Homogeneous Fractional Model Solution | 93 |
| 3.4.2.4 Limitation of Direct Laplace Method | 95 |
| 3.4.3 Investigation on Indirect Continuous Analytical Solution | 95 |
| 3.4.3.1 Oustaloup Rational Approximation Method | 96 |
| 3.4.3.2 Continued Fraction Expansions (CFE) Approximation Method | 98 |
| 3.4.3.3 Proposed Biquadratic Equiripple Approximation Method | 100 |
| 3.4.3.4 Proposed Biquadratic Exact Phase Approximation | 102 |
| 3.5 Summary | 104 |
| References | 105 |
| Publication | 109 |
| CHAPTER 4: Fractional Order Standalone and Augmented Control Strategies for Inverted Pendulum | 110 |
| 4.1 Introduction | 110 |

| | |
|--|------------|
| 4.2 Model Reference Adaptive Control (MRAC) | 111 |
| 4.2.1 Description | 112 |
| 4.2.2 Massachusetts Institute of Technology (MIT) Rule | 113 |
| 4.2.2.1 Traditional Adaptation Scheme of Feedforward Gain | 114 |
| 4.2.2.2 Proposed Fractional Adaptation Scheme of Feedforward Gain | 115 |
| 4.2.2.3 Closed Loop Traditional MIT Rule Formulation | 117 |
| 4.2.2.4 Closed Loop Proposed Fractional Order MIT Rule Formulation | 119 |
| 4.2.2.5 Modified proposed Fractional Order MIT Rule Formulation | 121 |
| 4.2.3 Lyapunov Stability Rule | 122 |
| 4.2.3.1 Proposed Fractional Adaptation Feedforward Gain | 123 |
| 4.2.3.2 Closed Loop Modified Fractional Order Lyapunov Stability Rule | 125 |
| 4.3 Fractional Order Augmented Strategies | 127 |
| 4.3.1 Proposed FOMIT-FOPI augmented control scheme | 127 |
| 4.3.2 2 DOF FOPI Control Strategy | 128 |
| 4.3.3 Proposed FOMIT-2 DOF FOPI augmented control scheme | 128 |
| 4.3.4 Proposed FOLY-FOPI/2 DOF FOPI augmented control schemes | 129 |
| 4.4 Investigation on Proposed Fractional Order Standalone and Augmented Control Schemes on Inverted Pendulum | 131 |
| 4.5 Summary | 145 |
| References | 145 |
| Publication | 148 |
| CHAPTER 5: Fractional Order Standalone and Augmented Control Strategies for Continuous Stirred Tank Reactor | 150 |
| 5.1 Introduction | 150 |
| 5.2 SCCS with dead time compensator | 151 |
| 5.2.1 Design of Controllers | 153 |
| 5.3 Fractional Order Dual-loop Strategy | 155 |
| 5.3.1 Dual-loop FOLY-FOPID strategy | 155 |
| 5.3.2 Dual-loop FOLY-FOIMC-FOPID strategy | 156 |
| 5.3.3 Dual-loop FOIMC-FOPD predictor | 158 |
| 5.4 Investigation on Proposed Fractional Order Standalone and Augmented Control Schemes on Continuous Stirred Tank Reactor | 160 |
| 5.5 Summary | 185 |
| References | 185 |
| Publication | 188 |
| CHAPTER 6: Fractional Order Standalone Backstepping Control Strategy for Unstable Processes | 190 |
| 6.1 Introduction | 190 |
| 6.2 Rule of Backstepping Scheme | 191 |
| 6.2.1 Implementation of Stabilizing Design | 191 |
| 6.2.2 Implementation of Tracking Design | 191 |
| 6.3 Design of Standalone Fractional Order Backstepping Strategy on Inverted Pendulum | 192 |
| 6.3.1 Proposed Fractional Order Backstepping (FOB) Rule | 193 |

| | |
|---|-----|
| 6.4 Design of Standalone Fractional Order Backstepping Strategy on CSTR | 196 |
| 6.4.1 Proposed Fractional Order Backstepping (FOB) Rule | 197 |
| 6.5 Investigation into The Performance of FOB Rule on Inverted Pendulum | 200 |
| 6.6 Investigation into The Performance of FOB Rule on CSTR | 208 |
| 6.7 Summary | 214 |
| References | 215 |
| Publication | 217 |
| CHAPTER 7: Conclusion & Future Work | 218 |
| 7.1 Conclusion | 218 |
| 7.2 Future Works | 220 |
| Appendix A: | 222 |
| Appendix B: | 226 |
| Appendix C: | 229 |

List of Symbols and Abbreviations

Symbols

| | |
|-------------------|---|
| τ | Residence time |
| T | Temperature |
| P | Pressure |
| h, U | Temperature transfer rates |
| C | Chemical species concentration |
| q_c | Inlet coolant flow rate |
| C_A | Concentration of substance A |
| Q | Fluid flow rate |
| A | Concentration of species |
| M | Mass of cart |
| m | Mass of pendulum |
| θ | Angle of pendulum |
| F_x | Input force |
| l | Length of pendulum |
| g | Centre of gravity |
| φ | Angle |
| k | Kinetic energy |
| p | Potential energy |
| F_y | Horizontal force |
| F_z | Vertical force |
| L | Total energy balance |
| d_1, d_2 | Disturbance |
| p | Centre of gravity |
| a | Acceleration |
| x_p, z_p | Coordinates of the centre of gravity |
| I | Moment of inertia |
| V, H | Balance of forces on vertical and horizontal directions |
| τ | Torque on pendulum |
| V | Volume of reactor |
| C_1, C_2 | Inlet and outlet concentrations |
| F_1, F_2 | Inlet and outlet flow rates |
| r_a | Rate of reaction |
| N_a | Total amount of substances |
| H_{in}, H_{out} | Enthalpy of inlet and outlet |
| ρ | Density |
| T_0, T_r | Inlet and outlet temperatures |
| k_0 | Exponential factor |
| E | Activation energy |
| R | Universal gas constant |
| c_{A_i} | Initial inlet concentration |
| F_i, F | Inlet and outlet flow rates |
| Q | Overall heat transfer of CSTR |
| k | Constant |

| | |
|---|---|
| U | Overall heat transfer coefficient |
| A_H | Heat transfer area |
| T_{c_o} | Temperature at the system boundary |
| λ, ν, μ, ρ | Extra degrees of freedom |
| $\theta_c(t)$ | Controller parameter vector |
| $W_m(s)$ | Reference model |
| G_p | Plant |
| e | Tracking error |
| y | Plant output |
| y_m | Model output |
| $\widetilde{G}_p(s)$ | Internal model |
| $G_c(s)$ | Controller function |
| ε | Model error |
| $\vartheta_1, \vartheta_2, \dots, \vartheta_r$ | Subsystems of nonlinear process |
| v | Control law |
| h | Step size of fractional calculus |
| α, β | Fractional orders |
| n | Smallest natural number of fractional calculus |
| a, t | Lower and upper limits of fractional integral |
| K_P, K_I, K_D | Proportional, integral and derivative gains |
| γ | Adaptive gain of model reference adaptive control |
| p, q_1, q_2, q_3 | Plant coefficients |
| θ_1, θ_2 | Control vectors |
| $q_{m_1}, q_{m_2}, q_{m_3}$ | Model coefficients |
| u_c | Command signal |
| b, l | Plant coefficients |
| a, b, a_m, b_m | Plant and model coefficients |
| P_1, P_2 | Unstable and stable plants |
| P_t | Total plant transfer function |
| r_1 | Reference signal |
| P_m | Internal model |
| $\theta_m s$ | Dead time |
| $\tau_1, \tau_{m2}, \tau_2, \tau_{m1}, \lambda_2$ | Time constants |
| K_2, K_1, K_{m2}, K_{m1} | Gains of plant and model |
| \ddot{x} | Acceleration of cart |

Abbreviations

| | |
|------|------------------------------------|
| DOF | Degree of freedom |
| SIMO | Single input-multi output |
| IO | Integer order |
| FO | Fractional order |
| MRAC | Model reference adaptive control |
| IMC | Internal model control |
| PID | Proportional-integral-derivative |
| DS | Direct synthesis |
| GUI | Graphical user interface |
| FOTF | Fractional order transfer function |
| G-L | Grunwald Letnikov |
| R-L | Riemann-Liouville |

| | |
|--------|--|
| FODE | Fractional order differential equation |
| FOMCON | Fractional order modeling and control |
| CFE | Continued Fraction Expansions |
| SBL | Stability boundary locus |
| PSE | Power series expansion |
| MIT | Massachusetts Institute of Technology |
| LJ | Luus-Jaakola |
| LY | Lyapunov |
| PSO | Particle swarm optimization |
| MPSO | Modified particle swarm optimization |
| SCCS | Series cascaded control structure |
| ABC | Artificial bee colony |
| MPC | Model predictive control |
| FOL | Fractional order Lyapunov |
| CB | Conventional backstepping |
| FOB | Fractional order backstepping |
| GA | Genetic algorithm |

***Symbols/Abbreviations appearing in this thesis other than mentioned ones are defined in the respective contexts.**

List of Figures

- Fig. 1.1. Basic model of linear inverted pendulum
- Fig. 1.2. Continuous stirred-tank reactor cross-section
- Fig. 1.3. a. Blockdiagram of a closed loop control system. b. Blockdiagram of a closed loop control system with noise and disturbance
- Fig. 1.4. Objective framework
- Fig. 1.5. Work Flow of Current Thesis
- Fig. 2.1. a. Classical inverted pendulum. b. Rotary inverted pendulum
- Fig. 2.2. An ideal CSTR
- Fig. 2.3. a. Vector schematic of X-inverted pendulum. b. X-Y inverted pendulum. c. X-Z inverted pendulum
- Fig. 2.4. Force equilibrium at the center of gravity
- Fig. 2.5. Interchanging the position of mass at the top of the rod
- Fig. 2.6. Isothermal and non-isothermal CSTR icon
- Fig. 2.7. CSTR Industrial Schematic
- Fig. 2.8. Schematic feature of single perfectly mixed CSTR
- Fig. 2.9. Schematic feature of a conventional PID controller
- Fig. 2.10. Fractional order PID controller
- Fig. 2.11. MPC schematic representation
- Fig. 2.12. Indirect MRAC scheme
- Fig. 2.13. Direct MRAC scheme
- Fig. 2.14. Direct MRAC based on MIT & Lyapunov schemes
- Fig. 2.15. Modified MRAC scheme
- Fig. 2.16. Modified MRAC scheme with two adaptive gains
- Fig. 2.17. Modified Lyapunov based MRAC scheme on CSTR
- Fig. 2.18. IMC scheme
- Fig. 2.19. Backstepping-sliding mode scheme
- Fig. 2.20. Augmented fuzzy-backstepping scheme
- Fig. 2.21. Adaptive fuzzy based backstepping scheme
- Fig. 2.22. Adaptive fuzzy based backstepping scheme on CSTR
- Fig. 3.1. Performance of function $y = x^2$ using classical calculus
- Fig. 3.2. Insight behavior of function using fractional orders between 0 and 1
- Fig. 3.3. Insight behavior of functions using fractional orders between 1 and 2
- Fig. 3.4. Insight behavior of function using fractional orders between 0 and 1
- Fig. 3.5. FOMCON platform
- Fig. 3.6. GUI (Graphical user interface) window
- Fig. 3.7. FOTF Time domain platform
- Fig. 3.8. Schematic of interacting tank level process
- Fig. 3.9. FOTF/IOTF entry dialog
- Fig. 3.10. Closed loop system using FOPID controller
- Fig. 3.11. Nominal outputs of AMIGO and Z-N methods
- Fig. 3.12. IOPID design tool
- Fig. 3.13. Identified FOPDT model
- Fig. 3.14. FOPID design tool
- Fig. 3.15. Fractional order realization tool
- Fig. 3.16. Fractional order PID optimization tool
- Fig. 3.17. Nelder-Mead local optimization algorithm step

- Fig. 3.18. Step response with IOPID controller
- Fig. 3.19. Step response with FOPID controller
- Fig. 3.20. Stable region for FOTF
- Fig. 3.21. Stability analysis for FOTF
- Fig. 3.22. Approximated outputs with different orders
- Fig. 3.23. Magnitude and phase effects of fractional order 0.4
- Fig. 3.24. Effect of magnitude and phase responses with higher frequency of 1000 rad/sec
- Fig. 3.25. Amplitude and phase outputs of model $s^{-0.4}$
- Fig. 3.26. Frequency domain outputs of outsaloup 5th order approximation, CFE 4th order approximation and model $s^{0.4}$
- Fig. 3.27. Time domain outputs of model $s^{0.4}$
- Fig. 3.28. Significant study on biquadratic equiripple method on FO model $s^{0.4}$
- Fig. 3.29. Comparative study between CFE approximation and proposed biquadratic equiripple approximation methods
- Fig. 3.30. Impact of modified biquadratic equiripple approximation method
- Fig. 3.31. Comprehensive analysis of the modified biquadratic equiripple precise phase method's performance
- Fig. 4.1. Basic MRAC architecture
- Fig. 4.2. Overview of adaptation strategy
- Fig. 4.3. Traditional adaptive feedforward scheme
- Fig. 4.4. Proposed fractional adaptive feedforward scheme
- Fig. 4.5. Overview of feedback-feedforward control strategy
- Fig. 4.6. Closed loop traditional MIT rule architecture
- Fig. 4.7. Closed loop proposed fractional order MIT rule architecture
- Fig. 4.8. Closed loop updated Fractional order MIT rule architecture
- Fig. 4.9. Proposed fractional adaptive feedforward scheme using Lyapunov stability rule
- Fig. 4.10. Closed loop proposed fractional Lyapunov stability architecture
- Fig. 4.11. Closed loop proposed a fractional modified FOLY scheme
- Fig. 4.12. Proposed FOMIT-FOPI/2 DOF FOPI augmented scheme
- Fig. 4.13. Proposed FOLY-FOPI/2 DOF FOPI augmented scheme
- Fig. 4.14. System output using traditional MIT rules
- Fig. 4.15. Servo-regulatory response using modified traditional MIT rules
- Fig. 4.16. Comparative study between FOMIT and IOMIT rules
- Fig. 4.17. Comparative study between proposed FOMIT and FOLY rules
- Fig. 4.18. Upright position tracking using FOMIT and FOLY rules
- Fig. 4.19. Upright position tracking in presence of noise
- Fig. 4.20. Comparative study between proposed FOLY and modified FOLY rules
- Fig. 4.21. Significant impact of proposed modified FOLY over existing rules under load disturbance
- Fig. 4.22. Control actions in presence of noise and disturbance
- Fig. 4.23. Nominal outputs for linearized model (a: FOLyapunov-2DOF FOPI, b: FOLyapunov-FOPI, c: FOMIT-2DOF FOPI, d:FOMIT-FOPI and e:Direct synthesis based PID)
- Fig. 4.24. Control efforts (a: FOLyapunov-2DOF FOPI, b: FOLyapunov-FOPI, c: FOMIT-2DOF FOPI, d:FOMIT-FOPI and e:Direct synthesis based PID)
- Fig. 4.25. Perturbed outputs for linearized model (a: FOLyapunov-2DOF FOPI, b: FOLyapunov-FOPI, c: FOMIT-2DOF FOPI, d:FOMIT-FOPI and e:Direct synthesis based PID)
- Fig. 4.26. System outputs for nonlinear model (a: FOLyapunov-2DOF FOPI, b: FOLyapunov-FOPI, c: FOMIT-2DOF FOPI and d:FOMIT-FOPI)
- Fig. 4.27. System outputs with noise (a: FOLyapunov-2DOF FOPI, b: FOLyapunov-FOPI,

- c: FOMIT-2DOF FOPI, d:FOMIT-FOPI and e:Direct synthesis based PID)
- Fig. 5.1. Proposed FOIMC-SCCS architecture with dead time compensator
 - Fig. 5.2. Dual-loop FOLY-optimal FOPID scheme
 - Fig. 5.3. Dual-loop FOLY-IMC FOPID scheme
 - Fig. 5.4. Dual-loop FOPD-FOIMC smith predictor
 - Fig. 5.5. Magnitude plots of stability for the proposed method
 - Fig. 5.6. Finding appropriate value of K_p
 - Fig. 5.7. Nominal outputs in presence of load disturbance
 - Fig. 5.8. Nominal control efforts
 - Fig. 5.9. Perturbed outputs
 - Fig. 5.10. Perturbed control actions
 - Fig. 5.11. Nominal outputs in presence of noise
 - Fig. 5.12. Control efforts in presence of noise
 - Fig. 5.13. Finding appropriate value of K_p
 - Fig. 5.14. Nominal outputs
 - Fig. 5.15. Nominal control actions
 - Fig. 5.16. Perturbed outputs
 - Fig. 5.17. Perturbed control actions
 - Fig. 5.18. System outputs amid noise
 - Fig. 5.19. Control efforts amid noise
 - Fig. 5.20. Magnitude graphs of stability for the proposed method
 - Fig. 5.21. Robustness of proposed method
 - Fig. 5.22. Nominal and perturbed control actions
 - Fig. 5.23. Nominal outputs with stand-alone and augmented control topologies
 - Fig. 5.24. Nominal control actions
 - Fig. 5.25. Perturbed outputs with stand-alone and augmented control topologies
 - Fig. 5.26. Perturbed control actions
 - Fig. 5.27. Nominal outputs under noise
 - Fig. 5.28. Nominal outputs with stand-alone and augmented control topologies
 - Fig. 5.29. Nominal control actions
 - Fig. 5.30. Perturbed outputs with stand-alone and augmented control topologies
 - Fig. 5.31. Perturbed control actions
 - Fig. 5.32. Nominal outputs in the presence of noise
 - Fig. 5.33. System outputs using different optimal FOMRAC rules
 - Fig. 5.34. Nominal Control actions
 - Fig. 5.35. Perturbed outputs using different optimal FOMRAC rules
 - Fig. 5.36. Perturbed Control efforts
 - Fig. 5.37. Noise measurement of outputs
 - Fig. 5.38. Noise impact on control efforts
 - Fig. 6.1. Physical model representation of inverted pendulum
 - Fig. 6.2. Proposed standalone fractional order backstepping scheme
 - Fig. 6.3. Proposed standalone fractional order backstepping scheme
 - Fig. 6.4. Upright trajectory from different locations
 - Fig. 6.5. Performance study between different fractional orders on Bode plots
 - Fig. 6.6. Time responses of fractional orders
 - Fig. 6.7. Nominal system output in presence of load disturbance
 - Fig. 6.8. Nominal responses under noise
 - Fig. 6.9. Nominal control actions
 - Fig. 6.10. Perturbed system outputs in presence of noise
 - Fig. 6.11. Global stability analysis of FOB with impulse 0.3 rad under disturbance

- Fig. 6.12. Robustness of FOB in presence of noise
- Fig. 6.13. Nominal outputs under load
- Fig. 6.14. Nominal performances under noise
- Fig. 6.15. Different control actions under noise
- Fig. 6.16. System outputs using different fractional orders
- Fig. 6.17. Nominal outputs using positive scalars = 5 and 15
- Fig. 6.18. Servo-regulatory outputs with load disturbance
- Fig. 6.19. Nominal outputs with noise
- Fig. 6.20. Nominal outputs with different molar concentration 1 Kmol/m³
- Fig. 6.21. Nominal and perturbed servo-regulatory outputs with FOB rule
- Fig. 6.22. Control efforts between CB and FOB
- Fig. 6.23. Perturbed outputs with noise
- Fig. 6.24. Servo-regulatory nominal outputs with load disturbance
- Fig. 6.25. Nominal outputs with noise
- Fig. 6.26. Input control actions with disturbance
- Fig. 6.27. Servo-regulatory perturbed outputs in presence of load disturbance
- Fig. 6.28. Servo-regulatory perturbed outputs in presence of noise

List of Tables

| | |
|------------|--|
| Table 1.1 | Quality metrics with desired condition |
| Table 1.2 | Investigation on performance of selected traditional schemes on Inverted pendulum and CSTR |
| Table 2.1 | Review on different control strategies for CSTR and Inverted pendulum processes |
| Table 3.1 | Review of fractional calculus |
| Table 3.2 | Tank specification |
| Table 3.3 | Optimal parameters and time domain metrics for IOPID controller |
| Table 3.4 | Optimal parameters for FOPID controller |
| Table 3.5 | Time domain metrics for FOPID controller |
| Table 3.6 | Computation of parameters for third and fifth order approximation of Oustaloup model $s^{0.4}$ |
| Table 3.7 | Approximated rational transfer function of Oustaloup model $s^{0.4}$ |
| Table 4.1 | Parameter specifications |
| Table 4.2 | Quantitative comparison under load disturbance |
| Table 4.3 | Quantitative comparison under noise |
| Table 4.4 | Quantitative comparison under noise |
| Table 4.5 | Approximations of fractional order |
| Table 4.6 | Quantitative comparison of closed-loop performances |
| Table 4.7 | Plant specifications |
| Table 4.8 | Summary of tuning parameters |
| Table 4.9 | Quantitative comparison of closed-loop performances |
| Table 5.1 | Approximated model of fractional order |
| Table 5.2 | Performance measures |
| Table 5.3 | Parameters of CSTR |
| Table 5.4 | Controller settings |
| Table 5.5 | Approximations of fractional order |
| Table 5.6 | Quantitative performance measures |
| Table 5.7 | Specifications of Jacketed CSTR |
| Table 5.8 | Parameters of controller tuning |
| Table 5.9 | Approximations of fractional order |
| Table 5.10 | Quantitative analysis |
| Table 6.1 | Parameters for newly transformed CSTR subsystems |
| Table 6.2 | Parameter specifications of inverted pendulum |
| Table 6.3 | Controller Settings |
| Table 6.4 | Approximations of fractional order |
| Table 6.5 | Quantitative measurement analysis |
| Table 6.6 | Actual parameters for CSTR |
| Table 6.7 | Summary of control functions |
| Table 6.8 | Quantitative measurement with load disturbance |

CHAPTER 1

Introduction

1.1 Introduction

Conventional control techniques can successfully and frequently tackle a wide range of nonlinear or unstable control issues in industry. The conventional controller's basic form, which has proven to be suitable for many often encountered control issues, such as disturbances and nonlinearities, is the reason for its wide spread acceptance. The process of controller tuning can be time-consuming even though tuning instructions are available, which leads to many mechanical or chemical plants control loops being poorly tuned and the control system's full potential not being realized. Auto-tuning on conventional techniques is preferred also not only to make the operator's job easier but also for reasons of robustness. For more than 15 years, industry has used conventional control relay auto-tuners with great success.

On the other hand, a remarkable quantity of investigation on the use of fractional calculus (FC) in various scientific and technical fields has been conducted recently. In terms of automatic control, fractional Order Control (FOC) requires the development of techniques for controller development, parameter tuning, and effective controller implementation in order to be applied in practical applications. By using the IO control technique, the system could oscillate or lead to low saturation robustness. It might aid to attain a greater harmony between stability and resiliency by allowing order to be a fraction between zero and one for fractional derivative or integral function. This trait emphasizes the positive aspects of using fractional order calculus in control engineering. The performance of nonlinear processes in various challenging areas can be studied more effectively using fractional order system (FOS). In recent decades, FC has become extensively employed in various fields of control theory, including operator layout, stability, flexibility, and error estimations.

The stabilization of an unstable system can be viewed as a task-based problem. Another way to look at it is as a regulation issue. Although task-based control is frequently more sophisticated than regulation and servoing, the latter two may be categorised as sub-tasks. The Segway transporter serves as an example of how stability is a crucial responsibility. In the realm of control engineering, the linear inverted pendulum (IP) which is among the most challenging systems to operate [1], based on the use of Segway transportation as a real-time application. It is challenging to contrast the control efficiencies among various control theories on the inverted pendulum. Better control topologies' efficacy levels attain the stabilization of the intended position and angle of inverted pendulum.

Apart from application on mechanical nonlinear under actuated system, unstable Continuous stirred tank reactor (CSTR) [2] is adopted to be another challenging application in chemical engineering, and they are mostly used in homogeneous liquid-phase flow processes in industrial processing, where continuous agitation is required. The primary goal of a reactor's design is to maximize the estimated current worth of a chemical reaction. Reactors are needed in industry to transform natural resources into consumer commodities. With a constant mass flow rate, reactants are continually added and products continuously removed. Controlling the concentration level and temperature in a tank reactor process is a difficult task, and stabilization of the process variables towards desired position is attained by using robust control topologies.

1.2 Overview of Unstable Process

Unstable processes are those that reveal behavior leading to unbounded growth or oscillations. It is challenging to regulate these systems since they are inherently unpredictable. The following sections provide the fundamental model representation and methodology of the chosen unstable processes.

1.2.1 Required Model of Inverted Pendulum

One of the standard control system issues is the handling of an inverted pendulum. It uses the analogy of a hand acting as a cart and a stick acting as a pendulum as the hand tries to balance the stick. The hand that is attempting to balance the stick has an advantage since it can move up and down, but the inverted pendulum has limited motion and can only move right and left. Inverted pendulum is intrinsically unstable and for the system to remain intact, force must be properly delivered. Here are two different varieties of inverted pendulum, including SISO (Single input single output) and SIMO (Single input multi output). SIMO is a control system that is more effective than SISO.

Only one input or manipulated variable can govern two or more controlled or output variables in a SIMO system which is known as the “X” plane inverted pendulum. The following part illustrates the system's mechanistic modelling. The basic required model representation of linear inverted pendulum [3] is depicted in Fig.1.1 below.

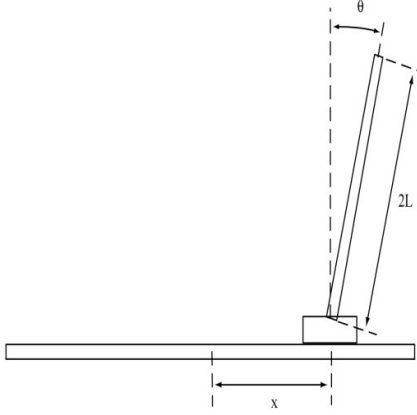


Fig. 1.1. Basic model of linear inverted pendulum.

The angular position must be kept close to zero as the main objective. The angle of the beam with the vertical is shown by the symbol θ . A second goal is to determine the track position because the pendulum can be stabilized at any point along the track. Standard techniques can be used to derive an inverted pendulum basic model as shown in Fig.1. The feedback linearization technique [3-4] is mostly leveraged to improve the tractability and efficiency of control design.

$$(I + mL^2)\ddot{\theta} + mL \cos(\theta)\ddot{x} = mgL \sin \theta \quad (1.1)$$

m is beam's mass, $2L$ is beam's length, $I = mL^2/3$ is moment of inertia, g is the acceleration, in case of small angles θ the following transfer function is obtained by feedback linearization as

$$\frac{4}{3}L\ddot{\theta} - g\theta = -\ddot{x} \quad (1.2)$$

Now, the overall transfer function is defined as

$$\frac{\theta(s)}{x(s)} = \frac{-s^2}{(4/3)Ls^2 - g} \quad (1.3)$$

The system's poles are at $s = \pm\sqrt{3g/4L}$. The instability of the positive root increases as the beam is short (as one might expect). Another challenging issue is that the system contains two zeros at the value of $s = 0$. This is because the cart needs to accelerate in order to affect the beam angle. However, this characteristic enables stabilization for any position of the cart.

Another mathematical expression illustrates how a first-order system's response causes the cart's velocity to be delayed.

$$x(s) = \frac{p}{s+p} x_{com}(s) \quad (1.4)$$

x_{com} is order for cart position, x is cart position and $p > 0$. The system's overall transfer function is then determined as

$$\frac{\theta(s)}{x_{com}(s)} = \frac{-ps^2}{((^4/3) Ls^2 - g)(s+p)} \quad (1.5)$$

By raising the value of p , the cart might react quickly. In order to stabilize, an uncompensated pendulum must be compensated, as will be featured in the following section.

1.2.2 Required Model of Continuous Stirred Tank Reactor (CSTR)

Reactors come in two varieties: batch and continuous stirred-tank (CSTR) (sometimes called stirred tank reactor, or STR) [5]. The primary distinction is the requirement for continuous component flow into the reactor by gravity or pump-assisted forced circulation in the case of the stirred tank reactor. Thoroughly stirring the resulting reaction mixture is necessary. Important process variables of CSTR include: Residence time (τ), Temperature (T), Pressure (P), Volume (V), temperature transfer rates (h, U), Chemical species concentration (C). The cross-section of a required CSTR [5-6] and its inside are shown in the Fig.1.2 below.

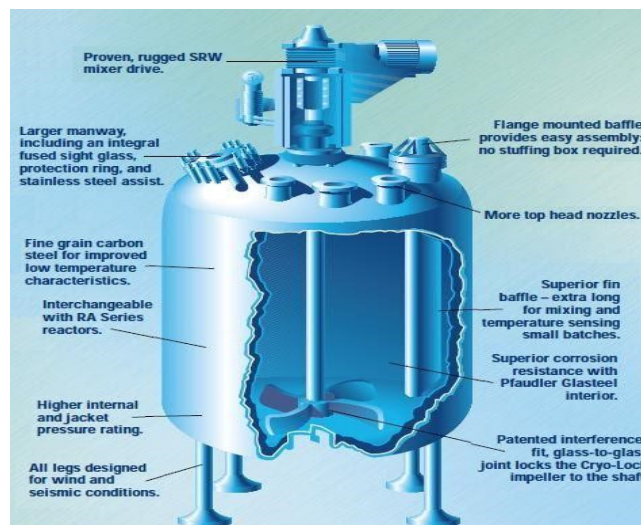


Fig. 1.2. Continuous stirred-tank reactor cross-section.

A hypothetical CSTR that takes perfect mixing into account typically approximates or models the performance of a CSTR. In a perfect reactor [5], when reagents are added, they instantly and uniformly mix across the entire reactor. As a result, the output combination matches the material composition within the reactor exactly, which is one of the goals of reaction rate and residence time. CSTR incorporates nonlinear, interdependent functions of temperature and concentration. Therefore, the model for the CSTR is linearized using a state space model based Jacobian matrix. In order to identify certain linear operating points around steady state, concentration (C_A), temperature (T), and inlet coolant flow rate (q_c) should be taken into account. Eigen vectors on the Jacobian matrix are found, and various stable and unstable states are adopted. As per the design equation of CSTR (Mass balance around the reactor)

$$\frac{dN_A}{dt} = F_{A_I} + F_{A_O} + Vv_A r_A \quad (1.6)$$

Where,

- F_{A_O} is the rate of molar flow of species A at the exit
- F_{A_I} is the rate of species A's molar flow in the intake
- r_A is the reaction rate
- v_A is stoichiometric coefficient
- N_A is the species A's mole count

The equations above are made simpler by using steady-state and $v_A = -1$ to create:

$$F_{A_I} + F_{A_O} - V r_A = 0 \quad (1.7)$$

Considering the species A concentration and the rate of flow (Q), the molar flow rates for those species can be rewritten as follows:

$$Q C_{A_I} - Q C_{A_O} - V r_A = 0 \quad (1.8)$$

$$r_A = \frac{Q}{V} (C_{A_I} - C_{A_O}) \quad (1.9)$$

$$r_A = \frac{1}{\tau} (C_{A_I} - C_{A_O}) \quad (1.10)$$

Where,

- C_{A_O} is the feed concentration at exit
- C_{A_I} is the feed concentration in inlet
- τ is residence time

1.3 Role of Controller

For any form of closed loop operation, accuracy, stability, and speed of action play a crucial role. A controller is used to increase steady state accuracy by reducing the steady state error between desired and measured variables toward the null position. In addition to this, a controller is utilized to limit the system's maximum amplitude and the amount of noise it produces. Using a controller, a slow response can be made faster. The open loop approach typically detects the process' starting behavior, but the closed loop method plays a significant task in moving the process in the direction of any desirable position to satisfy the desired criteria. Fig.1.3. (a) and (b) depict the fundamental schematic [7] of closed loop representation. Following these fundamental conditions, the control actions of certain widely used control schemes are investigated for mainly response time, overshoot and error using a nominal model as well as perturbations on selected unstable processes.

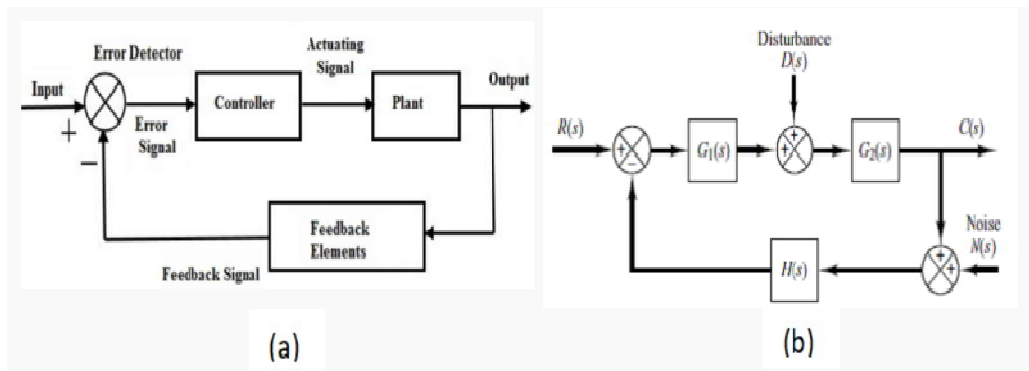


Fig. 1.3.a. Blockdiagram of a closed loop control system. b. Blockdiagram of a closed loop control system with noise and disturbance.

1.3.1 Design Objectives and Specifications of Basic Control Schemes

The controller in any feedback control system is made to meet the requirements [7] listed below:

- **Closed loop stability:** Algebraic techniques, like Routh's array, may be used to examine robustness; Bode graphs of models may be employed to determine stability as well.
- **Dynamic stability:** A satisfactory transient reaction indicates good dynamic stability. To achieve improvements in transient response, a suitable controller can be used.
- **Tracking error:** According to the position and velocity error constants of the loop transfer function, the steady-state error for prototype step input is calculated.

By adding the right controller to the feedback loop, the error may be avoided.

- **Sensitivity and Robustness:** It is impossible to prevent disturbance inputs when operating physical systems. High loop gain in the disturbance frequency spectrum is necessary for effective disturbance rejection. It is desirable for a well-designed control system to have minimal sensitivity to parameter changes and robustness to uncertainty in dynamics.

Inherent trade-offs are present in the system layout goals. A static controller, for instance, is unable to boost transient response while also bringing steady-state error down to a constant input. The design goals for disturbance rejection and reference tracking are also incompatible. Finding the ideal balance between meeting and prioritizing design objectives in such circumstances is not always simple. As a result, rather than being an exact science, ‘control system design’ is more of an art. The required characteristics for the transient and steady-state components of the system performance with regard to a prototype input are specified in the system layout specifications. To specify the desired transient response properties, a step input is needed. Table 1.1 provides a summary of the quality metrics for a prototype second order system.

Table 1.1
Quality metrics with desired condition

| Quality Indicator | Expression | Boundary Condition |
|-------------------------------------|---|--|
| Rise Time (t_r) | $t_r = \frac{\pi - \varphi}{\omega_d}$ | $\frac{\pi}{2\omega_d} \leq t_r \leq \frac{\pi}{\omega_d}$ |
| Peak Overshoot (M_p) | $M_p = 100e^{-\varepsilon\omega_n t_p}(\%)$ | $M_p \leq 10\%$ |
| Peak Time (t_p) | $t_p = \frac{\pi}{\omega_d}$ | - |
| Settling Time (t_s) | $t_s = \frac{4.5}{\varepsilon\omega_n}$ | $t_s \leq 2$ |
| IAE (Integral Absolute Error) | $\int_0^{t_s} e(t) dt$ | - |
| ISE (Integral Square Error) | $\int_0^{t_s} e(t) ^2 dt$ | - |
| ITAE (Integral Time Absolute Error) | $\int_0^{t_s} t e(t) dt$ | - |
| TV (Total variation) | $\sum_{i=1}^{\infty} u(i+1) - u(i) $ | - |

Where, ω_d is damped natural frequency, ω_n is natural frequency, ε is damping ratio, $e(t)$ is error, t is time, and u is control input.

1.4 Salient Features and Flaws of Traditional Schemes

Two key factors for investigating the control actions of various control topologies on unstable processes are noise rejection and set-point tracking. Some popular traditional methods struggle more to control the process amid disturbances because of the nonlinear impact of the plant, despite providing a reasonable solution on stable processes, according to documented research. The following Table 1.2 provides some of the pros and cons of the popular standalone and augmented traditional methods on inverted pendulum and CSTR systems.

Table 1.2
Investigation on performance of selected traditional schemes on Inverted pendulum and CSTR

| Traditional schemes | Salient features | Drawbacks |
|--|--|--|
| PID [8-9] | Capable of controlling process using widely used GA and PSO optimization methods | More struggle with higher integral errors and overshoot |
| 2 DOF PID [10-11] | Slightly improved speed of action with additional tuning parameters | No significant improvement on smoothness of control action |
| PI-PD [12] | Faster servo action | Still substantial degree of overshoot |
| IMC –PID [13-14] | Excelled over PID in presence of noise and disturbance using filter | Still lack of steady state control action |
| PI-PD based smith predictor [15] | Popular for disturbance rejection in industrial process | No significant improvement on overshoot and slow servo response |
| IOMIT rule of MRAC [16-18] | Effective technique in presence of model uncertainties and noise | No guarantee of stability for unstable process |
| IOLY stability rule of MRAC [19-20] | Popular for attaining global stability | Still higher integral errors, overshoot, and prolonged settling time |
| IOLY-PID [21] | Slight improvement of speed of action with lower overshoot using greater number of control settings | Still no significant improvement on smoothness of control action |
| Adaptive backstepping [22-23] | Well established technique for nonlinear system with strict feedback recursive method and robust technique | Complex tuning due to more control settings |
| Adaptive fuzzy backstepping [24] | Promising feature with robust solution | Complex tuning due to more control settings |

Higher integral errors with a substantial degree of overshoot were reported by the aforementioned conventional standalone techniques. A smooth performance was nevertheless unattainable despite the augmented traditional rules' relative improvement in action speed with the aid of a greater number of control settings, according to certain published works.

In contrast to the few documented experiments, the backstepping control approach is later discovered to be a more successful method of controlling nonlinear processes. Its relatively limited application is found on inverted pendulums and CSTRs. However, existing conventional augmented backstepping scheme relatively outperformed the other schemes with promising control action. However, there is still a lack of research on simple and straightforward backstepping scheme that needs to be explored. Using current techniques, it is discovered that some reported works lack case studies on model uncertainties and other crucial factors like the effect of a certain disturbance that needs to be taken into consideration. It is also imperative to explore on more insightful information on the behavior of the unstable systems because traditional schemes do not offer exact information due to its limitation to real numbers. This is accomplished by using the fractional order (FO) approach.

1.5 Issues on Implementing of Fractional Order Model

Compared to developing an IO model, implementing a fractional order transfer function [25] is a crucial undertaking. Unlike IO calculus, the FO derivative is essentially a nonlocal operator and retains historical data. The implementation of the FO model is computationally burdened as it necessitates more memory elements and results in a long memory effect. Therefore, one of the difficult roles in designing the FO control scheme is to approximate the behavior of fractional order by converting into an estimated integer order rational model. Research is currently underway to discover a suitable approximation method that could reveal a feasible approximation.

1.5.1 Existing Solution Technique

Contrary to some reported works, the popular optimal fractional order PID (FOPID) controller [26–30] outperformed PID controller in handling noise employing two extra degrees of freedom and was frequently employed on unstable processes to enhance the performance amid disturbance. By altering the derivative order between 0 and 1, these extra degrees of freedom aid to offer flexible results in contrast to standard rules and achieve better system performance balance. However, there was still no significant improvement in the overshoot, and the control action was sluggish even after adding a specific disturbance. Many experts recommended using the most popular indirect Oustaloup recursive filter [26–28] to realize additional degrees of freedom under the fractional order modeling and control (FOMCON) [27] toolset; nevertheless, this approach does not always result in a promising approximation. There is currently no study on alternate approximation techniques in any reported literature.

In order to deliver a more acceptable estimated outcome in the designed rule, further research into alternative approximation approaches is urgently needed. There is also a major scope of improvement on producing a more trustworthy control action by offering fastest speed of action, zero overshoot, lowest integral errors, and smoothest control efforts in presence of noise and disturbances on inverted pendulum and CSTR systems.

1.6 Motivation

As was covered in the previous sections, it is evident that an intriguing control method is needed to investigate more insight features about the performance of both CSTR and a linear inverted pendulum (IP). Finding more detailed, flexible information about the behavior of the systems is crucial for choosing the best course of control. The fractional order (FO) approach, which, in contrast to traditional methods, has infinite memory that preserves past information. Hence, this motivates us to modify the traditional control rules using fractional order. Achieving a viable solution for a nonlinear system also necessitates the use of appropriate approximation methods for transforming fractional order model into an appropriate estimated integer order model.

1.7 Objective

This thesis aims to develop various fractional order control architectures for nonlinear inverted pendulum and continuous stirred tank reactor systems.

1.8 Scope of Work

With the following scopes, the key technical contributions are summarized below:

- Investigation on different direct and indirect fractional order approximation methods to select the most trustworthy fractional order approximation technique.
- Development of fractional order control (FOC) based on standalone MIT rule, Lyapunov stability rule, and internal model control (IMC) strategy.
- Development of different FOC based on augmented FOMIT-1 DOF FOPI, FOMIT-2 DOF FOPI, FOLY-1 DOF FOPI, FOLY- 2 DOF FOPI, FOLY-FOPID, FOLY-IMC FOPID, FOPD-FOIMC predictor control strategies.
- Development of fractional order standalone backstepping control strategy using strict feedback recursive method.

- To investigate the significant impact of fractional order control schemes compared to traditional control schemes through various novel simulation case studies in presence of noise, load disturbance, delay time, model uncertainties, and nonlinear effect. Different quantitative performance analyses are subjected to all proposed standalone and augmented control strategies to compute the accuracy and total variation (TV) of the control signal is used to assess how smooth the control attempts are.
- To investigate for the most trustworthy and reliable fractional order control strategy also among various proposed fractional order control strategies.

The objective framework is depicted encompassing the aforementioned contributions in Fig. 1.4 below.

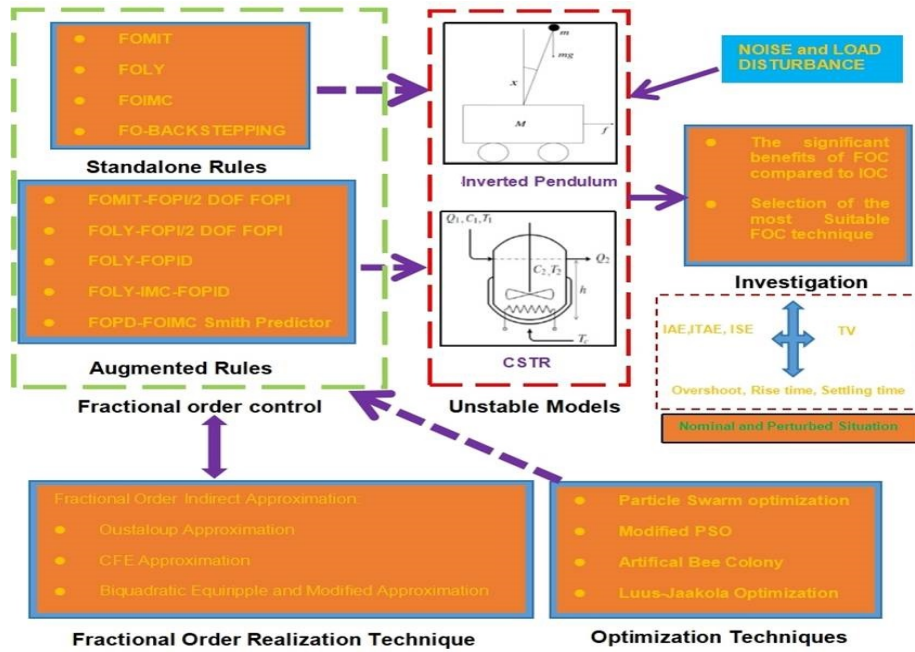


Fig. 1.4. Objective framework.

1.9 Thesis Outline

The current work is organized serially to comply with the objective through different chapters.

Chapter-1: This chapter discusses the purpose and relevance of the present work. Inverted pendulum and continuous stirred tank reactor models that must meet certain requirements have been emphasized. A controller's function with designed specifications is also discussed. In this chapter, existing control topology issues are discussed together with the necessary solutions for their application to continuous stirred tank reactors and inverted pendulums. The present study's purpose and motivation are unambiguously stated.

Chapter-2: This chapter performs a thorough mathematical analysis of inverted pendulum and continuous stirred tank reactor systems. To demonstrate the need for X plane SIMO based inverted pendulum and ideal continuous stirred tank reactor unstable systems, a brief review on different types of inverted pendulum models and continuous stirred tank reactors with pros and cons is discussed. In order to fulfil desired criteria, such as qualitative or time-domain metrics on unstable processes, pros and flaws of various popular control strategies are examined. This chapter discusses some of the most pressing issues related to tracking the angle, position, concentration level, or temperature of an inverted pendulum as well as a continuous stirred tank reactor. This discussion serves as a background for establishing research issues which need to be addressed along with the need for an improved technique that can be leveraged to overcome the issue for both of these systems.

Chapter-3: An in-depth mathematical postulations on fractional calculus is provided in this chapter, including discussions of G-L fractional differentiation or integration, R-L fractional differentiation or integration, and Caputo fractional differentiation or integration. In this chapter, the significance of FO is illustrated eloquently compared to integer order calculus. A brief overview of the FOMCON toolkit with pros and cons is discussed on benchmark process with dead time. In order to construct the necessary approximation approach for the solution of fractional orders on MATLAB platform, different direct and indirect fractional order approximation methods are discussed. The significant application of indirect fractional order approximation compared to direct approximation is illustrated through extensive simulation studies. The most acceptable indirect fractional order approximation method is explored with promising outcome.

Chapter-4: For use in two instances of the benchmark single input multi output (SIMO) linear inverted pendulum (IP), the fractional order based 1 degree of freedom (DOF) PI, 2 DOF PI, and direct modified MRAC are adopted in this chapter to investigate the level of efficacy compared to existing methods. Feedback linearization on different reported benchmark plants is suggested to improve tractability and efficiency of control design. The nonlinear impact is also investigated using proposed topologies. Different novel simulation endeavours are carried out to explore the impacts of proposed FOMRAC schemes amid disturbances. The global stability of the system is also investigated by fractional order Lyapunov (FOLY) stability rule. The significant impact of 2 DOF FOPI compared to 1 DOF FOPI is also explored augmenting these rules with FOMRAC rules in nominal, perturbed, and nonlinear simulations. Quantitative analysis is applied to all proposed methods and smoothness of control efforts is also explored.

Chapter-5: In this chapter, FOPID, MRAC, and IMC with fractional filters are adopted to investigate the level of efficacy compared to existing methods on continuous stirred tank

reactor (CSTR). Different reported benchmark CSTR plants with different linearized operating points around a stable zone are taken into account. Different stable and unstable states of nonlinear CSTR are explored for investigating closed-loop performances. In order to reject disturbances, the significant impact of proposed FOIMC based series cascaded control scheme (SCCS) with dead time compensator compared to traditional schemes is discussed in details. The significant impact of different FO dual-loop strategies of FOLY-FOPID, FOLY-IMC-FOPID, and FOIMC-FOPD smith predictor schemes compared to standalone FOLY rule is carried out on nominal and perturbed models amid disturbance. A combination of extensive simulation technique and optimization approaches, including modified PSO and ABC are conducted to obtain the control settings. Quantitative analysis is applied to all proposed methods and smoothness of control efforts is also explored.

Chapter-6: In this chapter, fractional order based linear standalone backstepping topology is proposed as a feasible alternative compared to augmented traditional backstepping schemes on nonlinear inverted pendulum and CSTR systems. The global stability is explored by strict feedback recursive methodology on nonlinear systems. The significant impact of fractional order backstepping (FOB) is explored on producing needless overshoot and fasted tracking compared to conventional backstepping and other proposed FO control schemes through a variety of novel simulation studies on closed-loop performances and control efforts amid disturbances.

Chapter-7: This chapter summarizes the research findings and proposes the scope of future study in the relevant area.

The work flow of the current thesis, including the outcomes as journal, patent, conference paper, and book chapter is presented in Fig. 1.5.

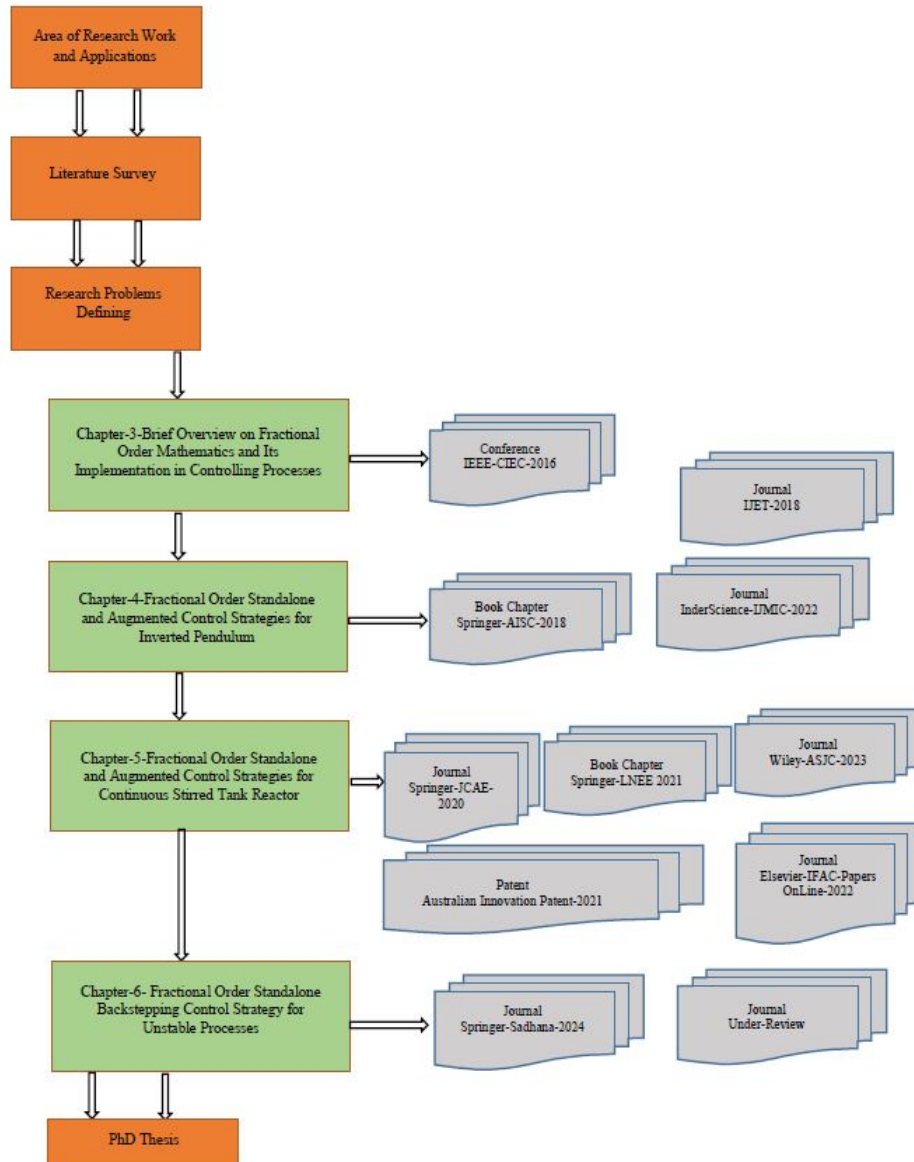


Fig. 1.5. Work Flow of Current Thesis.

References

- [1] Van den Berg, H. W. J. (2003). Introduction to the control of an inverted pendulum setup. (DCT rapporten; Vol. 2003.056). Technische Universiteit Eindhoven.
- [2] R. Lozano, I. Fantoni, and D. J. Block, "Stabilization of the inverted pendulum around its homoclinic orbit," *Systems & Control Letters*, vol. 40, pp. 197-204, 7/5/ 2000.

- [3] Leon Blitzer. Inverted pendulum. American Journal of Physics, 33(12):1076–1078, December 1965.
- [4] T. Sugie, and K. Fujimoto, "Controller design for an inverted pendulum based on approximate linearization," Int. J. of robust and nonlinear control, vol. 8, no 7, pp. 585-597, 1998.
- [5] Bhattachanyya B.C, (2005) "Introduction to chemical equipment design (Mechanical aspect)" 1 st Edition, CBS, New Delhi. PP 29, 39, 246.
- [6] Dimian C.A, (2005) "Integrated Design and Simulation of chemical processes", volume 13, 1st Edition, Elsevier Inc. USA page. 127.
- [7] H. T. K.J.Astrom, *PID Controllers: Theory, Design and Tuning [Import]*, 2nd ed.: ISA; 2nd Revised edition edition, 1995.
- [8] Muskinja, N. and Tovornik, B., Swinging up and stabilization of a real inverted pendulum, *IEEE Trans. Ind. Electron.*, 2006, vol. 53, pp. 631–639.
- [9] B.W. Bequette, Process Control Modelling Design and Simulation, Prentice Hall Professional, 2002.
- [10] Viet, T.D., Doan, P.T., Giang, H. *et al.* Control of a 2-DOF omnidirectional mobile inverted pendulum. *J Mech Sci Technol* **26**, 2921–2928 (2012).
- [11] William L. Luyben, "Temperature Control of Continuous Stirred Tank Reactors by Manipulation of Fresh Feed", Ind. Eng. Chem. Res. 2004, 43, 6430-6440.
- [12] Lloyds Raja, G., Ali, A. New PI-PD Controller Design Strategy for Industrial Unstable and Integrating Processes with Dead Time and Inverse Response. *J Control Autom Electr Syst* 32, 266–280, 2021.
- [13] Saxena, S., Hote, Y.V. Internal model control based PID tuning using first-order filter. *Int. J. Control Autom. Syst.* 15, 149–159, 2017.
- [14] Munna Kumar, Durga Prasad, Balendu Shekher Giri, Ram Sharan Singh, Temperature control of fermentation bioreactor for ethanol production using IMC-PID controller, Biotechnology Reports, Vol. 22, 2019.
- [15] Kaya, I. PI-PD controllers for controlling stable processes with inverse response and dead time. *Electr Eng* 98, 55–65, 2016.

- [16] P.Dostal, M.b., V.bobal, An approach to adaptive control of estr.chem.pap, 2004: pp. 184-190.
- [17] Selahattin Ozcelik, Julian DeMarchi, Howard Kaufman, Kevin Craig, Control of an Inverted Pendulum Using Direct Model Reference Adaptive Control, IFAC Proceedings Volumes, Vol. 30 (6), 1997, pp. 585-590.
- [18] M. Waszak and R. Łangowski, "An Automatic Self-Tuning Control System Design for an Inverted Pendulum," in *IEEE Access*, vol. 8, pp. 26726-26738, 2020.
- [19] Prasad, L.B., Tyagi, B. & Gupta, H.O. Optimal Control of Nonlinear Inverted Pendulum System Using PID Controller and LQR: Performance Analysis Without and With Disturbance Input. *Int. J. Autom. Comput.* 11, 661–670, 2014.
- [20] Goud, Harsh and Swarnkar, Pankaj. "Signal Synthesis Model Reference Adaptive Controller with Artificial Intelligent Technique for a Control of Continuous Stirred Tank Reactor" *International Journal of Chemical Reactor Engineering*, vol. 17, no. 2, 2019, pp. 20180145.
- [21] Kulthe, S., Purohit, C.S., Manna, S., Sudha, R., Pandian, B.J., Kazi, A. (2019). Performance Analysis of Interactive Thermal Process Using Various MRAC Techniques. In: Mishra, S., Sood, Y., Tomar, A. (eds) *Applications of Computing, Automation and Wireless Systems in Electrical Engineering. Lecture Notes in Electrical Engineering*, vol 553. Springer, Singapore.
- [22] Maruki, Y., Kawano, K., Suemitsu, H. *et al.* Adaptive backstepping control of wheeled inverted pendulum with velocity estimator. *Int. J. Control Autom. Syst.* 12, 1040–1048, 2014.
- [23] D. Dochain, M. Perrier, Adaptive Backstepping Nonlinear Control of Bioprocesses, IFAC Proceedings Volumes, Vol.37(1), 2004, pp. 77-82.
- [24] T. Zhang, M. Guay, Adaptive control of uncertain continuously stirred tank reactors with unknown actuator nonlinearities, *ISA Transactions*, Vol 44 (1), 2005, pp. 55-68.
- [25] J. Tenreiro Machado, Virginia Kiryakova, Francesco Mainardi, Recent history of fractional calculus, *Communications in Nonlinear Science and Numerical Simulation*, Vol.16 (3), 2011, pp.1140-1153.

- [26] Aleksei Tepljakov, Baris Baykant Alagoz, Celaleddin Yeroglu, Emmanuel Gonzalez, S. Hassan HosseinNia, Eduard Petlenkov, FOPID Controllers and Their Industrial Applications: A Survey of Recent Results, *IFAC-PapersOnLine*, Vol.51 (4), 2018, pp.25-30.
- [27] N. Lachhab, F. Svaricek, F. Wobbe and H. Rabba, "Fractional order PID controller (FOPID)-Toolbox," *2013 European Control Conference (ECC)*, Zurich, Switzerland, 2013, pp. 3694-3699.
- [28] Omar Elwy, Esraa M. Hamed, Somia H. Rashad, Amr M. AbdelAty, Lobna A. Said, Ahmed G. Radwan, Chapter 8 - On the Approximation of Fractional-Order Circuit Design, Editor(s): Ahmad Taher Azar, Ahmed G. Radwan, Sundarapandian Vaidyanathan, In *Advances in Nonlinear Dynamics and Chaos (ANDC)*, Fractional Order Systems, Academic Press, 2018, pp. 239-270.
- [29] Raafat Shalaby, Mohammad El-Hossainy, Belal Abo-Zalam, Fractional order modeling and control for under-actuated inverted pendulum, *Communications in Nonlinear Science and Numerical Simulation*, Vol. 74, 2019, pp. 97-121.
- [30] A. Singh and V. Sharma, "Concentration control of CSTR through fractional order PID controller by using soft techniques," *2013 Fourth International Conference on Computing, Communications and Networking Technologies (ICCCNT)*, Tiruchengode, India, 2013, pp. 1-6.

CHAPTER 2

A Brief Review on Various Control Methodologies and Its Applications on Unstable Systems

2.1 Introduction

The long-range missile and spacecraft developments are the inverted pendulum's major historical context. The establishment of long-range and subsequent intercontinental ballistic missiles made it crucial that the missile had suitable tracking capabilities, especially the ability to keep the proper angle and elevation through self-orientation. It was vital to build a feedback loop system that would enable control of the fins and rutters to help balance the rocket at lower speeds, which required the usage of an inverted pendulum [1], due to the problem that at lower speeds, aerodynamic stability would not be present. For a fundamental control-engineering problem in a real-world setting, either the classical or rotary inverted pendulum approaches is used. Using the dynamic behaviour of physical models as presented in Fig. 2.1.(a) and (b) below, the results of both approaches [2] are found to be very satisfying.

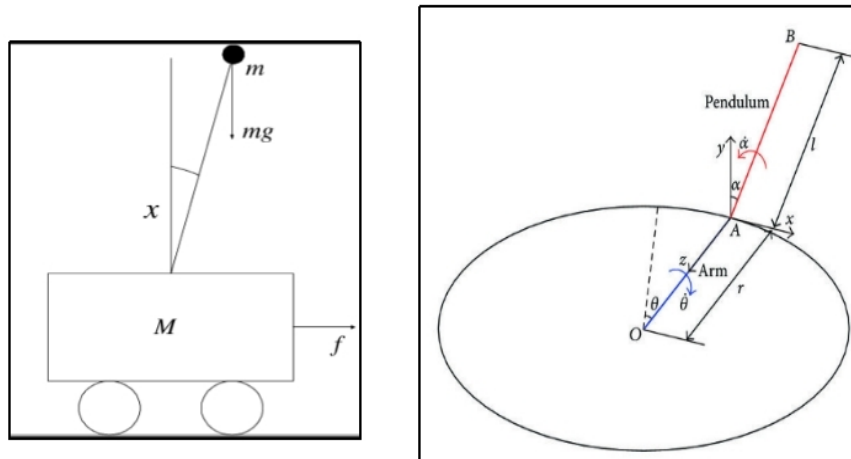


Fig. 2.1. a. Classical inverted pendulum. b. Rotary inverted pendulum.

The primary distinction between a classical and rotary inverted pendulum is that, in contrast to a classical inverted pendulum, a rotary inverted pendulum has more degrees of freedom

than control input. As a result, controlling the rotary inverted pendulum multi-variable system is a difficult work. Yet, sometimes it is particularly difficult to control the arm angle and pendulum angle simultaneously, as well as the arm angular position and pendulum angular position. In this case, a single control topology might not be appropriate for fixing the issue, necessitating the need for additional control efforts to satisfy the condition. Disturbances, however, which may originate internally or externally, may also exist in practical systems. As a result, control engineering finds a variety of control systems applications in linear or classical inverted pendulum systems.

Similar to this, in the chemical and food areas, continuous stirred-tank reactors (CSTRs) are frequently employed [3]. Because of the unpredictable behavior, numerous stationary states, thermal effect on chemical changes, time lag, and impact of various time-sensitive uncertainties, controlling CSTRs is a challenging task. The continuous-stirred tank reactor receives and expels material constantly. When there are no dead zones or bypasses and the CSTR is equally mixed, it performs at its best. It might or might not be perplexing. The composition and temperature of the tank are assumed to be consistent throughout [3], along with its operation at a steady state as seen in Fig. 2.2. The effluent composition is also assumed to be identical to that of the tank.

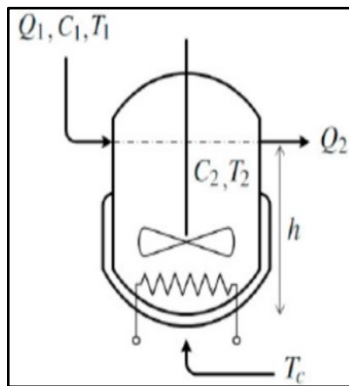


Fig. 2.2. An ideal CSTR.

CSTR is typically regarded as a mixing tank. The continuous stirred tank reactor receives and expels material constantly. When there are no dead zones or bypasses and the CSTR is equally mixed, it performs at its best. It might or might not be perplexing. The temperature and concentration level inside the reactor serve as the state variables, and the flow rate of coolant into the reactor jacket serves as the manipulated input, making the CSTR a tough plant for testing novel control algorithms.

2.2 Inverted Pendulum

The inverted pendulum may be controlled in three distinct ways, depending on its intended use. The swing-up control of an inverted pendulum is the first area that has received a lot of investigation [4]. The second factor is the inverted pendulum's stabilization [4]. The third factor is the inverted pendulum's tracking control [4]. In practical application, stabilization and tracking control are more beneficial.

2.2.1 Classification and Structures

There are three distinct kinds of inverted pendulums that can all rotate in different directions. The first type, which is the most prevalent, inverted pendulum, can only travel horizontally [5]. These reversed pendulums fall under the X category. The horizontal X-Y plane is a possible path for the second kind of inverted pendulum [5]. This type of reversed pendulum includes X-Y inversions. In the x-z plane, the third type of reversed pendulum can rotate in either direction [5]. This type of pendulum is known as a "X-Z inverted pendulum." The horizontal control force that controls the x-inverted pendulum is influenced by its horizontal displacements, which in turn define the control action. Two horizontal control forces acting on a pivot influence the x-y inverted pendulum, and the control action is reliant on the x-y horizontal displacements of the pivot.

One horizontal control force and one vertical control force influence the X-Z inverted pendulum, and the control action is dependent upon both the fulcrum's vertical and horizontal movements. The physical model based on structural representation [5] is shown in turn in Figs. 2.3 (a), (b), and (c).

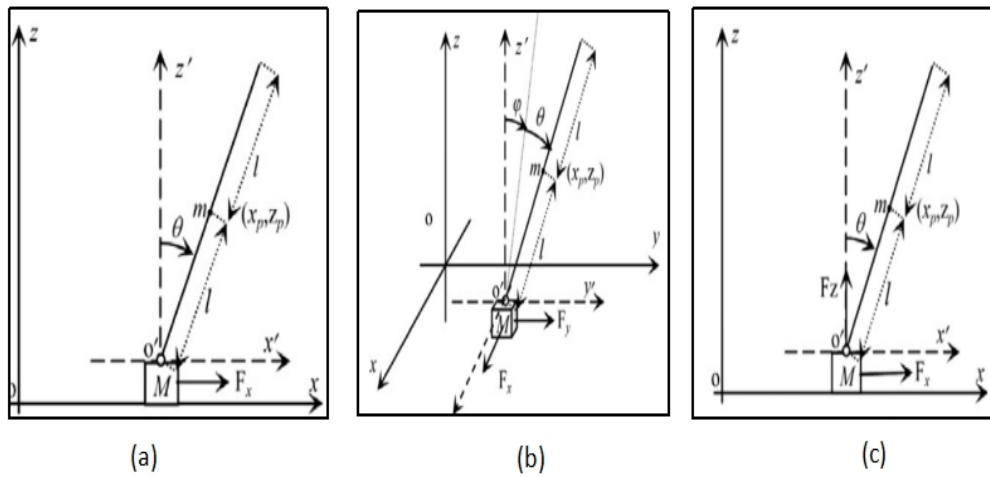


Fig. 2.3. a. Vector schematic of X-inverted pendulum. b. X-Y inverted pendulum. c. X-Z inverted pendulum.

2.2.2 Comparisons and Limitations between Three Types of Structures

The relationships between the three different types of structures [5] serve to emphasize the following points.

- The x-shaped solitary inverted pendulum is the most basic type. It is a unique instance of an X-Y and X-Z inverted pendulum.
- It is possible to separate the X-Y inverted pendulum into two separate inverted pendulums. It represents a broadening of the X model. The double inverted pendulum, also known as the X-Y, can be viewed as a pair of inverted pendulums with x axes combined. Hence, the cart, lower, and upper pendulum subsystems make up the double inverted pendulum in general.
- The X-Z inverted pendulum can be divided into two distinct inverted pendulums. While the z system cannot be stabilized using simply vertical control force, the X model may be regulated to be steady.
- Creating a controller that can implement stabilization and tracking control with regard to state equations is a challenging task.

Formulation of nonlinear dynamic equations is very important for describing dynamic behavior. Nonlinear dynamic equations are approached in two ways, such as the Lagrange model and Newton-Euler methods. Although the Lagrange model is more elegant [5] but the Newton-Euler approach [6] is also a well-established model for testing various control strategies and this method is significantly more straightforward, making it easy to understand and express with sophomore-level engineering dynamics. Both of the Newton-Euler and the Lagrangian-Euler mathematical methods are discussed in the following section.

2.2.3 Mathematical Modeling

2.2.3.1 Laglarange Method

The Lagrange-Euler method is used to represent those structures mathematically [5], and it is addressed as

✧ *X-Inverted Pendulum*

$$(M + m)\ddot{x} + ml \cos \theta \ddot{\theta} - ml \sin \theta \dot{\theta}^2 = F_x \quad (2.1)$$

$$\cos \theta \ddot{x} + l\ddot{\theta} - g \sin \theta = 0 \quad (2.2)$$

✧ ***X-Y Inverted Pendulum***

$$(M + m)\ddot{x} + ml \cos \theta \ddot{\theta} - ml \sin \theta \dot{\theta}^2 = F_x \quad (2.3)$$

$$(M + m)\ddot{y} + ml \cos \theta \cos \varphi \ddot{\varphi} - ml \sin \theta \sin \varphi \ddot{\theta} - 2ml \sin \theta \cos \varphi \dot{\theta} \dot{\varphi} - ml \cos \theta \sin \varphi (\dot{\theta}^2 + \dot{\varphi}^2) = F_y \quad (2.4)$$

$$l\ddot{\theta} + \cos \theta \ddot{x} - \sin \theta \sin \varphi \ddot{y} + l \cos \theta \cos \theta \dot{\varphi}^2 - g \sin \theta \cos \varphi = 0 \quad (2.5)$$

$$l \cos \theta \ddot{\varphi} + l \cos \varphi \ddot{y} - g \sin \varphi = 0 \quad (2.6)$$

✧ ***X-Z Inverted Pendulum***

$$(M + m)\ddot{x} + ml \cos \theta \ddot{\theta} - ml \sin \theta \dot{\theta}^2 = F_x \quad (2.7)$$

$$(M + m)\ddot{z} - ml \sin \theta \ddot{\theta} - ml \cos \theta \dot{\theta}^2 = F_z - (M + m)g \quad (2.8)$$

$$\cos \theta \ddot{x} - \sin \theta \ddot{z} + l\ddot{\theta} - g \sin \theta = 0 \quad (2.9)$$

The energy principle is used to create the aforementioned Lagrange equations for specific structures.

✧ ***X-Inverted Pendulum***

The entire kinetic energy and potential energy are followed as

$$\begin{cases} k = \frac{1}{2}M\dot{x}^2 + \frac{1}{2}m(\dot{x}_p^2 + \dot{z}_p^2) \\ p = mgz_p \end{cases} \quad (2.10)$$

✧ ***X-Y Inverted Pendulum***

$$\begin{cases} k = \frac{1}{2}M(\dot{x}^2 + \dot{y}^2) + \frac{1}{2}m(\dot{x}_p^2 + \dot{z}_p^2 + \dot{y}_p^2) \\ p = mgz_p \end{cases} \quad (2.11)$$

✧ ***X-Z Inverted Pendulum***

$$\begin{cases} k = \frac{1}{2}M(\dot{x}^2 + \dot{z}^2) + \frac{1}{2}m(\dot{x}_p^2 + \dot{z}_p^2) \\ p = mgz_p \end{cases} \quad (2.12)$$

Along with Eqs.(2.10), (2.11) and (2.12) the source of creating Lagrange models for all structures is shown below.

$$\text{X Inverted Pendulum} \rightarrow \begin{cases} \frac{d}{dt} \left(\frac{dL}{d\dot{x}} \right) - \frac{dL}{dx} = F_x \\ \frac{d}{dt} \left(\frac{dL}{d\dot{\theta}} \right) - \frac{dL}{d\theta} = 0 \end{cases} \quad (2.13)$$

$$\text{X - Y Inverted Pendulum} \rightarrow \begin{cases} \frac{d}{dt} \left(\frac{dL}{d\dot{x}} \right) - \frac{dL}{dx} = F_x \\ \frac{d}{dt} \left(\frac{dL}{d\dot{y}} \right) - \frac{dL}{dy} = F_y \\ \frac{d}{dt} \left(\frac{dL}{d\dot{\theta}} \right) - \frac{dL}{d\theta} = 0 \\ \frac{d}{dt} \left(\frac{dL}{d\dot{\varphi}} \right) - \frac{dL}{d\varphi} = 0 \end{cases} \quad (2.14)$$

$$\text{X - Z Inverted Pendulum} \rightarrow \begin{cases} \frac{d}{dt} \left(\frac{dL}{d\dot{x}} \right) - \frac{dL}{dx} = F_x \\ \frac{d}{dt} \left(\frac{dL}{d\dot{z}} \right) - \frac{dL}{dz} = F_z \\ \frac{d}{dt} \left(\frac{dL}{d\dot{\theta}} \right) - \frac{dL}{d\theta} = 0 \end{cases} \quad (2.15)$$

$$L = k - p \quad (2.16)$$

Now, following (2.1) and (2.2) state expression can be formed as

$$\begin{cases} \dot{x}_1 = x_2 \\ \dot{x}_2 = \frac{-mg \cos x_3 \sin x_3 + ml \sin x_3 \dot{x}_4^2 + F_x}{M + m \sin^2 x_3} + d_1 \\ \dot{x}_3 = x_4 \\ \dot{x}_4 = \frac{-mg \cos x_3 \sin x_3 \dot{x}_4^2 - \cos x_3 F_x + (M + m)g \sin x_3}{M + m \sin^2 x_3} + d_2 \end{cases} \quad (2.17)$$

For the other two structures, the disturbances are connected to each state equation as well.

2.2.3.2 Newton-Eular Method

The nonlinear dynamics with possible state equations [6] are formulated on only X inverted pendulum [5] in detail as it is a unique instance of other structures as discussed. Following vector representation of X model as presented in Fig.2.3. The physical representation of the inverted pendulum is demonstrated in this section. The aim of formulating the model differential equations is to balance the rod of length towards the vertical line and move the cart forward or reversing direction by applying input force F_x on the cart. The system's stability depends on the smaller value of the angle of the pendulum θ .

The dimensions of the centre of gravity with respect to the Cartesian axis on the X-Z plane of the X model are computed as

$$x_p = x + l \sin \theta \quad (2.18)$$

$$z_p = l \cos \theta \quad (2.19)$$

The balance of forces acting on the rod in the vertical direction at the centre of gravity is given as

$$V - mp = \sum F = ma = m \frac{d^2}{dt^2} l \cos \theta \quad (2.20)$$

By taking the double-time derivative of $\cos \theta$, it is as follows

$$V - mp = -ml\ddot{\theta} \sin \theta - ml\dot{\theta}^2 \cos \theta \quad (2.21)$$

Now, balance the forces (H) exerting on the rod in horizontal movement with respect to the centre of gravity is given as

$$H = m\ddot{x} + ml \frac{d^2}{dt^2} \sin \theta \quad (2.22)$$

By taking the double derivative of $\sin\theta$, the expression is followed as

$$H = m\ddot{x} + ml\ddot{\theta}\cos\theta - ml\dot{\theta}^2\sin\theta \quad (2.23)$$

Now, balance of force in horizontal direction on a cart is given as

$$\sum F = Ma \quad (2.24)$$

$$F_x - H = M\ddot{x} \quad (2.25)$$

Now, substituting (2.23) into (2.25) the expression of balance of force on cart is given as

$$F_x = M\ddot{x} + m\ddot{x} + ml\ddot{\theta}\cos\theta - ml\dot{\theta}^2\sin\theta \quad (2.26)$$

$$F_x = (M + m)\ddot{x} + ml\ddot{\theta}\cos\theta - ml\dot{\theta}^2\sin\theta \quad (2.27)$$

To compute the component of forces with regard to vertical and horizontal directions, as illustrated in Fig.2.4, it is imperative to illustrate how the forces at the center of gravity are in equilibrium.

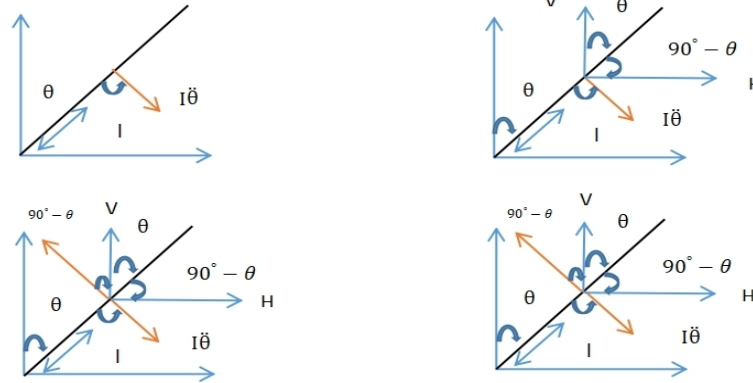


Fig. 2.4. Force equilibrium at the center of gravity.

The torque which is known as angular rotation, acting on this rod is defined as

$$\tau = I\ddot{\theta} \quad (2.28)$$

When the rod is moving towards a downward direction, then the torque should be applied in the opposite direction. Hence, vertical component of force in the required direction is given as

$$F_{x_1} = V\cos(90^\circ - \theta) \quad (2.29)$$

Now, the torque in the required direction is given as

$$\tau_1 = F_{x_1}l = Vl\sin\theta \quad (2.30)$$

Now, the horizontal component of force in the required direction is given as

$$F_{x_2} = H \cos(180^\circ - \theta) \quad (2.31)$$

Now, the torque in the required direction is given as

$$\tau_2 = F_{x_2} l = -H l \cos \theta \quad (2.32)$$

So, total torque acting on the centre of rod is given as

$$I \ddot{\theta} = V l \sin \theta - H l \cos \theta \quad (2.33)$$

Now, putting the value of V and H the following expressions are given as

$$I \ddot{\theta} = [m p - m l \ddot{\theta} \sin \theta - m l \dot{\theta}^2 \cos \theta] l \sin \theta - [m \ddot{x} + m l \ddot{\theta} \cos \theta - m l \dot{\theta}^2 \sin \theta] l \cos \theta \quad (2.34)$$

$$I \ddot{\theta} = m p l \sin \theta - m l^2 \ddot{\theta} \sin^2 \theta - m \ddot{x} l \cos \theta - m l^2 \dot{\theta}^2 \cos^2 \theta \quad (2.35)$$

$$I \ddot{\theta} = m p l \sin \theta - m l^2 \ddot{\theta} - m \ddot{x} l \cos \theta \quad (2.36)$$

$$I \ddot{\theta} + m l^2 \ddot{\theta} + m \ddot{x} l \cos \theta - m p l \sin \theta = 0 \quad (2.37)$$

$$(I + m l^2) \ddot{\theta} + m \ddot{x} l \cos \theta - m p l \sin \theta = 0 \quad (2.38)$$

So, (2.38) is a nonlinear expression related to all variables of the entire model and balancing the torque at the centre of gravity with balancing horizontal and vertical forces. This expression defines the inverted pendulum system along with the applied force on cart as shown in (2.27). This applied force is related to the displacement of the cart as \ddot{x} and the movement of the rod as $\ddot{\theta}$.

✧ *Linearization Approach on Nonlinear Model*

Every physical system is usually encountered with some popular nonlinear influences such as saturation, dead zone and backlash, which have a major role in introducing disturbances and noise in performance. Due to these effects, sometimes the system either may respond slow or may not respond in the desired manner in spite of applying input variables. Linear approximation, which is known as an effective technique, approaches a major solution to approximate any nonlinear functions linearly and this technique will be applicable on nonlinear system only when it will be considered on nearly operating point. So, Taylor series approximation [7] is the popular method of approximating nonlinear functions in a systematic manner.

Taylor series:

$$f(x) = f(x_0) + \frac{\partial f}{\partial x} \bigg|_{x_0} \frac{(x-x_0)}{1!} + \frac{\partial^2 f}{\partial x^2} \bigg|_{x_0} \frac{(x-x_0)^2}{2!} + \dots \quad (2.39)$$

From the above expression it clearly states that nonlinear function is expanded by Taylor series approximation with operating point at x_0 .

So, if it is very close to operating point then $x - x_0$ will be small and $(x - x_0)^2$ will be small. Other higher order terms also be further smaller. Now, neglecting the higher order terms Taylor series can be expressed with the final version:

$$f(x) - f(x_0) \approx \frac{\partial f}{\partial x}(x - x_0) \quad (2.40)$$

Based on the above background linearized approximation method is applied on inverted pendulum. Since it must keep the inverted pendulum vertical, that means $\theta(t)$ and $\dot{\theta}(t)$ are very small quantities, therefore as $\theta \rightarrow 0$ so, $\sin \theta \approx \theta$, $\cos \theta \approx 1$, $\theta \cdot \dot{\theta}^2 = 0$. Now, (2.27) and (2.38) can be written as

$$F_x = (M + m)\ddot{x} + ml\ddot{\theta} \quad (2.41)$$

$$(I + ml^2)\ddot{\theta} + m\ddot{x}l = mpl\theta \quad (2.42)$$

The above expressions are known as linearized model of inverted pendulum. Now, to find the transfer function it must take the Laplace transform of the above linearized differential equations.

$$F_x(s) = (M + m)X(s)s^2 + ml\theta(s)s^2 \quad (2.43)$$

$$(I + ml^2)\theta(s)s^2 - mpl\theta(s) = mlX(s)s^2 \quad (2.44)$$

Initial circumstances are meant to be zero to compute the overall transfer function of the system. The first expression of $X(s)$ from (2.44) is given as

$$X(s) = \left[\frac{(I + ml^2)}{ml} - \frac{p}{s^2} \right] \theta(s) \quad (2.45)$$

Now, substituting the value of $X(s)$ in (2.43) it is shown with the following expression

$$F_x(s) = (M + m) \left[\frac{(I + ml^2)}{ml} - \frac{p}{s^2} \right] \theta(s) \cdot s^2 + ml\theta(s)s^2 \quad (2.46)$$

Now, the entire transfer function is formulated as

$$\frac{\theta(s)}{F_x(s)} = \frac{ml}{\{(M + m)ml(I + ml^2)\} + (ml)^2s^2 - (M + m)mpl} \quad (2.47)$$

2.2.3.3 State Space Model Representation

Following vector representation [6] as depicted in Fig.2.4 the mass (m) is considered at the top of the rod and the centre of gravity is the centre of the pendulum as shown in Fig.2.5. Therefore, moment of inertia (I) will be zero.

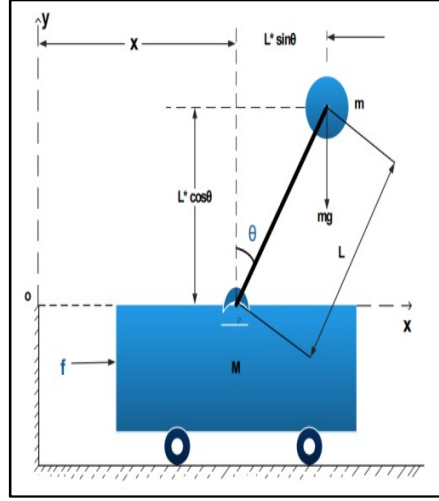


Fig. 2.5. Interchanging the position of mass at the top of the rod.

Following the above condition in (2.39) and (2.40), it can be defined as

$$(M + m)\ddot{x} + ml\ddot{\theta} = F_x \quad (2.48)$$

$$ml^2\ddot{\theta} + m\ddot{x}l = mpl\theta \quad (2.49)$$

$$\ddot{\theta} = \frac{mpl\theta}{ml^2} - \frac{m\ddot{x}l}{ml^2} = \frac{p}{l}\theta - \frac{1}{l}\ddot{x} \quad (2.50)$$

$$\ddot{x} = \frac{mpl\theta}{ml} - \frac{ml^2}{ml}\ddot{\theta} = p\theta - l\ddot{\theta} \quad (2.51)$$

Now, using (2.50) in (2.48) it is given as

$$(M + m)\ddot{x} + ml\left(\frac{p}{l}\theta - \frac{1}{l}\ddot{x}\right) = F_x \quad (2.52)$$

$$(M + m)\ddot{x} + mp\theta - m\ddot{x} = F_x \quad (2.53)$$

$$M\ddot{x} = F_x - mp\theta \quad (2.54)$$

Now, using (2.51) in (2.48) it is given as

$$M\ddot{x} + m\ddot{x} + ml\ddot{\theta} = F_x \quad (2.55)$$

$$M(p\theta - l\ddot{\theta}) + m(p\theta - l\ddot{\theta}) + ml\ddot{\theta} = F_x \quad (2.56)$$

$$Ml\ddot{\theta} = (M + m)p\theta - F_x \quad (2.57)$$

To convert state space, models x_1, x_2, x_3, x_4 are considered as state variables with the following expressions

$$\begin{cases} x_1 = \theta \\ \dot{x}_1 = \dot{\theta} = x_2 \\ \dot{x}_2 = \ddot{\theta} = \dot{x}_3 \\ x_3 = \ddot{\theta} \\ \dot{x}_3 = \ddot{\ddot{\theta}} = \dot{x}_4 \\ \dot{x}_4 = \ddot{\ddot{\ddot{\theta}}} = \ddot{x}_3 \end{cases} \quad (2.58)$$

Using state space variables (2.54) can be updated as

$$M\dot{x}_4 = F_x - mp x_1 \quad (2.59)$$

$$\dot{x}_4 = -\frac{mp}{M} x_1 + \frac{F_x}{M} \quad (2.60)$$

Now, using state space variables (2.57) can be updated as

$$Ml\dot{x}_2 = (M + m)px_1 - F_x \quad (2.61)$$

$$\dot{x}_2 = -\frac{(M+m)p}{Ml} x_1 - \frac{F_x}{Ml} \quad (2.62)$$

Now, following the above (2.60) and (2.62) state space model [6] is represented as

$$\begin{cases} \begin{bmatrix} \dot{x}_1 \\ \dot{x}_2 \\ \dot{x}_3 \\ \dot{x}_4 \end{bmatrix} = \begin{bmatrix} 0 & 1 & 0 & 0 \\ \frac{(M+m)p}{Ml} & 0 & 0 & 0 \\ 0 & 0 & 0 & 1 \\ -\frac{mp}{M} & 0 & 0 & 0 \end{bmatrix} \begin{bmatrix} x_1 \\ x_2 \\ x_3 \\ x_4 \end{bmatrix} + \begin{bmatrix} 0 \\ -\frac{1}{Ml} \\ 0 \\ \frac{1}{M} \end{bmatrix} [F_x] \\ \begin{bmatrix} y_1 \\ y_2 \end{bmatrix} = \begin{bmatrix} 1 & 0 & 0 & 0 \\ 0 & 0 & 1 & 0 \end{bmatrix} \begin{bmatrix} x_1 \\ x_2 \\ x_3 \\ x_4 \end{bmatrix} + [0] [F_x] \end{cases} \quad (2.63)$$

2.3 Continuous Stirred Tank Reactor (CSTR)

A precise model is required in order to effectively regulate the product concentration in the CSTR, a prototype chemical reactor system with complicated unstable features.

2.3.1 Classification and Characteristic of Chemical Reactors

A chemical reactor [8] is where reactants are transformed into products in a chemical plant. Chemical reactors come in a wide range of shapes and modes of operation. As a result, there are many different ways to categorize them. The primary categorization is based on several reaction systems and real-time assumptions.

✧ *Batch Reactor*

Typically, reactants are added to the reactor and given time to react [8]. As a result, products are created inside the reactor. The process is then repeated after the products and unreacted reactants have been eliminated. There is an unsteady mode of operation in batch reactors and the concentration of reactants is uniform throughout in batch reactor. This type of reactor is used for the preparation of specialty chemicals.

✧ *Plug Flow Reactor*

Plug flow reactors [8], often referred to as tubular reactors, are composed of a cylindrical plug like flow structure with apertures on each end through which reactants and products can pass.

Plug flow reactors typically operate only at steady state and there will be no back mixing. When reactants move down the reactor's length, they are continuously consumed. The percentage conversion achieved in CSTR is highest among CSTR, batch and PFR.

✧ *Continuous Stirred Tank Reactor*

The fact that CSTR [8] has a big heat capacity and an accessible interior makes it preferable to other reactors. Another significant advantage is that it is simple to maintain adequate temperature control. There is only one restriction: Compared to other flow reactors, the reactor's volume rate of reactant to product conversion is relatively low. In Fig.2.6, the fundamental characteristic is displayed.

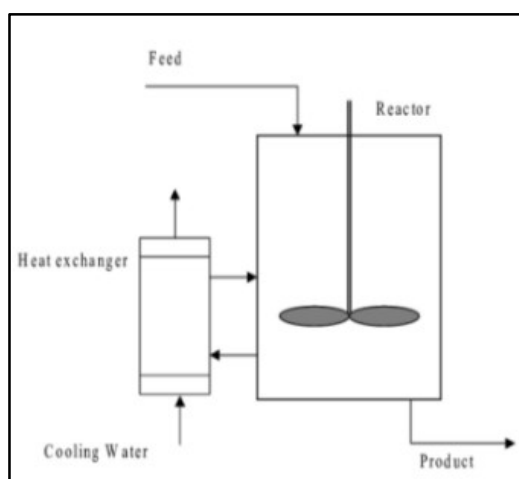


Fig. 2.6. Isothermal and non-isothermal CSTR icon.

The term "mixed flow reactor" (MFR) is another name for CSTR. Similar to batch and other reactors, the reaction in this reactor likewise takes place in a sealed tank. Moreover, the tank features an agitator to completely mix the reactants. It differs from a batch reactor in that its continuous equipment nature is implied by the name alone. The reactants enter the reactor at a specific mass flow rate, react for a period of time determined by the reactor's space time, and then produce the products. At the same mass flow rate, the products exit the reactor. The concentration of a reactant inside the reactor and at exit remains the same since the reactor is fully mixed one. The amount of time required to process single reactor volume is one space-time.

2.3.2 Characteristics and Limitation of Continuous Stirred Tank Reactor

A continuous flow into and out of the system distinguishes the CSTR [9–10] from a boiler reactor. Compared to batch reactors, CSTR is significantly more efficient. Both liquid phase processes and suspensions of liquids and solids can be handled by them. It is useful to

include a set of assumptions when modelling any piece of equipment because they will simplify the design calculations. The following two categories are employed to demonstrate the function of the CSTR process.

2.3.2.1 Ideal Version

The behaviour of an optimally CSTR is always leveraged to demonstrate the behaviour of CSTR (CISTR). Each reactor model must start with a general mole balance as a guide. The equation can then be modified to fit a set of presumptions. Every calculation is done using CISTR, which presupposes uniform mixing [10]. In a reactor with perfect mixing, the composition of the product is similar to the materials' composition inside the reactor, which is dependent on residence time and reaction rate. This estimate is appropriate for technical use if the residence time is 5–10 times the mixing time. The CISTR model is commonly used to simplify engineering calculations and can be used to characterise research reactors. In reality, it can only be approached, particularly in reactors of industrial capacity. Concentration and temperature are two crucial elements that must be balanced inside the reactor and depend on both isothermal and non-isothermal properties. Both isothermal and non-isothermal properties contribute to the knowledge on mole balance and energy balance, respectively. A general mathematical representation for molar concentration under isothermal property [10] is simplified as

$$\text{In} - \text{Out} + \text{Generation} - \text{Consumption} = \text{Accumulation} \quad (2.64)$$

Assumption I: Well mixed

$$F_1 C_1 - F_2 C_2 + \int r_a dV = \frac{dN_a}{dt} \quad (2.65)$$

Assumption II: Steady state

$$F_1 C_1 - F_2 C_2 + \int r_a dV = 0 \quad (2.66)$$

As, $r_a \neq fct(V)$ so, $\int r_a dV = r_a V$

$$F_1 C_1 - F_2 C_2 + \int r_a V = 0 \quad (2.67)$$

Now, following the steady state condition in (2.67) final concentration can be expressed with the following equation

$$C_2 = C_1 + \frac{r_a V}{F} \quad (2.68)$$

Now, the above isothermal derivation of mass balance can be expanded to convert into non-isothermal condition also with the function of conversion.

Currently, non-isothermal property is used to guide adiabatic and non-adiabatic circumstances [11–12] for illuminating the energy balance inside the reactor. Below is a discussion of how these key conditions compare and their limits.

- ✧ **Adiabatic situation** [12] is the procedure that prevents mass or heat from entering or leaving the reactor since the reactor is entirely encircled by a jacket as shown in Fig. 2.7, and the temperature inside the reactor will also fluctuate.

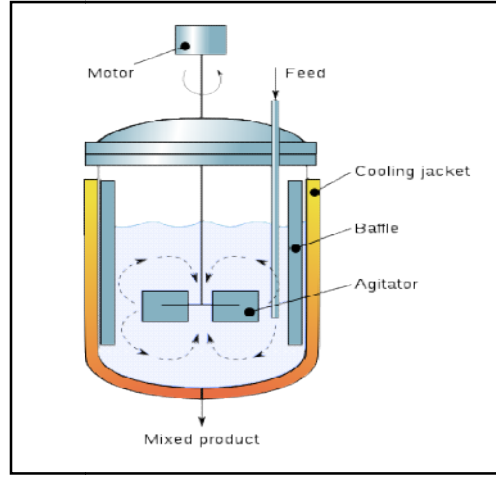


Fig. 2.7. CSTR Industrial Schematic.

$$\text{In} - \text{Out} \pm \text{Heat of reaction} = 0 \quad (2.69)$$

$$H_{in} - H_{out} \pm (-\Delta H_r)(r_a V) = 0 \quad (2.70)$$

Input and output heating energy can be shown as

$$F_1 \rho_0 C_1 (T_0 - T_r) - F_2 \rho C_2 (T - T_r) \pm (-\Delta H_r)(r_a V) = 0 \quad (2.71)$$

Now, under a steady state condition, if the reference temperature is considered as zero, then the final expression of temperature is shown as

$$T = \frac{\rho_0 C_1 T_0}{\rho C_2} \pm \frac{(-\Delta H_r)(r_a V)}{F \rho C_2} \quad (2.72)$$

If density is considered as constant then (2.72) can be followed as

$$T = \frac{c_1 T_0}{C_2} \pm \frac{(-\Delta H_r)(r_a V)}{F \rho C_2} \quad (2.73)$$

- ✧ **Non-adiabatic condition** [12] is the process which allows surrounding temperature outside the reactor and transfer of energy is considered with the final expression of energy balance as follows

$$T = \frac{c_1 T_0}{c_2} \pm \frac{(-\Delta H_r)(r_d V)}{F \rho c_2} - \frac{T - T_s}{F \rho c_2} \quad (2.74)$$

2.3.2.2 Non-Ideal Version

It is necessary to take into account non-ideal conditions because in practice, ideal conditions occasionally vary from ideality [12]. In the case of industry, there are reactors that deal with various types of fluids to produce the desired product. Ideal flow can therefore vary in this particular circumstance and change into different flow patterns. Real reactors never operate under ideal conditions, and the degree of mixing determines how ideal or non-ideal a flow pattern will behave throughout. The following factors are mainly responsible for non-ideal flow as

- I. There is a probability of getting a flow that is less than optimum if the reactor contains any kind of *recycled* stream.
- II. *Short-circuiting* is a phenomenon that occurs when the reactant does not participate in the reaction and exits the reactor in its original state without undergoing any form of conversion or reaction.
- III. *Vortices* may occur either at the reactor's entry point or its exit point. So, in this instance, as a result of the creation of vortices, both the velocity and the flow pattern will alter.
- IV. How the reactants or fluid are *mixed* is the main controlling factor that controls the flow patterns.
- V. There are a few places inside a reactor where reactants can simply be emptied without participating in the reaction.

Hence, it frequently occurs that reactants become stuck in the bottom-most portion of the reactor and are unable to participate in reactions there. Hence, a *dead zone* forms in some areas, which may cause the flow pattern to deviate from optimal. Since the outlet section of the reactor may not fit properly, producing a non-ideal flow pattern, and because reactant can easily bypass the entrance section, CSTR rarely behaves optimally in practice. The ideal uniform flow pattern may be disturbed by this. Yet, an optimal CSTR model is absolutely necessary to forecast the composition of any biological or chemical process.

2.3.3 Physical Modeling of Ideal CSTR

A typical nonlinear model of CSTR [13] with related variables is depicted as in Fig. 2.8.

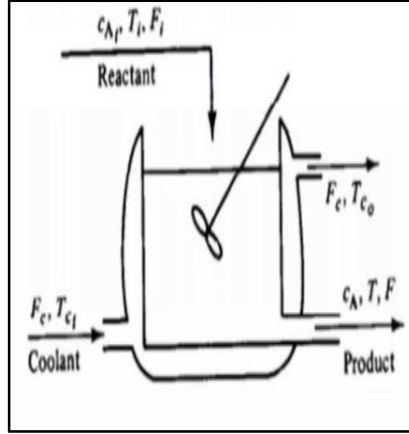


Fig. 2.8. Schematic feature of single perfectly mixed CSTR.

2.3.3.1 Mathematical approach for mass balance

As stated in the preceding section, isothermal properties are used to determine molar concentration. The basic qualities are as follows:

- ✧ Perfect mixing, i.e; temperature and concentration are identical everywhere in tank.
- ✧ Liquid density and heat output is fixed.
- ✧ There is no heat leakage from the reactor to the surroundings.
- ✧ No energy balance exists for the coolant, and the coolant is properly mixed.
- ✧ The CSTR's momentum is ignored because it remains constant under all working circumstances.

Now, based on conservation principles it is followed as

$$\frac{\text{Accumulation of total mass}}{\text{time}} = \frac{\text{Input of total mass}}{\text{time}} - \frac{\text{Output of total mass}}{\text{time}} \pm \frac{\text{Total mass generated or consumed}}{\text{time}} \quad (2.75)$$

$$\frac{d(\rho V)}{dt} = \rho_i F_i - \rho_o F \pm 0 \quad (2.76)$$

Since ρ is constant and the above expression can be re written as

$$\frac{dV}{dt} = F_i - F \quad (2.77)$$

Mass balance [14] on component A is represented as

$$\frac{\text{Accumulation of moles of A}}{\text{time}} = \frac{\text{Input of moles of A}}{\text{time}} - \frac{\text{Output of moles of A}}{\text{time}} - \frac{\text{Disappearance of moles of A due to reaction}}{\text{time}} \quad (2.78)$$

$$\frac{d}{dt}(n_A) = \frac{d}{dt}(c_A V) = c_{A_i} F_i - c_A F - rV \quad (2.79)$$

$$r = k_0 e^{-E/RT} c_A \quad (2.80)$$

Substituting, (2.80) into (2.79) it is expressed as

$$\frac{d}{dt}(c_A V) = c_{A_i} F_i - c_A F - (k_0 e^{-E/RT} c_A) V \quad (2.81)$$

$$c_A \frac{dV}{dt} + V \frac{dc_A}{dt} = c_{A_i} F_i - c_A F - (k_0 e^{-E/RT} c_A) V \quad (2.82)$$

$$V \frac{dc_A}{dt} = c_{A_i} F_i - c_A F - (k_0 e^{-E/RT} c_A) V - c_A \frac{dV}{dt} \quad (2.83)$$

Now, substituting (2.77) into (2.83) and it is expressed as

$$\frac{dc_A}{dt} = \frac{F_i}{V} (c_{A_i} - c_A) - (k_0 e^{-E/RT} c_A) \quad (2.84)$$

2.3.3.2 Mathematical modelling for Temperatures

An internal coil-based jacket that surrounds a non-isothermal CSTR [13] plays a crucial role in the reactor's temperature change. Reactor products typically release or absorb heat while being processed. Heat must be added to or withdrawn from the reactor contents by a cooling jacket in order to regulate the proper temperature. The reactor is heated and cooled using an external jacket. To add or remove heat, heat transfer fluid goes through the jacket. The performance of a jacket can be defined by three parameters:

- ✧ Response time to modify the jacket temperature
- ✧ Uniformity of jacket temperature
- ✧ Stability of jacket temperature

From above Fig. 2.8 it is shown that the agitation nozzle helps to pump heat transfer fluid that jacket circulates the fluid at a high velocity. The coolant moves at the flow rate of F_c and at feed temperature of T_{c_i} . The exit temperature of the coolant fluid is T_{c_o} . An irreversible, exothermic reaction ($A \rightarrow B$) is conducted in a single perfectly mixed CSTR under combined adiabatic and non-adiabatic conditions. As stated in the preceding section, isothermal properties [11-12] are used to determine molar concentration. The basic qualities are as follows:

- ✧ The temperature changes with time.
- ✧ Metal barriers are thought to have a negligible mass.
- ✧ The metal's thermal resistance must be considered.
- ✧ The amount of water in the jacket is maintained at a consistent level.
- ✧ Heat loss with constant densities is assumed to negligible.

The overall heat transfer is given as

$$Q = UA_H(T - T_{c_o}) \quad (2.85)$$

Reactor energy balance [13] is represented as

$$\text{Enthalpy In} - \text{Enthalpy Out} - \text{Enthalpy Generated} - \text{Energy removed by cooling coil} = \text{Energy Accumulated} \quad (2.86)$$

$$\rho F_i h_i - \rho F h - V k c_A - UA_H(T - T_{c_o}) = \frac{d(\rho V h)}{dt} \quad (2.87)$$

Under a steady state $F_i = F$

$$\rho F (h_i - h) - V k c_A - UA_H(T - T_{c_o}) = \rho \frac{d(Vh)}{dt} \quad (2.88)$$

Using $h = TC$ and $h_i = T_i C$ (2.88) can be updated as

$$\rho F C (T_i - T) - V k c_A - UA_H(T - T_{c_o}) = \rho C \frac{d(T)}{dt} \quad (2.89)$$

$$\frac{dT}{dt} = \frac{F}{V} (T_i - T) - \frac{k}{\rho C} c_A - \frac{UA_H(T - T_{c_o})}{\rho C V} \quad (2.90)$$

$$k = k_0 \exp\left(-\frac{E}{RT}\right) \quad (2.91)$$

$$\frac{dT}{dt} = \frac{F}{V} (T_i - T) - \frac{c_A}{\rho C} k_0 \exp\left(-\frac{E}{RT}\right) - \frac{UA_H(T - T_{c_o})}{\rho C V} \quad (2.92)$$

(2.84) and (2.92) are coupled non-linear equations in T and c_A , they need to solve after linearization using state space representation.

2.3.3.3 State variable form

The following non-linear equations need to be expressed in state space model.

$$\frac{dc_A}{dt} = f_1(c_A, T) = \frac{F_i}{V} (c_{A_i} - c_A) - (k_0 e^{-E/RT} c_A) \quad (2.93)$$

$$\frac{dT}{dt} = f_2(c_A, T) = \frac{F}{V} (T_i - T) - \frac{c_A}{\rho} k_0 \exp\left(-\frac{E}{RT}\right) - \frac{UA_H(T - T_{c_o})}{\rho C V} \quad (2.94)$$

2.3.3.4 Linearization

The nonlinear expressions are converted into linearized [13] version with state variable forms as follows.

$$\begin{cases} \dot{x} = Ax + Bu \\ y = Cx \end{cases} \quad (2.95)$$

$$\begin{cases} x = \begin{bmatrix} c_A - c_{As} \\ T - T_s \end{bmatrix} \\ y = \begin{bmatrix} c_A - c_{As} \\ T - T_s \end{bmatrix} \\ u = \begin{bmatrix} u_1 \\ u_2 \end{bmatrix} \begin{bmatrix} F_i - F_{is} \\ F_c - F_{cs} \end{bmatrix} \end{cases} \quad (2.96)$$

A jacobian matrix [14] plays very important role to identify the system whether it is stable or not determining the Eigen values of Jacobian matrix. It is also followed on near operating points to represent linearized version of nonlinear CSTR system.

$$A = \begin{bmatrix} A_{11} & A_{12} \\ A_{21} & A_{22} \end{bmatrix} = \begin{bmatrix} \frac{\partial f_1}{\partial x_1} & \frac{\partial f_1}{\partial x_2} \\ \frac{\partial f_2}{\partial x_1} & \frac{\partial f_2}{\partial x_2} \end{bmatrix} \quad (2.97)$$

$$\begin{cases} A_{11} = -\frac{F_i}{V} - K_s \\ A_{12} = -c_{As}K'_s \\ A_{21} = -\frac{c_A}{\rho C}K_s \\ A_{22} = -\frac{F_i}{V} + \left(\frac{c_{As}}{\rho C}\right)K'_s - \frac{UA_H}{\rho CV} \end{cases} \quad (2.98)$$

$$\begin{cases} K_s = k_0 \exp\left(-\frac{E}{RT_s}\right) \\ K'_s = k_0 \exp\left(-\frac{E}{RT_s}\right) \left(\frac{E}{RT_s^2}\right) \end{cases} \quad (2.99)$$

$$B = \begin{bmatrix} B_{11} & B_{12} \\ B_{21} & B_{22} \end{bmatrix} = \begin{bmatrix} \frac{\partial f_1}{\partial u_1} & \frac{\partial f_1}{\partial u_2} \\ \frac{\partial f_2}{\partial u_1} & \frac{\partial f_2}{\partial u_2} \end{bmatrix} \quad (2.100)$$

$$\begin{cases} B_{11} = \frac{c_{Ai} - c_{As}}{V} \\ B_{12} = 0 \\ B_{21} = \frac{T_i - T_s}{V} \\ B_{22} = \frac{(T_s - T_{c0})}{\rho CV} \end{cases} \quad (2.101)$$

$$\begin{cases} C = \begin{bmatrix} 1 & 0 \\ 0 & 1 \end{bmatrix} \\ D = \begin{bmatrix} 0 \\ 0 \end{bmatrix} \end{cases} \quad (2.102)$$

Now, the overall transfer function of the system can also be computed by using the above A B, C, and D matrices.

2.4 A Brief Survey on Different Control Algorithms for Unstable Processes

This section discusses current control actions of various emerging control schemes on two distinct systems, such as inverted pendulum and continuously stirred tank reactors.

2.4.1 PID (Proportional-Integral-Derivative) Controller

The PID controller mainly comprises of three tuning variables which individually play a very significant role in designing the process with satisfactory control action. The most crucial step in developing any control action is choosing the gain parameters, such as proportional, integral, and derivative gains.

To this end, there are numerous techniques available, including time domain method [15], frequency domain method [15], trial and error method, Ziegler-Nichols method [15] and optimization algorithm. The basic scheme of the conventional PID controller [16] is depicted as in Fig. 2.9.

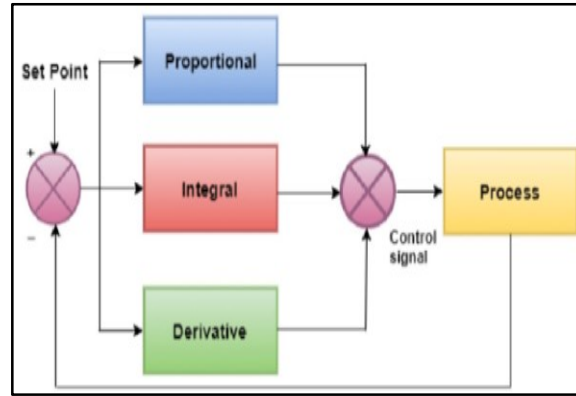


Fig. 2.9. Schematic feature of a conventional PID controller.

On inverted pendulum or continuous stirred tank reactor processes, experts have proposed PID control algorithms in a variety of ways, including single topology, dual topology, and combined topology. PID control ensured satisfactory performance in terms of desired time or frequency region metrics and error metrics.

✧ *Study on Inverted Pendulum*

For testing PID control actions, inverted pendulum models based on Newton-Euler are frequently found in literature, while studies based on Lagrange models are quite uncommon. In comparison, it is demonstrated that it is an inappropriate platform for verifying the control actions as mentioned above. Various architectures [5] of the Lagrange-based inverted pendulum are employed as testing platforms, including X, X-Y, and X-Z coordinate-based models separately using single and dual topologies with the trial-and-error approach and increased control efforts to tackle the systems. Dual topologies as two PID controllers [5] are used to test for fruitful action, however despite the use of more controllers, it is discovered that all of the models do not produce a smooth results. The X-inverted pendulum architecture [5] is still the best model among the three for testing any required control schemes, but other designs necessitate the use of additional controllers, which increases the amount of control work required. Later, a variety of control strategies, including LQR (Linear Quadratic Regulator) [17], fuzzy logic control (FLC) [18], and model predictive control (MPC) [19], are proposed for controlling the Newton-Eular 'X' coordinate based pendulum with fewer time domain metrics, such as rise time, settling time, and overshoot.

However, other than the MPC control scheme, LQR and FLC control methods outperformed PID controller in terms of control action. Experts recommended combination schemes [20-22] combining LQR, FLC, and PID control methods to speed up the tracking of the system's angle and position, but generally speaking, none of the strategies used have guaranteed the robustness of the plant. The amplitude level of tracking was reduced by a proposed PI-PD control method [23] in contrast to a PID scheme in a literary work, however the scheme eventually was not found to be very effective because it continued the tracking with some erratic behaviours towards the desired position. Trial and error on time and frequency domain platforms can be applied to tune a PID controller, however many experts advised using optimization algorithms [24-27] to achieve more manageable tuning results. A few optimization strategies have been shown to be effective in producing positive results. All of these traditional methods did, however, produce the system's current steady state or transient behaviors, and one of the drawbacks is the challenge of recovering continuous tracking performance in the face of disturbance. As a result of its constrained gain parameters, PID controller does not offer a very versatile solution. The specialists later discovered a potential solution by including two additional degrees of freedom with the integral (I) and derivative (D) actions [28], respectively. It was agreed that the values of these additional parameters should range between 0 and 1, establishing the term fractional order. In order to provide a promising solution than the conventional approach, it is now essential to choose additional degrees of freedom, and these parameters play a significant role in enhancing the system's performance. Fig. 2.10 depicts the fundamental design [28] along with numerical comparisons between fractional and traditional PID.

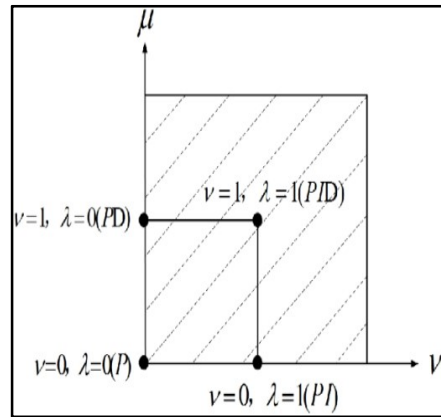


Fig. 2.10. Fractional order PID controller.

Mathematically [28] it is expressed as

$$\begin{cases} PID(s) = k_p + \frac{k_I}{s} + k_D s \\ FOPID(s) = k_p + \frac{k_I}{s^\lambda} + k_D s^\nu \end{cases} \quad (2.103)$$

Now, as s^λ and s^ν are not directly compatible with the MATLAB platform, approximation approaches are needed to make them compatible. The FOMCON toolbox [29-30] was frequently used in literature to realize fractional orders using only Oustaloup rational approximation techniques of irrational orders. Researchers used a variety of optimization techniques to create FOPID controllers for Newton-Euler and Lagrange based models, and in general, these controllers outperformed traditional ones with regard to settling time, overshoot, and integral errors. By employing a FOPID controller, sluggish servo and regulatory outcomes can occasionally be observed in the face of noise and disturbances. The FOMCON toolbox's shortcoming is that there are no alternative approximate methods available to study the behaviour of fractional order functions, leaving a gap in existing theories. Finding other suitable approximation methods that could generate approximations that are comparable to or better than those produced by the Oustaloup technique is therefore necessary.

✧ *Study on Continuous Stirred Tank Reactor*

PID controllers [31] are widely used in chemical reactor processes in addition to mechanical under-actuated systems to regulate molar concentration and reactor temperature. Several academic publications discuss the use of PID controllers [31], 2DOF PID controllers [32], and numerous mixed topologies using the PI-PD scheme [33] or fuzzy logic [34] to monitor the concentration level or temperature of an ideal CSTR process. It has been demonstrated that the goal of using several controllers for a given process is to improve performance with regard to desired settling time, rise time, overshoot, and other integral errors, such as IAE, ISE, or ITAE, respectively. Although fuzzy logic [34] controller applications are shown to be more effective, in a real-world setting fuzzy logic is unable to receive input for the temporary implementation of learning strategy. In contrast to boolean logic, there is no systematic way to solve any kind of problem using fuzzy logic, and none of its notions can be mathematically proven. 2 DOF scheme and PI-PD smith predictor [33] systems performed well with less time domain metrics to find higher performance and stability. Several specialists in the literature approached the tuning method [31-34] of the PID controller using either the time domain and frequency domain or the Ziegler-Nichols method. In CSTR, optimization techniques [35-37] that also worked very well, including mechanically under-actuated processes, assisted in lowering the level of amplitude over the course of the settling process. However, given that noise and disturbances have an impact on the aforementioned control schemes, it is necessary to further study how chemical reactants behave under these circumstances. Using conventional schemes, it was sometimes discovered that performance was disrupted by noise and other disturbances.

As a result, experts later switched to the most recent PID controller, which has two additional degrees of freedom [28] and is shown in 2.103 with Fig. 2.10, and which has proven to be much more effective at detecting performance disruption than traditional PID as documented in numerous academic publications. Several specialists contacted the FOMCON toolkit [29] to realize s^λ and s^ν the same mechanical under-actuated technique for CSTR with the support of the platform's exclusive Outstalaoup technology. In various books, experts explored various strategies such as trial-and-error or optimization algorithms [38-40], however, it was discovered that the obvious optimization method was more approachable to testing the performance. In CSTR as well, investigation into alternative suitable approximation techniques is required for better examination in order to find more adaptable solutions in challenging situations. This is because occasionally it was discovered that, despite offering better outcome than conventional PID controller, there were still some issues with measuring the performance indicators under the influence of disturbances.

2.4.2 MRAC (Model Reference Adaptive Control)

PID or FOPID controllers are not very good at handling noise, as was stated in earlier Section 2.4.1, and they exhibited several slow tendencies. Although the FOPID controller made several attempts to resolve the issue, the existing solution has not produced the needed accuracy. So, in contrast to PID controllers or FOPID controllers, the MRAC (Model reference adaptive control) control technique [41] is afterwards recommended by several specialists. The primary way that an adaptive controller adjusts is to changes in the dynamics of the process, which can occur for a variety of reasons. For instance, the environment may change and cause disruption, or in certain circumstances, variation may simply result from system uncertainty or dynamics that are not considered by the specific model. So, the controller should be configured in such a way to handle these variances. A robust controller is one approach to doing this, as it is designed with enough stability and performance margin to function effectively across the entire range of anticipated fluctuations.

In MRAC [41], the total control action is based on a reference model that determines the future behaviour of the current system and uses an adaptive gain mechanism to reduce the error signal between the ideal model and the current plant. For stable systems, MRAC controllers were very successful; however it is difficult to successfully tackle an unstable system when there are disturbances. In their literature, professionals demonstrated proper reference model selection and adaptive gain for reaching that goal. The choice of the reference model and the adaptive gain are crucial in MRAC.

Though the MPC (Model Predictive Control) scheme [42] is widely used in numerous research fields, it is primarily used in chemical reactors where the dynamics of the system are slow. Using the MPC controller has many drawbacks, including the fact that it uses a lot more computational resources and a relatively perfect model than MRAC. MPC [42] is merely an optimization-based control that relies on the right solver. Fig.2.11 shows the fundamental block diagram of the MPC approach.

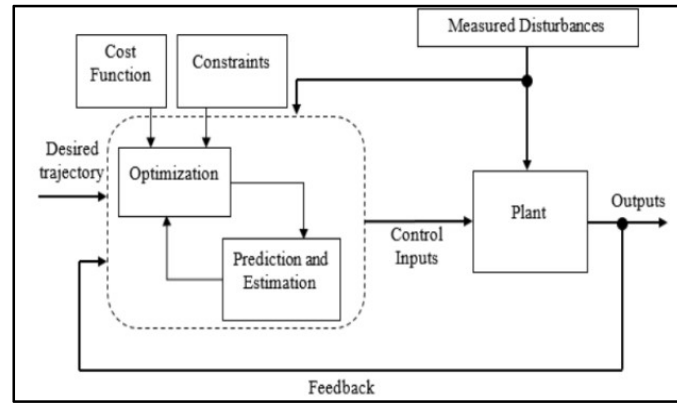


Fig. 2.11. MPC schematic representation.

The primary advantage of MRAC over MPC [43] is that it guarantees stability with less processing power while deviating from the nominal system. It can be categorized into direct and indirect forms [43], although direct MRAC only requires the estimation of controller parameters and does not require the calculation of plant parameters, whereas the computed parameters' convergence to the actual unknown values is necessary for indirect MRAC. For the most part, direct MRAC controllers are used in unstable process applications. In Fig. 2.12, the fundamental schematic diagram of indirect MRAC [43] is displayed.

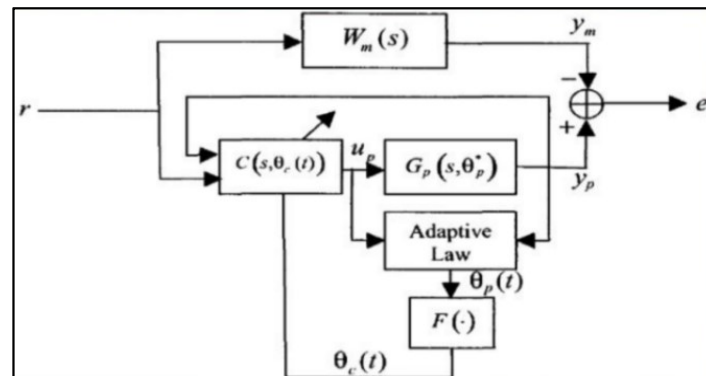


Fig. 2.12. Indirect MRAC scheme.

According to Fig. 2.12, the indirect MRAC adaptive control strategy results from using θ_p^* the certainty equivalence technique [43], where the estimated values of the unknown parameters are used in their place. Parameterizing the plant transfer function's parameters according to the intended controller parameter vector θ_c^* is another method [43] of designing MRAC schemes. The framework of the law is described in [43] as

$$\begin{cases} \theta_p^* = F^{-1}(\theta_c^*) \\ G_p(s, \theta_p^*) = G_p(s, F^{-1}(\theta_c^*)) = G_p(s, \theta_c^*) \end{cases} \quad (2.104)$$

The system is known as direct MRAC in this instance, since the controller variable $\theta_c(t)$ is modified directly without the need for any intermediary estimation, as seen in Fig. 2.13.

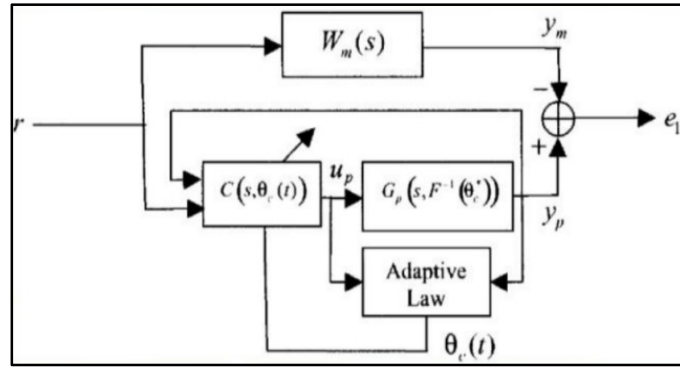


Fig. 2.13. Direct MRAC scheme.

While adaptation is employed to modify the variables in the control design, the controller is parameterized and offers tracking. There are two methods [43] for adjusting the system parameters: the gradient approach, sometimes known as the MIT (Massachusetts Institute of Technology) rule, and the Lyapunov stability theory. Since the MIT rule does not always guarantee stability [44], the Lyapunov direct rule is typically preferred. However, the Lyapunov rule can only produce a steady result if the proper Lyapunov function is chosen; otherwise, the tracking may be off. To approach Lyapunov stability rule some important rules [45] are followed as

Theorem 1.

- a. Derivative along the dynamical system trajectories is examined by generating a scalar energy like function.
- b. It is possible to draw conclusions regarding the stability of the system if the derivative of the Lyapunov function is not positive.

Theorem 2.

A constant scalar field Positive definite functions $P(x)$ are said to as locally or globally if

$$\begin{cases} P(0) = 0 \wedge (\forall x \neq 0 \wedge \|x\| < R) \Rightarrow P(x) > 0 \leftrightarrow \text{Local} \\ P(0) = 0 \wedge (\forall x \neq 0) \Rightarrow P(x) > 0 \leftrightarrow \text{Global} \end{cases} \quad (2.105)$$

Theorem 3.

$P(x)$ is considered the Lyapunov function for the system if it is a positive definite function with continuous partial derivatives and a negative semi-definite time derivative along any state trajectory of the system $\dot{x} = f(x)$, meaning that $\dot{P}(x) \leq 0$. The following is the Lyapunov function's time derivative.

$$\dot{P}(x) = \nabla P(x)f(x) \leq 0, \nabla P(x) = \left(\frac{dP(x)}{dx_1} \dots \frac{dP(x)}{dx_n} \right) \in R^n \quad (2.106)$$

✧ **Study on Inverted Pendulum**

When choosing a reference model, experts approach adaptive gain at random after finding a suitable solution [46] that meets the requirements of the current process, such as rise time, settling time, and overshoot, in the literature. In the literature, the MIT and Lyapunov rules are both tested on linearized versions of nonlinear systems considering different parameters in (2.47). In addition to single topologies, mixed topologies utilizing PID or FOPID controllers [53] are also used to test the performance of both of the rules. It is determined that the MRAC-MIT single rule [46] method is ineffective for balancing the pendulum with a single adaptive gain and is unable to tackle the system. The basic scheme of direct MRAC controller [46] is proposed as illustrated in Fig. 2.14.

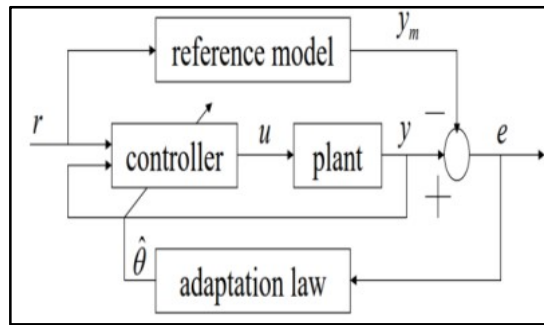


Fig. 2.14. Direct MRAC based on MIT & Lyapunov schemes.

Mathematically, the general MIT rule of MRAC controller [46] from Fig. 2.14 is represented as

$$\begin{cases} \frac{d\hat{\theta}}{dt} = -\gamma e y_m, \\ e = y - y_m \end{cases} \quad (2.107)$$

By selecting the proper Lyapunov function [46], the Lyapunov rule was able to resolve the problem of identifying some potential outcomes, but finding the right adaptive gain in the literature proved to be extremely challenging. Hence, experts tested the various control actions with various adaptive gains and found that performance could occasionally be either slow or fast with high or low peak overshoot. Lyapunov rule outperformed the PID system with a single adaptive gain while requiring less control effort, however adaptive gain adjustment plays a significant part in achieving desired performance. Therefore, it was suggested in Fig. 2.14 that the MRAC's modified structure [47] be used with both PID and FOPID controllers to increase tracking. The modified structure [47] is represented in Fig. 2.15.

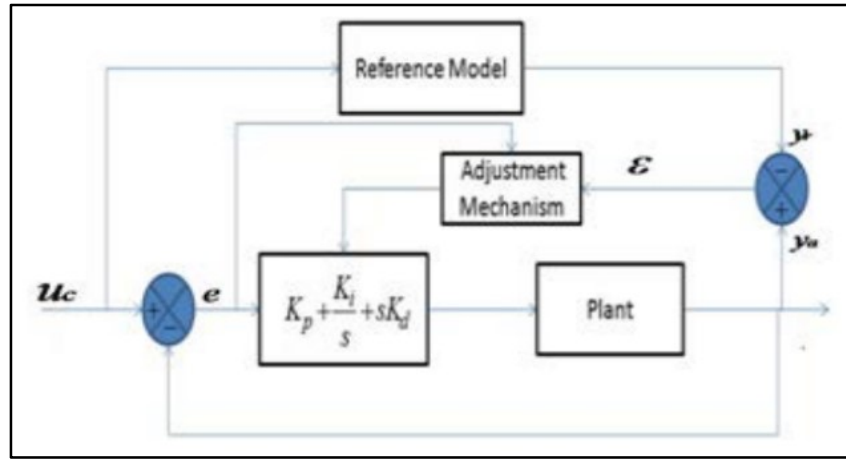


Fig. 2.15. Modified MRAC scheme.

The benefit of the combination approach is that performance may be better shaped by using more gain factors, although design complexity may rise. It also poses the significant issue of equally calculating all gain parameters within acceptable ranges. Whilst adopting the aforementioned structure with the aid of PID parameters [47] did not increase transient performance, FOPID controllers with two more gain parameters [48] were added to the same structure. There is also the option to choose a fractional order reference model [48]. Specialists have mostly concentrated [48] on the fractional order parameter adjustment rule for integer order plants. If so, it would also be necessary to apply fractional orders to current plants, which is not typically advised to avoid complexity and longer design computation times. Therefore, in the modified structure, even though the MRAC-FOPID scheme [48] tracked the pendulum's movement considerably better than the MRAC-PID scheme with a high adaptive gain value, there was still some tracking uncertainty, and as the adaptive gains were increased, the results became noisier as well. As a result, another modified MRAC structure with a PID controller [49] only was recommended in Fig. 2.16 as the single adaptive gain of MRAC in Fig. 2.15 is not found to be as much as capable of handling disturbances.

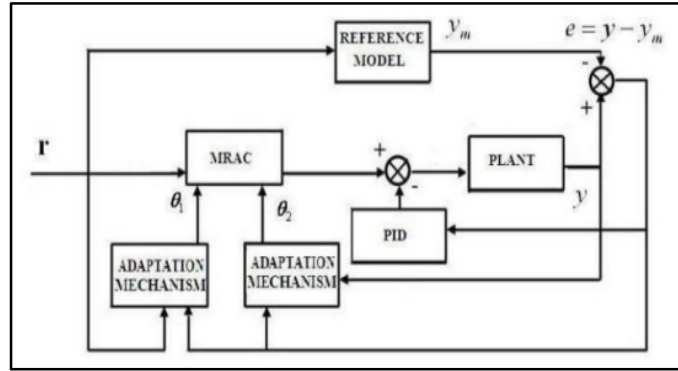


Fig. 2.16. Modified MRAC scheme with two adaptive gains.

According to MIT and Lyapunov rules, the aforementioned structure was shown to be more effective [49] in a stability setting. Both the single MIT rule and the MIT-PID rule [49] demonstrated smooth operation with two adaptive gains using this arrangement. Comparatively to single topology, combination rule showed faster control action. In addition, a single Lyapunov rule followed by combination logic enhances control action. Yet, there are situations where MIT-PID combination logic is discovered to be a faster control action than Lyapunov-PID logic, though Lyapunov PID successfully tracks disturbances with little peak overshoot [49]. Hence, total MRAC rules demonstrate robustness, but a single PID or FOPID scheme failed to provide the necessary goals for balancing the pendulum towards an upright position. As an alternative to certain works' use of random picks, a few optimization algorithms were also proposed to fine-tune PID settings, and it is clear that tracking has improved. The conventional MIT or Lyapunov rule itself, however, may be further modified by fractional order calculus to investigate improved tracking with less time domain metrics or error metrics than existing techniques, which is not found in any literature. These approaches should be counted as an absolute necessity for testing robust and flexible control actions on both nominal and perturbed models of the inverted pendulum with noise and disturbance. Another strategy might be to combine optimization techniques with random selection to determine the most acceptable adaptive gains for both MRAC scheme rules that can speed up computation. An innovative research for the smooth tracking of the angle and position of the system towards the target position can also be led by the approach of various augmented control methods based on fractional calculus.

✧ *Study on Continuous Stirred Tank Reactor*

Similar to the mechanical under-actuated process, after finding a solution that satisfies the criteria of the current process, such as rise time, settling time, and overshoot, in the literature, experts [50] approach adaptive gain at random when selecting a reference model.

The MIT and Lyapunov rules [51] are both investigated in the literature on linearized versions of nonlinear systems taking into account various specifications depending on chosen ranges of operating points in (2.84), (2.85) and (2.94). In a few selected publications [50-51], various stable transfer functions of the nonlinear CSTR model are used primarily dependent on chosen operating points. Model predictive controllers (MPCs) [52] were widely employed with single topology, fuzzy logic [53], and some analytical based methods to control process variables in chemical reactors, as was mentioned in the previous part. The MPC schemes [52] performed well when used with PID controllers, but occasionally showed inconsistent performance metrics when used with various CSTR models. So, these problems may be the result of this technique's limits, which were already addressed in the previous section. In order to demonstrate some acceptable control attempts with MIT as well as Lyapunov stability rules, MRAC (model reference adaptive control) technique became more popular than MPC scheme in the use of CSTR. It has been discovered through a small number of studies [50-51] that lower adaptive gain ranges that approximate the modified structure [54] depicted in Fig. 2.17 effectively handle temperature or concentration.

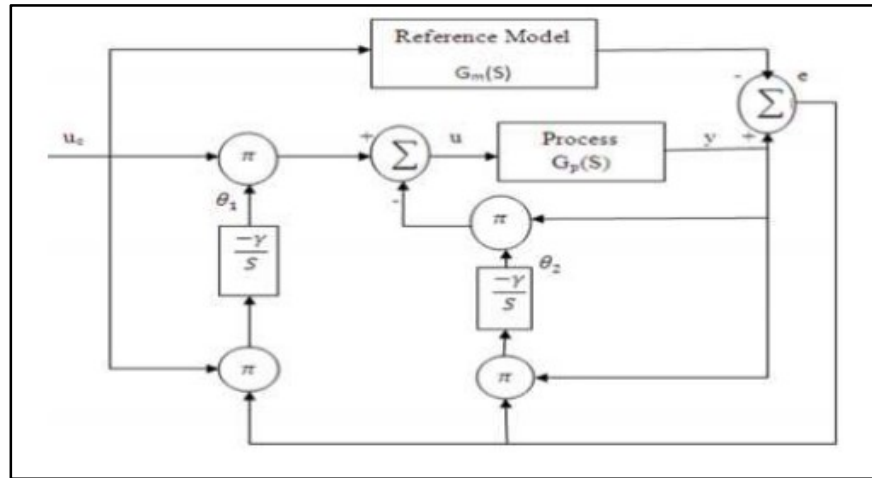


Fig. 2.17. Modified Lyapunov based MRAC scheme on CSTR.

The accuracy of ISE, IAE, or ITAE was occasionally found to be enhanced by gradually increasing adaptive gain beyond 20, but consistency on peak overshoot was not always found. Both MIT and PID controller were outperformed by the Lyapunov rule [54]. Unlike PID controllers, which are absolutely necessary for this purpose, Lyapunov rule demonstrated effective action on controlling temperature or concentration with a larger consistency level under the influence of disturbance and noise outside. Determining the proper Lyapunov function [54] for the specific process that plays a significant influence in performance is the most crucial task.

Yet, even changing feed concentration or temperature, which can also result in a robust analysis, there is no explanation found for the nominal CSTR process's disrupted model. The effectiveness of the rules must be supported by evidence regarding the impact of various parametric conditions present in the system but not considered by experts. The investigation should adopt non-integer order values at random between 0 and 1 in addition to the conventional or integer order based MRAC adjustment mechanism as shown in (2.104) so that, while keeping adaptive gain fixed, some better variations based solely on non-integer order values may be observed. Non-integer orders can only produce a result that is clear when analyzing system performance. This is how process variable behavior can be more adaptable and satisfyingly represented based on time domain or error metrics without needlessly increasing or decreasing adaptive gains. This technique can also assist in determining the efficacy level between integer order and non-integer order rule. Testing the stability of adjustment mechanisms with a lowering order of less than 1 while tracking the intended position while subject to noise and disturbance is another important challenge. The investigation of more rapid control action requires more than just the single non-integer order based MRAC rules approach. Another difficult task is choosing the best adaptive gain and non-integer order to prevent random selections and find a lower control effort to deal with unknown parameters during the process.

2.4.3 IMC (Internal Model Control)

Due to their sluggish performances, PID controllers were determined to be an inappropriate solution [55] for integrating processes and processes with significant dead time. Additionally, it cannot include a gradual disruption or a ramp-type set point change. As a result, in addition to PID and MRAC controllers, the additional control efficacy of IMC controllers is also examined in certain publications. IMC controllers [56] are sometimes referred to as model-based controllers since they can be approached directly or indirectly and do not require constant sample instants like PID methods. The control action is generated based on the actual quantitative relationship between the variables and is one sort of proactive controller. Currently, a small number of specialists use internal model control (IMC) tuning relationships to modify the PID controller's parameters. This technique assisted in designing the responses for input tracking and noise elimination. An IMC-based PID controller [56] might quickly correct some model imperfections, whereas a traditional PID technique could not. Fig. 2.18 shows the block diagrams for IMC [56], respectively.

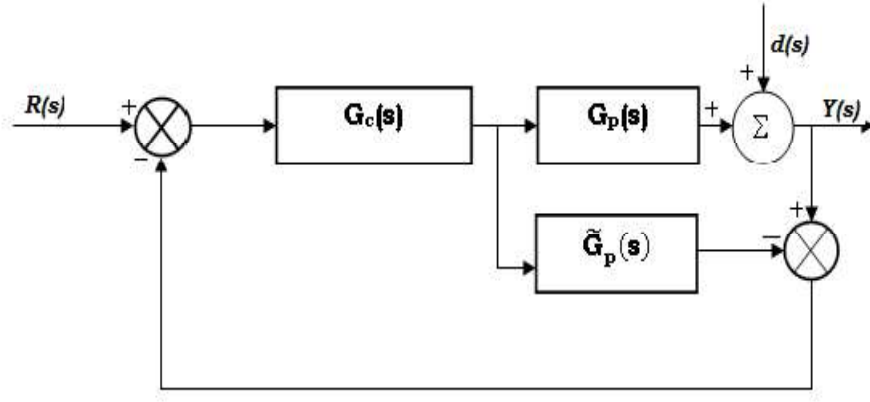


Fig. 2.18. IMC scheme.

The typical feedback structure permits the process model implicitly, allowing for the adjustment of PID tuning parameters on a model, but it does not explicitly state how the model influences the tuning choice. Now to construct the internal model control [56] as shown in the above Fig.2.18 (b), it may be assumed that the system can be demonstrated by the following dynamical model:

$$G_p(s) = \widetilde{G}_p(s)MV = \widetilde{K}_p \widetilde{G}_{dyn} MV \quad (2.108)$$

Now, associated static model can be proposed as follows

$$G_p(s) = \widetilde{K}_p MV \quad (2.109)$$

A few stages are used in certain literary works to illustrate the core concept of building an IMC controller for processes including an inverted pendulum and continuous stirred tank reactors. The steps [56] are discussed as follows

✧ *Static Optimization*

If input is considered as $MV = \frac{\text{Set point (SP)}}{\widetilde{K}_p}$ then process output (PV) will eventually reach $PV = SP$, after all dynamical effects are disappeared. It is assumed as the model gain is exact, i.e. $K_p = \widetilde{K}_p$.

A shortcoming is found, as if the model gain is not exact, $PV \neq SP$ and there is no way to influence the response, i.e, there is no feedback.

✧ **Model Error Update**

If the static model of the process is extended, then it is expressed as follows

$$G_p(s) = \widetilde{K}_p MV + \varepsilon \quad (2.110)$$

It needs to be implemented for steady state response $MV = \frac{\text{Set point (SP)} - \varepsilon}{\widetilde{K}_p}$

ε is obtained from a dynamical model of the process with the following expression:

$$\varepsilon = PV - \widetilde{K}_p \widetilde{G}_{dyn} MV \quad (2.111)$$

✧ **Boosting**

In the ideal case, i.e. model is exact, the manipulated value MV changes as a step. To accelerate the response, it suffices to introduce a well chosen boosting lead-lag filter in the control loop and it is known as dynamic optimization.

✧ **Final version of the law**

Dynamic optimization can be performed by imposing that $G_p(s) = SP$, i.e.

$$MV = \widetilde{G}_p^{-1}(SP - \varepsilon) \quad (2.112)$$

Using \widetilde{G}_p^{-1} is not always possible as the process might have a delay or might lead to unstable pole zero cancellations. \widetilde{G}_p^{-1} can be replaced by an approximate inverse G_{p-inv} . The filter (F) in design is approached for robustness. From the above Fig. 3.8 (b) the process transfer function's positive portion serves as the direct basis for the controller $G_c(s)$. Based on the above steps with different assumptions, the closed loop time constant, also known as the filter time constant, is the single tuning parameter that is often obtained from the IMC formulation. Now, from IMC topology, the process model can be divided into two components, as follows

$$\widetilde{G}_p = \widetilde{G}_{p+} \widetilde{G}_{p-} \quad (2.113)$$

Now, the overall transfer function using feedback control and internal model control is formulated [56] as follows:

$$\frac{Y(s)}{Y_{sp}(s)} = \frac{G_c G}{1 + G_c G} \quad (2.114)$$

$$\frac{Y(s)}{Y_{sp}(s)} = \frac{G_c G_p}{1 + G_c (G_p - \widetilde{G}_p)} \quad (2.115)$$

Under a best case scenario, the actual process and model are set to equal to find out how to make a standard controller act like an IMC controller. Now, filter is incorporated with the following expression as

$$G_c = \frac{1}{G_{p-}} F = \frac{1}{G_{p-}} \frac{1}{(\tau_c s + 1)^r} \quad (2.116)$$

Now, the final expression is approached as

$$\frac{Y(s)}{Y_{sp}(s)} = \widetilde{G_{p+}} \frac{1}{(\tau_c s + 1)^r} \quad (2.117)$$

According to the internal model concept, if the feedback path is modified to appropriately resemble the disturbance signal, a feedback regulator may be able to restore stability and regulation in the face of external disruptions, which is evident from the discussion above. This principle is the foundation of the IMC philosophy. Due to its ease of use, IMC has been widely used by the industry for PID tuning. Robustness [56] is crucial in PID design for any model-based PID tuning technique, such as IMC, due to model mismatch. Based on the IMC-PID technique, some useful case studies for the stability context on the inverted pendulum and continuously stirred tank reactor have been found.

✧ *Study on Inverted Pendulum*

IMC based PID controllers outperformed conventional PID or fractional order PID controllers by rejecting disturbances more quickly and tracking the set point more accurately under no-mismatch conditions between plant and model, according to a few previous studies [57-59] that reported on filtering technique using both integer and fractional orders in IMC controllers. Although theoretically, this technique can be demonstrated to be effective in a context of stability, in a practical setting it is very challenging to identify an internal model that is perfectly matched with the main process due to a variety of external uncertainties. In this situation, it is also challenging to reject disturbances smoothly, unlike in a no-mismatch condition. No successful control strategy for this situation has been documented in the literature, and despite utilizing first, second, or fractional filters in the controller, servo-regulatory behaviour occasionally turns slow with excessive overshoot. Still, no research on an IMC-based FOPID controller using a fractional filter approach has been disclosed. The IMC controller, in contrast to the MRAC rule, displayed sluggish control action in a practical mismatch situation, and it was determined that this made it unsuitable for further testing on an inverted pendulum.

✧ *Study on Continuous Stirred Tank Reactor*

The IMC controller is discovered as an approachable solution for dealing with concentration or temperature under the influence of noise or disturbance in chemical reactor. With the aid of IMC method, tuned parameters of PID controller also led to robust action with respect to lesser error metrics such as IAE, ISE or ITAE over conventional PID controller under linear or nonlinear version of CSTR model.

Experts [60-62] recommended integer or fractional filters in this application as well in order to eliminate the disturbance, although fractional filters [62] mainly aided in accelerating the smooth control action. To achieve smooth action, choosing the time constant and filter order is crucial, however, most of the time, random selection is found in the literature. For further investigating the performance, an approach of optimal algorithm to tune the best values of those parameters is necessary. IMC-PID performed well on platforms in both the time and frequency domains [59]. IMC-PID demonstrated an exceptional solution with larger gain or phase margins than Z-N or MIGO frequency-based design tuning in the frequency domain as well as lower error metrics like IAE, ISE, or ITAE than direct synthesis based PID or conventional PID controllers [63]. However, sometimes the best traditional PID controller [64] outperforms the IMC-PID technique with faster control action and reduced overshoot. Consequently, selecting the right filter settings is a crucial effort. The IMC-FOPID controller, which can also play a significant role with more parameter settings, has not yet been studied. Furthermore, to improve stability action compared to conventional methods, further research is required into an augmented strategy utilizing fractional order-based MRAC and IMC procedures.

In a few studies, the efficacy of control action is also examined without resorting to the linearized version. However, some controllers, in those circumstances, took occasionally tardy action to deal with the uncertainties. Backstepping controllers are a new type of emerging control system that is suggested in order to address uncertainties caused by the existence of nonlinear variables in the process.

2.4.4 Backstepping Controller

Backstepping [65] is useful for lower triangular strict-feedback systems. Backstepping is a recursive design technique that can be used to methodically address Lyapunov-based controller design. In general, the strict-feedback system is implemented as

$$\begin{cases} \dot{\vartheta}_1 = f_1(\vartheta_1) + \sigma_1(\vartheta_1)\vartheta_2 \\ \dot{\vartheta}_2 = f_2(\vartheta_1, \vartheta_2) + \sigma_2(\vartheta_1, \vartheta_2)\vartheta_3 \\ \vdots \\ \dot{\vartheta}_r = f_r(\vartheta_1, \vartheta_2, \dots, \vartheta_r) + \sigma_r(\vartheta_1, \vartheta_2, \dots, \vartheta_r)v \end{cases} \quad (2.118)$$

In the majority of situations, a conventional feedback linearization strategy results in the cancellation [65] of helpful nonlinearities. Since the resulting input-output dynamics are not required to be linear, the backstepping architecture [65] demonstrates greater flexibility than feedback linearization. It is possible to prevent the cancellation of potentially valuable nonlinearities, leading to fewer complex controllers.

The primary idea is to create intermediate control rules based on the dynamics of each state by using few state factors from (2.118) as "virtual controls" or "pseudo controls." In the backstepping design [65], the system as a whole is given a Lyapunov function through a recursive process. A state feedback control rule can be designed employing two different types of backstepping procedures, such as integrating and recursive methods. The backstepping design's salient characteristics and potentials, however, are better understood through the recursive method. Several control methods have been suggested in recent years to stabilize, regulate, and control both linear and nonlinear dynamical systems. It is simple to locate a control function in Lyapunov sense for stability and optimization issues in linear autonomous systems. For nonlinear control systems, however, determining a good Lyapunov function is a difficult task. The backstepping control approach is a recursive design process that ensures global asymptotic stability of stringent feedback systems by connecting the selection of a feedback device that uses a control Lyapunov function. A useful tool to get around the drawbacks of the method to feedback linearization in the control field is the active or linear backstepping control method [66]. One generic backstepping control technique that has been found to be more applicable in the control literature is the block backstepping control method [66]. An alternative backstepping control technique, the adaptive backstepping control method [66] employs estimations for the systems' unidentified parameters. An efficient backstepping method for control systems with uncertainty is the robust backstepping control method [66].

✧ *Study on Inverted Pendulum*

Backstepping controllers are currently recognized as a new tool for the use of underactuated processes, and research into various backstepping techniques is still ongoing. A few experts recommended using the inverted pendulum's adaptive backstepping law [67-69] to address the system's angle and position given a variety of initial positions. According to some comparative studies, backstepping outperformed the combined backstepping-sliding mode technique [67], model free backstepping rule [68], conventional sliding mode technique [69], and LQR method [67]. These studies were conducted to explore the efficacy of backstepping control. The model free backstepping method [68] estimates the unknown dynamics by using a normal form of the system model.

However, using fractional order calculus on a backstepping controller would give the new controller design concept a boost in popularity. There is no reported work so far on combining the fractional order with backstepping approach.

To demonstrate more robust control efficacy, investigation with fractional order on various backstepping methods, such as linear backstepping followed by adaptive or block backstepping methods, is worth-challenging task.

✧ *Study on Continuous Stirred Tank Reactor*

However, more recently, the backstepping method has been found to be a more fruitful solution for developing more practicable and approachable results with nonlinear effects. Previous literature demonstrated many successful results with various effective control actions for controlling temperature or concentration under many circumstances. The backstepping strategy was used in some contributions [70-73] on a CSTR process, and the outcomes were satisfactory despite the nonlinear effects. With adaptive backstepping method, applications of sliding mode controller [71] and fuzzy logic controller [73] are also reported. In literature adaptive backstepping method [72] was chosen over linear approach envisaging robust action in handling uncertainties. As a result, Figs. (2.19-2.22) depict some of the augmented backstepping systems reported [69, 71-73] in the aforementioned surveys. To demonstrate more robust control efficacy, it is also a worthwhile challenge to investigate fractional order on alternative backstepping methods, such as linear backstepping approach. No applications with fractional orders are still reported on backstepping control of CSTR. The fractional order backstepping approach might be considered a more demanding method in nonlinear processes due to its significant impact over other laws.

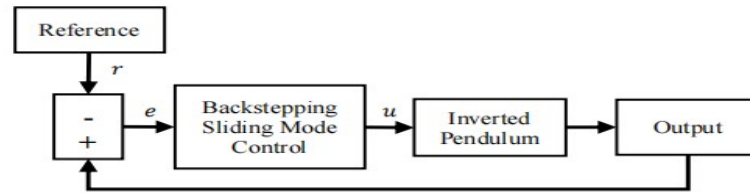


Fig. 2.19. Backstepping-sliding mode scheme.

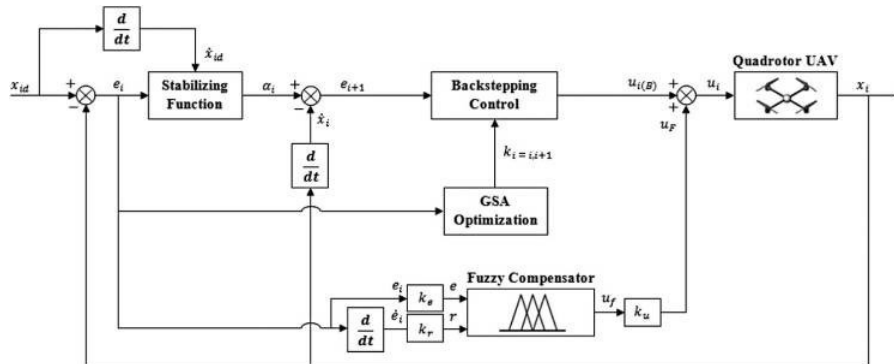


Fig. 2.20. Augmented fuzzy-backstepping scheme.

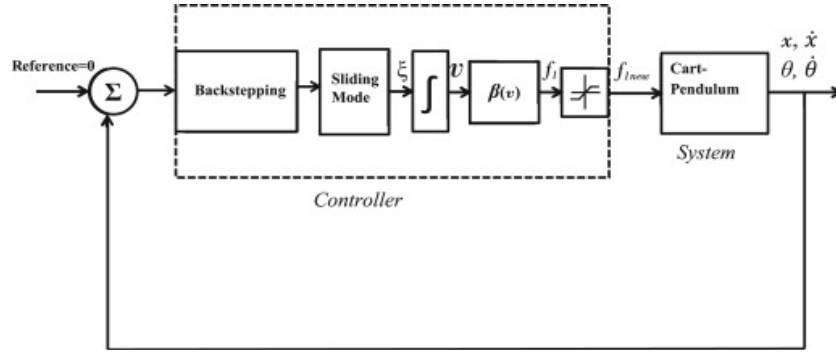


Fig. 2.21. Adaptive fuzzy based backstepping scheme.

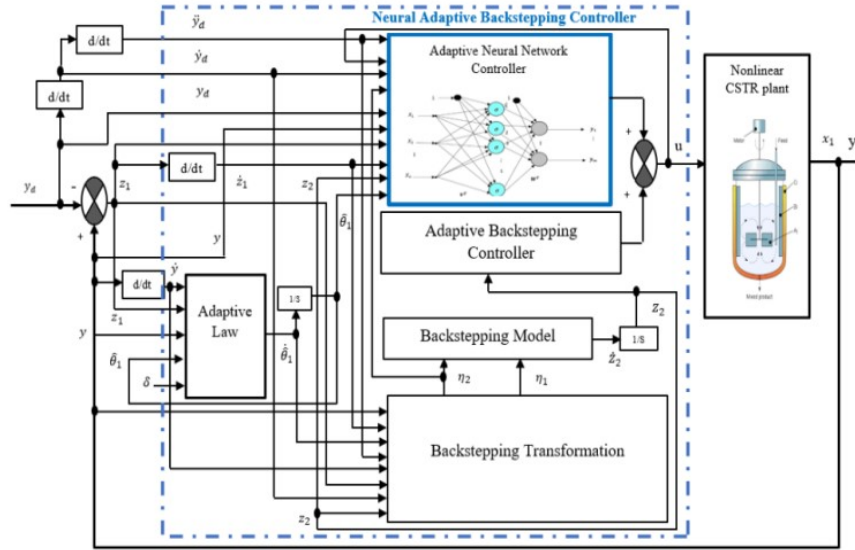


Fig. 2.22. Adaptive fuzzy based backstepping scheme on CSTR.

Although the augmented backstepping schemes outlined above provided a robust solution of managing nonlinear systems, they require a fairly sophisticated control algorithm to accomplish.

Therefore, it is vital to investigate the performance of nonlinear systems utilizing straightforward control backstepping techniques, which may be more effective than enhanced approaches. So that the important effects of a specific backstepping controller might be investigated. In this thesis, an effort has been made to design a straightforward standalone conventional backstepping rule. A brand-new fractional order backstepping rule is then reported to provide more detailed information than the traditional method, as there hasn't been

any work done on such a rule before. From the above discussions, a review of different controllers is summarized in Table 2.1.

Table 2.1
Review on different control strategies for CSTR and Inverted pendulum processes

| Controller | Merits | Drawbacks |
|-------------------------|--|--|
| Conventional PID | Provides the option to adjust the gains for optimal transient behaviour, particularly for well-behaving plants and suited for tracking issues. | It can be challenging to tune for unstable systems and is frequently not resilient in terms of parameter uncertainties. Cannot manage several inputs and outputs at once; cannot handle restrictions, noise, or disturbance. |
| LQR | Sensitive to plant models; better follows a reference trajectory. | Occasionally fails to eliminate steady-state error. |
| Fuzzy | Offers a practical solution to a difficult, ill-defined, and uncertain model; no accurate model is necessary. | Tuning parameters takes longer; There is an approximation error; There is a nonlinear function that is uncertain. |
| PID-LQR | Analytically effective and quick. | Occasionally fails to offer the ideal solution for a specific output's transient. |
| Fuzzy-PID | The capacity for self-tuning and live adaptation to uncertain, nonlinear, and time-varying systems. With a lot of appealing features, it offers a promising alternative for industrial uses. | Control rule and system analysis are challenging to create; They are not founded on a mathematical model and are frequently used to handle problems in ambiguous and uncertain environments with high nonlinearities. |
| PI-PD | Servo and regulatory measurements are better able to manage transient and steady state behaviours. | Offers occasionally sluggish movement amid disturbances. |
| MPC | It can manage numerous inputs and outputs at once, handle constraints at the input and output, and overcome noise and disturbances. It also predicts how the states will behave in the future. | Extremely sluggish tracking. |
| Optimal PID | Calculating tuning parameters is easy and quick; reliable solution; Improved set-point tracking | A challenge to select suitable methods; Different methods can speed up convergence at various rates; Boost precision depending on convergence rate. |
| FOPID | More degrees of freedom; improved speed of action. | Using the FOMCON toolkit does not guarantee the proper implementation of additional degrees of freedom; less efficient in handling noise. |
| Optimal FOPID | Offers a reliable and adaptable option. | A limited number of fractional order approximation techniques in the FOMCON toolkit; still lack of improvement on overshoot and integral errors. |
| Smith-predictor | Well-known and most commonly used dead-time compensation method; Better control over transient and steady-state conditions. | Still lack of robust disturbance rejection. |
| MRAC-MIT | Mechanism for managing adjustments automatically in uncertain situations. | No assurance of consistency. |

| | | |
|----------------------------------|---|---|
| MIT-PID | Improvement in stability with less control exertion. | No assurance of consistency in success metrics in a chaotic environment. |
| MRAC-Lyapunov | Greater regularity; global stability. | No established procedure for selecting the Lyapunov function; still higher overshoot. |
| Lyapunov-PID | Reduced control effort with regard to error metrics and temporal domain metrics; More stable and reliable action. | Offers occasionally sluggish action and still higher overshoot. |
| IO-filter based IMC-PID | Excellent set point monitoring. | Sometimes a lengthy settling period; Poor response to disturbances. |
| FO-filter based IMC-PID | Better noise rejection and good set point detection. | Random filter parameter selection; Occasionally sluggish set point monitoring; still no improvement on overshoot. |
| DS-PID | Intuitive strategy; Quick method to get a good outcome compared to PID. | Time-consuming and sluggish action with long-term response. |
| Conventional Backstepping | Increased capacity to handle nonlinear effects with linear, adaptive, or block methods; Simple Lyapunov function choosing for global stability; robust results. | Complex tuning scheme; Lack of detailed case studies in presence of noise, disturbance, and model uncertainties. |

2.5 Summary

The mathematical modeling of two benchmark unstable processes—the continuous stirred tank reactor systems (temperature and molar concentration) and the inverted pendulum (position and angle)—is covered in detail in this chapter. In order to clearly illustrate the influence of all initial conditions on the system's dynamic behavior, the transfer functions of the systems are also made simpler using the state space idea. Also covered in detail along with the necessary requirements is linearization of the models for both of the systems. Comparing the need for a certain 'X' type inverted pendulum system to others, is also reported. Comparing continuous stirred tank reactors to other reactors, a substantial use of this technology is also reported. Based on a comparison of control attempts made by several existing control schemes for the application of both of the aforementioned systems, a thorough analysis is given. The need for a fractional order controller is examined while examining the effectiveness of the currently used conventional control techniques, providing a sound justification for updating the laws.

References

- [1] C. Chandrasekara and A. Davari, "Inverted pendulum: an experiment for control laboratory," *Thirty-Sixth Southeastern Symposium on System Theory, 2004. Proceedings of the*, Atlanta, GA, USA, 2004, pp. 570-573.

- [2] K. Furuta and M. Iwase, "Swing-up time analysis of pendulum", *Bull. Polish Acad. Sci. Tech.* vol. 52, no. 3, pp. 153-163, 2004.
- [3] S. Engell and K.-U. Klatt, *Benchmark Problem: Continuous Stirred Tank Reactor with Consecutive and Parallel Reaction*, 1992.
- [4] B. Srinivasan, P. Huguenin, D. Bonvin, "Global stabilization of an inverted pendulum—Control strategy and experimental verification", *Automatica*, vol. 45, no.1, 2009, pp. 265-269.
- [5] Jia-Jun Wang, "Simulation studies of inverted pendulum based on PID controllers", *Simulation Modelling Practice and Theory*, vol. 19, no. 1, 2011, pp. 440-449.
- [6] E. Aranda-Escolástico, M. Guinaldo, F. Gordillo and S. Dormido, "A novel approach to periodic event-triggered control: design and application to the inverted pendulum", *ISA Trans.*, vol. 65, pp. 327-338, 2016.
- [7] M. Olivares and P. Albertos, "On the linear control of underactuated systems: The flywheel inverted pendulum," *2013 10th IEEE International Conference on Control and Automation (ICCA)*, Hangzhou, China, 2013, pp. 27-32.
- [8] Z. Prokopová and R. Prokop, "Modelling and simulation of chemical industrial reactors", *ECMS*, pp. 378-383, 2009.
- [9] H. Mihai, G. Bill and K. Sava, "Advanced control of batch reactor temperature", *American Control Conference 2002. Proceedings of the 2002*, pp. 1156-1161, 2002
- [10] S. Ben Mohamed, T. Bakir, B. Boussaid and M. N. Abdelkrim, "Dynamic modeling and simulation of an industrial chemical reactor," *2017 25th Mediterranean Conference on Control and Automation (MED)*, Valletta, Malta, 2017, pp. 755-760.
- [11] H. Wafik, "Batch processes monitoring based on statistical and engineering process control integration: case of alkyd polymerisation reactor", *International Journal of Automation and Control*, vol. 6, no. 3–4, pp. 291-309, 2012.
- [12] G. Botla, V. Kumar and R. K. Yamuna, "Modeling of batch processes using explicitly time-dependent artificial neural networks", *Neural Networks and Learning Systems IEEE Transactions on*, vol. 25, no. 5, pp. 970-979, 2014.

- [13] Luyben, W.L. (2007). Steady-State Design of CSTR Systems. In Chemical Reactor Design and Control, W.L. Luyben (Ed.).
- [14] P. Sanposh, W. Leenanithikul, S. Phoojaruenchanachai, P. Srinophakun, T. Srinophakun and C. Panjapornpon, "Feedback linearization controller design for continuous stirred-tank reactor (CSTR) in biodiesel production process," *2008 5th International Conference on Electrical Engineering/Electronics, Computer, Telecommunications and Information Technology*, Krabi, Thailand, 2008, pp. 613-616.
- [15] Kiam Heong Ang, G. Chong and Yun Li, "PID control system analysis, design, and technology," in *IEEE Transactions on Control Systems Technology*, vol. 13, no. 4, pp.559-576, July 2005.
- [16] K. J. Åström (Åstrom) and T. Hägglund (Hagglund), "The future of PID control", *Control Eng. Pract.*, vol. 9, no. 11, pp. 1163-1175, 2001.
- [17] Jinghu Xing, Workers Chen and Ming Jiang, "linear The study of inverted pendulum optimal control system based on LQR", *Industrial Instrumentation and Automation*, vol. 6, 2007.
- [18] J Yi and N Yubazaki, "Stabilization Fuzzy Control of Inverted Pendulum Systems", *Artificial Intelligence in Engineering*, vol. 14, pp. 153-163, 2000.
- [19] P. Bakaráč, M. Klaučo and M. Fikar, "Comparison of inverted pendulum stabilization with PID, LQR, and MPC control," *2018 Cybernetics & Informatics (K&I)*, Lazy pod Makytou, Slovakia, 2018, pp. 1-6.
- [20] L. Ming, "Self-adaptive fuzzy PID digital control method for linear inverted pendulum," *Proceedings of the 31st Chinese Control Conference*, Hefei, China, 2012, pp. 3563-3567.
- [21] S. A. Campbell, S. Crauford, K. Morris. "Friction and the Inverted Pendulum Stabilization Problem," *Journal of Dynamic system, Measurement, and Control*, 2008, vol. 130, pp. 054502 (1-7).
- [22] W. Li, H. Ding and K. Cheng, "An investigation on the design and performance assessment of double-PID and LQR controllers for the inverted pendulum," *Proceedings of 2012 UKACC International Conference on Control*, Cardiff, UK, 2012, pp. 190-196.

- [23] F. Peker and I. Kaya, "Identification and real time control of an inverted pendulum using PI-PD controller," *2017 21st International Conference on System Theory, Control and Computing (ICSTCC)*, Sinaia, Romania, 2017, pp. 771-776.
- [24] Prasad, L.B., Tyagi, B. & Gupta, H.O., "Optimal Control of Nonlinear Inverted Pendulum System Using PID Controller and LQR: Performance Analysis Without and With Disturbance Input", *Int. J. Autom. Comput.* 11, 661–670, 2014.
- [25] M. R. Dastranj, M. Moghaddas, S. S. Afghu and M. Rouhani, "PID control of inverted pendulum using particle swarm optimization (PSO) algorithm," *2011 IEEE 3rd International Conference on Communication Software and Networks*, Xi'an, China, 2011, pp. 575-578.
- [26] T. O. S. Hanafy, "Stabilization of inverted pendulum system using particle swarm optimization," *2012 8th International Conference on Informatics and Systems (INFOS)*, Giza, Egypt, 2012, pp. BIO-207-BIO-210.
- [27] Sudarshan K. Valluru & Madhusudan Singh, "Stabilization of nonlinear inverted pendulum system using MOGA and APSO tuned nonlinear PID controller", *Cogent Engineering*, 4:1.
- [28] K K Bhisikar, V A Vyawahare and M M. Joshi, "Design of fractional order PD Controller for Unstable and Integrating Systems[C]", *Intelligent Control and Automation. IEEE*, pp. 4698-4703, 2015.
- [29] S. Jiang, M. Li and C. Wang, "Design and simulation of fractional order PID controller for an inverted pendulum system," *2017 IEEE International Conference on Manipulation, Manufacturing and Measurement on the Nanoscale (3M-NANO)*, Shanghai, China, 2017, pp. 349-352.
- [30] Chunyang Wang, *Design of Fractional order Control System [M]*, Beijing: Defense Industry Press, 2014.
- [31] P. Cominos and N. Munro, "PID controllers: recent tuning methods and design to specification," *IEE Proc.-Control Theory Appl.*, vol. 149, no. 1, pp. 46-53, 2002.
- [32] W. Hu, G. Xiao and W. -J. Cai, "PID controller design based on two-degrees-of-freedom direct synthesis," *2011 Chinese Control and Decision Conference (CCDC)*, Mianyang, China, 2011, pp. 629-634.

- [33] Banu, U.S., and Uma, G, "Fuzzy gain scheduled CSTR with a GA based PID", *Chemical Engineering Communications*, 195 (10), pp. 1213-1226, 2008.
- [34] Kaya, I., "PI-PD controllers for controlling stable processes with inverse response and dead time", *Electr Eng*, 98, 55–65 (2016).
- [35] S. Baruah and L. Dewan, "A comparative study of PID based temperature control of CSTR using Genetic Algorithm and Particle Swarm Optimization," *2017 International Conference on Emerging Trends in Computing and Communication Technologies (ICETCCT)*, Dehradun, India, 2017, pp. 1-6.
- [36] Goud, H., Swarnkar, P. Investigations on Metaheuristic Algorithm for Designing Adaptive PID Controller for Continuous Stirred Tank Reactor. *MAPAN* 34, 113–119 (2019).
- [37] Wei-Der Chang, "Nonlinear CSTR control system design using an artificial bee colony algorithm", *Simulation Modelling Practice and Theory*, vol. 31, 2013, pp. 1-9.
- [38] Khanduja, N., Bhushan, B., "Optimal design of FOPID Controller for the control of CSTR by using a novel hybrid metaheuristic algorithm", *Sādhanā* 46, 104, 2021.
- [39] A. Singh and V. Sharma, "Concentration control of CSTR through fractional order PID controller by using soft techniques," *2013 Fourth International Conference on Computing, Communications and Networking Technologies (ICCCNT)*, Tiruchengode, India, 2013, pp. 1-6.
- [40] M. Chakraborty, D. Maiti and A. Konar, "The application of stochastic optimization algorithms to the design of a fractional-order PID controller," *IEEE, 3rd ICIIS*, pp. 1-6, 2008.
- [41] Raghupathy Prakash and Rajapalan Anita, "Robust Model Reference Adaptive Intelligent Control", *International Journal of Control Automation and Systems (springer)*, vol. 10, no. 2, pp. 396-406, 2012.
- [42] M. Morari and J. H. Lee, "Model predictive control: Past present and future", *Comput. Chemical Eng.*, vol. 23, no. 4–5, pp. 667-682, May 1999.
- [43] W.S. Black, P. Haghi and K.B. Ariyur, "Adaptive Systems: History Techniques Problems and Perspectives", *Systems*, vol. 2, no. 4, pp. 606-660, 2014.
- [44] D. Zang and B. Wei, "A Review on Model Reference Adaptive Control of Robotic Manipulators", *Annual Reviews in Control Elsevier*, pp. 1-11, February 2017.

- [45] D. Shevitz and B. Paden, "Lyapunov stability theory of nonsmooth systems," in *IEEE Transactions on Automatic Control*, vol. 39, no. 9, pp. 1910-1914, Sept. 1994.
- [46] C. A. Ibañez, O. G. Frias and M. S. Castanon, "Lyapunov-based controller for the inverted pendulum cart system", *Nonlinear Dynamics*, vol. 40, no. 4, pp. 367-374, 2005.
- [47] Daniel E. Miller and Naghmeh Mansouri, "Model reference adaptive control using simultaneous probing estimation and control", *IEEE Transactions on Automatic Control*, vol. 55, no. 9, pp. 2014-2029, 2010.
- [48] S. B. Pingale, S. P. Jadhav and V. P. Khalane, "Design of fuzzy model reference adaptive controller for inverted pendulum," *2015 International Conference on Information Processing (ICIP)*, Pune, India, 2015, pp. 790-794.
- [49] Bejarbaneh, E.Y., Bagheri, A., Bejarbaneh, B.Y. *et al.*, "Optimization of Model Reference Adaptive Controller for the Inverted Pendulum System Using CCPSO and DE Algorithms", *Aut. Control Comp. Sci.* 52, 256–267, 2018.
- [50] Manna, S., Akella, A.K. (2021). Design and Performance Analysis of Second-Order Process Using Various MRAC Technique. In: Singh, A.K., Tripathy, M. (eds) *Control Applications in Modern Power System. Lecture Notes in Electrical Engineering*, vol 710. Springer, Singapore.
- [51] Goud, Harsh and Swarnkar, Pankaj. "Signal Synthesis Model Reference Adaptive Controller with Artificial Intelligent Technique for a Control of Continuous Stirred Tank Reactor" *International Journal of Chemical Reactor Engineering*, vol. 17, no. 2, 2019, pp. 20180145.
- [52] Smt. U.V. Ratnakumari and M. Babu Triven, "Implementation of Adaptive Model Predictive Controller and Model Predictive Control for Temperature Regulation and Concentration Tracking of CSTR", *2016 International Conference on Communication and Electronics Systems (ICCES)*.
- [53] J. Mendes, F. Souza and R. Araújo, "Online evolving fuzzy control design: An application to a CSTR plant," *2017 IEEE 15th International Conference on Industrial Informatics (INDIN)*, Emden, Germany, 2017, pp. 218-225.

- [54] M. Naeijian and A. Khosravi, "Stability Analysis of Model Reference Adaptive Control with the New Theorem of Stability," *2020 28th Iranian Conference on Electrical Engineering (ICEE)*, Tabriz, Iran, 2020, pp. 1-6.
- [55] K. H. Ang, G. Chong and Y. Li, "PID control system analysis design and technology", *IEEE Transactions on Control Systems Technology*, vol. 13, no. 4, pp. 559-576, July 2005.
- [56] T. Liu and F. Gao, "New insight into internal model control filter design for load disturbance rejection", *IET Control Theory Appl.*, vol. 4, no. 3, pp. 448-460, 2010.
- [57] X. Li, Y. Gao, Y. You and B. Gu, "IMC-PID controller design for power control loop based on closed-loop identification in the frequency domain," *2018 Chinese Control And Decision Conference (CCDC)*, Shenyang, China, 2018, pp. 6355-6360.
- [58] M. Shamsuzzoha and M. Lee, "IMC-PID controller design for improved disturbance rejection of time-delayed processes," *Industrial Engineering Chemistry Research*, vol. 46, no. 7, pp. 2077-2091, 2007.
- [59] M. Hou, Z. Zhao, J. Zhang, and J. Tian, "An IMC-PID control method with set-point weight," *Proc. IEEE Int. Conf on Computational Intelligence and Security*, 2009, pp. 45-49.
- [60] Kumar, M., Prasad, D. & Singh, R.S., "Performance enhancement of IMC-PID controller design for stable and unstable second-order time delay processes", *J. Cent. South Univ.* 27, 88–100, 2020.
- [61] S. Sen, C. Dey and U. Mondal, "IMC based Fractional-order Controller for a Level Process," *2019 International Conference on Opto-Electronics and Applied Optics (Optronix)*, Kolkata, India, 2019, pp. 1-5.
- [62] R. Ranganayakulu, G. Uday Bhaskar Babu and A. Seshagiri Rao, "Fractional filter IMC-PID controller design for second order plus time delay processes", *Cogent Eng*, vol. 4, pp. 1366888, 2017.
- [63] H. Ikeda, "PID controller design methods for multi-mass resonance system", *PID Control for Industrial Processes*, Sep 2018.

- [64] N. Khanduja and B. Bhushan, "Intelligent Control of CSTR using IMC-PID and PSO-PID controller," *2016 IEEE 1st International Conference on Power Electronics, Intelligent Control and Energy Systems (ICPEICES)*, Delhi, India, 2016, pp. 1-6.
- [65] Sundarapandian Vaidyanathan, Ahmad Taher Azar, Chapter 1 - An introduction to backstepping control, In *Advances in Nonlinear Dynamics and Chaos (ANDC)*, Backstepping Control of Nonlinear Dynamical Systems, Academic Press, 2021, Pages 1-32.
- [66] W. Wang, J. Zhou, C. Wen and J. Long, "Adaptive Backstepping Control of Uncertain Nonlinear Systems With Input and State Quantization," in *IEEE Transactions on Automatic Control*, vol. 67, no. 12, pp. 6754-6761, Dec. 2022.
- [67] C. Ghorbel, A. Tiga, S. Rannen and N. Benhadj Braiek, "Combined backstepping-PID control of inverted pendulum," *2017 14th International Multi-Conference on Systems, Signals & Devices (SSD)*, Marrakech, Morocco, 2017, pp. 779-784.
- [68] Y. Maruki, K. Kawano, H. Suemitsu and T. Matsuo, "Adaptive backstepping control of wheeled inverted pendulum with velocity estimator", *International Journal of Control Automation and Systems*, vol. 12, no. 5, pp. 1040-1048, 2014.
- [69] S. Rudra, R. Kumar Barai and M. Maitra, "Nonlinear state feedback controller design for underactuated mechanical system: A modified block backstepping approach", *ISA Transactions*, vol. 53, no. 2, pp. 317-326, 2014.
- [70] R.Gopaluni, I. Mizumoto and S.Shah, "A robust nonlinear adaptive backstepping controller for a CSTR", *Ind. Eng. Chem. Res.*, Vol. 42, 4628-4644, 2003.
- [71] Li-Ping Xin, Bo Yu, Lin Zhao, Jinpeng Yu, "Adaptive fuzzy backstepping control for a two continuous stirred tank reactors process based on dynamic surface control approach", *Applied Mathematics and Computation*, Volume 377, 2020.
- [72] C. Hua, P. X. Liu and X. Guan, "Backstepping Control for Nonlinear Systems With Time Delays and Applications to Chemical Reactor Systems," in *IEEE Transactions on Industrial Electronics*, vol. 56, no. 9, pp. 3723-3732, Sept. 2009.
- [73] C. Hua, X. Guan and P. Shi, "Robust backstepping control for a class of time delayed systems", *IEEE Trans. Autom. Control*, vol. 50, no. 6, pp. 894-899, Jun. 2005.

CHAPTER 3

Brief Overview on Fractional Order Mathematics and Its Implementation in Controlling Processes

3.1 Introduction

Integrals and derivatives of functions are investigated in fractional calculus. However, in this area of mathematics, non-integer order integrals and derivatives are examined rather than the customary integer order. These are known as fractional derivatives and fractional integrals, which also include integer orders and can have real or complex orders. Fractional calculus, or fractional derivatives and integrals, is not a brand-new concept. Nevertheless, FO integration and differentiation do not follow this pattern, which represent a rapidly expanding subject in terms of both theory and applicability to real-world issues. There hasn't been a suitable geometric or physical interpretation of these operations for more than 300 years, ever since the concept of differentiation as well as integration of random order first emerged. The fractal characterization [1] of FO integration as "gloom on the fortifications" and its physical explanation as "gloom of the precedent" were made public. Function has been used in many scientific and technical fields recently, including the study of visco-elastic materials, fluid flow, elasticity, electrical systems, electromagnetism, and randomness. Visco-elasticity, fractional-order multiples in electromagnetism, electrical chemistry, tracer in hydraulic flows, dynamical structures in the theory of control, electrical networks with fractance, generalized voltage dividers, dynamical systems in nature, and physical networks with fractance all use fractional calculus. Applications of fractional calculus in both scientific and technological fields are emphasized, with a focus on numerical computation of FO derivatives and integrals. But this observation has changed recently. It has been suggested that fractional calculus [2] may be useful and even powerful.

Fractional calculus and its applications are currently experiencing rapid development with ever-more attractive real-world applications. A fast-connectivity strategy [3] for the computational solution of fractional differentiation and fractional integration is presented.

Matrix methodology [4] was further developed to incorporate non-equidistant grids, varied step dimensions, and distributed ordering in the differentiation of non-integer derivatives and integrals. The fractional calculus has its roots in the quest of academics for extension of significance, just like many other mathematical disciplines and ideas. It broadens an integer order's derivative to any order. This freedom of order offers up a brand-new perspective, and fractional calculus can be used to approach many applied scientific problems more succinctly. Numerous definitions of FO derivatives as well as integrals are going to be looked at in this chapter. For a number of simple functions, the explicit formula of the fractional calculus is available. This chapter uses a universal technique on any functions to achieve the goal of using FO derivatives or integrals. For the purpose of implementing the fractional order operator on the MATLAB platform, a few well-liked rational approximation techniques are explored. Their benefits over the alternatives are also highlighted. An overview of some research studies on fractional calculus is summarized in Table 3.1.

Table 3.1
Review of fractional calculus

| Method | Year | Development |
|-------------------------|------|---|
| Rossikhin[5] | 2001 | Formulation and analysis of the viscoelastic rod using a mathematical model that incorporates fractional derivatives. |
| Yuan [6] | 2002 | A mathematical approach similar to fractional derivatives of displacements for the dynamic analysis of mechanical systems. |
| Bahuguna et.al.[7] | 2003 | A set of integro differential equations in any arbitrary Banach space, Mittag-lefflar distribution and discretization technique on fractional order differentiator and integrator. |
| Agrawal et al[8] | 2004 | Fractional semi integral and derivative approach, Issue with semilinear nonlocal functional differentials, R-L(Riemann-Liouville) fractional integration and differentiation. |
| Saxena [9] | 2005 | Cauchy-type issue with caputo fractional derivatives. |
| Kilbas et al [10] | 2006 | Nonsequential linear fractional differential equations pertaining to the Caputo fractional derivatives with constant coefficients. |
| Yadav [11] | 2008 | Fractional q-integral operator. |
| Srivastav [12] | 2009 | Fractional calculus through integral operator pertaining to Mittag lefflar functions. |
| Herrmann [13] | 2011 | Optimisation criteria for various variational functions that have left- and right-handed Caputo fractional derivatives. |
| Changpin [14] | 2011 | Main characteristics of R-L(Riemann-Liouville) fractional derivative and partial fractional derivatives. |
| Haubold et al [15] | 2011 | Brief description on Mittag lefflar functions. |
| Purohit [16] | 2011 | solutions of generalised fractional partial differential equations involving the Caputo time-fractional derivative and the Liouville space-fractional derivative with laplace and fourier transforms. |
| Ansari [17] | 2012 | Flexible operational technique on fractional derivative. |
| Prajapati [18] | 2012 | Function in the form truncated series of powers and its numerous features, such as the integral representation and the derivative. |
| Kalla et al. [19] | 2012 | Mittag lefflar type based new generalized function. |
| Odziejewicz et al. [20] | 2012 | Proper fractional extension of classical calculus. |
| Faraj et al. [21] | 2013 | More properties for generalized Mittag lefflar function. |
| Srivastava et al. [22] | 2014 | New extended theory incorporating a generalized Hurwitz-Lerch zeta function. |
| Kumari [23] | 2014 | Some differentiation formulas for I function of two variables. |

3.2 Preliminaries of Fractional Calculus

By allowing differentiation and integration orders that are not required to be positive integers, fractional calculus expands the traditional definitions of derivatives and indefinite integrals [5]. Fractional transfer functions are typically replaced in practical applications by approximations, either continuous or discrete, that only use integer differentiation and integration orders. These estimations rely on the assumption that the approximated fractional orders of differentiation and integration don't change over time. This section discusses some fundamental methods and formulas for various functions.

3.2.1 Gamma Function

In fractional calculus, the gamma function is crucial.

Definition 3.2.1. One of the fundamental features of gamma function [24] is as follows

$$\Gamma(p + 1) = p\Gamma(p) \quad (3.1)$$

Gamma function is followed as

$$\Gamma(p) = \int_0^{\infty} \exp(-t)t^{p-1}dt \quad (3.2)$$

The above integral intersects for $\Re(p) > 0$ (right side of the intricate plane). Now, the above (3.2) can be integrated with the help of (3.1) as follows

$$\Gamma(p + 1) = \int_0^{\infty} \exp(-t)t^p = [-\exp(-t)t^p]_0^{\infty} + p \int_0^{\infty} \exp(-t)t^{p-1}dt \quad (3.3)$$

If the first part is eliminated and the second part is equal to $p\Gamma(p)$.

Another property is as follows

$$\Gamma(1) = 1 \quad (3.4)$$

Now, applying (3.4) in (3.1) is as follows

$$\left\{ \begin{array}{l} \Gamma(2) = 1. \Gamma(1) = 1 = 1! \\ \Gamma(3) = 2. \Gamma(2) = 2.1! = 2! \\ \Gamma(4) = 3. \Gamma(3) = 3.2! = 3! \\ \vdots \\ \Gamma(n + 1) = n. \Gamma(n) = n. (n - 1)! = n! \end{array} \right. \quad (3.5)$$

Therefore, it is quite evident from the aforesaid expressions that the gamma function is simply an expansion of the factorial function.

3.2.2 Beta Function

For better use in fractional derivatives, beta function may occasionally be favored over gamma function.

Definition 3.2.2. Let, $p, w \in \mathbb{C}$ then beta function can be followed as [25]

$$B(p, w) = \int_0^1 \tau^{p-1} (1 - \tau)^{w-1} d\tau \quad (3.6)$$

The above expression is considered for $\Re(p) > 0$ and $\Re(w) > 0$. The gamma function can be used to express the beta function using the Laplace transform for convolution by

$$B(p, w) = \frac{\Gamma(p)\Gamma(w)}{\Gamma(p+w)} \quad (3.7)$$

And it follows from (3.7) that

$$B(p, w) = B(w, p) \quad (3.8)$$

3.2.3 Mittag-Leffler Function

In differential equations of IO, the exponential function e^p is extremely crucial. This can be expressed [15] in series form by

$$e^p = \sum_{k=0}^{\infty} \frac{p^k}{\Gamma(k+1)} \quad (3.9)$$

The following general representation of the aforementioned (3.9) can be used as

$$E_{\alpha, \beta}(p) = \sum_{k=0}^{\infty} \frac{p^k}{\Gamma(\alpha k + \beta)} \quad (3.10)$$

Where, $\alpha, \beta \in \mathbb{C}$ and $\Re(\alpha) > 0$. In special case of $\alpha = 1$ and $\beta = 1$ $E_{1,1}(p) = e^p$. The term "mittag-leffler function" refers to this generalisation. In fractional calculus, particularly in fractional differential equations, the two parameter functions play a significant role. Given that (3.10)'s series is uniformly convergent on all compact subsets, it can be differentiated term by term to produce the following expression with a n times differentiated function as shown by

$$E_{\alpha, \beta}^{(n)}(p) = \sum_{k=0}^{\infty} \frac{(k+n)!}{k!} \frac{p^k}{\Gamma(\alpha k + \alpha n + \beta)} \quad (3.11)$$

3.3 Overview of Fractional Derivatives and Integrals

In actuality, the phrase "Fractional Calculus" is inappropriate because it does not refer to either the calculus of fractions or the fraction of any calculus. Actually, it is the area of mathematics [6] that extends the concepts of differentiation as well as integration of IO functions to encompass derivatives and integrals of arbitrary orders. If the sequence of integers order integral and derivatives is as follows

$$\int_a^t f(\tau_1) d\tau_1, f(t), \frac{df(t)}{dt}, \frac{d^2}{dt^2} f(t), \dots$$

Then the derivative of arbitrary order is then described in the above sequence as an insertion between two operators. This method is known as fractional derivative. The following statement denotes fractional derivative:

$$a^D_t^\alpha f(t), \alpha > 0.$$

But, with reference to the above expression, if $\alpha < 0$ then it will be defined as fractional integral with the expression as follows

$$a^{D_t^{-\alpha}} f(t).$$

The next section goes into the value of fractional calculus.

3.3.1 Application of Fractional Order Derivative

In contrast to integer order derivative, fractional order derivative provides more insight into the behavior of all functions, giving the user more freedom to select the desired behavior based on the function. A function like $y = x^2$ and its behavior together with first and second order derivatives are depicted in Fig. 3.1, which provides a clear explanation of the need for fractional order calculus in this research work.

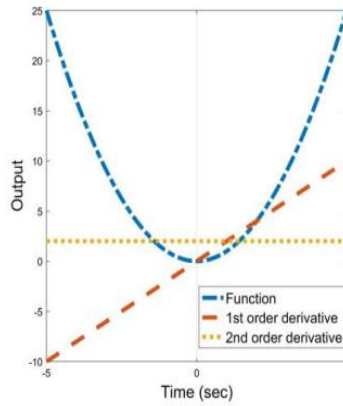


Fig. 3.1. Performance of function $y = x^2$ using classical calculus.

The behaviour of the aforementioned function is depicted using classical calculus in Fig. 3.1, but one drawback of this calculus is that it does not adequately explain how parabolic to linear polynomials are transformed because it does not explain clearly what the derivative lying between zero and first order derivative means. Therefore, it is easy to comprehend the internal feature of how the parabolic curve is progressively converted to a straight line curve, exactly the same as shown in the above Fig. 3.1 using fractional calculus if it is addressed with derivative order as between 0 and 1 such as 0.2, 0.5, and 0.75 accordingly as shown in Fig. 3.2.

Likewise, if it is addressed with a derivative order between 1 and 2, such as 1.2, 1.5, and 1.75, respectively, it will likewise reveal more about the gradual transformation towards the graphical behaviour of the second order derivative also, as depicted in Fig. 3.3.

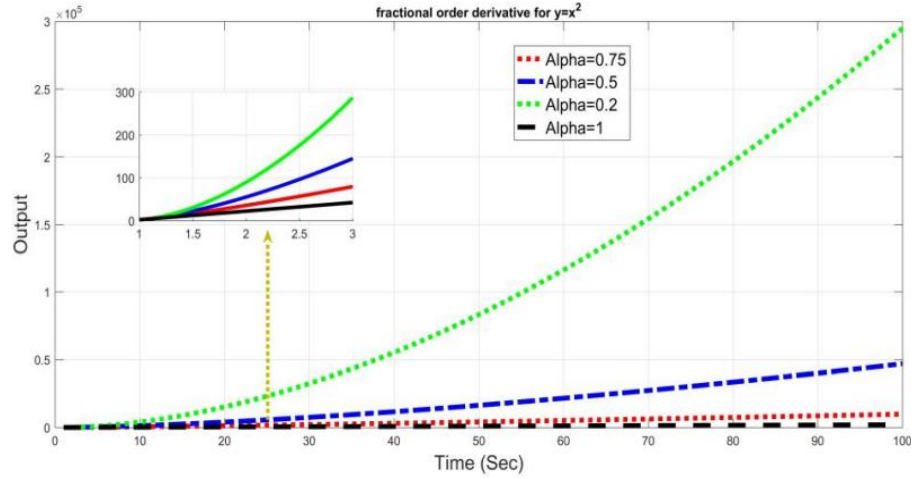


Fig. 3.2. Insight behavior of function using fractional orders between 0 and 1.

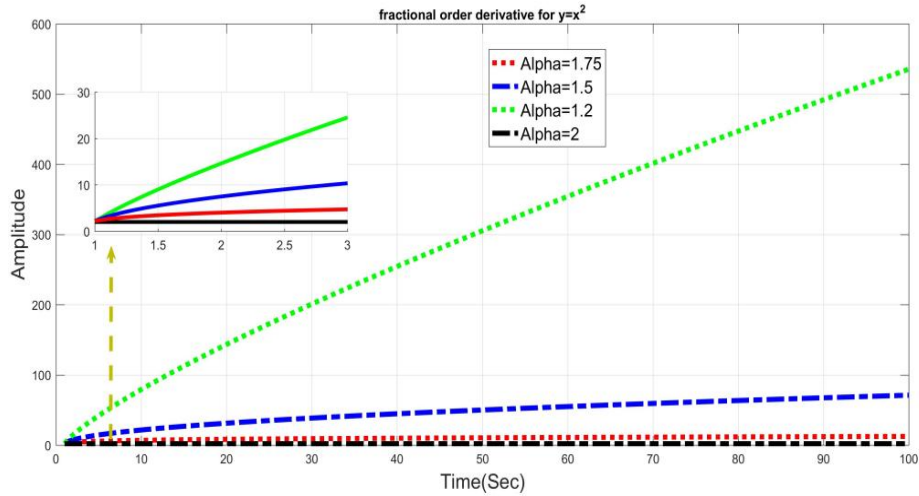


Fig. 3.3. Insight behaviour of functions using fractional orders between 1 and 2.

The above fractional derivative and integral for the aforementioned function with various fractional orders are illustrated using the features of the gamma function presented by Euler as detailed in section 3.2.1. The MATLAB codes are displayed in Appendix A. The aforementioned claim opens up the possibility of broad application to all different kinds of functions, and along with idea of fractional calculus, other well-known approaches like G-L, R-L, and Caputo procedures are also well-established for a variety of uses. In the following sections, the mathematical reinforcements of such techniques are covered.

3.3.2 Grunwald-Letnikov (G-L) Construction

Grunwald-Letnikov construction [26] is based on the forward difference derivative shown by

$$f'(t) = \lim_{h \rightarrow 0} \left\{ \frac{f(t) - f(t-h)}{h} \right\} \quad (3.12)$$

Now, second order derivative is constructed by using the above (3.12) as shown by

$$f''(t) = \lim_{h \rightarrow 0} \left\{ \frac{f'(t) - f'(t-h)}{h} \right\} \quad (3.13)$$

$$f''(t) = \lim_{h \rightarrow 0} \left\{ \frac{\left(\frac{f(t) - f(t-h)}{h} \right) - \left(\frac{f(t-h) - f(t-2h)}{h} \right)}{h} \right\} \quad (3.14)$$

$$f''(t) = \lim_{h \rightarrow 0} \frac{1}{h^2} \{ f(t) - 2f(t-h) + f(t-2h) \} \quad (3.15)$$

Applying the above (3.15) third order derivative is also constructed, as shown by

$$f'''(t) = \lim_{h \rightarrow 0} \frac{1}{h^3} \{ f(t) - 3f(t-h) + 3f(t-2h) - f(t-3h) \} \quad (3.16)$$

Now, the above (3.16) can be generalized with the following binomial term as shown by

$$f'''(t) = \lim_{h \rightarrow 0} \frac{1}{h^3} \sum_{j=0}^3 (-1)^j \binom{3}{j} f(t-jh) \quad (3.17)$$

Now, n^{th} derivative of function is shown by

$$f^n(t) = \lim_{h \rightarrow 0} \left(\frac{1}{h} \right)^n \sum_{j=0}^n (-1)^j \binom{n}{j} f(t-jh) \quad (3.18)$$

The above (3.18) with integer number can be replaced with α^{th} order to obtain the following definition.

Definition 3.3.2. Assume that n is the smallest real number such that $|\alpha| \leq n$ then G-L differ-integral is followed as

$$D^\alpha f(t) = \lim_{h \rightarrow 0} \left(\frac{1}{h} \right)^\alpha \sum_{j=0}^n (-1)^j \binom{\alpha}{j} f(t-jh) \quad (3.19)$$

Now, the above binomial coefficient $\binom{\alpha}{j}$ can be extended by property of gamma function as shown by

$$\binom{\alpha}{j} = \frac{\alpha!}{j!(\alpha-j)!} = \frac{\Gamma(\alpha+1)}{j!\Gamma(\alpha-j+1)} \quad (3.20)$$

Now, applying (3.20) into (3.19) it is found as

$$D^\alpha f(t) = \lim_{h \rightarrow 0} \left(\frac{1}{h} \right)^\alpha \sum_{j=0}^n (-1)^j \frac{\Gamma(\alpha+1)}{j!\Gamma(\alpha-j+1)} f(t-jh) \quad (3.21)$$

Now, if it is assumed as $n = \frac{t-a}{h}$ following the condition as $h \rightarrow 0, n \rightarrow \infty$ and $a < t$, then the final expression is constructed by

$$D^\alpha f(t) = \lim_{n \rightarrow \infty} \left(\frac{n}{t-a} \right)^\alpha \sum_{j=0}^n (-1)^j \frac{\Gamma(\alpha+1)}{j! \Gamma(\alpha-j+1)} f\left(t - j \left(\frac{t-a}{n} \right)\right) \quad (3.22)$$

However, it may be inferred that the above definition, which incorporates a limit (lim), is highly complex and that the definition will only make sense if limits exist. As a result, the Riemann-Liouville (R-L) technique, which is covered in the following section, modifies the definition above.

3.3.3 Riemann-Liouville (R-L) Construction

As opposed to the G-L approach, which starts with the derivative, the R-L method [27] starts with the integral by changing the sign of α in (3.19) to negative to reflect fractional integral as shown by

$$D^{-\alpha} f(t) = \lim_{h \rightarrow 0} \left(\frac{1}{h} \right)^{-\alpha} \sum_{j=0}^n (-1)^j \binom{-\alpha}{j} f(t - jh) \quad (3.23)$$

Now, the above binomial coefficient $\binom{-\alpha}{j}$ can be extended by property of the gamma function as shown by

$$\binom{-\alpha}{j} = \begin{cases} \frac{(-\alpha)(-\alpha-1)\dots(-\alpha-j+1)}{j!} \\ \frac{(-1)^j \alpha(\alpha+1)\dots(\alpha+j-1)}{j!} \\ \frac{(-1)^j (\alpha+j-1)\dots(\alpha+1)\alpha(\alpha-1)!}{j! (\alpha-1)!} \\ \frac{(-1)^j (\alpha+j-1)!}{j! (\alpha-1)!} \\ \frac{(-1)^j \Gamma(\alpha+j)}{j! \Gamma(\alpha)} \end{cases} \quad (3.24)$$

Now, applying (3.24) into (3.22) it is obtained as

$$D^{-\alpha} f(t) = \lim_{n \rightarrow \infty} \left(\frac{1}{h} \right)^{-\alpha} \sum_{j=0}^n (-1)^j \frac{(-1)^j \Gamma(\alpha+j)}{j! \Gamma(\alpha)} f\left(t - j \left(\frac{t-a}{n} \right)\right) \quad (3.25)$$

$$D^{-\alpha} f(t) = \lim_{n \rightarrow \infty} h^\alpha \sum_{j=0}^n \frac{\Gamma(\alpha+j)}{j! \Gamma(\alpha)} f\left(t - j \left(\frac{t-a}{n} \right)\right) \quad (3.26)$$

Now, (3.26) is replaced with an integral term to define R-L integral.

Definition 3.3.3. Integrals and integer order derivatives are combined to produce the R-L differ-integral.

$$I^\alpha f(t) = \lim_{n \rightarrow \infty} h^\alpha \sum_{j=0}^n \frac{\Gamma(\alpha+j)}{j! \Gamma(\alpha)} f(t - jh) \quad (3.27)$$

Now, if $\alpha = 1$ then it is obtained as

$$I^1 f(t) = \lim_{n \rightarrow \infty} h \sum_{j=0}^n f(t - jh) \quad (3.28)$$

Suppose, considering a function $y = f(t)$ whose area may lie within boundary $0 \rightarrow t - a$. So, the total area under the complete region of function is derived from (3.28) as shown by

$$I^1 f(t) = \int_0^{t-a} f(t-x) dx \quad (3.29)$$

Where, $x = jh$

Assume, $t - x = u$, so $-dx = du$

$$I^1 f(t) = - \int_t^a f(u) du \quad (3.30)$$

If $f(u)$ is integrable in every finite interval (a, t) then it is obtained as

$$I^1 f(t) = \int_a^t f(u) du \quad (3.31)$$

Now, if $\alpha = 2$ then it is also constructed by the gamma function's characteristic as

$$I^2 f(t) = \begin{cases} \lim_{n \rightarrow \infty} h^2 \sum_{j=0}^n \frac{\Gamma(2+j)}{j! \Gamma(2)} f(t-jh) \\ \lim_{n \rightarrow \infty} h^2 \sum_{j=1}^{n+1} j f(t-(j-1)h) \\ \lim_{n \rightarrow \infty} h^2 \sum_{j=1}^{n+1} j f(t+h-jh) \\ \lim_{n \rightarrow \infty} h^2 \sum_{j=1}^{n+1} j f(y-jh), \text{ where } t+h=y \\ \lim_{n \rightarrow \infty} \sum_{j=1}^{n+1} (jh) h f(y-jh) \\ \int_0^{t-a} t f(t-x) dx \end{cases} \quad (3.32)$$

Under the same assumption, the above expression is obtained as

$$I^2 f(t) = \int_a^t (t-u) f(u) du \quad (3.33)$$

Similarly, for $\alpha = 3$ it is followed as

$$I^3 f(t) = \frac{1}{2!} \int_a^t (t-u)^2 f(u) du \quad (3.34)$$

Now, finally, for arbitrary order, R-L fractional integral is followed as

$$I^\alpha f(t) = \frac{1}{\Gamma(\alpha)} \int_a^t (t-u)^{\alpha-1} f(u) du, a < t \quad (3.35)$$

Now, R-L fractional derivative may be defined using (3.35) as shown by

$$D^\alpha f(t) = \frac{d^m}{dt^m} I^{m-\alpha} f(t) \quad (3.36)$$

$$D^\alpha f(t) = \frac{d^m}{dt^m} \frac{1}{\Gamma(m-\alpha)} \int_a^t (t-u)^{\alpha-1} f(u) du \quad (3.37)$$

3.3.3.1 Application of R-L Fractional Integral

In contrast to classical integral, fractional order integral also provides more insight into the behavior of all functions, giving the user more freedom to select the desired behavior based on the function. As illustrated in Fig. 3.4, the fractional integral also tells more about the gradual conversion of the same function $y = t^2$ to traditional calculus-based performance. The aforementioned function is computed using the final R-L fractional integral expression presented in (3.35), as demonstrated by

$$I^\alpha(t^m) = \frac{1}{\Gamma(\alpha)} \int_a^t (t-u)^{\alpha-1} u^m du, f(t) = t^m, f(u) = u^m \quad (3.38)$$

$$I^\alpha(t^m) = \frac{1}{\Gamma(\alpha)} \int_a^t [t(1 - \frac{u}{t})]^{\alpha-1} u^m du \quad (3.39)$$

$$I^\alpha(t^m) = \frac{t^{\alpha-1}}{\Gamma(\alpha)} \int_a^t \left(1 - \frac{u}{t}\right)^{\alpha-1} u^m du \quad (3.40)$$

Now, it is assumed as $\frac{u}{t} = v$ then $u = vt, du = t dv$

Now, changing upper and lower limits with respect to v the above (3.40) is modified as shown by

$$I^\alpha(t^m) = \frac{t^{\alpha-1}}{\Gamma(\alpha)} \int_{a/t}^1 (1-v)^{\alpha-1} (tv)^m t dv \quad (3.41)$$

$$I^\alpha(t^m) = \frac{t^{\alpha+m}}{\Gamma(\alpha)} \int_{a/t}^1 v^m (1-v)^{\alpha-1} dv \quad (3.42)$$

Now, assuming lower limit as $a = 0$ to correlate with beta function as discussed in section 3.2.2 and applying the property of beta function the above (3.42) is illustrated by

$$I^\alpha(t^m) = \frac{t^{\alpha+m}}{\Gamma(\alpha)} \int_0^1 v^m (1-v)^{\alpha-1} dv \quad (3.43)$$

$$I^\alpha(t^m) = \frac{t^{\alpha+m}}{\Gamma(\alpha)} B(m+1, \alpha) \quad (3.44)$$

$$I^\alpha(t^m) = \frac{t^{\alpha+m} \Gamma(m+1) \Gamma(\alpha)}{\Gamma(\alpha) \Gamma(\alpha+m+1)} \quad (3.45)$$

$$I^\alpha(t^m) = \frac{t^{\alpha+m} \Gamma(m+1)}{\Gamma(\alpha+m+1)} \quad (3.46)$$

The aforementioned fractional integral expression is utilized to create a graphical representation as depicted in Fig. 3.4.

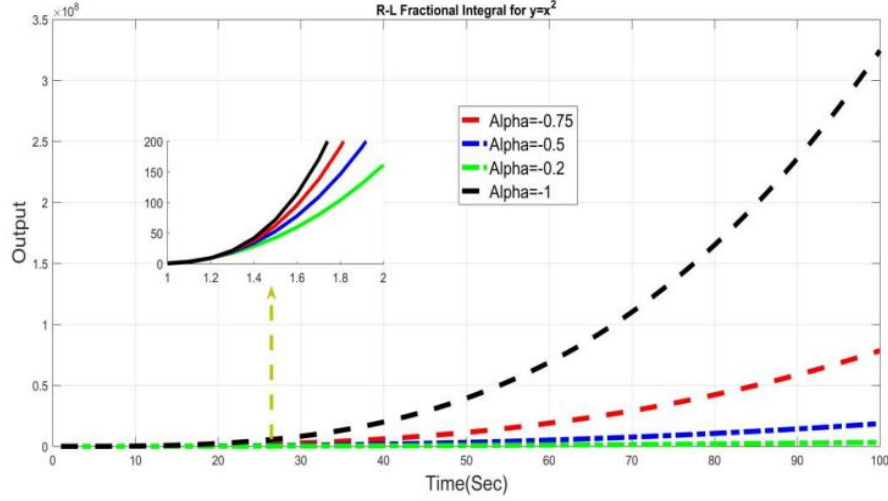


Fig. 3.4. Insight behavior of function using fractional orders between 0 and 1.

3.3.4 Caputo Construction

Definition 3.3.4. Caputo fractional derivative [28] is proposed as

$$D^\alpha f(t) = I^{m-\alpha} \left\{ \frac{d^m}{dt^m} f(t) \right\} \quad (3.47)$$

$$D^\alpha f(t) = \frac{1}{\Gamma(m-\alpha)} \int_a^t (t-u)^{m-\alpha-1} \frac{d^m}{du^m} f(u) du, \quad m-1 < \alpha < m \quad (3.48)$$

In order to present more analytical features based on progressive transformation that may be observed with different fractional orders applying on the function $y = t^2$, another investigation is now carried out in this study with Caputo fractional derivative on the same previously described function.

So, (3.47) is replaced with $f(t) = t^\beta$ as shown by

$$D^\alpha [t^\beta] = I^{m-\alpha} \left\{ \frac{d^m}{dt^m} t^\beta \right\} \quad (3.49)$$

$$D^\alpha [t^\beta] = \frac{1}{\Gamma(m-\alpha)} \int_a^t (t-u)^{m-\alpha-1} \frac{d^m}{du^m} u^\beta du, \quad f(u) = u^\beta \quad (3.50)$$

$$D^\alpha [t^\beta] = \frac{1}{\Gamma(m-\alpha)} \int_a^t (t-u)^{m-\alpha-1} \left\{ \frac{\beta!}{(\beta-m)!} u^{\beta-m} \right\} du \quad (3.51)$$

Now, applying the gamma function's characteristic into (3.51) as

$$D^\alpha [t^\beta] = \frac{\Gamma(1+\beta)}{\Gamma(m-\alpha)\Gamma(1+\beta-m)} \int_a^t (t-u)^{m-\alpha-1} u^{\beta-m} du \quad (3.52)$$

$$D^\alpha [t^\beta] = \frac{\Gamma(1+\beta)}{\Gamma(m-\alpha)\Gamma(1+\beta-m)} \int_a^t t^{m-\alpha-1} \left(1 - \frac{u}{t}\right)^{m-\alpha-1} u^{\beta-m} du \quad (3.53)$$

Now, it is assumed as $\frac{u}{t} = y$ then $u = yt, du = tdy$

Now, changing the higher and lower bounds with respect to y the above (3.53) is modified as shown by

$$D^\alpha[t^\beta] = \frac{\Gamma(1+\beta)}{\Gamma(m-\alpha)\Gamma(1+\beta-m)} \int_{a/t}^1 t^{m-\alpha-1} (1-y)^{m-\alpha-1} (ty)^{\beta-m} t dy \quad (3.54)$$

$$D^\alpha[t^\beta] = \frac{\Gamma(1+\beta)t^{m-\alpha+1+\beta-m+1}}{\Gamma(m-\alpha)\Gamma(1+\beta-m)} \int_{a/t}^1 (1-y)^{m-\alpha-1} y^{\beta-m} dy \quad (3.55)$$

Now, assuming lower limit as $a = 0$ to correlate with beta function as discussed in section 3.2.2 and applying the property of beta function the above (3.55) is illustrated by

$$D^\alpha[t^\beta] = \frac{\Gamma(1+\beta)t^{\beta-\alpha}}{\Gamma(m-\alpha)\Gamma(1+\beta-m)} B(m-\alpha, \beta-m+1) \quad (3.56)$$

$$D^\alpha[t^\beta] = \frac{\Gamma(1+\beta)t^{\beta-\alpha}}{\Gamma(m-\alpha)\Gamma(1+\beta-m)} \frac{\Gamma(m-\alpha)\Gamma(\beta-m+1)}{\Gamma(m-\alpha+\beta-m+1)} \quad (3.57)$$

$$D^\alpha[t^\beta] = \frac{\Gamma(1+\beta)}{\Gamma(1+\beta-\alpha)} t^{\beta-\alpha} \quad (3.58)$$

The fractional derivative approach for the function $y = t^2$ presented in section 3.2.1 computes using the same expression as the caputo method, however the caputo method defines it more analytically than the Euler method does. Similar to the aforementioned function, any other type of function's graphical characteristic may likewise be determined more analytically using R-L or Caputo fractional differ-integral calculus.

3.4 Theoretical Background of Implementation of Fractional Calculus

Fractional order system models [2] allow for a more precise description of actual systems and have been employed to find more trustworthy responses to a variety of scientific and technical difficulties. For instance, the field of control engineering has profited considerably over the past 20 years from the positive effects of non-integer order modelling to enhance control behavior and generate more trustworthy plant modelling. Since there are infinite number of tuning possibilities for non-integer order integral and derivative parts, FOPID scheme [29] have generally been regarded as a feasible and logical replacement for traditional scheme. However, optimal implementation of fractional order systems introduces substantially more computing difficulty than ideal implementation of conventional systems, despite the fact that fractional calculus assures notable improvements in modelling and control system efficiency. The primary explanation is as the FO derivative function, which is a not a local operator [30] that necessitates all previous values of the function, is required. As a result, computing fractional parameters requires additional memory components to retain all historical signal or function values across time.

This phenomenon is known as the long memory effect. Because the long memory effect uses up increasing amounts of computational resources over time, it causes the computational load of fractional order items to increase significantly over time. This basic difficulty prohibits engineering issues from fully utilizing the benefits of optimal fractional order behavior. Approximate integer order models were developed to address these issues and implement fractional order elements with a manageable processing overhead. These models may approximately predict the performances of FO elements within certain operating regions. In real-world control applications, these approximations were frequently used to implement FOPID controllers in less-than-ideal ways. Because analytical tuning approaches primarily presume a hypothetical implementation of FOPID controller functions, the performance of approximate models inherently degrades the practical performance of optimal tuning methods. As a result, estimated computations of fractional parameters result in real-world control performance that is significantly lower than the best possible control performance that may be attained theoretically. Due to these factors, choosing a suitable estimated model to establish fractional order systems should be a top priority for applications that require fractional order control systems to function in the real world. The most important characteristics of approximation models are important from the perspective of control practice:

✧ *Approximated Performance on Time and Frequency region platform*

In order to prevent a significant decline in control nature due to differences between the performances of the original system and the estimated systems, it is crucial that the time and frequency outcomes of the main FO systems and its estimated forms match characteristically. The effects of incorrectly realizing FOPID controllers have previously been examined in a number of researches. For minimal difficulty and realistic realization of fractional derivative operators, a variety of approximation techniques are offered in the literatures [31-35]. In terms of broad definition, these techniques are continuous systems in the frequency region platform and discrete models in the time region platform. Following is a list of some frequency domain approximation techniques that have been proposed and are methodologically important: The serial filter banks used by Oustaloup's [31] Method have zeros and poles that are set up to roughly approximate the amplitude behavior of fractional order operators. A rational integer-order function that roughly corresponds to elements of fractional order is produced by the CFE Method [31]. The manipulation of frequency points can be approximated using Matsuda's Method, which is based on continuing fraction expansion utilizing in logarithmic manner separated set points.

Stability with the use of the boundary locus (SBL) fitting method, a rational model is fitted to SBL curves with a FO model in the necessary frequency range. In order to create a continuous approximate model, improved iterations of these techniques as well as various methodologically modern approaches were provided, such as Carlson's Method and its enhanced types [31], Charef's Method [31], phase shaping approaches by ideal pole-zero placing [33], Mittag-Leffler function based solutions [32]. Two distinct ways to obtaining discrete models in the time domain using discrete approximation methods are discussed. Firstly, the discretization of continuous processes generated by frequency domain [34-35] aspects is enabled by indirect discretization. The second is direct discretization [36-37], which applies direct PSE for the Euler operator or CFE for the Tustin operator to discretize model in the z-domain. For fractional-order linear differential problems, there are also a number of approximate or numerical solution techniques, such as homotopy variation [36], variational iteration [37], and Grünwald-Letnikov definition-based methods; however, these mathematical solutions have not been applied extensively in the field of control.

Therefore, the primary goal of this work is to evaluate effective approximation techniques for any fractional differentiation equations or transfer functions in comparison to some direct or indirect approximation methods.

3.4.1 FOMCON Toolkit

For the modelling, investigation, and development of linear fractional or conventional processes, it is widely known that the FOMCON (Fractional order modeling and control) Toolkit [38] of MATLAB offers a very easy and straightforward approach. A Simulink block set, graphical user interfaces (GUIs), convenience functions, ways to identify models in the time and frequency regions, and fractional PID controller formulation and efficiency are all included in the FOMCON toolkit for MATLAB, which is an addition to the small toolkit [38] previously addressed. The toolbox aims to offer a user-friendly, practical, and useful toolset to a variety of users.

3.4.1.1 Toolkit Features

Following G-L fractional derivative and R-L fractional derivative or integral in (3.22), (3.35) and (3.37) under section 3.3.2 and 3.3.3 the Laplace transform [38] of α^{th} derivative with $\alpha \in \mathbb{R}_+$ of a signal $x(t)$ assuming zero initial condition is shown by

$$\mathcal{L}(D^\alpha x(t)) = s^\alpha X(s) \quad (3.59)$$

So, fractional order linear differential equation can be approached as

$$p_n D^{\alpha_n} y(t) + p_{n-1} D^{\alpha_{n-1}} y(t) + \dots + p_0 D^{\alpha_0} y(t) = q_m D^{\beta_m} u(t) + q_{m-1} D^{\beta_{m-1}} u(t) + \dots + q_0 D^{\beta_0} u(t) \quad (3.60)$$

Now, by following Laplace transform in above (3.60) the following FOTF is shown as

$$G(s) = \frac{q_m s^{\beta_m} + q_{m-1} s^{\beta_{m-1}} + \dots + q_0 s^{\beta_0}}{p_n s^{\alpha_n} + p_{n-1} s^{\alpha_{n-1}} + \dots + p_0 s^{\alpha_0}} \quad (3.61)$$

This type of system is described as a commensurate order system. Usually, for commensurate order system denoting $\lambda = s^\alpha$ or s^β the transfer function can be presented as a rational order as shown by

$$G(s) = \frac{q_m \lambda^m + q_{m-1} \lambda^{m-1} + \dots + q_0 \lambda}{p_n \lambda^n + p_{n-1} \lambda^{n-1} + \dots + p_0 \lambda} = \frac{\sum_{k=0}^m q_k \lambda^k}{\sum_{k=0}^n p_k \lambda^k} \quad (3.62)$$

The FOTF presented in (3.61) serves as the primary focus of analysis in FOMCON. The SISO and LTI (linear time-invariant) systems are the main emphasis of the toolkit. The modules that comprise the toolkit are as follows: the primary module, which does fractional system investigation, the identification module, which identifies systems in the time and frequency domain platforms, and the Control module, which includes tools for designing, fine-tuning, and optimizing fractional PID controllers as well as some extra features. The main module GUI, shown in Fig. 3.5, can be used to access all of the modules, which are all connected. The toolkit also includes a Simulink block set that enables the execution of sophisticated modelling tasks. The following MATLAB software is necessary for the FOMCON toolbox [38]:

- Control System Toolbox, which is necessary for the majority of features;
- Optimization Toolbox, which is necessary for time-zone understanding and standard PID tuning for approximating typical system.

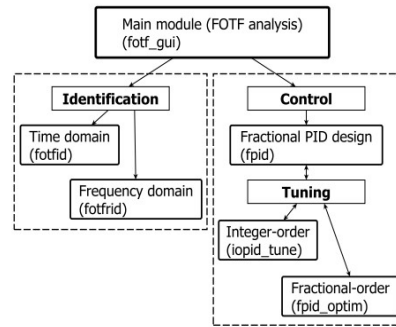


Fig. 3.5. FOMCON platform.

3.4.1.2 Computation of Fractional Order Model

This causes the FOTF Viewer [38], the primary toolbox GUI, to be shown in Fig. 3.6. Two panels make up its layout:

- The Fractional Order Transfer Functions panel on the left is where FOTF objects are entered, edited, deleted, and converted.
- The right panel, System analysis, has tools for FO system investigation in the time and frequency domain platforms. The tool works directly with MATLAB base workspace variables.

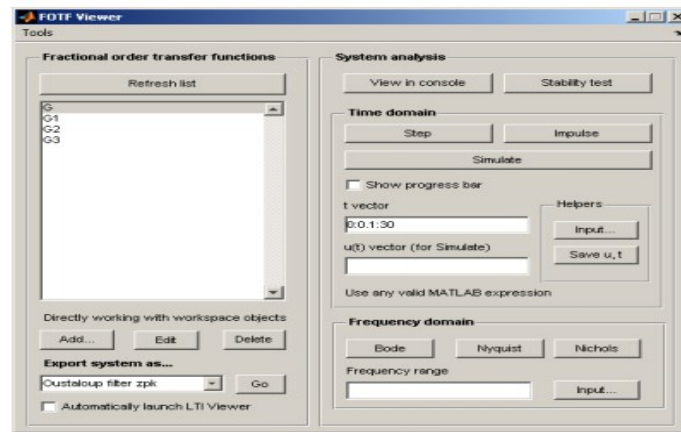


Fig. 3.6. GUI (Graphical user interface) window.

✧ *Time domain platform*

A modified Grünwald-Letnikov formulation [38] is used to simulate the system performance to a random input signal during time-domain analysis of the fractional systems as shown in Fig.3.7.

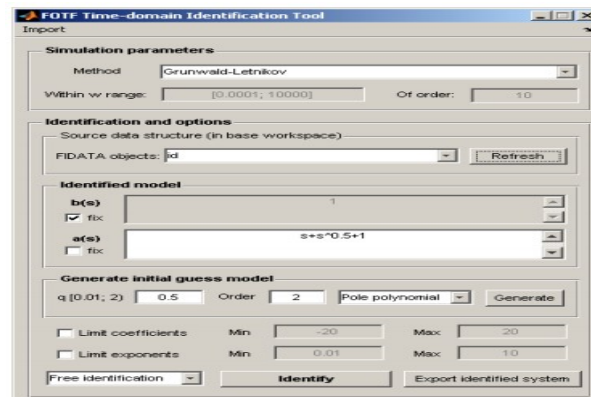


Fig. 3.7. FOTF Time domain platform.

Now, denoting left hand side of (3.60) by

$$v(t) = q_m D^{\beta_m} u(t) + q_{m-1} D^{\beta_{m-1}} u(t) + \dots q_0 D^{\beta_0} u(t) \quad (3.63)$$

The FO linear differential form can be represented in form as

$$p_n D^{\alpha_n} y(t) + p_{n-1} D^{\alpha_{n-1}} y(t) + \dots p_0 D^{\alpha_0} y(t) = v(t) \quad (3.64)$$

Substituting (3.22) in the above expression as shown by

$$\frac{p_n}{h^{\alpha_n}} \sum_{j=0}^{\{(t-a)/h\}} w_j^{\alpha_n} y(t-jh) = v(t) \quad (3.65)$$

Binomial coefficients $w_j^{\alpha_n}$ can be obtained iteratively with

$$w_0^{\alpha_0} = 1, w_j^{\alpha_i} = \left(1 - \frac{\alpha+1}{j}\right) w_{j-1}^{\alpha_i}, j = 1, 2, \dots \quad (3.66)$$

The closed loop version of a FO process can be expressed as follows with a modest term rearrangement:

$$y(t) = \frac{1}{\sum_{i=0}^n \frac{p_i}{h^{\alpha_i}}} \left[v(t) - \sum_{i=0}^n \frac{p_i}{h^{\alpha_i}} \sum_{j=1}^{\{(t-a)/h\}} w_j^{\alpha_i} y(t-jh) \right], \quad (3.67)$$

Where, h is step length of estimation. The correctness of the simulation may be affected by the step length h due to the fixed-step computation. As a result, it is advised to gradually reduce h until there is no longer any fluctuation in the simulation findings before using them. It could take a long time to simulate a lot of points.

✧ *Frequency domain platform*

The frequency zone investigation [38] is explored by replacing $s = j\omega$. The primary GUI's export feature enables the conversion of FOTF systems into the following types of objects:

- Oustaloup filter zpk;
- Oustaloup refined filter zpk;

The fractional operators [38] are extremely accurately solely approximated by the Oustaloup filters in the given frequency range (ω_l, ω_h) and order N . Fractional operator s^α is approximated by

$$G(s) = z \prod_{i=-N}^N \frac{s + \omega_z'}{s + \omega_z} \quad (3.68)$$

Where,

$$\begin{cases} z = \omega_h^\alpha, \\ \omega'_z = \omega_l \left(\frac{\omega_h}{\omega_l} \right)^{\frac{z+N+0.5(1-\alpha)}{2N+1}}, \\ \omega_z = \omega_l \left(\frac{\omega_h}{\omega_l} \right)^{\frac{z+N+0.5(1+\alpha)}{2N+1}} \end{cases} \quad (3.69)$$

A refined Oustaloup filter [64] is given by

$$s^\alpha = \left(\frac{d\omega_h}{l} \right)^\alpha \left(\frac{ds^2 + l\omega_h s}{d(1-\alpha)s^2 + l\omega_h s + d\alpha} \right) Q(s) \quad (3.70)$$

Where,

$$\begin{cases} Q(s) = \prod_{z=-N}^N \frac{s + \omega'_z}{s + \omega_z}, \\ \omega'_z = \left(\frac{d\omega_l}{l} \right)^{\frac{\alpha-2z}{2N+1}}, \\ \omega_z = \left(\frac{l\omega_h}{d} \right)^{\frac{\alpha+2z}{2N+1}} \end{cases} \quad (3.71)$$

3.4.1.3 Application of FOMCON Toolkit

The design of a FOPID scheme [29] for an integer order interacting cylindrical tank level process with a dead-time is the main topic of the current study. Fig. 3.8 depicts the fundamental concept of the interaction tank level process.

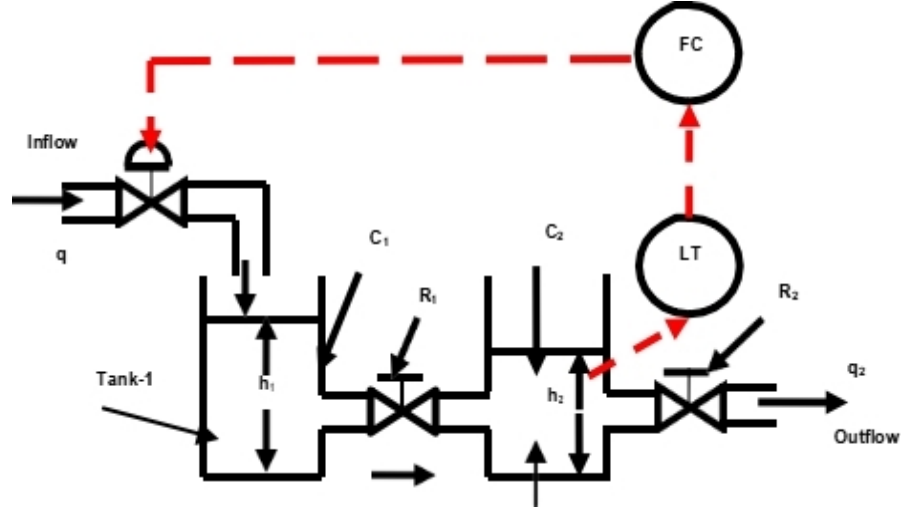


Fig. 3.8. Schematic of interacting tank level process.

Process specification [39] is given as in Table 3.2.

Table 3.2
Tank specification

| Parameter | Specification |
|---|---------------------------|
| D (Diameter) | 92 cm |
| H (Height) | 300 mm |
| q (Maximum flow in to tank 1) | 20 cm ³ /sec |
| C ₁ (Volume of tank 1) | 0.00948 cm ³ |
| C ₂ (Volume of tank 2) | 0.00475 cm ³ |
| R ₁ (Restriction parameter of storage chamber 1) | 10800 min/cm ² |
| R ₂ (Restriction parameter of storage chamber 2) | 10800 min/cm ² |

✧ *Modeling of System*

For tank 1:

$$C_1 \frac{dh_1}{dt} = q_1 - q, q = \frac{(h_1 - h_2)}{R_1} \quad (3.72)$$

$$C_2 \frac{dh_2}{dt} = q - q_2, q_2 = \frac{h_2}{R_2} \quad (3.73)$$

The overall IO model with dead-time is computed as

$$G(s) = \frac{10800 e^{-5s}}{5252.2s^2 + 256.28s + 10801} \quad (3.74)$$

Again, the overall transfer function is computed with 1st order pade approximation on delay time is shown as

$$G(s) = \frac{22500 s^2 - 27000s + 1080}{109042.08 s^4 + 1366.41 s^3 + 2839.9 s^2 + 27258.28 s + 10801} \quad (3.75)$$

Now, in the ADD...dialog, as shown in Fig. 3.9, the system should enter the following information to supply it as "G".

Create... — □ ×

System name:
G

Zero polynomial (e.g. s+1):
22500s^2-27000s+10800

Pole polynomial (e.g. -s^1.5-1):
64.41s^3+28394.9s^2+27258.28s+10801

Delay [sec]:
0

OK Cancel

Fig. 3.9. FOTF/IOTF entry dialog.

✧ Investigation, Tuning and design of Fractional Order PID (FOPID) Controller

The fundamental contrast between FOPID and IOPID schemes is already covered in the previous chapter's section 2.4.1, and the closed loop diagram employing FOMCON is displayed as illustrated in Fig. 3.10.

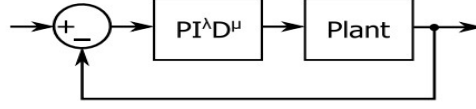


Fig. 3.10. Closed loop system using FOPID controller.

Obviously, when considering $\lambda = 1$ and $\mu = 1$, the result is IOPID controller. There are various fractional PID design strategies that vary depending on the plant that needs to be managed. So, in this study, first classical tuning technique is used to acquire integer-order PID parameters as the plant is described by a conventional system. The function of the FOPID controller is modified.

● IOPID Controller

In Fig. 3.11, a comparison of the two methods' FOMCON performances reveals that AMIGO tuning is favored over the Ziegler-Nichols (Z-N) approach for designing IOPID controllers.

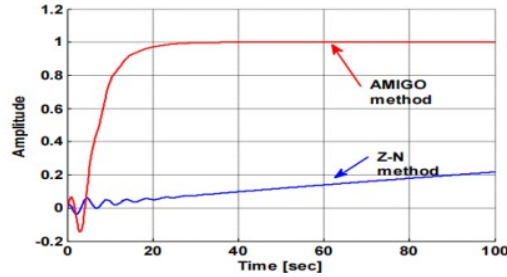


Fig. 3.11. Nominal outputs of AMIGO and Z-N methods.

The parameters of the system are determined using the two point curve fitting method. Astrom and Hagglund (AMIGO) [40] utilized this technique to obtain the FOPDT model as shown in Figs. 3.12 and 3.13. A static gain K ($K = 1.009$) is obtained by dividing the uniform output variation ratio by the step alteration. The step response's intercept of tangent is used to calculate the lag time ($L = 4.314$), and the difference between the lag time and the step response's time to reach a gain value of 0.63 is used to compute the time constant ($T = 0.06958$).

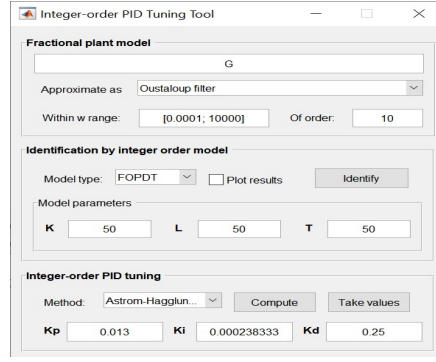


Fig. 3.12. IOPID design tool.

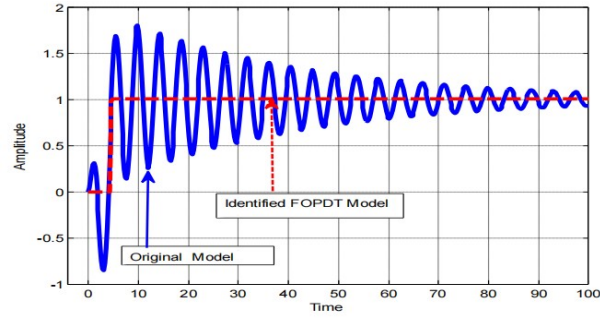


Fig. 3.13. Identified FOPDT model.

IOPID controllers are designed using the procedures listed below:

Step I: The transfer function is defined by $\frac{K e^{-L}}{T_s + 1}$, where K is the process gain, L is the delay time, and T is the time constant.

Step II: Identified by an integer order model that approximates the FOPDT model.

Step III: Tuning rules

$$\begin{cases} K_c = \frac{1}{K} (0.2 + 0.45 \frac{T}{L}) \\ T_i = \frac{0.4L + 0.8T}{L + 0.1T} L \\ T_d = \frac{0.5LT}{0.3L + T} \end{cases} \quad (3.76)$$

● FOPID Controller

As illustrated in Fig. 3.14, the FOPID design tool is opened by using the `fpid` command or by selecting Tools→Fractional PID design from the main GUI. For the traditional negative feedback unity system, it makes it possible to create a FOPID controller.

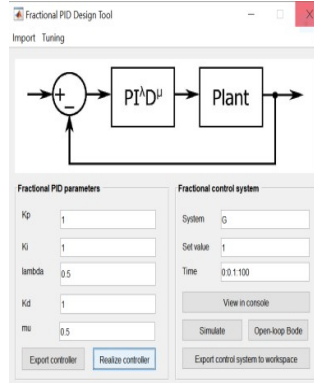


Fig. 3.14. FOPID design tool.

The differential equation for FOPID controller follows (2.103) in the previous chapter is shown as

$$U(t) = K_p e(t) + K_I D^{-\lambda} e(t) + K_D D^{\mu} e(t) \quad (3.77)$$

Applying the Laplace transform method on the above expression is shown by

$$U(s) = K_p E(s) + K_I s^{-\lambda} E(s) + K_D s^{\mu} E(s) \quad (3.78)$$

As shown in Fig. 3.15, the continuous Oustaloup filter approach is used in this work to approximate $s^{-\lambda}$ and s^{μ} and this method is commonly chosen over the G-L time domain method due to processing speed. Frequency ranges (ω_l, ω_h) are selected as $\omega_l = 10^{-3}$ and $\omega_h = 10^3$ and order (N) is selected as 5.

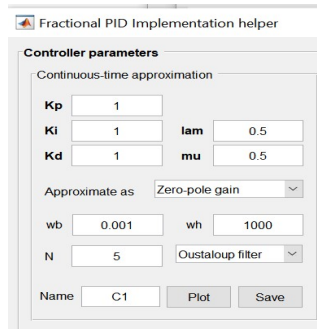


Fig. 3.15. Fractional order realization tool.

Due to its flexibility, an optimization tool is then utilized to determine the best parameters for both a FOPID and an IOPID controller. As seen in Fig. 3.16, the tool is accessible through the PID design tool menu *Tuning* \rightarrow *Optimize*.

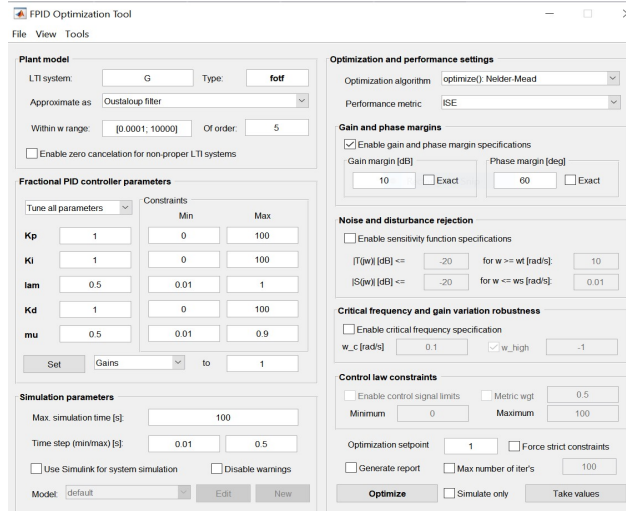


Fig. 3.16. Fractional order PID optimization tool.

● Optimization Method

Only Nelder-Mead and FMINCON are available as numerical optimization methods in the FOMCON toolkit, but Nelder-Mead is preferred in this study because it is a more computationally efficient method [41] compared to FMINCON (interior point or active set). It can lead to unpredictable regions using a single objective function with performance metrics like IAE, ISE, and it essentially employs the idea of simplex [41] to find the optimal value of a target function $f(x)$ with multiple variables, where simplex is a triangle with $n+1$ vertices. The three triangle vertices, designated as $f(x_G)$, $f(x_B)$ and $f(x_W)$, are contrasted using this procedure. Here, the triangle's good to worst points are x_G , x_B and x_W . After the iteration phase, the simplex approach minimizes the function by reflecting (R), expanding (E), contracting (C), and reducing (S). The base of a triangle (M) is determined for every vertex other than x_W .

- Reflection (x_R) = $M + \alpha(M - x_W)$, where $\alpha = 1$
- Expansion (x_E) = $M + \gamma(M - x_W)$, $\gamma = 2$
- Contraction (x_C) = $x_W + \beta(M - x_W)$, $\beta = 0.5$ or -0.5
- Reduction (x_S) = $(x_S + x_B)/2$

Fig. 3.17 illustrates the entire iteration procedure for determining the smallest function using a geometrical approach and designing an algorithm.

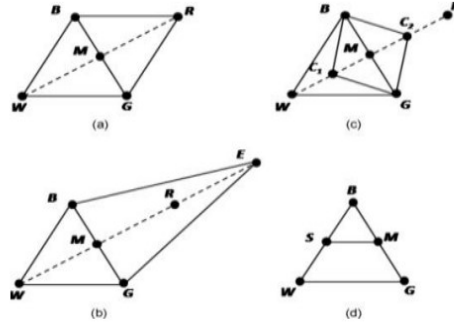


Fig. 3.17. Nelder-Mead local optimization algorithm step.

Steps

1. Order the vertices $x_B < x_G < x_W$. Compute centroid.
2. If $f(x_R) < f(x_B)$ then carry out either (R) reflect and (E) extend or (C) contract.
3. If $f(x_G) < f(x_R)$ then adopt x_R and evaluate.
4. If $f(x_R) < f(x_G)$ then $R \rightarrow E$ and evaluate x_E .
5. If $f(x_E) \leq f(x_R)$ then adopt x_E and select 1 else adopt x_R .
6. If $f(x_R) < f(x_W)$ then $x_W \rightarrow R$ and evaluate C with $\beta = 0.5$
7. If $f(x_R) \geq f(x_W)$ then C with $\beta = -0.5$
8. If $f(x_C) < f(x_W)$ then $x_W \rightarrow C$ else reduce.
9. Proceed to step 1 if the stopping criterion is not met, then continue.

✧ **Result**

Tables 3.3, 3.4, and 3.5, which includes all of the ideal settings for both controllers, respectively, shows the comparative performance of IOPID and FOPID controllers. This is shown in Figs. 3.18 and 3.19. For the IOPID controller, the minimal objective function $F(x)$ is 5.26, 5.57, and 14.06 under IAE, ISE, and ITSE. The best value objective function is $F(x)$ of 4.85 for the ISE metric, 5.22, and 13.34 under IAE, and ITSE error metrics are found for the FOPID controller are found for the FOPID controller.

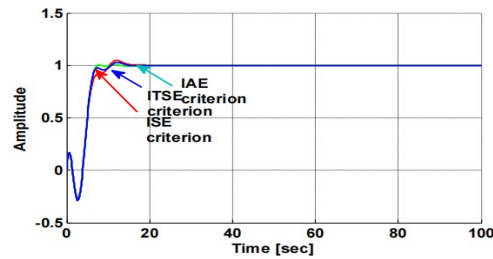


Fig. 3.18. Step response with IOPID controller.

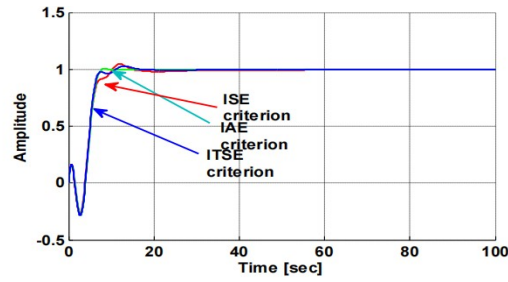


Fig. 3.19. Step response with FOPID controller.

Table 3.3

Optimal parameters and time domain metrics for IOPID controller

| Performance metric | K_P | K_I | K_D | Rise Time(s) | %Overshoot | Settling time(s) |
|--------------------|-------|-------|-------|--------------|------------|------------------|
| ISE | .3866 | .1823 | .2964 | 6.79 | 4.8 | 15.55 |
| IAE | .4286 | .1849 | .2841 | 6.10 | 0.5 | 17.16 |
| ITSE | .4151 | .1852 | .3083 | 6.33 | 2.4 | 17.85 |

Table 3.4

Optimal parameters for FOPID controller

| Performance metric | K_P | K_I | K_D | λ_m | μ |
|--------------------|-------|-------|-------|-------------|---------|
| ISE | .3296 | .2001 | .3149 | .96003 | 0.89803 |
| IAE | .3974 | .1868 | .2726 | .9955 | 0.9 |
| ITSE | .3517 | .1960 | .3161 | .97948 | .8375 |

Table 3.5

Time domain metrics for FOPID controller

| Performance metric | Rise time(s) | Settling time(s) | % overshoot |
|--------------------|--------------|------------------|-------------|
| ISE | 7.02 | 36.98 | 4.5% |
| IAE | 6.33 | 9.56 | 0.1% |
| ITSE | 6.33 | 16.01 | 2.4% |

Under the IAE performance metric, FOPID outperforms IOPID with a minimum overshoot of 0.1% and tracks the desired level at 9.56 seconds, but under ISE, IOPID outperforms FOPID with a rise time of 6.79 seconds and an extremely quick reach of the desired level, whereas FOPID requires quite more time to settle. Under the ITSE performance metric, both controllers exhibit nearly identical performance.

3.4.1.4 Stability Solution of FOTF

In comparison to IO systems, FO systems have a distinct stability assessment. The only approach for determining stability [42] for commensurate-order systems is currently available.

Although the Toolkit directly aids in stability determination, in this study the following analytical procedures are used to measure stability.

Condition I. If all the poles' absolute angles of λ in a commensurate order system with no time delay are larger than $\alpha\pi/2$, where $\lambda = s^\alpha$ then the system is stable [42]. Fig. 3.20 depicts the stable zone of the commensurate order system.

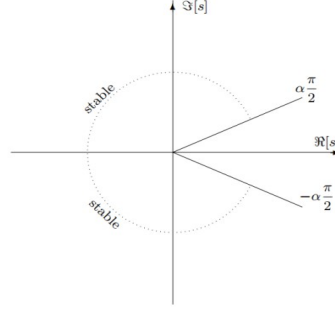


Fig. 3.20. Stable region for FOTF.

Condition II. For evaluating the stability [42] of FOTFs, the MATLAB function *isstable()* is used. The orders' greatest common factor is identified and indicated by α for a given FOTF. The minimum value of α is set to 0.01, making it possible to automatically create an approximation commensurate-order model without obtaining an excessively high-order system.

Condition III. The argument values of roots of polynomial of λ are computed and verified. The stability is made based on the position of the roots of λ . Using the command *isstable()* if return value is 1, then the system is said to be stable. To determine potential roots for a closed loop system's characteristic equation as $1 + G(s)C(s) = 0$ is evaluated under Riemann's principle [42] $-\pi < \arg(jw) < \pi$.

Now, the fractional order PID (FOPID) controller under ISE performance metric as stated in section 3.4.1.3 is established as follows:

$$C(s) = \frac{.3269 s^{.96003} + .2001 + .3149 s^{1.858}}{s^{.96003}} \quad (3.79)$$

The overall fractional order transfer function (FOTF) is developed using (3.75) and (3.79). The FOTF is investigated by the FOMCON toolkit as well, but in a more comprehensible manner.

The Overall transfer function is defined as

$$H(s) = \frac{3530.5 s^{.96003} + 3400.92 s^{1.858} + 216 .08}{5252.2 s^{2.96003} + 256.28 s^{1.96003} + 108 s^{.96003} + 3530.5 s^{.96003} + 3400.92 s^{1.858} + 216 .08} \quad (3.80)$$

Now, the aforementioned expression is transformed into the polynomial of λ with greatest common factor 0.01 as illustrated by

$$H(\lambda) = \frac{3530.5 \lambda^{96} + 3400.92 \lambda^{185} + 2161.08}{5252.2 \lambda^{296} + 256.28 \lambda^{196} + 10 \lambda^{96} + 353 \lambda^{96} + 3400.92 \lambda^{185} + 2161.08} \quad (3.81)$$

The characteristic equation using (3.80) is computed as

$$5252.2 \lambda^{296} + 256.28 \lambda^{196} + 10801 \lambda^{96} + 3530.5 \lambda^{96} + 3400.92 \lambda^{185} + 2161.08 = 0 \quad (3.82)$$

A method for establishing FOTF stability as described in (3.80) is also developed using the MATLAB code presented in Appendix A. After implementing the MATLAB statement, the value of K is obtained as 1 and the common factor is obtained as 0.01. So, the FOTF system is said to be stable. Now, following (3.82) one of the roots is also found as $|\arg(jw)| = 1.052$ which satisfies condition III with $1.052 < \pi$. The stable zone of the current system is shown as in Fig. 3.21.

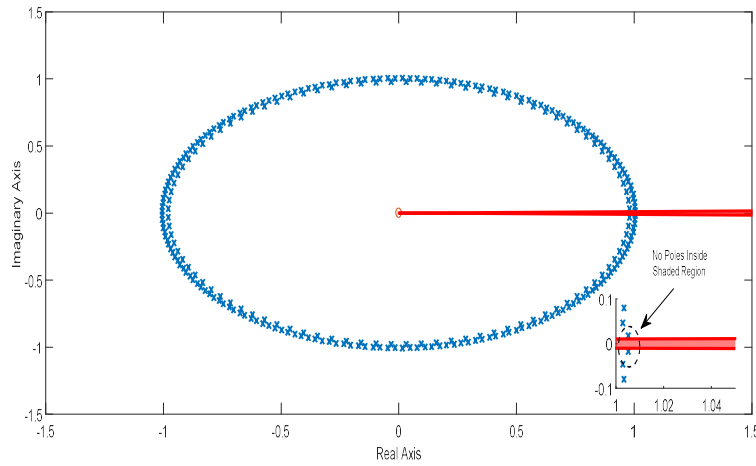


Fig. 3.21. Stability analysis for FOTF.

No poles are seen in the shaded area of Fig. 3.21, demonstrating the stability of the system. The FOMCON toolset discovers also the same stability performance. Similar to the above, it is possible to undertake a stability study of additional overall fractional order transfer functions under IAE and ITSE performance error metrics.

3.4.1.5 Limitation of FOMCON Toolkit

For the realization of a fractional operator, the FOMCON tool-set is only limited to time domain-based G-L fractional derivatives and frequency domain-based Oustaloup filter approximation methods.

The FOMCON toolkit only permits local optimization approaches, not global ones. Thus, achieving the best values for the controller is not always guaranteed by the local optimization strategy.

3.4.2 Investigation on Direct Continuous Laplace Analytical Solution

This section presents R-L fractional differ-integral and Caputo technique based time domain mathematical solutions to common fractional calculus problems. With the aid of the Laplace transformation and MLF function approaches, a closed-form analytical direct solution for linear FO processes with homogeneous and non-homogeneous forms is investigated. Linear FODE are the main governing equations for linear fractional-order systems, just like they are for conventional linear systems. First, Laplace transforms for specific functions are presented. Some important properties [43-45] of Laplace transform of R-L fractional differ-integral, Caputo fractional derivatives and MLF function are summarized as

- **Property I**

$$L(I^\alpha f(t)) = s^{-\alpha} F(s) \quad (3.83)$$

- **Property II**

$$L({}^{RL}_0 D_t^\alpha f(t)) = s^\alpha F(s) - \sum_{k=0}^{n-1} s^k {}^{RL}_0 D_t^{\alpha-k-1} f(0) \quad (3.84)$$

- **Property III**

$$L({}_0^C D_t^\alpha f(t)) = s^\alpha F(s) - \sum_{k=0}^{n-1} s^{\alpha-k-1} f^{(k)}(0) \quad (3.85)$$

- **Property IV**

$$L(t^{\beta-1} E_{\alpha,\beta}(\lambda t^\alpha)) = \frac{s^{\alpha-\beta}}{s^\alpha - \lambda} \quad (3.86)$$

3.4.2.1 R-L Based Linear Homogeneous Fractional Model Solution

First, a straightforward linear homogeneous R-L fractional differential equation is explored for the aim of solving the FODE. The Fractional differential equations are described as

$${}^{RL}_0 D_t^{0.5} y(t) + y(t) = 0, t > 0, 0 < \alpha < 1 \quad (3.87)$$

With initial condition as $[D^{-0.5} y(t)]_{t=0} = z$, The above expression is transformed using the Laplace method, as demonstrated by

$$L\{{}^{RL}_0 D_t^{0.5} y(t)\} + L\{y(t)\} = 0 \quad (3.88)$$

The above expression is transformed to FOTF using property II, as demonstrated by

$$s^{0.5} Y(s) - \sum_{k=0}^{n-1} s^k {}^{RL}_0 D_t^{0.5-k-1} y(0) + Y(s) = 0 \quad (3.89)$$

$$s^{0.5}Y(s) - s^0 {}^{RL}D_t^{0.5-1}(0) + Y(s) = 0 \quad (3.90)$$

$$s^{0.5}Y(s) - z + Y(s) = 0 \quad (3.91)$$

$$Y(s) = z \frac{1}{s^{0.5}+1} \quad (3.92)$$

Now, applying inverse Laplace transform into property IV it is shown by

$$L^{-1}\left\{\frac{s^{\alpha-\beta}}{s^{\alpha}-\lambda}\right\} = t^{\beta-1}E_{\alpha,\beta}(\lambda t^{\alpha}) \quad (3.93)$$

The above (3.92) is demonstrated by inverse Laplace transform as shown by

$$y(t) = z \cdot L^{-1}\left\{\frac{1}{s^{0.5}+1}\right\} \quad (3.94)$$

Now, comparing (3.93) and (3.94) it is computed as

$$\begin{cases} \alpha - \beta = 0 \\ \alpha = \beta = 1/2 \\ \lambda = -1 \end{cases} \quad (3.95)$$

So, the final approximated version of FODE with MLF function is realized by

$$y(t) = t^{-0.5}E_{0.5,0.5}(-1 \cdot t^{0.5}) \quad (3.96)$$

3.4.2.2 Caputo Based Linear Homogeneous Fractional Model Solution

Caputo linear homogeneous fractional differential equation is explored now for the aim of solving the FODE. The Fractional differential equations are described as

$${}_0^CD_t^{0.5}y(t) + y(t) = 0, t > 0, 0 < \alpha < 1 \quad (3.97)$$

With the initial condition as $y(0) = z$, the above expression is transformed using the Laplace method, as demonstrated by

$$L\{{}_0^CD_t^{0.5}y(t)\} + L\{y(t)\} = 0 \quad (3.98)$$

The above expression is transformed to FOTF using property III, as demonstrated by

$$s^{0.5}Y(s) - \sum_{k=0}^{n-1} s^{0.5-k-1} y^k(0) + Y(s) = 0 \quad (3.99)$$

$$s^{0.5}Y(s) - \sum_{k=0}^0 s^{0.5-k-1} y^k(0) + Y(s) = 0, n = 1 \quad (3.100)$$

$$s^{0.5}Y(s) - \sum_{k=0}^0 s^{0.5-1} y(0) + Y(s) = 0 \quad (3.101)$$

$$s^{0.5}Y(s) - z s^{0.5-1} + Y(s) = 0 \quad (3.102)$$

$$Y(s) = z \frac{s^{0.5-1}}{s^{0.5}+1} \quad (3.103)$$

Applying inverse Laplace transform into (3.103) it is shown by

$$y(t) = z L^{-1} \left\{ \frac{s^{0.5-1}}{s^{0.5}+1} \right\} \quad (3.104)$$

Now, using property IV and (3.104), it is computed as

$$\begin{cases} \beta = 1 \\ \lambda = -1 \end{cases} \quad (3.105)$$

So, the final approximated version of FODE using the MLF function is realized by

$$y(t) = z. E_{0.5,1} (-t^{0.5}) \quad (3.106)$$

Along with using fractional order 0.5, the effectiveness of the Caputo operator-based direct approximation method is examined using (3.106) with various orders, such as 0.6, 0.8, 0.9, and 1 as shown in Fig. 3.22. It is found that the approximated results attempt to lead to follow first order differential equation.

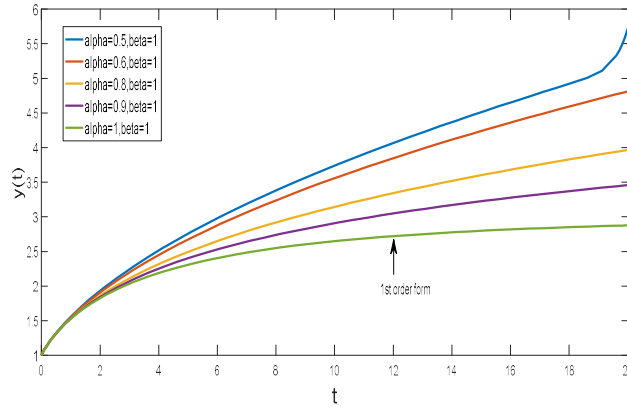


Fig. 3.22. Approximated outputs with different orders.

3.4.2.3 Caputo Based Non-Homogeneous Fractional Model Solution

Two terms non-homogenous fractional differential equation with Caputo operator is described as

$${}^C_0 D_t^{0.5} y(t) + {}^C_0 D_t^{0.8} y(t) = u(t), t > 0, 0 < \gamma < \mu < 1 \quad (3.107)$$

Where, $\alpha = 0.5$ and $\beta = 0.8$ with initial condition as $y(0) = K$.

Applying Laplace method into (3.107) it is demonstrated as

$$L\{{}^C_0 D_t^{0.5} y(t)\} + L\{{}^C_0 D_t^{0.8} y(t)\} = L\{u(t)\} \quad (3.108)$$

The above expression is transformed to FOTF using property III, as demonstrated by

$$s^{0.5} Y(s) - \sum_{k=0}^{n-1} s^{0.5-k-1} y^k(0) + s^{0.8} Y(s) - \sum_{k=0}^{n-1} s^{0.8-k-1} y^k(0) = U(s) \quad (3.109)$$

$$s^{0.5}Y(s) - \sum_{k=0}^0 s^{0.5-1} y(0) + s^{0.8}Y(s) - \sum_{k=0}^0 s^{0.8-1} y(0) = U(s), n = 1 \quad (3.110)$$

$$Y(s)[s^{0.5} + s^{0.8}] - y(0)[s^{0.5-1} + s^{0.8-1}] = U(s) \quad (3.111)$$

$$Y(s)[s^{0.5} + s^{0.8}] = U(s) + Z[s^{0.5-1} + s^{0.8-1}] \quad (3.112)$$

$$Y(s) = U(s) \cdot \frac{1}{s^{0.5} + s^{0.8}} + \frac{s^{0.5 \frac{1}{s} + s^{0.8 \frac{1}{s}}}}{s^{0.5} + s^{0.8}} \cdot Z \quad (3.113)$$

$$Y(s) = U(s) \cdot \frac{1}{s^{0.5} + s^{0.8}} + \frac{1}{s} Z \quad (3.114)$$

Now, applying inverse Laplace transform into (3.114) it is demonstrated by

$$y(t) = L^{-1}\{U(s) \cdot G(s)\} + Z \cdot (1) \quad (3.115)$$

$$\text{Where, } G(s) = \frac{1}{s^{0.5} + s^{0.8}}$$

The above FOTF is rewritten as

$$G(s) = \frac{1}{s^{0.5} \left(1 + \frac{s^{0.8}}{s^{0.5}}\right)} \quad (3.116)$$

$$G(s) = \frac{s^{-0.5}}{s^{0.8-0.5} + 1} \quad (3.117)$$

Applying again, inverse Laplace transforms into (3.117) it is demonstrated by

$$g(t) = L^{-1} \left\{ \frac{s^{-0.5}}{s^{0.8-0.5} + 1} \right\} \quad (3.118)$$

Now, comparing (3.118) with MLF function property IV it is computed as

$$\begin{cases} \alpha = 0.3 \\ \alpha - \beta = -0.5, \beta = 0.8 \\ \lambda = -1 \end{cases} \quad (3.119)$$

So, modified approximation of (3.118) with MLF function is evaluated as

$$g(t) = t^{-0.2} E_{0.5,0.8}(-1 \cdot t^{0.5}) \quad (3.120)$$

In light of the convolution property [46] demonstrated by the foregoing (3.115), convolution function of f and g as

● **Property V**

$$\begin{cases} f * g = \int_0^t f(t-\tau) g(\tau) d\tau \\ L(f * g) = F(s) G(s) \\ f * g = L^{-1}\{F(s) G(s)\} \end{cases} \quad (3.121)$$

So, (3.115) is rewritten as

$$y(t) = [g(t) * u(t)] + Z \quad (3.122)$$

Using the definition of a static function above (3.122) is rearranged as

$$y(t) = \int_0^t g(t-\tau)u(\tau)d\tau + Z \quad (3.123)$$

So, following (3.115), Eq.(3.123) is rewritten with modified approximation as

$$y(t) = \int_0^t (t - \tau)^{-0.2} E_{0.5,0.8} (-1. (t - \tau)^{0.5}) u(\tau) d\tau + Z \quad (3.124)$$

3.4.2.4 Limitation of Direct Laplace Method

Due to the lack of acceptable algebraic equation, the Laplace transform method is typically not very useful for nonlinear problems. It is discovered also from the above investigations that the issue of inverting the transform to resolve it arises when employing the Laplace transform for the FO derivative, but it is found also that the Laplace transform of a convolution is simply a product, which is useful. Although the Laplace transform approach is appropriate for solving constant coefficient fractional differential equations but also found that not all constant coefficient FODE can be solved by the Laplace method, since it requires forcing terms. In addition to requiring infinite approximation [46] at various time intervals, it also incurs higher computing costs. For some classes of unstable processes, this approach might not be appropriate.

3.4.3 Investigation on Indirect Continuous Analytical Solution

By replacing FO derivatives with their estimated models, approximation of fractional-order function is produced and employed exclusively for approximation modelling of original fractional-order models. This method leads to an approximate model whose response converges to a fractional order derivative element's response. Investigation on indirect approximation modelling is the subject of the current study. In control applications, the indirect approaches [33–35] are frequently used. Despite the fact that the Laplacian operator s is often raised to an integer order, i.e., s^2, \dots, s^n , it is technically valid to raise to a non-integer order s^α , where $0 < \alpha < 1$ as well; this represents a fractional order process. A fractional derivative according to R-L fractional derivatives as shown in (3.37) is represented as

$$D^\alpha f(t) = \frac{d^m}{dt^m} \frac{1}{\Gamma(m - \alpha)} \int_a^t (t - u)^{\alpha-1} f(u) du \quad (3.125)$$

Where $\Gamma(.)$ is the gamma function, and (3.125) is transformed using a Laplace transform with a zero initial condition to produce

$$L\{D^\alpha f(t)\} = s^\alpha F(s) \quad (3.126)$$

There are various engineering fields where this fractional Laplacian operator is useful. Therefore, approximations of integer order are utilized to realize the fractional Laplace sole operators ^{α} . Continued Fraction Expansions (CFEs) and various other rational techniques can be used to approximate s^α solely in a variety of ways. These approaches offer a wide range

of approximations with different orders and precision, with the accuracy and approximated frequency band growing with the order of the approximation. Research into indirect approximation methods is ongoing and some of the important indirect approximation techniques are investigated analytically in this research.

3.4.3.1 Oustaloup Rational Approximation Method

A technique called the Oustaloup approximation [34] uses an IO, correct model to explain FO systems. Digital filters are designed using this recursive approximation process. Oustaloup approximation [34] is demonstrated with the given form

$$G(s) = z \prod_{z=1}^N \frac{s + \omega'_z}{s + \omega_z} \quad (3.127)$$

Where, z is the gain, ω'_z and ω_z are periodic zero and pole frequencies.

The approximation model $G(s)$ contains $2N + 1$ zeros and poles, and frequencies are dispersed in geometric manner, hence the order of Oustaloup's model is odd number $n = 2N + 1$. This characteristic enables approximate Oustaloup models of odd order. The computation of the aforementioned parameters are already discussed in Eq.(9.9) under section 3.4.1.2. A crucial factor in achieving a better approximation of the Laplace fractional sole operator is frequency band selection. Usually, higher (ω_h) and lower (ω_l) frequencies are set as $\omega \in (100, 0.01)$ rad/sec. Table 3.6 shows the computation of different parameters with the third and fifth orders only of the model $s^{0.4}$ utilizing the aforementioned frequency ranges.

Table 3.6
Computation of parameters for third and fifth order approximation of Oustaloup model $s^{0.4}$

| N | ω_z | ω'_z | z |
|---|------------|-------------|---|
| 1 | .15848 | .63095 | 7 |
| 2 | 39810715.3 | 251886412.9 | 7 |

The approximate rational transfer functions of the aforementioned FO model is shown in Table 3.7.

Table 3.7
Approximated rational transfer function of Oustaloup model $s^{0.4}$

| N | Approximated transfer functions $G(s)$ |
|---|--|
| 1 | $\frac{6.31s^3 + 77.14s^2 + 41.74s + 1}{s^3 + 41.74s^2 + 77.14s + 6.31}$ |
| 2 | $\frac{6.31s^5 + 206.5s^4 + 924s^3 + 639.3s^2 + 68.37s + 1}{s^5 + 68.37s^4 + 639.3s^3 + 924s^2 + 206.5s + 6.31}$ |

Based on the aforementioned transfer function computations, the magnitude and phase effects are examined in Fig. 3.23.

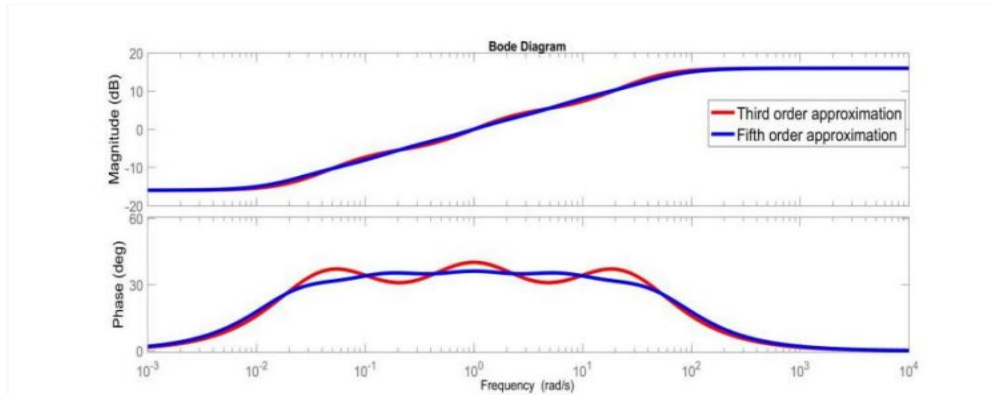


Fig. 3.23. Magnitude and phase effects of fractional order 0.4.

It is discovered that, within the aforementioned frequency band, higher order approximation has provided sharp gain and appropriate magnitude with less ripple. As shown in Fig. 3.24, changing the higher frequency range to 1000 rad/sec for 5th order approximation has a notable impact on magnitude and phase effects. This widens the frequency gap, but it also causes more ripples to appear, which has an impact on both amplitude and phase.

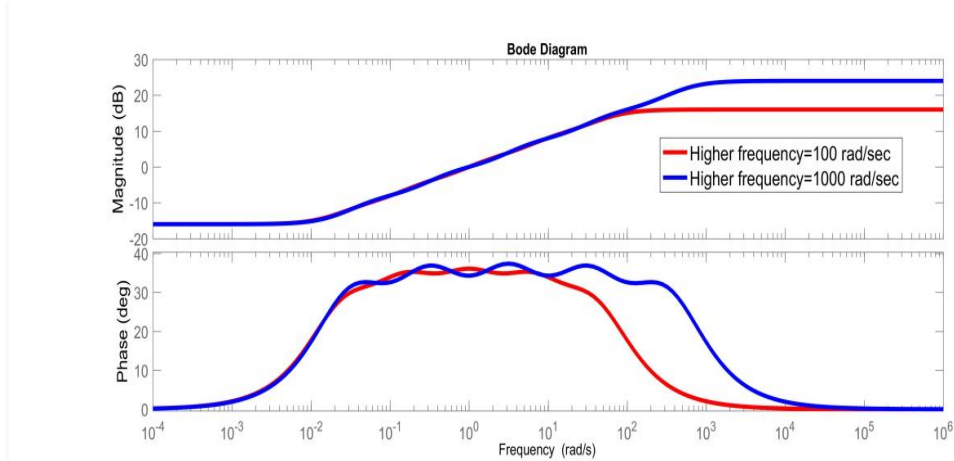


Fig. 3.24. Effect of magnitude and phase responses with higher frequency of 1000 rad/sec.

In Fig. 3.25, the phase and magnitude responses based on 3rd and 5th order approximations for the fractional integral model $s^{-0.4}$ are also examined.

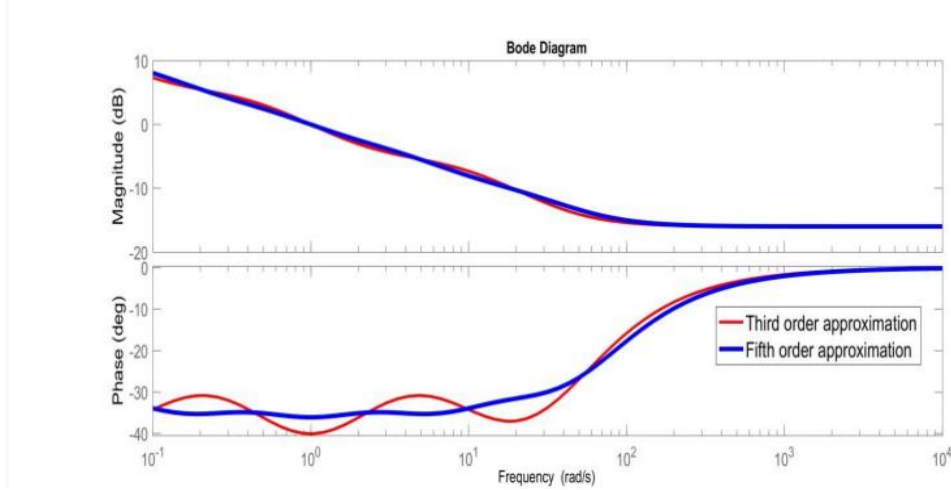


Fig. 3.25. Amplitude and phase outputs of model $s^{-0.4}$.

So even though the Oustaloup approximation method is a well-liked and low-complexity calculation approach, a significant downside is the restriction of model orders to odd numbers.

3.4.3.2 Continued Fraction Expansions (CFE) Approximation Method

In addition to the Oustaloup method of approximation, the CFE method [35] stretches the FO derivative s^α to an estimated IO by employing continuing fractions. The CFE strategy, which is essentially a series expansion technique, demonstrates traits like series expansion technique properties including truncation and recursive computation of series elements. To find the CFE of FO model, CFE of the term $(1+z)^\alpha$ is used [35] as

$$(1+z)^\alpha = 1 + \frac{\alpha z}{1 + \frac{(1-\alpha)z}{2 + \frac{(1+\alpha)z}{3 + \frac{(2-\alpha)z}{2 + \frac{(2+\alpha)z}{5 + \dots}}}}} = c_0 + \frac{d_1}{c_1 + \frac{d_2}{c_2 + \frac{d_3}{c_3 + \frac{d_4}{c_4 + \frac{d_5}{c_5 + \dots}}}}} \quad (3.128)$$

$$(1+z)^\alpha = c_0 + \frac{d_1}{c_1 +} \frac{d_2}{c_2 +} \frac{d_3}{c_3 + \dots} \quad (3.129)$$

Where, $c_0 = 1, c_j = 2, c_{j+1} = j + 1$ for $j = 2k, k \geq 1$ and $d_1 = \alpha z, d_j = (k - \alpha)z, d_{j+1} = (k + \alpha)z$

Now, $(1+z)^\alpha$ is truncated for computing first order approximation of fractional order derivative model as follows

$$(1+z)^\alpha \cong 1 + \frac{\alpha z}{1 + \frac{(1-\alpha)z}{2}} \cong \frac{2+(1+\alpha)z}{2+(1-\alpha)z} \quad (3.130)$$

Now, substituting, $z = s - 1$ first order and second approximation [35] are as follows

$$s^\alpha \cong \frac{(1+\alpha)s+(1-\alpha)}{(1-\alpha)s+(1+\alpha)} \quad (3.131)$$

$$s^\alpha \cong \frac{(\alpha^2+3\alpha+2)s^2+(-2\alpha^2+8)s+(\alpha^2-3\alpha+2)}{(\alpha^2-3\alpha+2)s^2+(-2\alpha^2+8)s+(\alpha^2+3\alpha+2)} \quad (3.132)$$

Following the above truncation, the 2nd, 3rd and 4th order approximation models can also be found and to compared with Oustaloup's fifth order approximation fourth, order CFE approximation [35] of fractional derivative $s^{0.4}$ is only demonstrated as

$$s^\alpha \cong \frac{(\alpha^4+10\alpha^3+35\alpha^2+50\alpha+20)s^4+(-4\alpha^4-20\alpha^3+40\alpha^2+320\alpha+384)s^3+(6\alpha^4-150\alpha^2+864)s^2+(-4\alpha^4+20\alpha^3+40\alpha^2-320\alpha+384)s+(\alpha^4-10\alpha^3+35\alpha^2-50\alpha+20)}{(\alpha^4-10\alpha^3+35\alpha^2-50\alpha+20)s^4+(-4\alpha^4+20\alpha^3+40\alpha^2-320\alpha+384)s^3+(6\alpha^4-150\alpha^2+864)s^2+(-4\alpha^4-20\alpha^3+40\alpha^2+320\alpha+384)s+(\alpha^4+10\alpha^3+35\alpha^2+50\alpha+20)} \quad (3.133)$$

$$s^{0.4} \cong \frac{26.26s^4+517.01s^3+840.15s^2+263.58s+8.98}{8.98s^4+26.26s^3+840.15s^2+517.01s+26.26} \quad (3.134)$$

Now, a significant comparison between the fifth order Oustaloup approximation and the fourth order CFE approximation [35] is made using the phase, magnitude and step responses in Fig. 3.26 and Fig. 3.27 respectively.

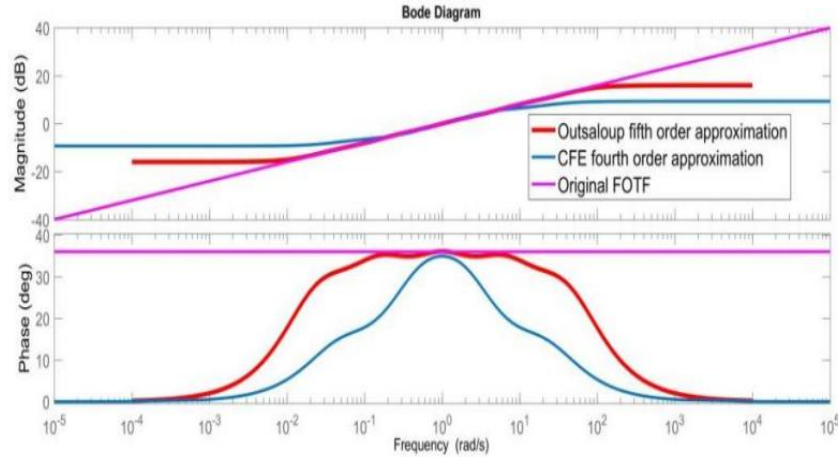


Fig. 3.26. Frequency domain outputs of ousaloup 5th order approximation, CFE 4th order approximation and model $s^{0.4}$.

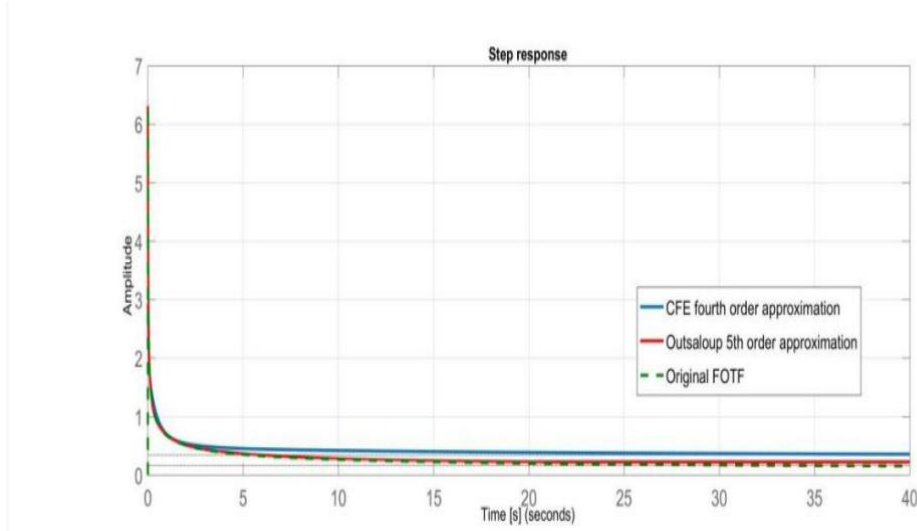


Fig. 3.27. Time domain outputs of model $s^{0.4}$.

It is found that, compared to time domain platforms, frequency domain platforms clearly study the behavior of approximated rational functions for irrational functions. While a higher order model requires more computing time, Fig. 3.26 illustrates that a 5th order approximation outperforms a CFE fourth order approximation in terms of the magnitude at 10.2 dB and phase of the original FO model. Though it is also observed that the CFE 4th order approximation is closer to the original model, it does not produce the desired sharp gain and flat magnitude output with a broad band gap. Another flaw in CFE is that it is not able to customize the frequency range of approximation. Therefore, it cannot be concluded that CFE approximation is a better method for computing fractional order processes.

Further research into improved alternative versions of rational approximation that can replace Oustaloup and CFE techniques is also required, as lower order approximation can perform with more accurate approximation than higher order model with less computing time.

3.4.3.3 Proposed Biquadratic Equiripple Approximation Method

According to [47], the biquadratic equiripple approximation method is a more advanced and efficient technique for realizing FO models. Based on 2nd order CFE approximation, it is modified by including tuning parameters [47] to minimize error ripples around an operational frequency.

$$s^{\pm\alpha} \cong \frac{c_0 s^2 + c_1 s + c_2}{c_2 s^2 + c_1 s + c_0}, 0 < \alpha \leq 1 \quad (3.135)$$

Where, $c_0 = (\alpha^2 + 3\alpha + 2)$, $c_2 = (\alpha^2 - 3\alpha + 2)$, and $c_1 = \{\beta(1 - \alpha^2) + 6\}$ are real constants. The ripple error can be changed by introducing β both the magnitude and phase

outputs. The addition of β places restrictions on the set of values that can produce more stable approximation. Fractional differentiator and integrator approximation are decided by the following conditions as demonstrated by (3.135).

$$\begin{cases} s^\alpha \rightarrow 0 < c_2 < c_0 \\ s^{-\alpha} \rightarrow 0 < c_0 < c_2 \end{cases}$$

In order to obtain more stable approximation it must choose [47] as

$$\beta > 6/\alpha^2 - 1 \quad (3.136)$$

Though the value of β as 3.83 is decided to produce a stable approximation, some other values are also investigated as illustrated in Fig. 3.28.

For approximating the same aforementioned fractional derivative model $s^{0.4}$, the value of alpha 0.4 is used to compute the required parameters to develop rational form. The parameters are obtained as $c_0 = 3.36$ and $c_2 = .96$ and c_1 is computed with different values of β as 3, 3.83 and 4 respectively as 8.52, 9.21 and 9.36. So, replacing the values of all parameters with different values of β (3.135) is rewritten as

$$\left\{ \begin{aligned} s^{0.4} &= \frac{3.36s^2 + 8.52 + .96}{.96s^2 + 8.52s + 3.36} \\ &\frac{3.36s^2 + 9.21 + .96}{.96s^2 + 9.21 + 3.36} \\ &\frac{3.36s^2 + 9.36 + .96}{.96s^2 + 9.36s + 3.36} \end{aligned} \right. \quad (3.137)$$

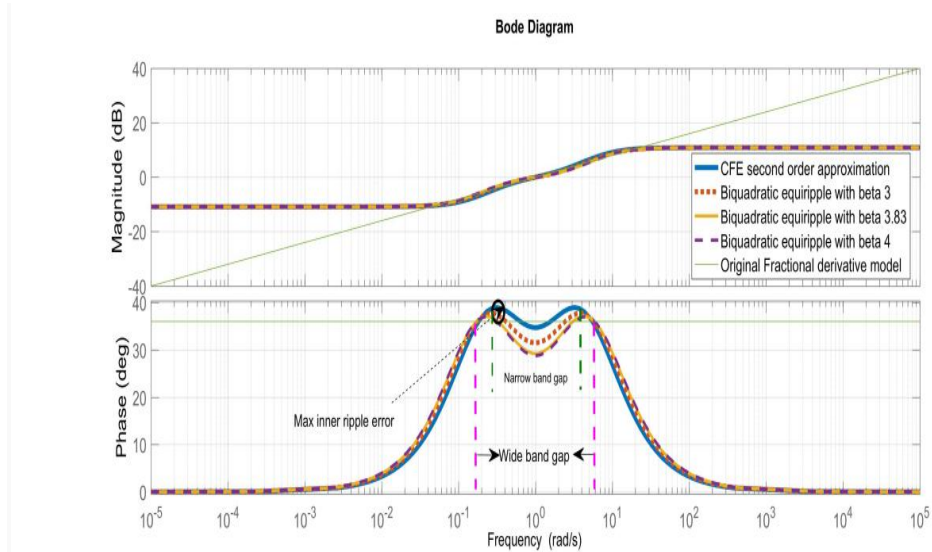


Fig. 3.28. Significant study on biquadratic equiripple method on FO model $s^{0.4}$.

Fig. 3.29 depicts that biquadratic equiripple technique gradually minimizes the maximum inner ripple error caused by CFE 2nd order approximation by selecting the values of β as 3.83,

which results in a more stable approximation of the original model with broad band gap frequency.

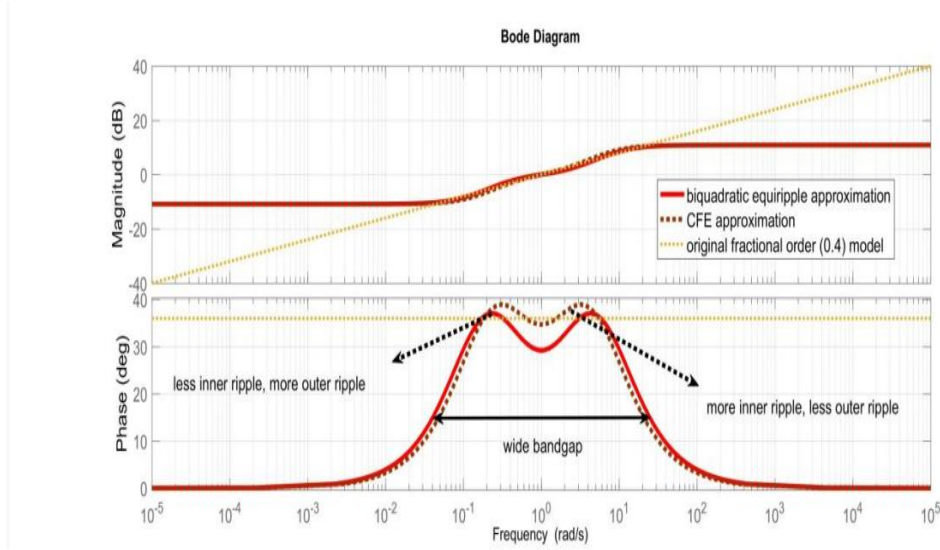


Fig. 3.29. Comparative study between CFE approximation and proposed biquadratic equiripple approximation methods.

Despite having a stable approximation, biquadratic equiripple approximation has a large outer ripple error in phase and also causes a very minor gain variation. Again, employing a lower order approximated transfer function to reduce outer ripple error with less phase variation and gain is a difficult operation. In order to improve the efficiency of the biquadratic equiripple strategy, another alternative exact phase approximation method is proposed to attain smooth approximation.

3.4.3.4 Proposed Biquadratic Exact Phase Approximation

Biquadratic approximation in (3.135) is further improved by ensuring

- Flat phase response at corner frequency (ω_c) is 1, i.e., $\arg\left\{G\left(\frac{s}{\omega_c}\right)\right\} = \frac{\alpha\pi}{2}, 0 < \alpha < 1$.
- Exact amplitude response at $\omega = 10\omega_c$. This can be obtained by forcing $\left|G\left(\frac{s}{\omega_c}\right)\right| = 10^\alpha$.

So, (3.135) is rewritten with corner frequency as

$$\left(\frac{s}{\omega_c}\right)^\alpha \cong \frac{c_0 s^2 + c_1 s \omega_c + c_2 \omega_c^2}{c_2 s^2 + c_1 s \omega_c + c_0 \omega_c^2} \quad (3.138)$$

For the aforementioned expression, the parameters [47] are computed as

$$\begin{cases} c_0 = (\alpha + 1)(\alpha + l) \\ c_2 = (\alpha - 1)(\alpha - l) \\ c_1 = (c_0 - c_2) \tan \frac{(2-\alpha)\pi}{4} \end{cases} \quad (3.139)$$

The aforementioned conditions for phase and amplitude can be satisfied by the parameters c_1 and l . l is a real constant and it can be computed by [47] the following formula

$$l = \left| \frac{-h - \sqrt{h^2 - 4ga}}{2g} \right| \quad (3.140)$$

Where,

$$g = [200 \left(\alpha \tan \frac{(2-\alpha)\pi}{4} \right)^2 + (100\alpha)^2 + 99^2](1 - 10^{2\alpha}) + 19998\alpha(1 + 10^{2\alpha}) \quad (3.141)$$

$$h = [600 \left(\alpha \tan \frac{(2-\alpha)\pi}{4} \right)^2 + (100\alpha)^2 + 99^2](1 - 10^{2\alpha}) + 19998\alpha(1 + 10^{2\alpha}) \quad (3.142)$$

$$a = 200 \left[\left(\alpha \tan \frac{(2-\alpha)\pi}{4} \right)^2 + 980\alpha^4 + 12000\alpha \right](1 - 10^{2\alpha}) + 19998\alpha^3(1 + 10^{2\alpha}) \quad (3.143)$$

Now, the value of l 4.3852 is obtained by replacing the aforementioned values in (3.140) by 0.4. Consequently, c_0 , c_2 and c_1 are calculated as 9.025, 3.545, and 16.88 respectively using the value of l . The influence of the modified biquadratic approximation technique—the precise phase approximation method—is now contrasted with the biquadratic equiripple approximation approach, as shown in Fig. 3.30. It displays a precise, steady phase approximation of $\pi/5$ at ω_c .

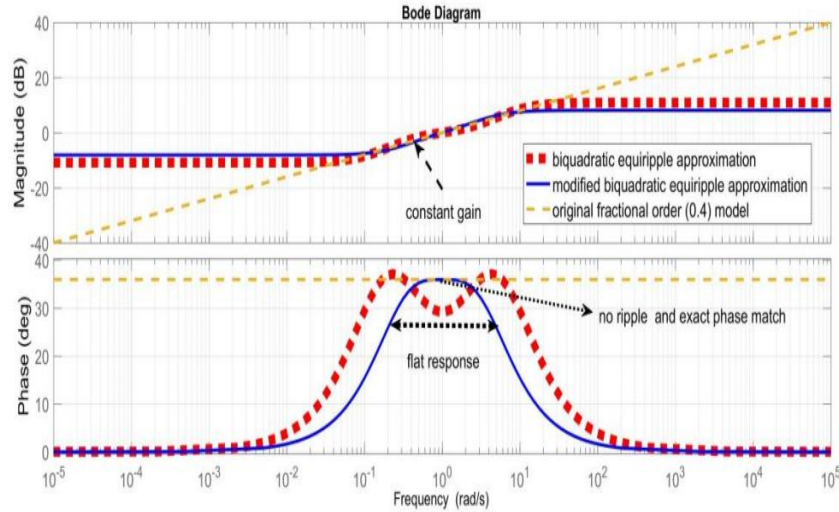


Fig. 3.30. Impact of modified biquadratic equiripple approximation method.

Consequently, it is shown in Fig. 3.31 that the modified biquadratic exact phase approximation approach entirely eliminates ripple on phase response and establishes no fluctuation, in contrast to the Oustaloup and CFE approximation methods. This establishes

that modified biquadratic exact phase lower order approximation is superior to higher order oustaloup approximation methods for approximating fractional order model.

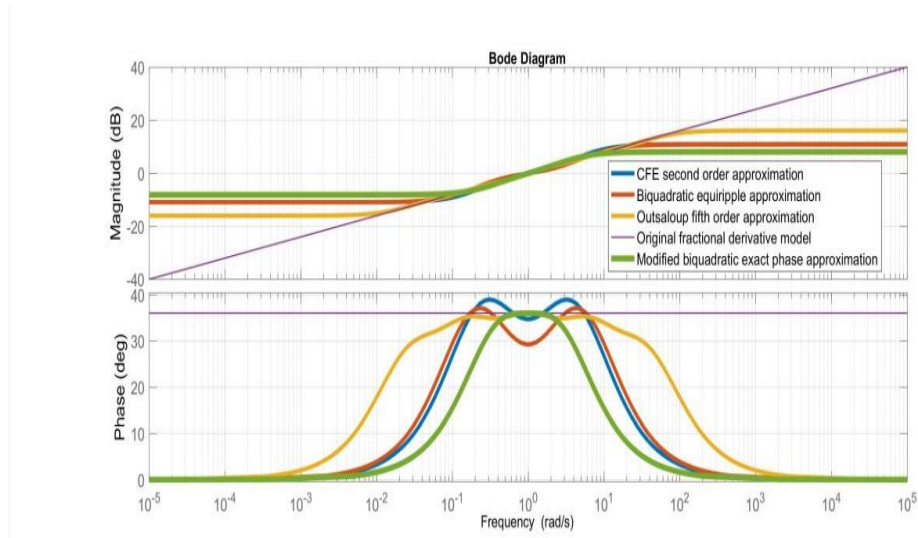


Fig. 3.31. Comprehensive analysis of the modified biquadratic equiripple precise phase method's performance.

However, it produces a tiny frequency band gap and Research is still in progress to find ways to make the performance even better with a larger frequency gap.

3.5 Summary

This chapter explores a significant application of fractional calculus with various fractional orders for a specific function in order to demonstrate its benefits over integer order calculus. With the use of FO differentiation and integration techniques, the deeper properties of a given function are investigated. With analytical and graphical representations, various fractional calculus techniques are proposed along with their applications to various functions. Using the FOMCON toolbox, a simple application of the Oustaloup recursive filter approximation, an indirect approximation technique, is explained for a typical second order plus delay time based model. Later, analytical solutions for several direct and indirect fractional order approximation strategies are put forth, and their significance in comparison to a toolkit is also explained unambiguously. A comparative analysis with some existing indirect approximations with lower and higher orders is investigated on a specific fractional order model under frequency domains in detail, along with an explanation of the advantages of the indirect method over the direct method. Using those techniques, ripples or oscillations are found. In order to investigate the performance in phase and magnitude in comparison with other methods such as Oustaloup or CFE techniques, a novel indirect approximation method known as modified biquadratic equiripple approximation method is recommended. This method appears at the smooth and flat response of gain or phase.

Therefore, this suggested method outperforms the alternatives and more gracefully approximates the model with a waveform that has sharp gain and a flat phase. Consequently, in our current research, the entire set of proposed fractional order control techniques makes use of this recommended technique to approximate various fractional orders.

References

- [1] H.M. Srivastava and R.K. Saxena, “Operators of fractional integration and their applications”, *Applied Mathematics and Computation*, 118(1), 1-52, 2001.
- [2] Samko, S, “Fractional integration and differentiation of variable order: an overview”. *Nonlinear Dyn*, 71, 653–662, 2013.
- [3] Ross, B, “A brief history and exposition of the fundamental theory of fractional calculus”. In: Ross, B. (eds) *Fractional Calculus and Its Applications*. Lecture Notes in Mathematics, 457, 1975, Springer, Berlin.
- [4] Bertram Ross, “The development of fractional calculus 1695–1900”, *Historia Mathematica*, 4(1), 75-89, 1977.
- [5] Rossikhin, Y.A and Shitikova, M.V, “Analysis of Dynamic Behaviour of Viscoelastic Rods Whose Rheological Models Contain Fractional Derivatives of Two Different Orders”. *Z. angew. Math. Mech.*, 81, 363-376, 2001.
- [6] Yuan, L and Agrawal, O.P, “A numerical scheme for dynamic systems containing fractional derivatives”, *J.Vib. Acoust*, 124(2), 321-324, 2002.
- [7] Bahuguna, D, “Integrodifferential equations with analytic semigroups”, *Journal of Applied Mathematics and Stochastic Analysis*, 16(2), 177-189, 2003.
- [8] Agrawal, O, “Application of fractional derivatives in thermal analysis of disk brakes. *Nonlinear Dyn*, 38, 191–206, 2004.
- [9] Saxena, R.K, and Kalla, S.L, “Solution of volterra-type integro-differential equations with a generalized lauricella confluent hypergeometric function in the kernels, *International Journal of Mathematics and Mathematical Sciences*, 2005.
- [10] Kilbas, A.A., Rivero, M, Rodríguez-Germá, L, and Trujillo, J.J, “Caputo linear fractional differential equations, *IFAC Proceedings*, 39(11), 52-57, 2006.

- [11] Yadav, R.K., Purohit, S.D., and Kalla, S., “On generalized weyl fractional q-integral operator involving generalized basic hypergeometric functions”, *Fractional Calculus and Applied Analysis*, 11(2), 129-142, 2008.
- [12] Srivastava, H.M., and Tomovski, Ž, “Fractional calculus with an integral operator containing a generalized Mittag-Leffler function in the kernel”, *Applied Mathematics and Computation*, 211(1), 198-210, 2009.
- [13] Herrmann, R., Fractional calculus: an introduction for physicists, *World Scientific*, 2011.
- [14] Changpin, L, Zhengang, Z, and Yang Q.C., “Numerical approximation of nonlinear fractional differential equations with subdiffusion and superdiffusion”, *Computers & Mathematics with Applications*, 62(3), 855-875, 2011.
- [15] Haubold, H.J., Mathai, A.M., and Saxena, R.K., “Mittag-Leffler functions and their applications”, *Journal of Applied Mathematics*, 2011.
- [16] Purohit, S.D., and Kalla, S.L., “On fractional partial differential equations related to quantum mechanics”, *Journal of Physics A: Mathematical and Theoretical*, 44(4), 2011.
- [17] Ansari, A, Darani, M.A., and Moradi, M., “On fractional Mittag-Leffler operators”, *Reports on Mathematical Physics*, 70(1), 119-131, 2012.
- [18] Prajapati, J.C., and Shukla, A.K., “Decomposition of generalized Mittag-Leffler function and its properties”, *Advances in Pure mathematics*, 2(1), 2012.
- [19] Kalla, S.L., Haidey, V., and Virchenko, N., “A generalized multiparameter function of Mittag-Leffler type”, *Integral Transforms and Special Functions*, 23(12), 901-911, 2012.
- [20] Odziejewicz, T., Malinowska, A.B., and Torres, D.FM., “Fractional variational calculus with classical and combined Caputo derivatives”, *Nonlinear Analysis: Theory, Methods & Applications*, 75(3), 1507-1515, 2012.
- [21] Faraj, A., Salim, T., Sadek, S., and Jamal, I., “Generalized Mittag-Leffler function associated with weyl fractional calculus operators”, *Journal of Mathematics*, 2013.
- [22] Srivastava, H.M., Gaboury, S., and Bayad, A., “Expansions formulas for an extended Hurwitz-Lerch zeta function obtained via fractional calculus”, *Advances in Continuous and Discrete Models*, 169, 2014.

- [23] Kumari, S.K., and Nambisan, V.T.M., “On some summation formulae for the I-function of two variables”, *Applications and Applied Mathematics: An International Journal*, 9(1), 2014.
- [24] Miller, S., and Ross, B., “An introduction to the fractional calculus and fractional differential equations”, *John Wiley & Sons Inc.*, New York, 1993.
- [25] Gutierrez, R.E., Rosario, J.M., and Machado, J.T., “Fractional order calculus: Basic concepts and engineering applications, *Mathematical Problems in Engineering*, 2010.
- [26] Hemalatha, S., and Anouncia, S.M., “G-L fractional differential operator modified using auto-correlation function: Texture enhancement in images”, *Ain Shams Engineering Journal*, 9(4), 1689-1704, 2018.
- [27] Machado, J.T., Fractional calculus: Application in modeling and control. In: constanda, C., Bodmann, B., Velho, H. (eds) *Integral Methods in Science and Engineering*. Birkhäuser, New York, 2013.
- [28] Gohar, M., Li, C. and Li, Z., “Finite difference methods for Caputo–Hadamard fractional differential equations”, *Mediterr. J. Math*, 17, 194, 2020.
- [29] Tepljakov, A., “Fractional-order PID controller design”, In: *Fractional-order modeling and control of dynamic systems*, Springer, 2017.
- [30] Das, S., Pan, I., “Fractional order system identification”, In: *Fractional order Signal Processing*, Springer Briefs in Applied Sciences and Technology. Springer, Berlin, Heidelberg.
- [31] El-Khazali, R., Batiha, I.M., Momani, S., “Approximation of fractional-order operators”, In: Agarwal, P., Baleanu, D., Chen, Y., Momani, S., Machado, J. (eds) *Fractional Calculus. ICFDA 2018. Springer Proceedings in Mathematics & Statistics*, vol 303. Springer, Singapore.
- [32] Khanra, M., Pal, J., and Biswas, K., “Rational approximation and analog realization of fractional order transfer function”. *Asian Journal of Control*, 15, 723-735, 2013.
- [33] Chen, Y.Q., Vinagre, B.M., and Pudlubny, I., “Continued fraction expansion approaches to discretizing fractional order derivative: An expository review”, *Nonlinear Dynamics*, 38, 155-170, 2004.

- [34] Deniz, F.N., Alagoz, B.B., Tan, N. and Koseoglu, M. “Revisiting four approximation methods for fractional order transfer function implementations: Stability preservation, time and frequency response matching analyses”, *Annual Reviews in Control*, 49, 239-257, 2020.
- [35] Bayat, F.M. “Rules for selecting the parameters of Oustaloup recursive approximation for the simulation of linear feedback systems containing $PI^\lambda D^\mu$ controller”, *Communications in Nonlinear Science and Numerical Simulation*, 17, 1852-1861, 2012.
- [36] Trigub, R.M., and Bellinsky, E.S., Discretization direct and inverse theorems of approximation theory. In: *Fourier Analysis and Approximation of Functions*. Springer, 2004.
- [37] Swarnakar, S., Sarkar, P., and Singh, L.J., “Direct discretization method for realizing a class of fractional order system in delta domain – a unified approach”, *Aut. Control Comp. Sci*, 53, 127–139, 2019.
- [38] X. -J. Wen, Z. -M. Wu and J. -G. Lu, "Stability Analysis of a Class of Nonlinear Fractional-Order Systems," in *IEEE Transactions on Circuits and Systems II: Express Briefs*, vol. 55, no. 11, pp. 1178-1182, Nov. 2008.
- [39] M. U. Khalid and M. B. Kadri, "Liquid level control of nonlinear Coupled Tanks System using linear model predictive control," *2012 International Conference on Emerging Technologies*, Islamabad, Pakistan, 2012, pp. 1-5.
- [40] Astrom and Hagglund, “Design of PID controllers based on constrained optimization,” *IEE Proc.: Control Theory Appl.*, 149(1), 32-40, 2014.
- [41] Koscianski, A., and Luersen, M., “Globalization and parallelization of nelder-mead and powell optimization methods,” In: Elleithy, K. (eds) *Innovations and Advanced Techniques in Systems, Computing Sciences and Software Engineering*. Springer, 2008.
- [42] Luo, X., “On the foundation of stability”, *Econ Theory*, 40, 185–201, 2009.
- [43] West, B.J., Bologna, M., Grigolini, P., “Fractional laplace transforms. In: *Physics of Fractal Operators. Institute for Nonlinear Science*, Springer, New York, 2003.
- [44] Brzeziński, D.W., Ostalczyk, P., “Numerical calculations accuracy comparison of the Inverse Laplace Transform algorithms for solutions of fractional order differential equations”, *Nonlinear Dyn*, 84, 65–77, 2016.

- [45] Meerschaert, M.M., Schilling, R.L., Sikorskii, A., “Stochastic solutions for fractional wave equations”, *Nonlinear Dyn*, 80(4), 1685–1695, 2014.
- [46] Badrieh, F., Properties of the fourier transforms. *In: Spectral, Convolution and Numerical Techniques in Circuit Theory*, Springer, Cham, 2018.
- [47] El-Khazali, R, “On the biquadratic approximation of fractional-order Laplacian operators”. *Analog Integr Circ Sig Process*, 82, 503–517, 2015.

Publication

D. Mukherjee, P.K. Kundu, A. Ghosh, “PID Controller Design for an Interacting Tank Level Process With Time delay Using MATLAB FOMCON Toolbox”, IEEE 2nd International Conference on Control, Instrumentation, Energy & Communication (**CIEC-2016**), ISSN:978-1-5090-0035-7, pp. 1-5, 2016.

CHAPTER 4

Fractional Order Standalone and Augmented Control Strategies for Inverted Pendulum

4.1 Introduction

Since nonlinear systems make up the majority of real-world practical models, adaptive identification and control for these models are active study fields. Feedback linearization techniques [1] are among the innovative adaptive control of nonlinear models' methods that are made possible. MRAC technique delivers a different solution for the nonlinear controller layout, which is an effective way for regulating the models with unpredictable variable and unmodeled errors by means of adaptive learning to account for the models' characteristic variations. A MRAC typically consists of three components: a reference model to generate the ideal signals, an identifier to figure out the system, and a controller to build the control rule using the identifier's data. However, the system's nonlinearity does not greatly profit from it, which has motivated of this chapter to find effective technique for unstable systems. The controller in the traditional MRAC rule is created to achieve the system response convergence to the ideal model output under the presumption that the system can be linearized. The technique is therefore successful in regulating a linear system with unpredictable variables, but it may not always be successful in controlling an unstable model with uncertain behaviors. It is clear from the literature review in chapter 2 that direct combination techniques, like MRAC-PID/FOPID [2–5], were reported by many experts who used the trial-and-error method or other optimization techniques to stabilize the under-actuated unstable model as an inverted pendulum towards its upright position. However, rather than relying on the Lyapunov stability rule of MRAC for the use of CSTR or inverted pendulum, the Massachusetts Institute of Technology (MIT) rule and its combination with fuzzy logic controller or sliding mode controller were primarily used. However, there is still no information available on the stability recovery method using a single MRAC based on MIT rule that is proposed in this chapter.

A linear proportional-derivative (PD)-like controller is employed with the MRAC-MIT tuning rule as a reliable solution for both of the nonlinear systems to assure the robustness of the

closed loop system. Moreover, the importance of MRAC-based Lyapunov stability rule over modified MIT rule is emphasized in this chapter, and the performance of stability is also tested by using linear PD controller with MRAC-Lyapunov rule. In addition to the conventional methods, the use of fractional order -based control techniques to stabilize these unstable systems and achieve acceptable closed-loop performances is growing in popularity. This is because it is very difficult to control an inverted pendulum system because of its upright posture, which is an unstable equilibrium. The key contribution of this research is the conversion of the traditional MRAC's MIT and Lyapunov stability rules into fractional order rules after developing the aforementioned technique with the use of PD controller. This chapter includes a brief discussion of mathematical modelling of traditional and fractional order control rules. Compared to PID controller design for unity feedback systems, there are comparatively fewer studies on multi-loop control structures. Multi-loop control techniques perform [6-7] somehow better than traditional single-loop control for processes that are unstable.

On fractional order dual-loop control techniques, there is a dearth of literature. Therefore, by adopting FO controllers, the closed-loop behaviors of the prevalent dual-loop control techniques on particular aforementioned unstable systems are yet to be explored. The effectiveness of fractional order based MRAC control rules compared to standard MRAC rules is examined in this chapter for the application of the inverted pendulum process. In addition to unity feedback schemes, a novel augmented version of MRAC rules with various controllers is also proposed. Even though the MRAC method is popular for handling noise, the unity feedback scheme may not always produce the desired results when there is noise and disturbance. On unstable processes, it can occasionally become involved in significant problems handling set-point and noise simultaneously. In order to fix this issue, an enhanced technique is proposed. 1 DOF FOPI, and 2 DOF FOPI control schemes are proposed to be augmented with FOMRAC rules. These are all intended to investigate the robust closed loop performance over unity feedback schemes. The main focus of the inquiry is on extensive simulation techniques to explore the efficacy of proposed control schemes. Quantitative analysis of all proposed approaches is conducted. Lower value of integral errors and total variation in control efforts is preferable.

4.2 Model Reference Adaptive Control (MRAC)

There are two different types of control systems utilized in engineering: conventional feedback control and adaptive control. Traditional feedback control systems are developed to reject the impact of disturbances on the controlled variables and return them to the target levels in accordance with a specific performance index. Contrarily, adaptive control systems

offer a systematic method [8] for automatic controller modification in real time to preserve a desired degree of efficacy when the parameter values of the plant dynamic model are unknown or change over time. The effectiveness is determined by the following factors:

- ✧ The required control loop performances should be specified.
- ✧ The controllable plant's dynamic architecture should be identified.
- ✧ A reliable controller design approach should be possessed that enables relevant plant model to behave as planned.
- ✧ Modelling of real-world systems is never without its uncertainties. Therefore, using the appropriate knowledge of the system, adaptation can lessen the uncertainties.

4.2.1 Description

When there are disruptions in the parameters, the system's performance is tracked by an adaptive control system [9] that includes a supplemental loop acting on the controller's adjustable parameters along with a feedback control with adjustable parameters. There are two loops in it. While the process must adhere to the ideal reference model in the external loop, the standard feedback process is found in the inner loop. To obtain the re-tuned control settings, the outputs of the process or plant (y) and the model (y_M) are contrasted, and the error function (e) is minimized using an appropriate optimization method [9] as illustrated in Fig. 4.1.

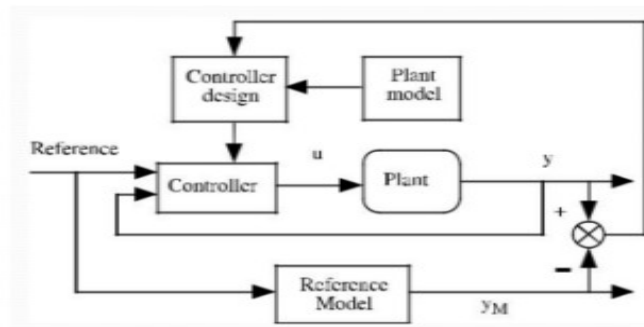


Fig. 4.1. Basic MRAC architecture.

The ideal model, which comprises of a realistic closed-loop description of how the process should react to a set-point alteration, is a critical part of the MRAC scheme. The reference model output is contrasted to the real process outcome, and the measured error is utilized to guide some adaptation strategy that triggers the controller settings to be manipulated in order to diminish error to zero. The adoption technique could be a control variable optimization method that diminishes the error metrics such as ISE, IAE etc. This is an adaptive control

strategy in which the performance specifications are expressed as a model. The model depicts the process's optimum reaction to a command input (u) as again illustrated in Fig. 4.2.

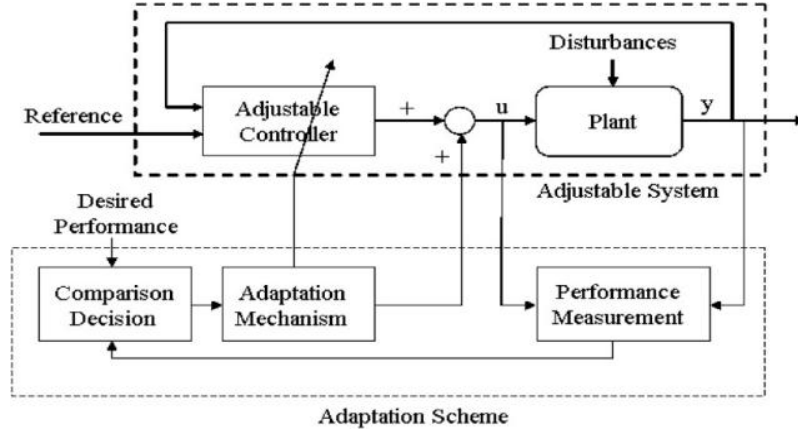


Fig. 4.2. Overview of adaptation strategy.

In an MRAC, there are two approaches for altering system parameters. In the next sections, each method's traditional and its transition into fractional technique formulation is addressed briefly.

4.2.2 Massachusetts Institute of Technology (MIT) Rule

Let e be the error between the ideal model and actual process outputs. Cost function [10] is set as

$$J(\theta) = \frac{1}{2} e^2 \quad (4.1)$$

Where, θ is vector of the controller, which must be influenced. To reduce J , it is fair to modify the parameters in the direction of J 's negative gradient as

$$\frac{d\theta}{dt} = -\gamma \frac{dJ}{d\theta} = -\gamma e \frac{de}{d\theta} \quad (4.2)$$

This is known as gradient method of MIT rule.

The term $\frac{de}{d\theta}$ is known as sensitivity derivative. It is thought to be a slower response to parameter changes than the other elements in the system. Then the sensitivity derivative can be computed by considering θ as a constant. However, if the controller's vector is undiscovered, the control scheme cannot be formulated; therefore, direct or indirect adaptive schemes, as discussed in chapter 2, aid in establishing an absolute identical strategy to replace the undiscovered element in the control rule with its estimated outcome. The MIT rule of the MRAC controller serves as the basic framework for direct adaptive control. In this scenario, the tracking target is stated with regard to rise time and peak overshoot; for a step input, it can

also be defined as the input-output characteristics of a transfer function. The controller is developed in such a way that the closed loop system has the required dynamic system behaviors for a real plant. As a result, the direct adaptive scheme is based on the fact that the disparity between the outcomes of the plant and the ideal model (referred to as plant-model error) is a function of the difference between the actual and desired performances. As shown in Fig. 4.1.a, the adaptation mechanism (later referred to as the parameter adaptation method) uses this data, together with additional data, to directly alter the controller's settings in real time in order to compel the process-model error to zero asymptotically. Now, using Figs.4.1.(a) and (b), feedforward adaptive gain (also known as an open loop scheme), and feedback-feedforward scheme with transformation into fractional order schemes are covered in the next sections.

4.2.2.1 Traditional Adaptation Scheme of Feedforward Gain

Let the actual plant or process be defined [9] as

$$Y(s) = cG(s) \quad (4.3)$$

Where, $G(s)$ is known but c is an unknown parameter. Now a feedforward control scheme is designed to yield a desired outcome as

$$Y_M(s) = c'G(s)U_c(s) \quad (4.4)$$

The controller is defined as

$$u(t) = \theta u_c \quad (4.5)$$

Applying Laplace transforms into (4.5) it is rewritten as

$$U(s) = \theta U_c(s) \quad (4.6)$$

So, using (4.6) the actual process is defined as

$$y(s) = cG(s)\theta U_c(s) \quad (4.7)$$

(4.6) provides the accurate $y_M(s)$ if $\theta = c'/c$.

Now, the error function is defined as

$$e(t) = y(t) - y_M(t) \quad (4.8)$$

(4.8) is rewritten with Laplace transform as

$$E(s) = cG(s)\theta U_c(s) - c'G(s)U_c(s) \quad (4.9)$$

Therefore, sensitivity derivative is computed as

$$\frac{de}{d\theta} = \frac{dE(s)}{d\theta} = cG(s)U_c(s) \quad (4.10)$$

Now, (4.10) is modified as

$$\frac{de}{d\theta} = \frac{dE(s)}{d\theta} = \frac{c}{c'} Y_M \quad (4.11)$$

Now, assuming c and c' as constants and applying MIT rule in (4.2) it is formulated as

$$\frac{d\theta}{dt} = -\gamma e Y_M \quad (4.12)$$

$$\theta = -\frac{\gamma}{s} e Y_M \quad (4.13)$$

The aforementioned process is referred to as the classic MIT rule of the MRAC scheme. First order, conventional MIT rule is defined clearly, and turning this rule into a fractional order scheme is given utmost priority in this chapter because it is crucial to investigate the behavior of an actual plant or process in greater depth in order to match the behaviour of the ideal model with more dependable and adaptable operation.

4.2.2.2 Proposed Fractional Adaptation Scheme of Feedforward Gain

The traditional MIT rules of the MRAC scheme are simply modified as

$$\frac{d^\alpha \theta}{dt^\alpha} = -\gamma e Y_M \quad (4.14)$$

$$\theta = -\frac{\gamma}{s^\alpha} e Y_M \quad (4.15)$$

The FOMIT rule of the MRAC scheme refers to the aforementioned differ-integral equation. The rational indirect solo approximation is used to solve the fractional integral operator $\frac{1}{s^\alpha}$ in (4.15) by using a biquadratic exact phase approximation methodology. The details of the analytical method are already provided in chapter 3. So, following (3.138) and (3.139) the adaptive gain method is modified as

$$\theta = -\gamma \frac{c_2 s^2 + c_1 s \omega_c + c_0 \omega_c^2}{c_0 s^2 + c_1 s \omega_c + c_2 \omega_c^2} e Y_M \quad (4.16)$$

$$\theta = -\gamma \frac{(\alpha-1)(\alpha-l)s^2 + (c_0 - c_2) \tan \frac{(2-\alpha)\pi}{4} s + (\alpha+1)(\alpha+l)}{(\alpha+1)(\alpha+l)s^2 + (c_0 - c_2) \tan \frac{(2-\alpha)\pi}{4} s + (\alpha-1)(\alpha-l)} e Y_M, \omega_c=1 \quad (4.17)$$

The aforementioned modified representation is referred to as the MRAC scheme's FOMIT rule. The open loop adaptive control strategies are shown in Fig. 4.3 and Fig. 4.4 by the obtained rules.

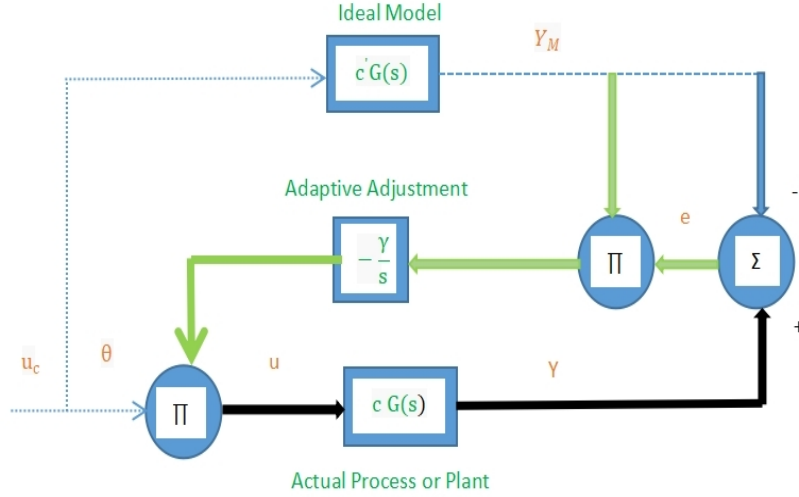


Fig. 4.3. Traditional adaptive feedforward scheme.

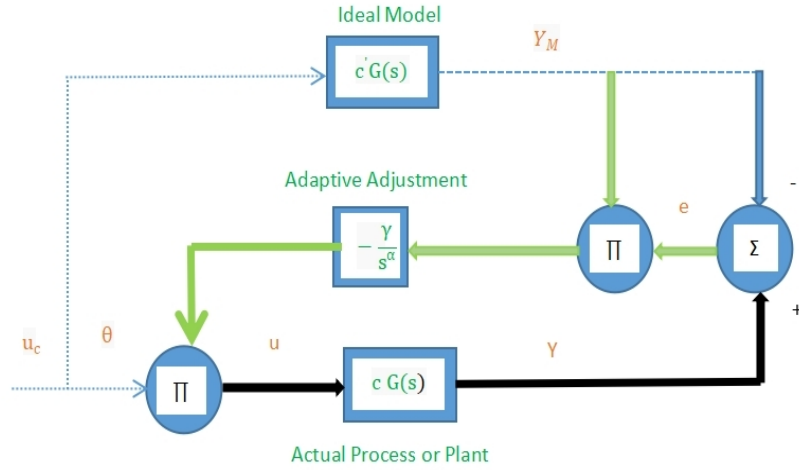


Fig. 4.4. Proposed fractional adaptive feedforward scheme.

Despite the fact that the aforementioned feedforward adaptive methods make it simple to control the process' transient behavior and steady state error, there are a few drawbacks [8-9] to employing the feedforward scheme that are stated as

- ✧ The system may not be stable (it may fluctuate or deviate substantially from the anticipated output), despite the same open-loop system being stable.
- ✧ To compare two states, an error detector is required.
- ✧ A change in an output will impact a system input.

In order to examine a robust solution for the process or plant, feedback strategy is therefore required in addition to the feedforward scheme as illustrated in Fig. 4.5.

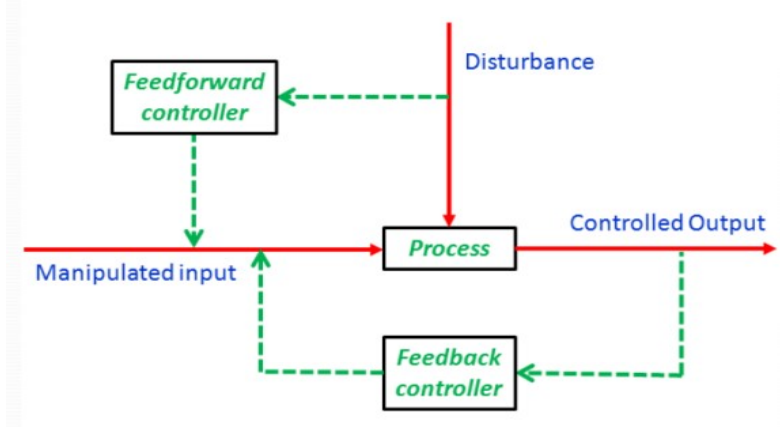


Fig. 4.5. Overview of feedback-feedforward control strategy.

Although there are closed loop schemes for only first order processes accessible in the literature [11], using closed loop MIT rule schemes to second order processes opens up new opportunities to examine control action. In order to create the closed loop conventional and fractional order MIT rules of the MRAC control scheme, second order model and plant are identified directly in accordance with the aforementioned real-time applications.

4.2.2.3 Closed Loop Traditional MIT Rule Formulation

Let the second order, actual plant or process is defined as

$$G_p = \frac{p}{q_1 s^2 + q_2 s + q_3} \quad (4.18)$$

A new version of the controller in (4.5) is constructed based on closed loop feedback technology as

$$u = \theta_1 u_c - \theta_2 Y \quad (4.19)$$

An error function between actual process and reference model is modified using (4.4) and (4.6) as

$$e = Y - Y_M \quad (4.20)$$

$$e = G_p u - G_m u_c \quad (4.21)$$

$$Y = G_p u \quad (4.22)$$

Using (4.18) and (4.19) in (4.22) it is shown as

$$Y = \frac{p}{q_1 s^2 + q_2 s + q_3} (\theta_1 u_c - \theta_2 Y) \quad (4.23)$$

$$Y = \frac{p}{q_1 s^2 + q_2 s + q_3} \theta_1 u_c - \frac{p}{q_1 s^2 + q_2 s + q_3} \theta_2 Y \quad (4.24)$$

$$Y + \frac{p}{q_1 s^2 + q_2 s + q_3} \theta_2 Y = \frac{p}{q_1 s^2 + q_2 s + q_3} \theta_1 u_c \quad (4.25)$$

$$Y(q_1 s^2 + q_2 s + q_3) + p \theta_2 Y = p \theta_1 u_c \quad (4.26)$$

$$Y = \frac{p \theta_1}{q_1 s^2 + q_2 s + q_3 + p \theta_2} u_c \quad (4.27)$$

Now, substituting (4.27) in (4.21) it is rewritten as

$$e = \frac{p \theta_1}{q_1 s^2 + q_2 s + q_3 + p \theta_2} u_c - G_m u_c \quad (4.28)$$

Now, the modified sensitivity derivatives are computed as

$$\frac{de}{d\theta_1} = \frac{p}{q_1 s^2 + q_2 s + q_3 + p \theta_2} u_c \quad (4.29)$$

$$\frac{de}{d\theta_2} = - \frac{p^2 \theta_1}{(q_1 s^2 + q_2 s + q_3 + p \theta_2)^2} u_c \quad (4.30)$$

Substituting (4.27) in (4.30) it is rewritten as

$$\frac{de}{d\theta_2} = - \frac{p}{q_1 s^2 + q_2 s + q_3 + p \theta_2} Y \quad (4.31)$$

If the reference model is reasonably close to the real process or facility, it can be roughly approximated as

$$q_1 s^2 + q_2 s + q_3 + p \theta_2 \cong q_{m_1} s^2 + q_{m_2} s + q_{m_3} \quad (4.32)$$

The sensitivity derivatives are now reorganized in relation to the ideal model as

$$\frac{de}{d\theta_1} = \frac{p_m}{q_{m_1} s^2 + q_{m_2} s + q_{m_3}} u_c \quad (4.33)$$

$$\frac{de}{d\theta_2} = - \frac{p_m}{q_{m_1} s^2 + q_{m_2} s + q_{m_3}} Y \quad (4.34)$$

Now, the modified traditional adaptive gain mechanism in (4.2) using the gradient approach is achieved as

$$\frac{d\theta_1}{dt} = -\gamma' \frac{de}{d\theta_1} e \quad (4.35)$$

$$\frac{d\theta_2}{dt} = -\gamma' \frac{de}{d\theta_2} e \quad (4.36)$$

$$\frac{d\theta_1}{dt} = -\gamma \left(\frac{q_{m_2} s + q_{m_3}}{q_{m_1} s^2 + q_{m_2} s + q_{m_3}} u_c \right) e \quad (4.37)$$

$$\frac{d\theta_2}{dt} = \gamma \left(\frac{q_{m_2} s + q_{m_3}}{q_{m_1} s^2 + q_{m_2} s + q_{m_3}} Y \right) e \quad (4.38)$$

$$\text{Where, } \gamma = \frac{\gamma' p}{q_{m_2} s + q_{m_3}}$$

$$\theta_1 = -\frac{\gamma}{s} \left(\frac{q_{m_2} s + q_{m_3}}{q_{m_1} s^2 + q_{m_2} s + q_{m_3}} u_c \right) e \quad (4.39)$$

$$\theta_2 = \frac{\gamma}{s} \left(\frac{q_{m_2}s + q_{m_3}}{q_{m_1}s^2 + q_{m_2}s + q_{m_3}} Y \right) e \quad (4.40)$$

The traditional modified MIT rule is now proposed into a closed loop FO scheme, as detailed in the section below.

4.2.2.4 Closed Loop Proposed Fractional Order MIT Rule Formulation

By utilizing (4.37) and (4.38) as the starting point, the traditional modified MIT rule is converted into a fractional order rule as

$$\frac{d^\alpha \theta_1}{dt^\alpha} = -\gamma \left(\frac{q_{m_2}s + q_{m_3}}{q_{m_1}s^2 + q_{m_2}s + q_{m_3}} u_c \right) e \quad (4.41)$$

$$\frac{d^\alpha \theta_2}{dt^\alpha} = \gamma \left(\frac{q_{m_2}s + q_{m_3}}{q_{m_1}s^2 + q_{m_2}s + q_{m_3}} Y \right) e \quad (4.42)$$

So, from (4.41) and (4.42) θ_1 and θ_2 are obtained as

$$\theta_1 = -\frac{\gamma}{s^\alpha} \left(\frac{q_{m_2}s + q_{m_3}}{q_{m_1}s^2 + q_{m_2}s + q_{m_3}} u_c \right) e \quad (4.43)$$

$$\theta_2 = \frac{\gamma}{s^\alpha} \left(\frac{q_{m_2}s + q_{m_3}}{q_{m_1}s^2 + q_{m_2}s + q_{m_3}} Y \right) e \quad (4.44)$$

With the assistance of (3.138) and (3.139), the aforementioned fractional order adaptive mechanisms are now updated as follows:

$$\theta_1 = -\gamma \left[\frac{(\alpha-1)(\alpha-l)s^2 + (c_0-c_2) \tan \frac{(2-\alpha)\pi}{4} s + (\alpha+1)(\alpha+l)}{(\alpha+1)(\alpha+l)s^2 + (c_0-c_2) \tan \frac{(2-\alpha)\pi}{4} s + (\alpha-1)(\alpha-l)} \right] \left(\frac{q_{m_2}s + q_{m_3}}{q_{m_1}s^2 + q_{m_2}s + q_{m_3}} u_c \right) e \quad (4.45)$$

$$\theta_2 = \gamma \left[\frac{(\alpha-1)(\alpha-l)s^2 + (c_0-c_2) \tan \frac{(2-\alpha)\pi}{4} s + (\alpha+1)(\alpha+l)}{(\alpha+1)(\alpha+l)s^2 + (c_0-c_2) \tan \frac{(2-\alpha)\pi}{4} s + (\alpha-1)(\alpha-l)} \right] \left(\frac{q_{m_2}s + q_{m_3}}{q_{m_1}s^2 + q_{m_2}s + q_{m_3}} Y \right) e \quad (4.46)$$

The closed loop traditional and fractional order MIT rules are illustrated in Fig. 4.6 and Fig.4.7.

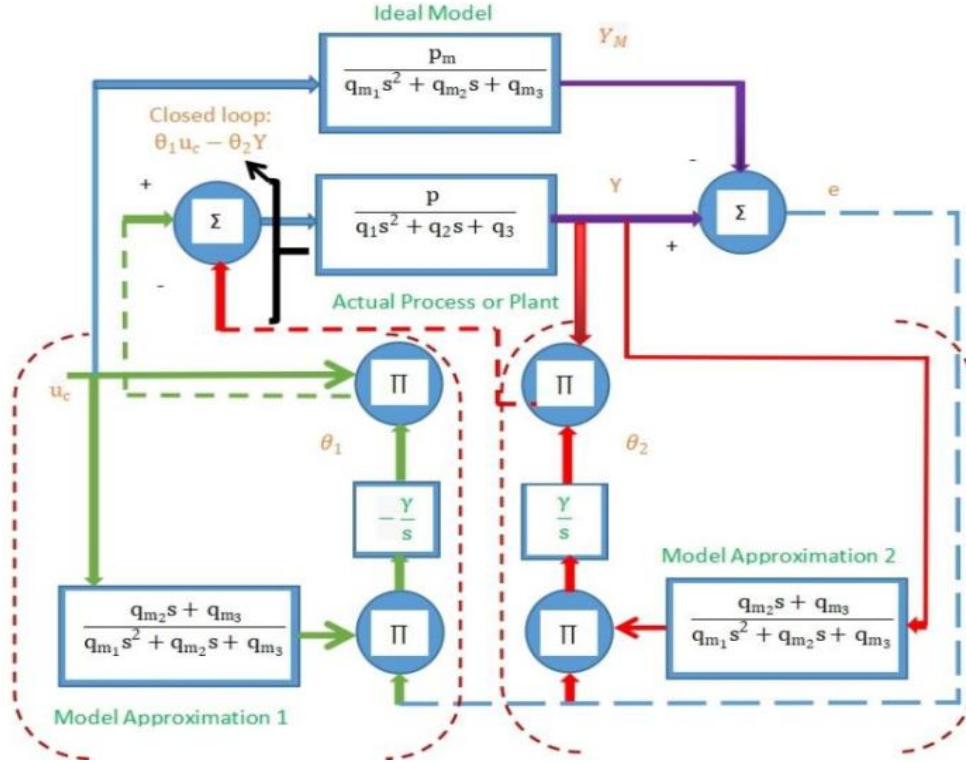


Fig. 4.6. Closed loop traditional MIT rule architecture.

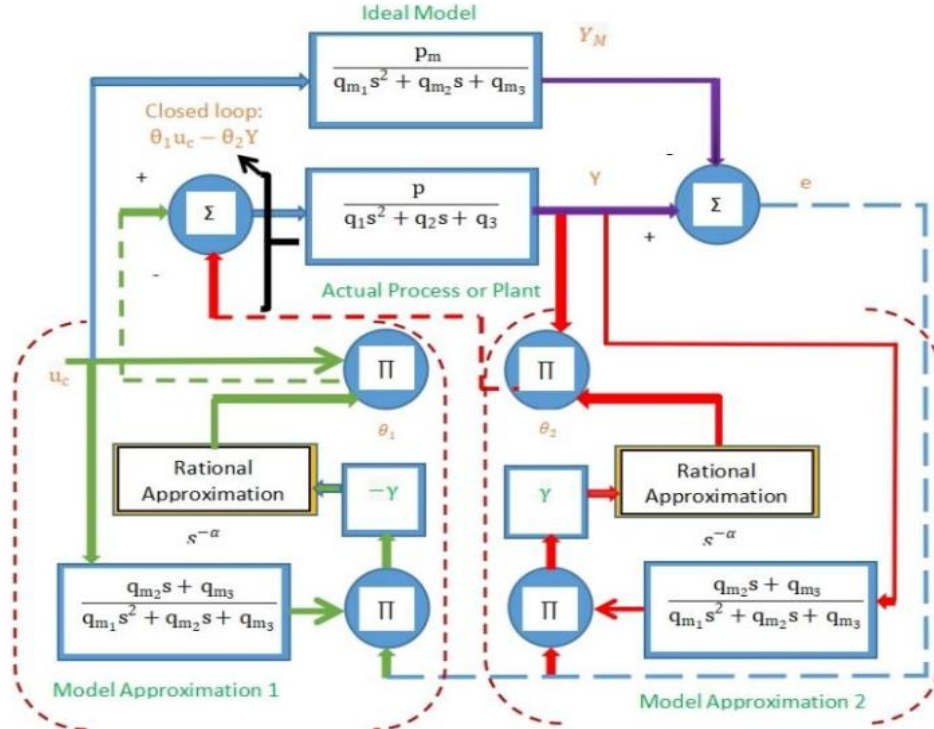


Fig. 4.7. Closed loop proposed fractional order MIT rule architecture.

The control rule is now modified to further strengthen the aforementioned traditional and fractional order feedback MIT rules because MIT rules do not always guarantee stability in unstable systems. The following section discusses the updated version of the MIT rules.

4.2.2.5 Modified proposed Fractional Order MIT Rule Formulation

The controller in (4.5) is proposed by integrating with the Proportional-derivative (PD) control scheme as

$$u(t) = \theta u_c(K_p + K_d s) \quad (4.47)$$

For the purpose of modifying the control law, the PD controller [12] is preferred over the PID controller because it has the potential to improve damping and overshoot, and diminish high-frequency noise. As a follow-up to the closed loop MIT rule, the control law in [4.19] is once more proposed as

$$u(t) = \theta_1 u_c(K_p + K_d s) - \theta_2 Y \quad (4.48)$$

The traditional law is revised as a result of the aforementioned method,

$$\theta_1 = -\frac{\gamma}{s} \left(\frac{q_{m_2}s + q_{m_3}}{q_{m_1}s^2 + q_{m_2}s + q_{m_3}} u_c[K_p + K_d s] \right) \quad (4.49)$$

$$\theta_2 = \frac{\gamma}{s} \left(\frac{q_{m_2}s + q_{m_3}}{q_{m_1}s^2 + q_{m_2}s + q_{m_3}} Y \right) e \quad (4.50)$$

Similar to this, the fractional order law is modified as

$$\theta_1 = -\frac{\gamma}{s^\alpha} \left(\frac{q_{m_2}s + q_{m_3}}{q_{m_1}s^2 + q_{m_2}s + q_{m_3}} u_c[K_p + K_d s] \right) e \quad (4.51)$$

$$\theta_2 = \frac{\gamma}{s^\alpha} \left(\frac{q_{m_2}s + q_{m_3}}{q_{m_1}s^2 + q_{m_2}s + q_{m_3}} Y \right) e \quad (4.52)$$

The closed loop fractional order MIT rule structure is updated as per the determined rules.

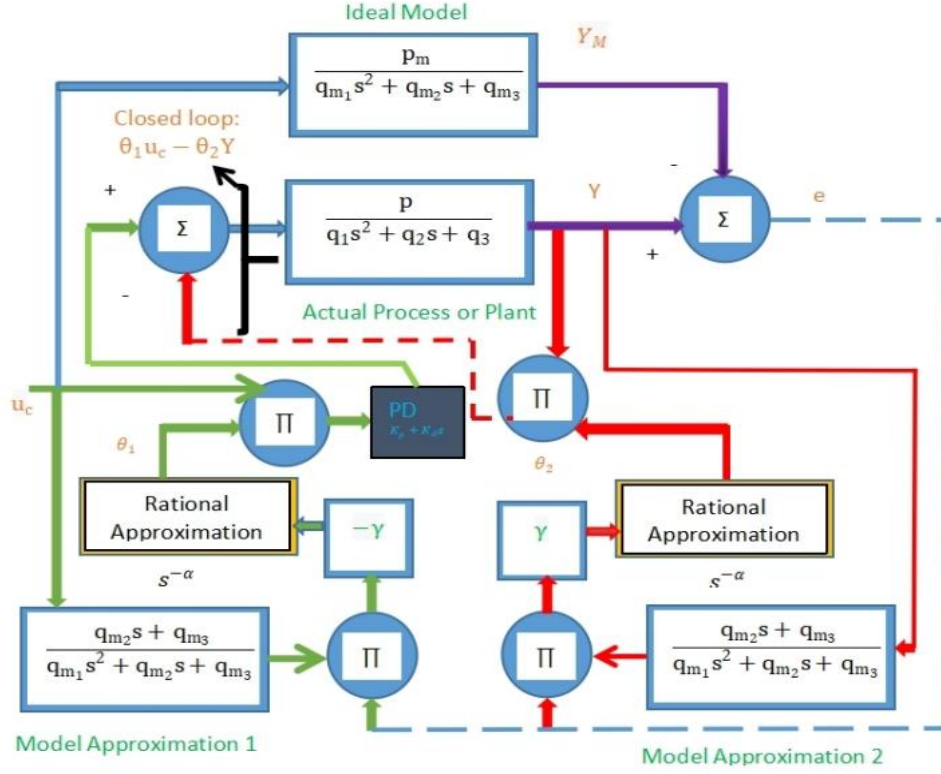


Fig. 4.8. Closed loop updated Fractional order MIT rule architecture.

If α is taken to be 1 in the structure above, it will be converted to the standard MIT rule. The aforementioned scheme is employed to investigate the performance of the inverted pendulum and CSTR. The significant application of the FOMIT rules is discussed in section 4.5. To attain a more stable result of the system, investigation is further carried out with the Lyapunov stability rule which modifies the MIT rule architecture with a simpler structure and aids to enhance stability by choosing appropriate Lyapunov function.

4.2.3 Lyapunov Stability Rule

Lyapunov stability theory [13–15] was approached as a robust method of revamping the adaptive scheme to ensure system stability. The modified laws are identical to the MIT rule, except instead of sensitivity functions, they use additional functions that are covered in the following sections.

Definition 1: The result $p(t) = 0$ is stable if given $\rho > 0$ there remains a number $\delta(\rho) > 0$ such that all solutions with initial circumstances

$\|p(0)\| < \delta$ have the property $\|p(t)\| < \rho$ for $0 \leq t < \infty$.

Definition II: An ever-differentiable function $V: \mathbb{Z}^n \rightarrow \mathbb{Z}$ is defined as positive definite in a region $U \subset \mathbb{Z}^n$ including the origin if

- $V(0) = 0$
- $V(p) > 0, p \in U, x \neq 0$

If $V(p) \geq 0$ then it is known as positive semidefinite.

Theorem I If there exists a function $V: \mathbb{Z}^n \rightarrow \mathbb{Z}$ that is positive definite such that

$\frac{dV}{dt} = \frac{dV^T}{dp} \frac{dp}{dt} = \frac{dV^T}{dx} f(p) = -K(p)$, represents negative semidefinite, then result $p(t) = 0$ is stable.

Furthermore, the finding is asymptotically stable if $\frac{dV}{dt}$ is negative definite.

4.2.3.1 Proposed Fractional Adaptation Feedforward Gain

The actual process, reference model, and controller are identified as follows, adopting the aforementioned Lyapunov stability scheme:

$$\dot{Y}(t) = -bY + lu \quad (4.53)$$

$$\dot{Y}_m(t) = -bY_M + l'u_c \quad (4.54)$$

$$\dot{Y}^{(\alpha)}(t) = -bY + lu \quad (4.55)$$

$$\dot{Y}_M^{(\alpha)}(t) = -bY_M + l'u_c \quad (4.56)$$

$$u(t) = \theta u_c \quad (4.57)$$

Same error function between actual process and ideal model is introduced as

$$e(t) = Y(t) - Y_M(t) \quad (4.58)$$

First order of derivatives is applied as follows: (4.58) as

$$\dot{e}(t) = \dot{Y}(t) - \dot{Y}_m(t) \quad (4.59)$$

Fractional order derivative is proposed as follows: (4.59) as

$$\dot{e}^{(\alpha)}(t) = \dot{Y}^{(\alpha)}(t) - \dot{Y}_M^{(\alpha)}(t) \quad (4.60)$$

Using (4.55-4.57) in (4.60) it is determined that

$$\dot{e}^{(\alpha)}(t) = -be + u_c(l\theta - l') \quad (4.61)$$

Now, to reduce the output error to zero, a common Lyapunov function $V(p)$ is suggested with the error function and controller vector using the following expression:

$$V(e, \theta) = \frac{1}{2}\gamma e^2 + \frac{l}{2}l\left(\theta - \frac{l'}{l}\right)^2 \quad (4.62)$$

The Lyapunov function's fractional order derivative is now defined as

$$\dot{V}^{(\alpha)}(t) = \gamma e[-be + u_c(l\theta - l')] + l\left(\theta - \frac{l'}{l}\right)\frac{d^\alpha \theta}{dt^\alpha} \quad (4.63)$$

$$\dot{V}^\alpha(t) = -\gamma be^2 + \gamma eu_c l\left(\theta - \frac{l'}{l}\right) + l\left(\theta - \frac{l'}{l}\right)\frac{d^\alpha \theta}{dt^\alpha} \quad (4.64)$$

$$\dot{V}^\alpha(t) = -\gamma be^2 + l\left(\theta - \frac{l'}{l}\right)\left(\gamma eu_c + \frac{d^\alpha \theta}{dt^\alpha}\right) \quad (4.65)$$

$\dot{V}^\alpha(t) < 0$, satisfies Theorem I which shows stability of the system. Now, from (4.62), fractional feedforward adaptive gain scheme is established following the aforementioned definitions in 4.2.3 as

$$\gamma eu_c + \frac{d^\alpha \theta}{dt^\alpha} = 0 \quad (4.66)$$

$$\frac{d^\alpha \theta}{dt^\alpha} = -\gamma eu_c \quad (4.67)$$

$$\theta = -\frac{\gamma}{s^\alpha} eu_c \quad (4.68)$$

As previously discussed in earlier sections, rational approximation is now used to present the feedforward gain as

$$\theta = -\gamma \frac{(\alpha-1)(\alpha-1)s^2 + (c_0-c_2) \tan \frac{(2-\alpha)\pi}{4} s + (\alpha+1)(\alpha+1)}{(\alpha+1)(\alpha+1)s^2 + (c_0-c_2) \tan \frac{(2-\alpha)\pi}{4} s + (\alpha-1)(\alpha-1)} e u_c \quad (4.69)$$

So, the fractional order feedforward adaptive gain structure is modified as per determined rule.

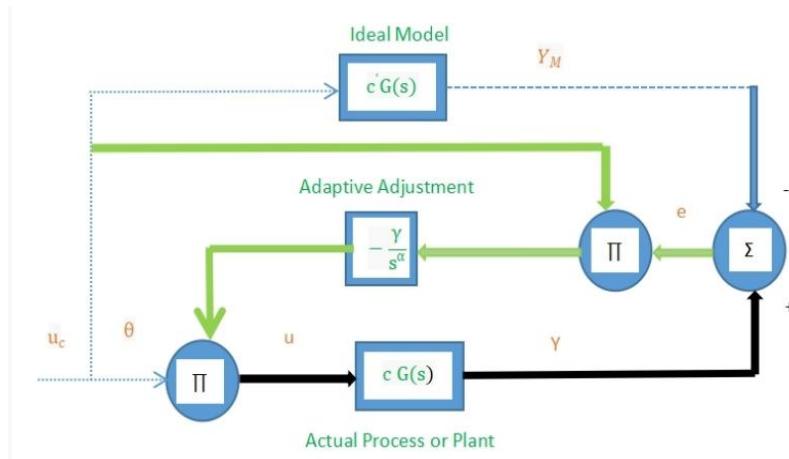


Fig. 4.9. Proposed fractional adaptive feedforward scheme using Lyapunov stability rule.

4.2.3.2 Closed Loop Modified Fractional Order Lyapunov Stability Rule

To design FOLY rule, the second order plant and ideal model are adopted as follows:

$$\frac{d^2 Y(t)}{dt^2} = -a \frac{dY(t)}{dt} - bY(t) + bu(t) \quad (4.70)$$

$$\frac{d^2 Y_M(t)}{dt^2} = -a_m \frac{dY_M(t)}{dt} - b_m Y_M(t) + b_m u(t) \quad (4.71)$$

The first-order plant and model are adopted as given below:

$$\frac{dY(t)}{dt} = -aY(t) + bu(t) \quad (4.72)$$

$$\frac{dY_M(t)}{dt} = -a_m Y_M(t) + b_m u(t) \quad (4.73)$$

The second order derivative is applied as follows: (4.58) as

$$\ddot{e}(t) = \ddot{Y}(t) - \ddot{Y}_M(t) \quad (4.74)$$

Following (4.70 - 4.74) second order derivative of error function is formulated as

$$\frac{d^2 e}{dt^2} = a^2 Y - abu - bY + bu + a_m^2 Y - a_m^2 e - a_m b_m u_c - b_m Y + b_m e + b_m u_c \quad (4.75)$$

$$\ddot{e}(t) = -e(a_m^2 - b_m) + Y_p(ab\theta_2 - b - b\theta_2 + a_m^2 - b_m) - u_c(ab\theta_1 - b\theta_1 + a_m b_m - b_m) \quad (4.76)$$

Now, an appropriate Lyapunov quadratic function is selected as

$$V(t) = \frac{1}{2} \left(e^3 + \frac{1}{\lambda(ab-b)} [(ab-b)\theta_2 + a_m^2 - b - b_m]^2 + \frac{1}{\lambda(ab-b)} [(ab-b)\theta_1 + a_m b_m - b_m]^2 \right) \quad (4.77)$$

Now, closed loop conventional Lyapunov rule is expressed using (4.77) as follows

$$\dot{V}(t) = -1.5e^2(a_m^2 - b_m) + \frac{3}{2\gamma} [(ab-b)\theta_2 + a_m^2 - b - b_m] \left(\frac{2}{3} \frac{d\theta_2}{dt} + eY_p \gamma \right) + \frac{3}{2\gamma} [(ab-b)\theta_1 + a_m b_m - b_m] \left(\frac{2}{3} \frac{d\theta_1}{dt} + eu_c \gamma \right) \quad (4.78)$$

Following (4.78) closed loop fractional Lyapunov rule is established as

$$\dot{V}^\alpha(t) = -1.5e^2(a_m^2 - b_m) + \frac{3}{2\gamma} [(ab-b)\theta_2 + a_m^2 - b - b_m] \left(\frac{2}{3} \frac{d^\alpha \theta_2}{dt^\alpha} + eY_p \gamma \right) + \frac{3}{2\gamma} [(ab-b)\theta_1 + a_m b_m - b_m] \left(\frac{2}{3} \frac{d^\alpha \theta_1}{dt^\alpha} + eu_c \gamma \right) \quad (4.79)$$

$\dot{V}^\alpha(t) < 0$, Satisfies Theorem I which shows stability of the system.

Now, the fractional adaptation law is established as

$$\theta_2 = -1.5e \frac{\gamma}{s^\alpha} Y_p \quad (4.80)$$

$$\theta_1 = 1.5e \frac{\gamma}{s^\alpha} u_c \quad (4.81)$$

Now, applying biquadratic equiripple approximation the aforementioned laws are obtained as follows

$$\theta_2 = -1.5 e \gamma \frac{(\alpha-1)(\alpha-l)s^2 + (c_0-c_2) \tan \frac{(2-\alpha)\pi}{4} s + (\alpha+1)(\alpha+l)}{(\alpha+1)(\alpha+l)s^2 + (c_0-c_2) \tan \frac{(2-\alpha)\pi}{4} s + (\alpha-1)(\alpha-l)} Y_p \quad (4.82)$$

$$\theta_1 = 1.5 e \gamma \frac{(\alpha-1)(\alpha-l)s^2 + (c_0-c_2) \tan \frac{(2-\alpha)\pi}{4} s + (\alpha+1)(\alpha+l)}{(\alpha+1)(\alpha+l)s^2 + (c_0-c_2) \tan \frac{(2-\alpha)\pi}{4} s + (\alpha-1)(\alpha-l)} u_c \quad (4.83)$$

So, closed loop fractional order Lyapunov rule scheme is designed as per determined rule.

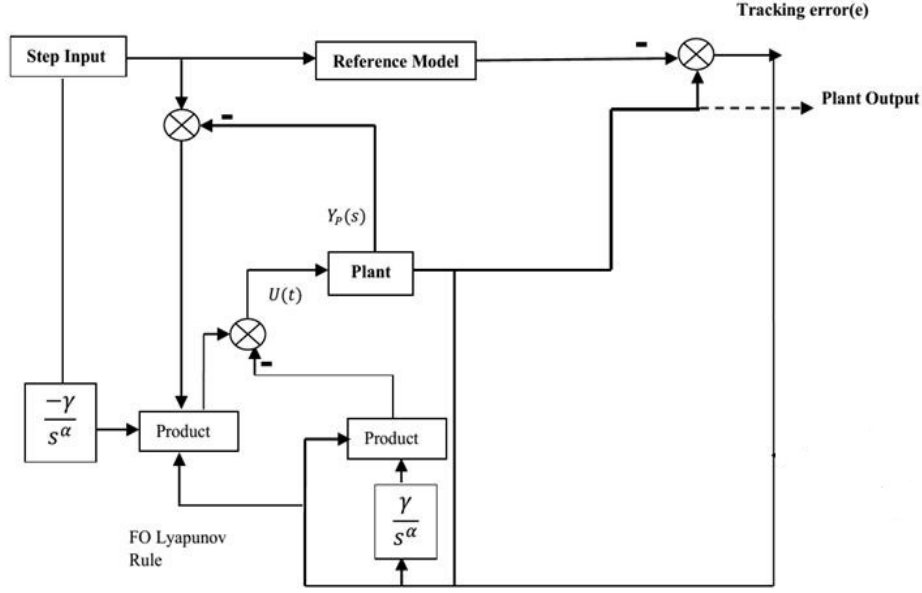


Fig. 4.10. Closed loop proposed fractional Lyapunov stability architecture.

In section 4.4, the significant application of this design is discussed in relation to error measurements that can ensure the system's consistent performance. PD feedback laws, like the FOMIT rule that was previously discussed in section 4.2.2.5, have since further modified the aforementioned rule, and the resulting architecture is depicted in Fig. 4.11. FOLY itself has the capability of controlling the system more steadily as discussed in section 4.4, but still, the aforementioned rule has been further modified by PD feedback laws. The effectiveness of the redesigned topology's control must also be examined, and section 4.4 explores the use of the updated architecture on another benchmark model.

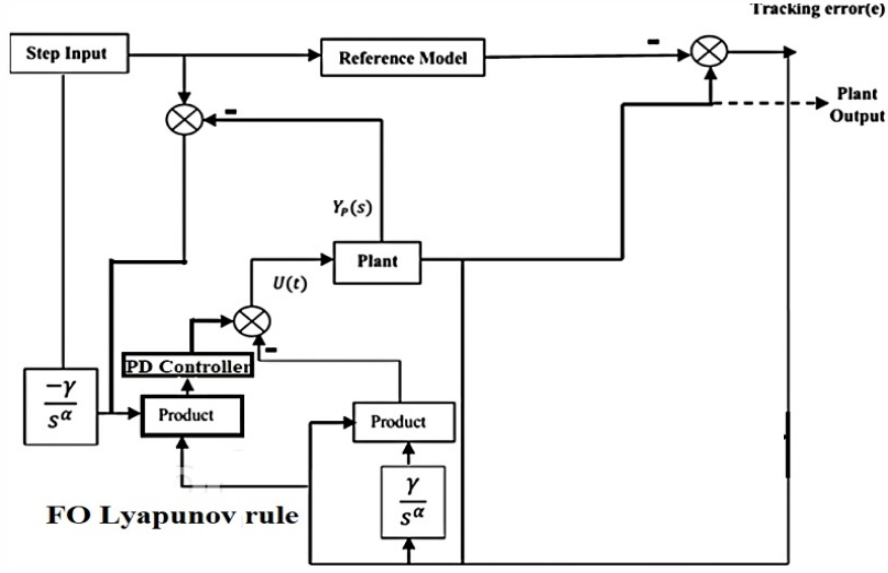


Fig. 4.11. Closed loop proposed a fractional modified FOLY scheme.

The aforementioned law in (4.83) is further modified as

$$\theta_1 = -1.5e\gamma \frac{(\alpha-1)(\alpha-l)s^2 + (c_0 - c_2) \tan \frac{(2-\alpha)\pi}{4} s + (\alpha+1)(\alpha+l)}{(\alpha+1)(\alpha+l)s^2 + (c_0 - c_2) \tan \frac{(2-\alpha)\pi}{4} s + (\alpha-1)(\alpha-l)} u_c [K_p + K_d s] \quad (4.84)$$

The effectiveness of augmented approaches on unstable processes must be thoroughly investigated in addition to stand-alone strategies, and no widespread use of fractional augmented schemes has been investigated. Though some 1 DOF based controllers such as PID or FOPID were frequently employed with traditional MRAC schemes and produced desirable results, enhancing the control action with lower error metrics is the primary goal of employing a fractional augmented scheme. In this chapter, 2 DOF method is also adopted along with 1 DOF method and detailed proposals are presented in the following sections.

4.3 Fractional Order Augmented Strategies

Due to high stability region and suitability for nonlinear systems, FOPI controller has been chosen over FOPID controller [16] for augmenting with proposed FO schemes. So, the significant application of 1 DOF and 2 DOF FOPI schemes with the FOMRAC rules are yet to be explored.

4.3.1 Proposed FOMIT-FOPI augmented control scheme

The FOPI controller is defined as follows:

$$C(s) = K_p + \frac{K_I}{s^\lambda} \quad (4.85)$$

By subtracting the output of the FOPI control method from the output of the FOMIT, an additional modification to the FOMIT rule of the MRAC controller is established as shown below:

$$U(t) = \theta_1 u_c - \theta_2 Y_P - \left(K_p + \frac{K_I}{s^\lambda} \right) \quad (4.86)$$

$$U(t) = -\frac{\gamma}{s^\alpha} \left(\frac{q_{m2}s + q_{m3}}{q_{m1}s^2 + q_{m2}s + q_{m3}} u_c [K_p + K_d s] \right) e - \frac{\gamma}{s^\alpha} \left(\frac{q_{m2}s + q_{m3}}{q_{m1}s^2 + q_{m2}s + q_{m3}} Y_P \right) e - \left(K_p + \frac{K_I}{s^\lambda} \right) \quad (4.87)$$

4.3.2 2 DOF FOPI Control Strategy

The quantity of independently controllable closed-loop transfer functions is referred to as the degree of freedom of any control method. Servo controllers may not always produce satisfactory regulatory action, and vice versa, for servo controllers. Due to the fact that 1 DOF control method cannot satisfactorily satisfy these two needs at the same time. According to reports, a 2-DOF control strategy produces more effective servo and regulatory actions than a 1-DOF scheme [17-19]. In other words, the 2-DOF approach results in improved disturbance rejection without appreciable increases in peak overshoot during set point shift. The control action of a normal FOPI controller is as shown below:

$$U(s) = K_p E_P(s) + \frac{K_I}{s^\lambda} E_I(s) \quad (4.88)$$

For 2 DOF FOPI controller, error terms of proportional and integral action are as follows:

$$E_P(s) = bR(s) - Y(s) \quad (4.89)$$

$$E_I(s) = R(s) - Y(s) \quad (4.90)$$

where, $R(s)$ is the reference signal, $Y_P(s)$ is the output signal and b is the proportional set point weighting parameter. Since the integral term's error term is not weighted, steady state error is eliminated, unlike the proportional term. Therefore, the expression for 2DOF FOPI control action becomes as follows:

$$U(s) = (K_{P1} * b + \frac{K_{I1}}{s^\lambda}) R(s) - \left(K_{P2} + \frac{K_{I2}}{s^\lambda} \right) Y(s) \quad (4.91)$$

4.3.3 Proposed FOMIT-2 DOF FOPI augmented control scheme

A novel combination of control algorithms is proposed by subtracting the output of 2-DOF FOPI from (4.87) from that of FOMIT modified control law in (4.48) as follows:

$$u(t) = [\theta_1 u_c (K_p + K_d s) - \theta_2 Y_P] - \left[\left(K_{P1} * b + \frac{K_{I1}}{s^\lambda} \right) R(s) - \left(K_{P2} + \frac{K_{I2}}{s^\lambda} \right) Y(s) \right] \quad (4.92)$$

Using (4.51) and (4.52) it is obtained as

$$u(t) = -\frac{\gamma}{s^\alpha} \left(\frac{q_{m2}s + q_{m3}}{q_{m1}s^2 + q_{m2}s + q_{m3}} u_c [K_p + K_d s] \right) e - \frac{\gamma}{s^\alpha} \left(\frac{q_{m2}s + q_{m3}}{q_{m1}s^2 + q_{m2}s + q_{m3}} Y_p \right) e - [(K_{p1} * b + \frac{K_{I1}}{s^\lambda}) R(s) - (K_{p2} + \frac{K_{I2}}{s^\lambda}) Y(s)] \quad (4.93)$$

The control architecture of the proposed FOMIT-FOPI/2DOF FOPI is illustrated in Fig. 4.12.

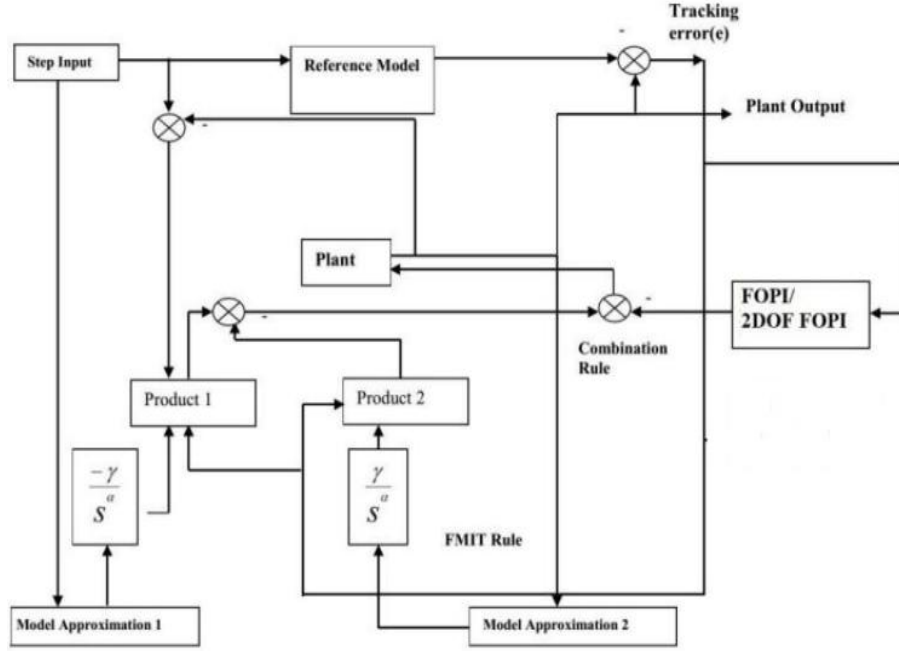


Fig. 4.12. Proposed FOMIT-FOPI/2 DOF FOPI augmented scheme.

4.3.4 Proposed FOLY-FOPI/2 DOF FOPI augmented control schemes

A novel combination of stability rules is developed by augmenting the FOPI controller's rule with the FOLY rule as follows:

$$V^\alpha(t) = -1.5e^2(a_m^2 - b_m) + \frac{3}{2\gamma} [(ab - b)\theta_2 + a_m^2 - b - b_m] \left(\frac{2}{3} \frac{d^\alpha \theta_2}{dt^\alpha} + eY_p \gamma \right) + \frac{3}{2\gamma} [(ab - b)\theta_1 + a_m b_m - b_m] \left(\frac{2}{3} \frac{d^\alpha \theta_1}{dt^\alpha} + eu_c \gamma \right) + (ab - b) \left(K_p + \frac{K_I}{s^\lambda} \right) \quad (4.94)$$

Using (4.82) and (4.83) control law is found as

$$u(t) = -1.5e\gamma \frac{(\alpha-1)(\alpha-l)s^2 + (c_0 - c_2) \tan \frac{(2-\alpha)\pi}{4} s + (\alpha+1)(\alpha+l)}{(\alpha+1)(\alpha+l)s^2 + (c_0 - c_2) \tan \frac{(2-\alpha)\pi}{4} s + (\alpha-1)(\alpha-l)} u_c - 1.5e\gamma \frac{(\alpha-1)(\alpha-l)s^2 + (c_0 - c_2) \tan \frac{(2-\alpha)\pi}{4} s + (\alpha+1)(\alpha+l)}{(\alpha+1)(\alpha+l)s^2 + (c_0 - c_2) \tan \frac{(2-\alpha)\pi}{4} s + (\alpha-1)(\alpha-l)} Y_p - \left(K_p + \frac{K_I}{s^\lambda} \right) \quad (4.95)$$

Similarly, augmenting 2DOF-FOPI with FO-Lyapunov rule, the following equation is computed:

$$V^\alpha(t) = -1.5e^2(a_m^2 - b_m) + \frac{3}{2\gamma} [(ab - b)\theta_2 + a_m^2 - b - b_m] \left(\frac{2}{3} \frac{d^\alpha \theta_2}{dt^\alpha} + eY_p \gamma \right) + \frac{3}{2\gamma} [(ab - b)\theta_1 + a_m b_m - b_m] \left(\frac{2}{3} \frac{d^\alpha \theta_1}{dt^\alpha} + eu_c \gamma \right) + (ab - b) \left[(K_{p1} * b + \frac{K_{I1}}{s^\lambda}) R(s) - (K_{p2} + \frac{K_{I2}}{s^\lambda}) Y(s) \right] \quad (4.96)$$

$$u(t) = -1.5\epsilon\gamma \frac{(\alpha-1)(\alpha-l)s^2 + (c_0 - c_2) \tan \frac{(2-\alpha)\pi}{4} s + (\alpha+1)(\alpha+l)}{(\alpha+1)(\alpha+l)s^2 + (c_0 - c_2) \tan \frac{(2-\alpha)\pi}{4} s + (\alpha-1)(\alpha-l)} u_c - 1.5\epsilon\gamma \frac{(\alpha-1)(\alpha-l)s^2 + (c_0 - c_2) \tan \frac{(2-\alpha)\pi}{4} s + (\alpha+1)(\alpha+l)}{(\alpha+1)(\alpha+l)s^2 + (c_0 - c_2) \tan \frac{(2-\alpha)\pi}{4} s + (\alpha-1)(\alpha-l)} Y_p - [(K_{p1} * b + \frac{K_{j1}}{s\lambda})R(s) - (K_{p2} + \frac{K_{j2}}{s\lambda})Y(s)] \quad (4.97)$$

FOMRAC control parameters are selected by extensive simulation technique where as parameters of FOPI/2 DOF FOPI schemes are investigated by global optimization technique known as Luus-Jaakola optimization. A nonlinear programming-based [20-21] approach to global optimization is the Luus-Jaakola algorithm. This nonlinear programming method is used since the additivity assumption of linear programming problems for the choice variables may not hold true for the objective function or the constraints, and the linear programming issues' linear assumptions may not hold true for real-world problems. Constraints are handled easily with this method. Additionally, the iteration process is quicker than other global optimization algorithms such as the GA and PSO. Because of superior performance, it serves as an efficient optimization tool in variety of problems. Dimensional vector (q) and interval of random vector ($-d, d$) are assumed prior to the optimization process. The interval is initially chosen as $[-0.5, 0.5]$ and can be constructed in search space as $d(a_l + a_u)$, where a_l and a_u are lower and upper limits of decision variables. To explore the entire region, the size of region vector is chosen as $0.5(a_l + a_u)$. During the optimization process, the following constraints must be met:

$$l_1 \leq K_P \leq u_1, l_2 \leq K_I \leq u_2, l_3 \leq \lambda \leq u_3 \quad (4.98)$$

The multi-objective function using IAE, ISE and ITAE error metrics is formulated as follows:

$$J = \int_0^{\infty} |e(t)| dt + \int_0^{\infty} |e(t)|^2 dt + \int_0^{\infty} t|e(t)| dt \quad (4.99)$$

The pseudo code for obtaining global optimum of K_P, K_I, λ is discussed in Appendix B.

4.4 Investigation on Proposed Fractional Order Standalone and Augmented Control Schemes on Inverted Pendulum

This simulation-based study compares conventional and fractional MRAC-based schemes employing (2.47) for benchmark X-inverted pendulum subjected to quantitative performance analysis. Figs. 4.6, 4.7, 4.8, s4.10, and 4.11 are employed to implement FO/IO-MIT and FO/IO-Lyapunov rules independently with modified versions in a Simulink environment. The significant application of FOLY and its modified version is discussed in the following case study I.

Case study I: Investigation into The Performance on Fractional Order Standalone MRAC Rules

Following the specifications [22] of the reported benchmark inverted pendulum in Table 4.1 the overall transfer function is used as

Example 1 [22]:

$$Y(s) = \frac{\theta(s)}{F_X(s)} = \frac{.102}{.0446s^2 - 1} \quad (4.100)$$

Table 4.1
Parameter specifications

| Symbol | Quantity | Value |
|--------|-------------------|-----------------------|
| M | mass of cart | 900 gm |
| m | mass of pendulum | 1000 gm |
| l | length of rod | 1.09 m |
| g | Gravity | 9.81 m/s ² |
| I | Moment of inertia | 5.3 gm/m ² |

The ideal model is adopted in accordance with the intended performance of the closed loop system. The settling time (T_s) of 3.73 seconds and overshoot (M_P) of 1.25% are selected to predict the performance of the stable reference model. Using these values, damping ratio (ε)

and natural frequency (ω_n) are obtained as 1.93 and 4.977 respectively and the reference model is shown as

$$Y_M(s) = \frac{3.72}{s^2 + 4.977s + 3.72} \quad (4.101)$$

As shown in Fig. 4.14, the feed-forward based MIT rule of the MRAC scheme does not ensure the stability of the system using Fig. 4.6. Even with an extensive range of adaptive gain (γ) between 0.1 and 500, the inverted pendulum oscillates continuously and cannot be stabilized.

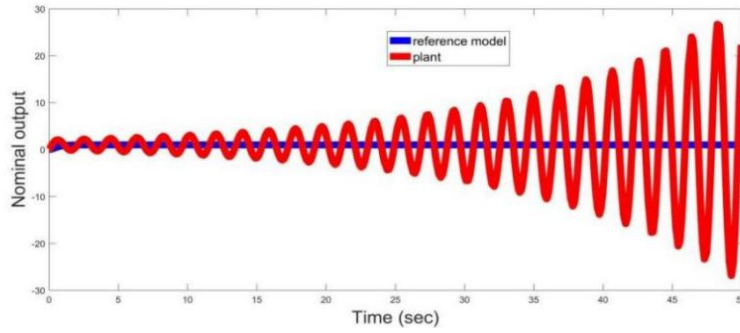


Fig. 4.14. System output using traditional MIT rules.

Although multiple FOs between 0 and 1 are attempted, no discernible improvement in stability is discovered when feed-forward based proposed FOMIT is also applied to the same plant and another reported plant. In order to overcome the aforementioned issue, feedback topology with PD control law is used with the MRAC architecture's reference input, as shown in Fig. 4.8. To tackle the system depicted in Fig. 4.15, the servo-regulatory performance of the modified classic MIT rule using Figs. 4.7 and 4.8 is investigated with different adaptive gains applying load disturbance at $t = 25$ sec from a real-time perspective.

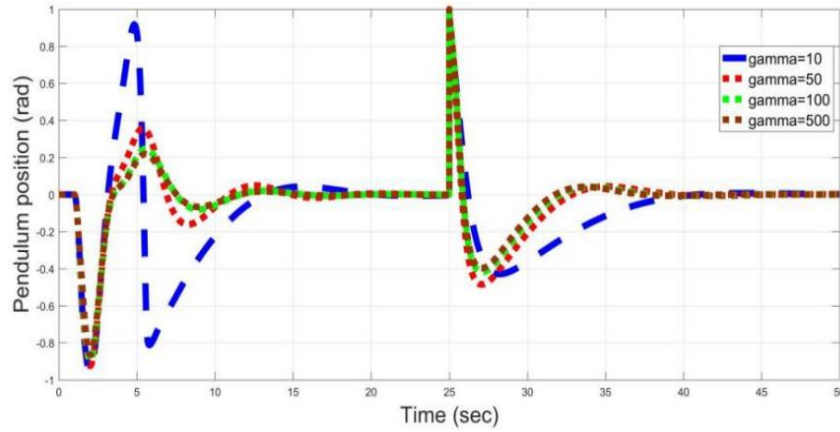


Fig. 4.15. Servo-regulatory response using modified traditional MIT rules.

The system is successfully tracked by the modified classic MIT rule in its upright position, and peak overshoot is reduced by employing a higher adaptive gain value, such as 500, as shown in Fig. 4.15. Choosing the appropriate adaptive gain is essential to achieving the required stable performance. This high adaptive gain value enables the system to stabilize more quickly even under load. Now, the significant application of the modified FOMIT rule is illustrated in Fig. 4.16, while adaptive gain is kept fixed at 500.

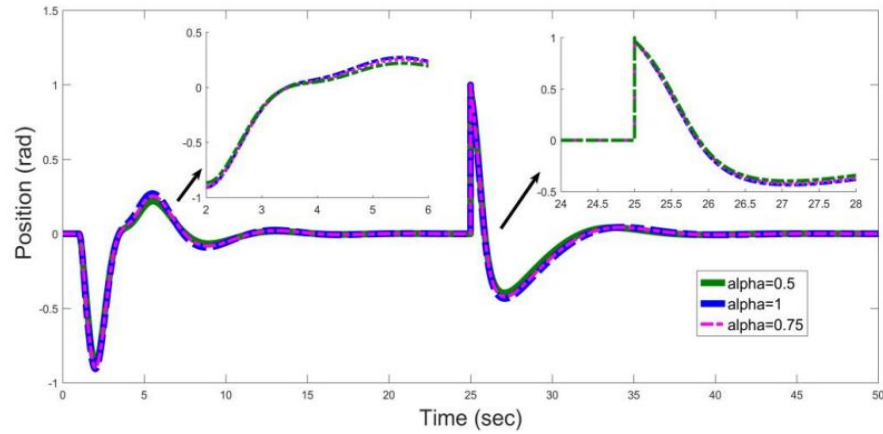


Fig. 4.16. Comparative study between FOMIT and IOMIT rules.

Figure 4.16 illustrates the significant application of the FOMIT rule, which, in contrast to standard rules, exhibits more adaptable and trustworthy behaviors by altering the additional degree of freedom between 0 and 1. The rational approximation of different fractional orders are presented in Table 4.5. It is obvious that the system can be handled more efficiently by utilizing a lower range of fractional order, such as 0.5, but if the fractional order is increased towards 1, the system responds more slowly and with more overshoot. This trait explores FOMIT's benefit over IOMIT for this particular system. Later, the research is carried out utilizing the FOLY stability law (4.79–4.83) in comparison to FOMIT to help the system stand upright more swiftly and gracefully with step input ($t=1$ sec) as depicted in Fig. 4.17.

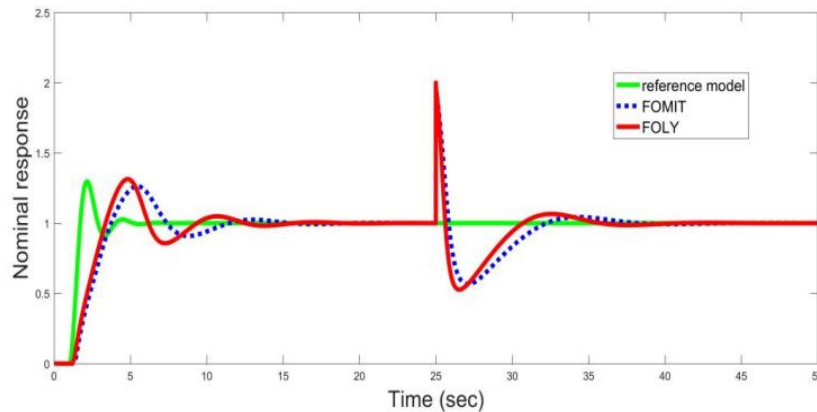


Fig. 4.17. Comparative study between proposed FOMIT and FOLY rules.

Fig. 4.17 illustrates how FOLY, which follows the reference model with a shorter rise time of 3.13 sec, tracks the system better than FOMIT. However, overshoot of 35.2% is discovered when tracking the system with FOLY, but FOMIT produces a smaller overshoot of 30.2%. Now, following Figs. 4.8 and 4.10, servo-regulatory performances are therefore carried out using impulse and step inputs at $t = 1$ sec with the same adaptive gain and fractional order as 500 and 0.5 in the presence of positive and negative unit step disturbances at $t = 25$ and 35 seconds and white noise source (seed = 81, noise strength = 0.01 and sample time = 1) as depicted in Figs. 4.18 and 4.19. (4.80–4.81) is used to compute the adaptive gain for FOLY as 750.

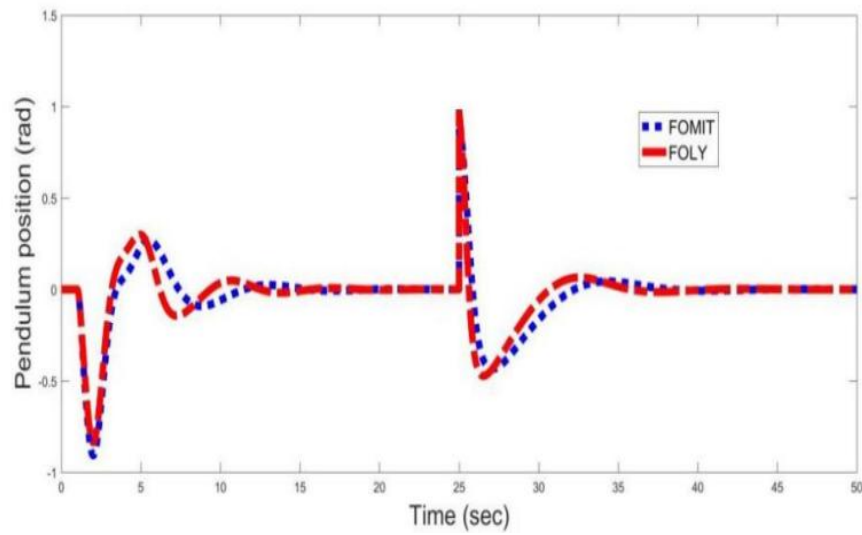


Fig. 4.18. Upright position tracking using FOMIT and FOLY rules.

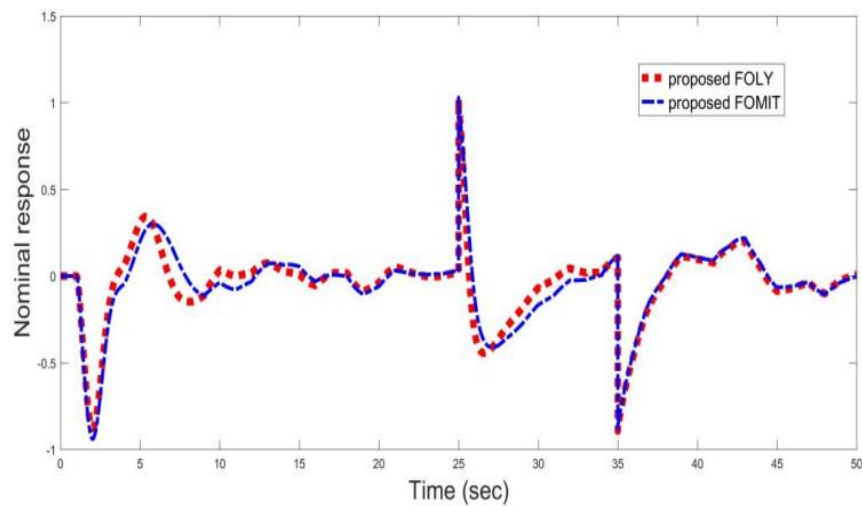


Fig. 4.19. Upright position tracking in presence of noise.

The upright posture of the system is found to be efficiently tracked by both the FOLY and FOMIT rules despite the presence of noise and load disturbances (25-35 seconds). The system is more swiftly and elegantly tackled by FOLY's effective control action despite the fact that it produces a slightly higher overshoot. The lower readings of IAE, ISE, and ITAE measurement in Table 4.2 and 4.3 show the effectiveness of the proposed FOLY strategy over proposed modified FOMIT and modified IOMIT laws.

Table 4.2
Quantitative comparison under load disturbance

| Control Scheme | Servo response | | | | Regulatory response | | | |
|--------------------------------|----------------|-------------|-------------|----------------------|---------------------|-------------|-------------|----------------------|
| | IAE | ISE | ITAE | T _s (sec) | IAE | ISE | ITAE | T _s (sec) |
| MIT | ---- | ---- | ---- | ---- | ---- | ---- | ---- | ---- |
| Modified MIT | 5.73 | 3.83 | 82.2 | 17.573 | 5.93 | 3.86 | 83.4 | 39.425 |
| Proposed modified FOMIT | 4.48 | 3.25 | 69.7 | 15.483 | 4.53 | 3.18 | 71.2 | 36.382 |
| Proposed FOLY | 4.05 | 2.25 | 45.5 | 12.755 | 4.08 | 2.19 | 45.7 | 35.362 |

'----': unstable

Table 4.3
Quantitative comparison under noise

| Control Scheme | IAE | ISE | ITAE |
|--------------------------------|-------------|-------------|-------------|
| Proposed modified FOMIT | 7.21 | 4.08 | 138.2 |
| Proposed FOLY | 5.83 | 2.89 | 94.2 |

Now, in order to take better control actions, Fig. 4.11 is employed to examine the effectiveness of the FOLY rule's updated control law with noise and load disturbance (25-35 seconds) as illustrated in Fig. 4.20.

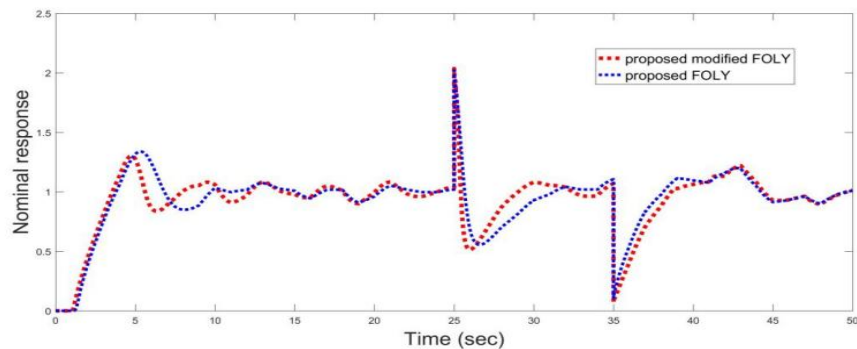


Fig. 4.20. Comparative study between proposed FOLY and modified FOLY rules.

According to Fig. 4.20, the suggested improved FOLY rule controls the system more effectively and elegantly with a rise time of 2.56 sec, an overshoot of 28.5%, and error metrics listed in Table 4.4.

Table 4.4
Quantitative comparison under noise

| Method | IAE | ISE | ITAE |
|-------------------------------|-------------|-------------|-------------|
| Proposed FOLY | 5.83 | 2.89 | 94.2 |
| Proposed modified FOLY | 3.82 | 1.49 | 88.3 |

The effectiveness of proposed modified FOLY is now validated in the presence of load disturbance at $t = 25$ seconds by comparison to the existing IOPID, FOPID, GA-FOPID, MIT-PID, IOLY, and IOLY-PID topologies [23-25] using step input $t = 0$ sec as illustrated in Fig. 4.21. The input control actions under noise are also presented within saturation limit -1 and 1 in Fig. 4.22.

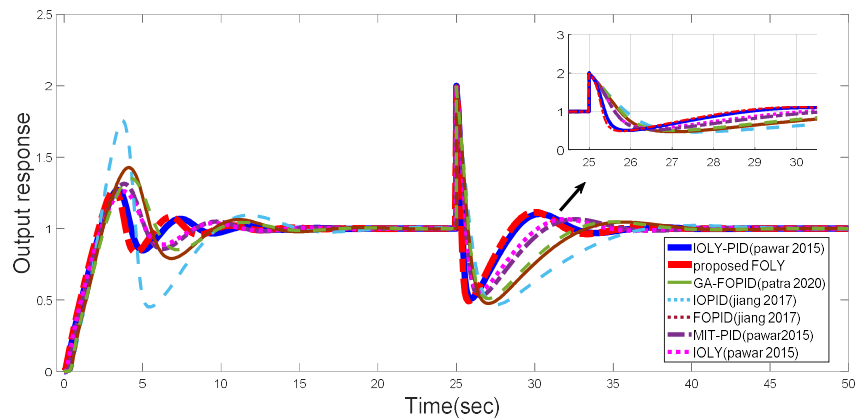


Fig. 4.21. Significant impact of proposed modified FOLY over existing rules under load disturbance.

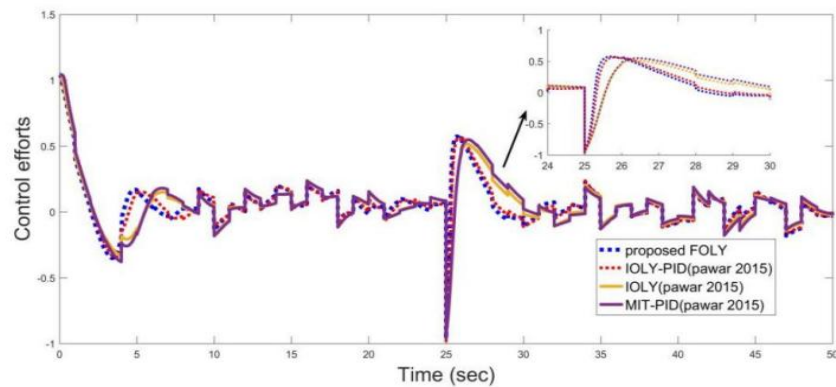


Fig. 4.22. Control actions in presence of noise and disturbance.

Table 4.5
Approximations of fractional order

| Fractional order | Approximated transfer functions $G(s)$ |
|------------------|---|
| $s^{0.5}$ | $\frac{5.025s^2 + 36.88s + 6.525}{6.525s^2 + 36.88s + 5.025}$ |
| $s^{0.75}$ | $\frac{8.026s^2 + 24.73s + 4.536}{4.536s^2 + 24.73s + 8.026}$ |

Table 4.8 discusses the controller settings of various topologies. On the basis of in-depth simulation, Fig. 4.21 shows a thorough comparison of standard MIT and Lyapunov rules with single and dual topologies utilizing different adaptive gains. Only servo action was used to study the effectiveness of the aforementioned rules in the literatures. In this study, the servo-regulatory performance is introduced using the recommended controller settings. Although the IOMIT-PID enhanced technique effectively handles the system, it performs somewhat slowly. At 14.856 seconds, the system is controlled, and at 35.645 seconds, after applying a load disturbance, it is stabilized. Tracking the system also reveals a higher amplitude level of 38.45%. The IOLY rule with the correct Lyapunov function marginally improves the problem's solution while slightly reducing overshoot. However, the settling time independently is not significantly improved by IOLY. Further research is therefore conducted on the IOLY-PID enhanced strategy, which tracks the desired position significantly faster than other schemes with lower rise times. To further study the stability of the system using servo action alone, standard and fractional PID controllers are suggested. This study compares servo-regulatory action to conventional MIT and Lyapunov rules from a real-time perspective. When compared to conventional MRAC systems, its performances are not found to be satisfactory. FOPID controllers control the system more quickly than IOPID controllers, and both IOPID and FOPID rules produce larger overshoot than MRAC rules. However, as demonstrated in Table 4.6, both of these rules result in high values for error metrics like IAE, ISE, and ITAE. FOPID control settings were recently optimized by genetic algorithm to examine robust servo action; however, despite producing less rise time and settling time than IOPID and FOPID schemes, it is unable to reduce peak overshoot. So, the aforementioned PID controller schemes do not work well and provide larger values of error metrics when compared to typical MRAC systems. IOPID or FOPID controllers cannot be suggested as a way to deal with such a nonlinear system more effectively. Therefore, MRAC system exhibits satisfactory servo-regulatory behaviors with low error metric values. Now, among existing MRAC rules, proposed FOLY rule outperforms with lower reading of IAE, ISE and ITAE as shown in Table

4.6 and a lower amplitude level of 28.5%. In FOLY laws, the fractional order of 0.5 is favored for comparative research.

Lower fractional orders are also appropriate for investigation, but larger fractional orders cause the system to perform slowly. When there is noise present, the after load disturbance system is controlled more effectively utilizing the FOLY rule, as shown in Fig. 4.21.

Table 4.6
Quantitative comparison of closed-loop performances

| Methods | Set response | | | | Load response | | | |
|-------------------------------|--------------|-------------|-------------|--------------|---------------|-------------|-------------|--------------|
| | IAE | ISE | ITAE | TV | IAE | ISE | ITAE | TV |
| Proposed modified FOLY | 2.85 | 1.15 | 43.8 | 131.5 | 2.87 | 1.08 | 44.2 | 134.2 |
| MIT-PID (pawar 2015) | 4.55 | 3.79 | 57.3 | 228.3 | 4.58 | 3.82 | 57.9 | 228.9 |
| IOLY (pawar 2015) | 4.26 | 3.27 | 52.5 | 285.2 | 4.29 | 3.12 | 53.9 | 285.7 |
| IOLY-PID (pawar 2015) | 4.12 | 2.86 | 47.3 | 168.2 | 4.18 | 2.83 | 47.8 | 169.3 |
| IOPID (jiang 2017) | 8.23 | 5.02 | 123.4 | 362.5 | 8.49 | 5.04 | 124.2 | 360.2 |
| FOPID (jiang 2017) | 6.03 | 3.85 | 81.2 | 310.8 | 6.08 | 3.89 | 83.4 | 304.2 |
| GA-FOPID (patra 2020) | 4.79 | 3.42 | 64.3 | 234.2 | 4.82 | 3.46 | 68.3 | 229.4 |

$$TV = \sum_{i=1}^{\infty} |u(i+1) - u(i)|$$

All proposed FO-MRAC topologies maintain consistency in following the intended upright posture despite noise, however the proposed modified FOLY rule reveals more robust control action. As described in Case Study II, the FOLY and FOMIT rules have now been further expanded with novel augmented procedures to evaluate potential control action for stabilizing the inverted pendulum.

Case study II: Investigation into The Performance on Fractional Order Augmented MRAC Rules

FOMRAC rules are augmented to the controllers of both the 1 DOF and 2 DOF FOPI, and another reported benchmark system [26] is employed in this case study for performance assessment. A common trade-off in 1 DOF rules is between noise elimination and set-point tracking. However, by providing independent tuning for set-point tracking and noise elimination, the 2 DOF rule may be able to attain a better balance in process control. In addition to exploring the substantial application of augmented methods compared to standalone

approach, a thorough simulation study is conducted to investigate the significant impact of 2 DOF FOPI rule compared to 1 DOF FOPI rule in the presence of noise.

Example 2 [26]:

$$Y(s) = \frac{\theta(s)}{F_x(s)} = \frac{1}{s^2 - 9} \quad (4.102)$$

In this study, the second order stable ideal model with settling time of 2.73s and overshoot of 4.19% is chosen.

$$Y_M(s) = \frac{4.76}{s^2 + 3.1s + 4.76} \quad (4.103)$$

The parameter specifications for the model [26] are presented in Table 4.7.

Table 4.7
Plant specifications

| Symbol | Quantity | Value |
|--------|-------------------|-----------------------|
| m | mass of pendulum | 0.8417 Kg |
| l | length of rod | 1.09 m |
| g | Gravity | 9.81 m/s ² |
| I | Moment of inertia | 2.3 gm/m ² |

Due to the fact that the 2 DOF rule has never been used in augmented methods before, this study conducts an inquiry. This section discusses the major benefits of the 2 DOF method over the 1 DOF method. A set point weighting parameter [27] is taken into account for the proportional term in the case of a 2 DOF-FOPI controller to mitigate overshoot during set-point change. A multi-objective function is used in the LJ optimization technique to determine the variables of the FOPI and 2 DOF FOPI strategies. The IAE, ISE, and ITAE reduction are all part of the multi-objective function. In this case study, standalone direct synthesis-based PID control scheme [28] simulation tests were conducted because they produced more reliable results than the conventional IOPID scheme. It has been determined through thorough simulation tests that selecting $\gamma = 100$ results in reduced peak overshoot and settling time. In order for the system output to match that of the ideal model, the aforementioned value of γ is fixed and the parameter (α) of the fractional derivative can be changed between 0 and 1. In order to successfully track the reference model, the fractional order is gradually reduced from 1 to 0.1, stabilizing the tilt of the inverted pendulum. It is found that using a fractional order of 0.5 results in better tracking performance than other fractional order values. The controller settings for FOMIT and FOLY rules are discussed in Table 4.8. Using the LJ optimization algorithm, optimal values of FOPI and 2 DOF FOPI controller settings are obtained as $K_p = 18.54$,

$K_I = 2.67, K_{P1} = 11.24, K_{I1} = 2.67, K_{P2} = 18.54, K_{I2} = 2.67, \lambda = 0.45$ for the linearized model of inverted pendulum obtained in (4.102).

The set point weighting parameter of 2 DOF FOPI controller is selected as $b = 0.65$ by thorough simulation studies for attaining improved performance. Direct synthesis [28-29] based on PID controller design technique [30] yields $K_p = 12.01, T_i = 12.01$ and $T_d = 0.250$. In this section, the following combinations of control schemes are contrasted using the aforementioned controller settings: Direct synthesis-based PID controller, FOLY FOPI/2DOF-FOPI, and FOMIT FOPI/2DOF are all proposed. An overview of the controller settings obtained using each of the aforementioned approaches is provided in Table 4.8. While regulatory action is examined by providing a unit step load disturbance at $t = 15s$, servo action is studied by taking into account a unit step change in set-point. The closed-loop results and control actions of the five combinational control schemes are depicted using step input $(t) = 0$ sec in Figs. 4.23 and 4.24, respectively, for the linearized plant model given in (4.104). The control signals of the FOLY and FOMIT schemes are restricted by adding a saturation block so that the control signal does not go above the following range to ensure a fair comparison: $-20 < u < 20$. This is due to the fact that in real-world applications, sudden changes in the control signal might cause actuator saturation. The performance metrics in Table 4.9 and Fig. 4.23 makes it clear that the FOLY-2 DOF-FOPI combination produces enhanced closed-loop result in presence of noise. With the aid of the following perturbed plant model with delay time, the stability of the proposed and reported works to parametric uncertainties is investigated:

$$Y(s) = \frac{\theta(s)}{F_x(s)} = \frac{1.2e^{0.01}}{s^2 - 10.8} \quad (4.104)$$

The suggested approaches produce superior closed-loop performance even when the plant model is perturbed, as indicated by the system outputs of the perturbed plant in Fig. 4.25 and the quantitative performance measurements provided in Table 4.9. Despite having somewhat higher integral errors, the FOLY-2 DOF FOPI rule achieves smooth long-term stability by providing reduced TV readings. The impact of nonlinearities on the system response is worthwhile researching. The closed-loop results for the subsequent nonlinear plant model are thus depicted in Fig. 4.26.

$$T(t) = \ddot{\theta}(t) - 9\sin\theta(t) \quad (4.105)$$

Since the PID controller based on direct synthesis produces unbounded output, it is not depicted in Fig. 4.25. Table 4.9 clearly shows that the suggested strategy can enhance the performance even when there are nonlinearities in the process dynamics. FOLY augmented schemes relatively outperforms FOMIT augmented schemes in presence of nonlinear effect in the system. The speed of control action is improved by FOLY augmented schemes compared to

FOMIT augmented schemes and despite getting deviation from set-point FOLY augmented schemes control the system more swiftly and gracefully after applying disturbance. The system output is augmented with a Rayleigh noise source ($\sigma=0.1$, initial seed=1, sampling time=1 second) to evaluate the impact of measurement noise on system response. Fig. 4.28 displays servo-regulatory responses amid noise. From Fig. 4.27 and Table 4.9, it is discovered that the proposed approach can follow the set-point and reject the noise efficiently.

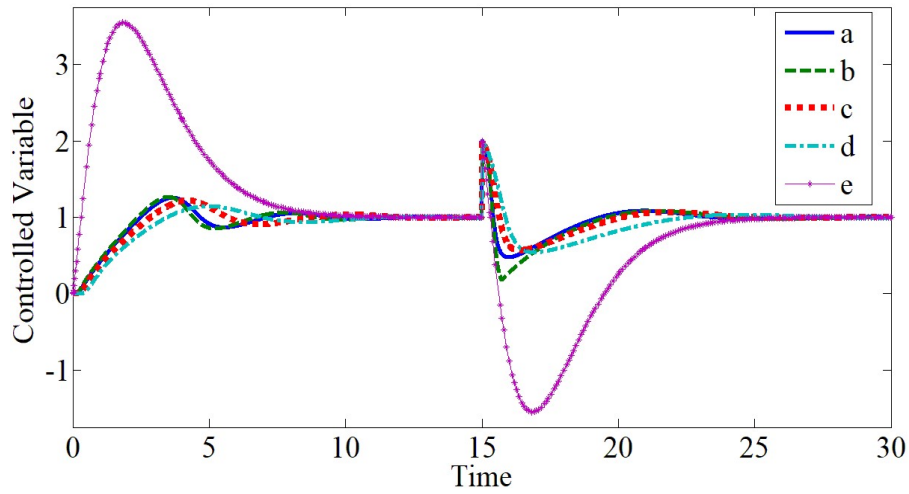


Fig. 4.23. Nominal outputs for linearized model (a: FOLyapunov-2DOF FOPI, b: FOLyapunov-FOPI, c: FOMIT-2DOF FOPI, d: FOMIT-FOPI and e: Direct synthesis based PID).

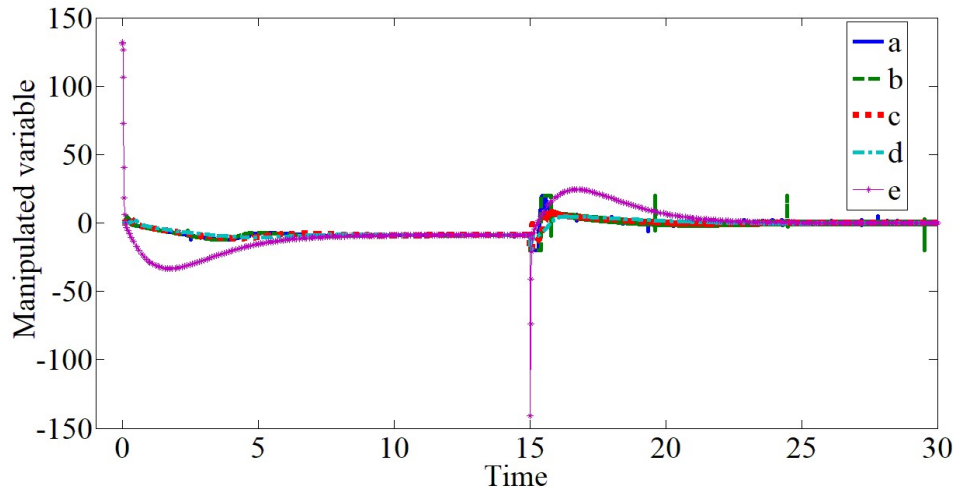


Fig. 4.24. Control efforts (a: FOLyapunov-2DOF FOPI, b: FOLyapunov-FOPI, c: FOMIT-2DOF FOPI, d: FOMIT-FOPI and e: Direct synthesis based PID).

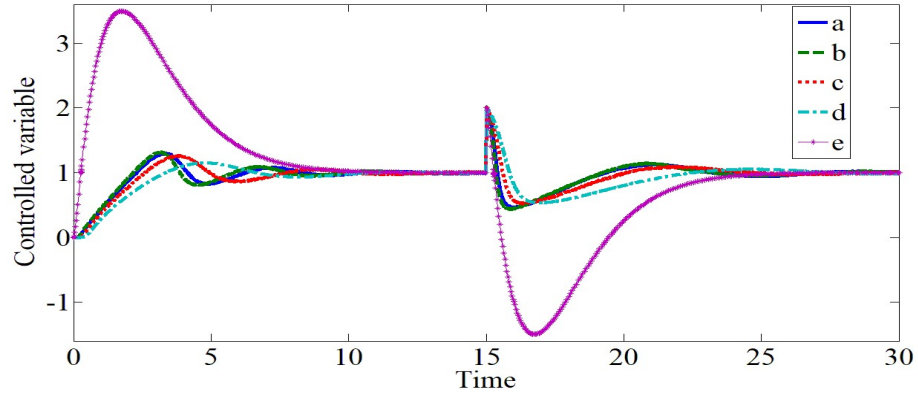


Fig. 4.25. Perturbed outputs for linearized model (a: FOLYapunov-2DOF FOPI, b: FOLYapunov-FOPI, c: FOMIT-2DOF FOPI, d:FOMIT-FOPI and e:Direct synthesis based PID).

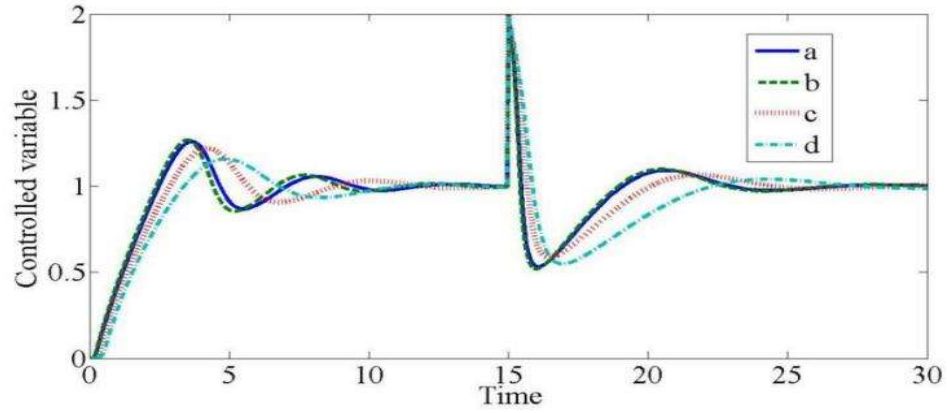


Fig. 4.26. System outputs for nonlinear model (a: FOLYapunov-2DOF FOPI, b: FOLYapunov-FOPI, c: FOMIT-2DOF FOPI and d:FOMIT-FOPI).

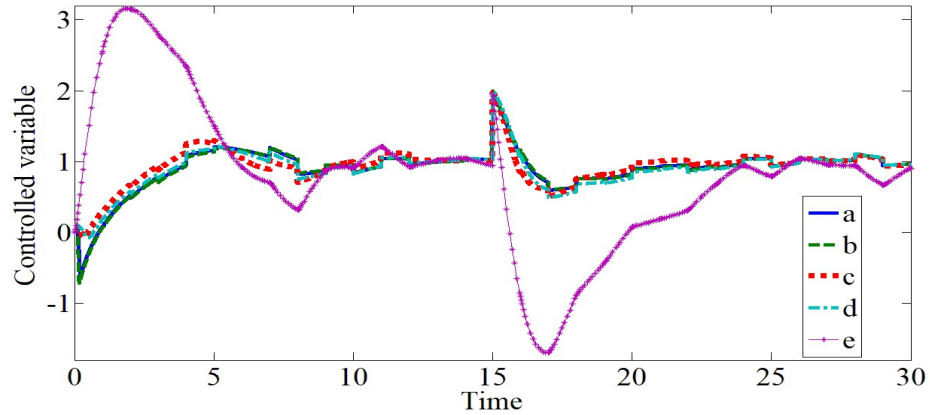


Fig. 4.27. System outputs with noise (a: FOLYapunov-2DOF FOPI, b: FOLYapunov-FOPI, c: FOMIT-2DOF FOPI, d:FOMIT-FOPI and e:Direct synthesis based PID).

Table 4.8
Summary of tuning parameters

| Case study | Methods | Controller settings |
|------------|----------------------------|--|
| I | Proposed modified MIT rule | $\gamma = 10,50,100,500$ $\theta_1 = -\frac{\gamma}{s} \left(\frac{2.1s+8.45}{s^2+2.1s+8.45} u_c[1+1.5s] \right) e$ $\theta_2 = \frac{\gamma}{s} \left(\frac{2.1s+8.45}{s^2+2.1s+8.45} * \frac{.102}{.0446s^2-1} \right) e$ |
| | MIT-PID (pawar 2015) | $\theta_1 = -\frac{2000}{s} \left(\frac{2.1s+8.45}{s^2+2.1s+8.45} u_c \right) e$ $\theta_2 = \frac{2000}{s} \left(\frac{2.1s+8.45}{s^2+2.1s+8.45} * \frac{.102}{.0446s^2-1} \right) e$ $C_{PID} = -343.8 + \frac{-175.3}{s} + (-20.32)s$ |
| | IOLY (pawar 2015) | $\theta_2 = -e \frac{8000}{s^{0.7}} \frac{.102}{.0446s^2-1}$ $\theta_1 = e \frac{8000}{s^{0.7}} u_c$ |
| | IOLY-PID (pawar 2015) | $\theta_2 = -e \frac{8000}{s^{0.7}} \frac{.102}{.0446s^2-1}$ $\theta_1 = e \frac{8000}{s^{0.7}} u_c$ $C_{PID} = -343.8 + \frac{-175.3}{s} + (-20.32)s$ |
| | Proposed modified FOMIT | $\theta_1 = -\frac{500}{s^{0.5}} \left(\frac{2.1s+8.45}{s^2+2.1s+8.45} u_c[1+1.5s] \right) e$ $\theta_2 = \frac{500}{s^{0.5}} \left(\frac{2.1s+8.45}{s^2+2.1s+8.45} * \frac{.102}{.0446s^2-1} \right) e$ |
| | Proposed modified FOLY | $\theta_2 = -e \frac{750}{s^{0.5}} \frac{.102}{.0446s^2-1}$ $\theta_1 = e \frac{750}{s^{0.5}} u_c[1+1.5s]$ |
| | IOPID (jiang 2017) | $C_{PID} = 243.8 + \frac{53.4}{s} + 30.45s$ |
| | FOPID (jiang 2017) | $C_{FOPID} = 63.2 + \frac{32.7}{s^{0.484}} + 16.25s^{0.382}$ |
| | GA-FOPID (patra 2020) | $C_{FOPID} = 1.04 + \frac{0.537}{s^{0.634}} + 0.226s^{0.532}$ |
| II | Proposed modified FOMIT | $\theta_1 = -\frac{100}{s^{0.5}} \left(\frac{3.1s+4.76}{s^2+3.1s+4.76} u_c[1+1.5s] \right) e$ $\theta_2 = \frac{100}{s^{0.5}} \left(\frac{3.1s+4.76}{s^2+3.1s+4.76} * \frac{1}{s^2-9} \right) e$ |

| | | |
|--|---|---|
| | Proposed modified FOLY | $\theta_2 = -e^{\frac{150}{s^{0.5}} \frac{1}{s^2-9}}$ $\theta_1 = e^{\frac{150}{s^{0.5}}} u_c [1 + 1.5s]$ |
| | Proposed optimal FOPI | $K_p = 11.24, K_I = 2.67, \lambda = 0.45,$ |
| | Proposed optimal 2 DOF-FOPI | $K_{p1} = 11.24, K_{I1} = 2.67, K_{p2} = 18.54,$ $K_{I2} = 2.67, \lambda = 0.45, b = 0.65$ |
| | Direct synthesis based PID (vanavil et al. 2015) | $K_C = 12.01, T_I = 12.01, T_d = 0.250$ |

Table 4.9
Quantitative comparison of closed-loop performances

| Control Scheme | Unperturbed linearized model | | | | Perturbed linearized model | | | | Nonlinear model | | | | Unperturbed model in presence of noise | | | |
|---|------------------------------|-------|-------|-------------------|----------------------------|-------|-------|-------------------|-----------------|------|-------|-------------------|--|-------|-------|-------------------|
| | IAE | ISE | ITAE | TV | IAE | ISE | ITAE | TV | IAE | ISE | ITAE | TV | IAE | ISE | ITAE | TV |
| Direct synthesis Based PID (vanavil et al. 2015) | 18.60 | 32.62 | 194.1 | 9.2×10^5 | 18.65 | 31.75 | 193.2 | 9.4×10^5 | ---- | ---- | ----- | ---- | 19.52 | 30.07 | 224.3 | 8.8×10^5 |
| Proposed FOMIT-FOPI | 4.39 | 2.13 | 44.71 | 3.3×10^3 | 4.53 | 2.18 | 48.27 | 4.1×10^3 | 4.33 | 2.06 | 43.74 | 4.6×10^3 | 5.40 | 2.41 | 56.51 | 4.3×10^3 |
| Proposed FOMIT-2 DOF FOPI | 3.73 | 1.71 | 34.53 | 3.1×10^3 | 3.97 | 1.77 | 39.28 | 3.5×10^3 | 3.66 | 1.64 | 33.26 | 4.4×10^3 | 4.59 | 2.00 | 44.25 | 3.8×10^3 |
| Proposed FOLY-FOPI | 3.90 | 1.89 | 39.75 | 2.4×10^3 | 3.77 | 1.61 | 38.45 | 2.9×10^3 | 3.38 | 1.43 | 30.78 | 3.7×10^3 | 5.51 | 3.05 | 50.56 | 3.5×10^3 |
| Proposed FOLY-2 DOF FOPI | 3.58 | 1.60 | 33.59 | 1.7×10^3 | 3.82 | 1.63 | 38.92 | 2.6×10^3 | 3.42 | 1.47 | 30.87 | 3.9×10^3 | 5.43 | 2.90 | 49.97 | 2.9×10^3 |

It is evident that fractional augmented MRAC schemes tackle the system more swiftly and gracefully with lesser error metrics. Both FOMIT and FOLY augmented 2 DOF FOPI rules outperform augmented 1 DOF FOPI rule in presence of noise. In particular, FOLY augmented strategies outperform the other schemes.

4.5 Summary

For two distinct reported benchmark models of the inverted pendulum, different fractional order standalone and augmented novel control topologies are proposed in this chapter. All proposed control methods' underlying mathematical presuppositions are thoroughly explained. Fractional orders are approximated by rational modified biquadratic exact phase approximation method. A combination of sophisticated simulation and optimization techniques are used to set the controller's parameters. The significant impacts of proposed fractional order Lyapunov stability rule and its modified version in comparison to proposed fractional order modified MIT rule and other existing different conventional standalone and augmented control topologies are explored from real time perspective. Both standalone modified FOMIT and FOLY schemes yield satisfactory control actions with lower error metrics in presence of load disturbances and noise but standalone FOLY comparatively outperforms by tackling the system more swiftly and gracefully. By examining the superior action of the standalone FOLY rule, fractional order MIT and Lyapunov rules are extended by a novel augmented scheme with 1 DOF FOPI and 2 DOF FOPI rules to investigate the control effectiveness of the augmented version. Compared to FOMIT enhanced variants, FOLY augmented versions likewise exhibit more robust control action. Although, FOLY-2 DOF FOPI relatively outperforms with lesser error metrics, under perturbed situation it is discovered to have slightly higher error metrics. However, in terms of noise rejection, FOLY-2 DOF FOPI is superior to FOLY-FOPI. Although standalone modified FOLY and its augmented versions offer lower level of overshoot but still there is a scope of improvement on closed-loop servo-regulatory performance with zero overshoot.

References

- [1] Garces, F., Becerra, V.M., Kambhampati, C., and Warwick, K., "Introduction to feedback linearisation. In: strategies for feedback linearization", *Advances in Industrial Control*. Springer, London, 2003.
- [2] Bejarbaneh, E.Y., Bagheri, A., Bejarbaneh, B.Y., "Optimization of Model Reference Adaptive Controller for the Inverted Pendulum System Using CCPSO and DE Algorithms", *Aut. Control Comp. Sci.* 52, 256–267, 2018.

- [3] Bensafia, Y. & Ladaci, S. (2018), "Fractional order model reference adaptive control", *International Journal of Industrial and Systems Engineering*, Vol. 30, No. 2, pp. 138-156.
- [4] Begum, K. G., Rao, A. S., & Radhakrishnan, T. K. (2018), "Optimal controller synthesis for second order time delay systems with at least one RHP pole". *ISA transactions*, Vol. 73, pp. 181-188.
- [5] Kennedy, E., King, E., and Tran, H. (2019), "Real-time implementation and analysis of a modified energy based controller for the swing-up of an inverted pendulum on a cart", *European Journal of Control*, Vol. 50, pp. 176-187.
- [6] Molin, A., and Hirche, S., "Price-based adaptive scheduling in multi-loop control systems with resource constraints", *IEEE Transactions on Automatic Control*, 59(12), 3282-3295, 2014.
- [7] Zhou, J., Wen, C., and Wang, W., "Adaptive control of uncertain nonlinear systems with quantized input signal", *Automatica*, 95, 152-162, 2018.
- [8] Yadav, A. K., Pathak, P. K., Sah, S. V., & Gaur, P. (2019), "Sliding Mode-Based Fuzzy Model Reference Adaptive Control Technique for an Unstable System", *Journal of The Institution of Engineers (India): Series B*, Vol. 100, No. 2, pp. 169-177.
- [9] Yazdani, E. and Bagheri, A. (2018), "Optimization of model reference adaptive controller for the inverted pendulum system using CCPSO and DE algorithms", *Automatic Control & Computer Sciences*, Vol. 52, No. 4, pp. 256- 267.
- [10] Dydek, Z.T., Annaswamy, A.M., and Lavretsky, E., "Adaptive control of quadrotor UAVs: A design trade study with flight evaluations", *IEEE Transactions on Control Systems Technology*, 21(4), 1400-1406, 2013.
- [11] Jalil, M.A, Rahiman, M.F., and Hamdan, R., "Real time implementation of first order model reference adaptive control (MRAC) without integral on regulation temperature of glycerin bleaching process", *ARPJ. Eng. Appl. Sci.*, 10(22), 17158-17164, 2015.
- [12] Marquez-Rubio, J.F., del Muro-Cuellar, B., and Álvarez Ramírez, J., "Stabilization region of PD controller for unstable first order process with time delay", *Int. J. Control Autom. Syst.* 12, 265–273, 2014.
- [13] J. Y. Ishihara and M. H. Terra, "On the Lyapunov theorem for singular systems", in *IEEE Transactions on Automatic Control*, vol. 47, no. 11, pp. 1926-1930, Nov. 2002.

- [14] Z. Man, H. R. Wu, S. Liu and X. Yu, "A New Adaptive Backpropagation Algorithm Based on Lyapunov Stability Theory for Neural Networks," in *IEEE Transactions on Neural Networks*, vol. 17, no. 6, pp. 1580-1591, Nov. 2006.
- [15] Duarte-Mermoud, M. A., Aguila-Camacho, N., Gallegos, J. A., & Castro-Linares, R. (2015), "Using general quadratic Lyapunov functions to prove Lyapunov uniform stability for fractional order systems", *Communications in Nonlinear Science and Numerical Simulation*, Vol. 22, No.1-3, pp. 650-659.
- [16] Kar, B., and Roy, P., "A comparative study between cascaded FOPI-FOPD and IOPI-IOPD controllers applied to a level control problem in a coupled tank system", *J Control Autom Electr Syst*, 29 340–349, 2018.
- [17] Acharya, D.S., Swain, S.K. and Mishra, S.K., "Real-time implementation of a stable 2 DOF PID controller for unstable second-order magnetic levitation system with time delay", *Arab J Sci Eng*, 45, 6311–6329, 2020.
- [18] Bingi, K., Ibrahim, R., Karsiti, M. N., Hassan, S. M. & Harindran, V. R. (2018) "A comparative study of 2DOF PID and 2DOF fractional order PID controllers on a class of unstable systems", *Archives of Control Sciences*, Vol. 28, No. 4, pp. 635–682.
- [19] Mondal, R. and Dey, J. (2019) "Fractional order 2-degree of freedom control of linear time invariant plants", *ISA Transaction*, Vol. 5, No. 10, pp.68-81.
- [20] Damara, S. and Kundu, M. (2015), "Design of robust fractional PID controller using triangular strip operational matrices", *Fractional Calculus and Applied Analysis*.
- [21] He, Z., Ma, Z., Xu, Y., Zhang, Y., Hu, F., Sun, Y., & Zhou, D. (2015), "Analysis of forced expiratory flow signals using the new luus-jaakola optimization procedure", *IEEE Transactions on Biomedical Engineering*, Vol. 62, No. 6, pp. 1644-1651.
- [22] Prasad, L.B., Tyagi, B., and Gupta, H.O., "Optimal control of nonlinear inverted pendulum system using PID controller and LQR: performance analysis without and with disturbance input. *Int. J. Autom. Comput*, 11, 661–670, 2014.
- [23] R. J. Pawar and B. J. Parvat, "Design and implementation of MRAC and modified MRAC technique for inverted pendulum", *2015 IEEE International Conference on Pervasive Computing (ICPC)*, Pune, India, 2015, pp. 1-6.

- [24] A. K. Patra, A. Patra, D. K. Subudhi, A. Nanda, A. K. Mishra and R. Agrawal, "Genetic Algorithm based FOPID Controller Design for Balancing an Inverted Pendulum (IP)", *2020 International Conference on Computational Intelligence for Smart Power System and Sustainable Energy (CISPSSE)*, Keonjhar, India, 1-5, 2020.
- [25] S. Jiang, M. Li and C. Wang, "Design and simulation of fractional order PID controller for an inverted pendulum system", *2017 IEEE International Conference on Manipulation, Manufacturing and Measurement on the Nanoscale (3M-NANO)*, Shanghai, China, 349-352, 2017.
- [26] Zangeneh-Madar, M.R., Mazinan, A.H., "Control of the inverted pendulum system: a Smith fractional-order predictive model representation", *Sādhanā*, 45, 105, 2020.
- [27] Wang, J.J., "Simulation studies of inverted pendulum based on PID controllers", *Simulation Modelling Practice and Theory*, 19(1), 440-449, 2011.
- [28] Hezeng Wang and Xiaoming Jin, "Direct synthesis approach of PID controller for second-order delayed unstable processes", *Fifth World Congress on Intelligent Control and Automation (IEEE Cat. No.04EX788)*, Hangzhou, China, 2004, pp. 19-23 Vol.1.
- [29] A. Seshagiri Rao, V.S.R. Rao, M. Chidambaram, "Direct synthesis-based controller design for integrating processes with time delay", *Journal of the Franklin Institute*, 346 (1), 2009, pp. 38-56.
- [30] Balakrishnan, Vanavil & Chaitanya, K. & Rao, A (2015), "Improved PID controller design for unstable time delay processes based on direct synthesis method and maximum sensitivity", *International Journal of Systems Science*, 46.

Publication

1. **D. Mukherjee**, G.L. Raja, P. Kundu, A. Ghosh, "Modified augmented fractional order control schemes for cart Inverted Pendulum using constrained Luus-Jaakola optimisation", **International Journal of Modelling, Identification and Control (IJMIC)**, Inderscience, Vol.38 No.3/4, pp. 367 – 379, 2022.
2. **D. Mukherjee**, P. Kundu, A. Ghosh, "A Stability Analysis of Inverted Pendulum System Using Fractional-Order MIT Rule of MARC Controller", *Advances in Intelligent Systems and Computing*, Vol.701, ISBN:978-981-10-7562-9, **Springer**, 2018.

3. **D. Mukherjee**, P.K. Kundu, A. Ghosh, “A performance analysis of fractional order based MARC controller over optimal fractional order PID controller on inverted pendulum”, International Journal of Engineering & Technology, Vol. 7, no. 2.21, pp. 29–33, 2018.

CHAPTER 5

Fractional Order Standalone and Augmented Control Strategies for Continuous Stirred Tank Reactor

5.1 Introduction

Noise rejection is a more difficult problem than set point tracking in industrial unstable processes. Some direct combination techniques, like MRAC-PID and MRAC-FOPID [1–5], were already reported by many experts who used the trial-and-error method or other optimization techniques to stabilize the concentration or temperature of a stable approximation model based on different operating points of the CSTR nonlinear process. Those techniques quite canceled out noise. So, later on to reject disturbances during tracking the temperature at its desired level, the series cascade control structures [6–12] were frequently utilized in chemical processes. However, they did not yield desired servo response for plants with large delay time. In the primary loop, a PI-PD structure [13] was used, whereas the IMC method was used to create the secondary controller. To control the integration process, three different methods were suggested: an IMC-based secondary controller [14], a PID for set-point tracking in series with a lead-lag compensator, and a PD for disturbance rejection in series with a lead-lag filter. The direct synthesis (DS) approach was used in the construction of the aforementioned PID and PD schemes that were connected in series with lead-lag compensators. A generalized predictor cascade control (GPCC) technique based on output prediction was reported by GarcíŁa et al. [15] in the discrete platform. To increase robustness and noise attenuation, the previously mentioned GPCC structure includes three filters beyond the primary and secondary control strategies. Process control is one area where fractional calculus has seen significant use recently [16–17]. The benefits of fractional calculus, parallel cascade control, and the Smith predictor have only been coupled in Pashaei and Bagheri's [17] work to date to produce satisfactory closed-loop performance. As a result, the series cascade control approach introduced by Pashaei and Bagheri [17] is expanded upon in this work. Therefore, a unique series cascade control structure (SCCS) with a dead time compensator is recommended for this application as shown in Fig. 5.1.

Three controllers, referred to as the primary, secondary, and stabilizing controllers, are included in the proposed SCCS. FOIMC is proposed to construct both main and secondary controllers. The stabilizing PD controller is constructed using maximal sensitivity assumptions and Routh-Hurwitz (RH) stability requirements. The FO and temporal constants of IMC filters are optimized by the utilization of the constrained artificial bee colony (ABC) technique. IAE, ITAE, and ISE are all multi-objective functions that must be minimized in this ABC algorithm.

In addition to the SCCS investigation, an MRAC scheme with modified FOMIT and FOLY rules are recommended to test the effectiveness of the control on handling disturbance. Moreover, the importance of FOLY stability rule over modified FOMIT rule is emphasized in this application. Compared to PID controller design for unity feedback systems, there are comparatively fewer studies on multi-loop control structures. Dual-loop control techniques perform [18] somehow better than traditional single-loop control [19-23] for processes that are unstable. On fractional order multi-loop control techniques, there is a dearth of literature. Therefore, by adopting FO controllers, the behaviors of the prevalent dual-loop control techniques on particular aforementioned unstable systems are yet to be explored. In addition to unity feedback schemes, a novel augmented version of MRAC rules with different controllers is also proposed. These controllers include FOPID and internal model based FOPID (IMC-FOPID) control schemes. These are all intended to investigate the robust closed loop performance over unity feedback schemes. Later on, the control effort of the augmented FOLY control rules is contrasted with that of another novel multi-loop predictor that uses fractional order internal model control (FOIMC) and FOPD topologies. The main focus of the inquiry is on extensive simulation techniques to demonstrate the effectiveness of suggested control schemes, and afterwards, some global optimization algorithms are offered to determine the most workable tuning parameters for a more thorough investigation.

This chapter includes a brief discussion of mathematical modelling of proposed different fractional order control topologies.

5.2 SCCS with dead time compensator

Fig. 5.1 shows the recommended control scheme: is equipped with a primary controller (G_c), secondary IMC filter (C_2), and a stabilizing controller (C_s). Both C_1 and C_2 are designed by FOIMC whereas C_s is corresponds to PD type as presented below:

$$C_s(s) = K_P(1 + T_d s) \quad (5.1)$$

The secondary process (G_{A2}) is computed as follows:

$$G_{A2}(s) = \frac{y_2(s)}{r_2(s)} = \frac{P_2(s)}{1 + C_2(s)(P_2(s) - P_{m2}(s))} \quad (5.2)$$

$$P_t(s) = \frac{y_1(s)}{r_2'(s)} = \frac{G(s)}{1 + G(s)C_s(s)} \quad (5.3)$$

where $G(s) = P_1(s)G_{A2}(s)$. In case of ideal matching, $P_2(s) = P_{m2}(s)$. Hence, $G_{A2}(s) = P_2(s)$ and hence $G(s) = P_1(s)P_2(s)$. The process's total dead time is compensated for by the Smith dead-time compensator. For servo response, the fundamental model is represented as

$$\frac{y_1(s)}{r_1(s)} = \frac{G_c(s)P_t(s)}{1 + G_c(s)(P_m(s) + P_t(s) - P_m(s)e^{-\theta_m s})} \quad (5.4)$$

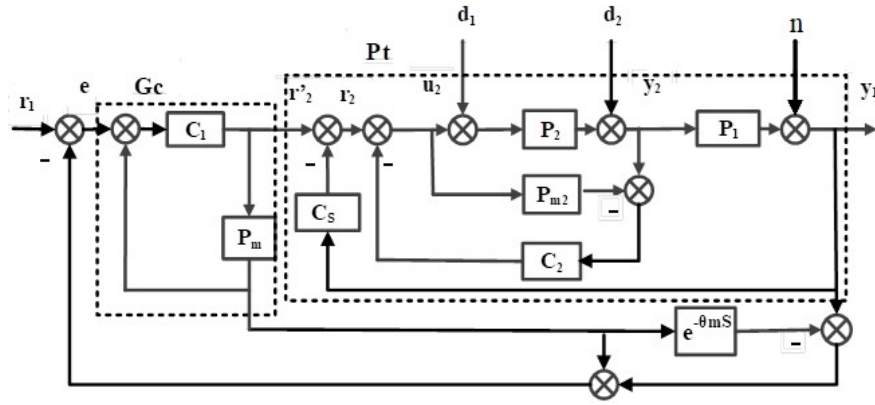


Fig. 5.1. Proposed FOIMC-SCCS architecture with dead time compensator.

Considering perfect-matching conditions ($P_t(s) = P_m(s)e^{-\theta_m s}$), (5.4) results

$$\frac{y_1(s)}{r_1(s)} = \frac{G_c(s)P_m(s)e^{-\theta_m s}}{1 + G_c(s)P_m(s)} \quad (5.5)$$

where $G_c(s) = C_1(s)/(1 - P_m(s)C_1(s))$ is the primary controller. It is clear the auxiliary equation's independence on θ_m from the aforementioned formula. Thus, the model P_m is the only one that influences the design of C_1 . This is a merit of augmenting SCCS to boost the dead-time compensator. P_2 's dynamics is typically consistent in nature while that of P_1 's dynamics may be stable, unsteady or integrated [24]. In this investigation, the models of P_2 and P_1 are adopted as,

$$P_2(s) = \frac{K_2}{\tau_2 s + 1} e^{-\theta_2 s} \quad (5.6)$$

$$P_1(s) = \frac{K_1}{\tau_1 s - 1} e^{-\theta_1 s} \quad (5.7)$$

Plants with unsteady first order plus dead time (UFOPDT) and steady first order plus dead time (FOPDT) are shown in (5.6) and (5.7), accordingly. Process gain, dead time and time constant are represented by K , θ and τ , accordingly.

5.2.1 Design of Controllers

Three control parameters (G_C , C_2 and C_S) need to be designed for the suggested dead-time compensator based SCCS. The model of G_C can be evaluated by developing the FOIMC. The step for computing the distinct control functions is outlined below

❖ *Design of C_2*

The model of P_2 is adopted as

$$P_{m2}(s) = \frac{K_{m2} e^{-\theta_{m2}s}}{\tau_{m2}s + 1} \quad (5.8)$$

By 1st order Pade's approximation of $e^{-\theta_{m2}s}$ in (5.8) results

$$P_{m2}(s) = \frac{K_{m2} (1 - 0.5\theta_{m2}s)}{(\tau_{m2}s + 1)(1 + 0.5\theta_{m2}s)} \quad (5.9)$$

(5.9) is factorized as

$$P_{m2}(s) = P_{m2}^-(s)P_{m2}^+(s) \quad (5.10)$$

where the non-minimum phase zeros and delay time are indicated by $P_{m2}^+(s)$. Following IMC rule [25], $C_2(s)$ is developed as

$$C_2(s) = \frac{1}{P_{m2}^-(s)} f(s) \quad (5.11)$$

where $P_{m2}^-(s) = K_{m2} / ((\tau_{m2}s + 1)(1 + 0.5\theta_{m2}s))$. For designing a FOIMC rule, the filter $f(s)$ in (5.11) is proposed as

$$f(s) = \frac{1}{(\lambda_2 s^\beta + 1)^2} \quad (5.12)$$

where β is the FO and replacing (5.12) in (5.11), we get

$$C_2(s) = \frac{(\tau_{m2}s + 1)(1 + 0.5\theta_{m2}s)}{K_{m2} (\lambda_2 s^\beta + 1)^2}, \quad \beta > 1 \quad (5.13)$$

where λ_2 is the additional time constant. If $\theta_{m2} = 0$, C_2 is developed as

$$C_2(s) = \frac{(\tau_{m2}s + 1)}{K_{m2} (\lambda_2 s^\beta + 1)} \quad (5.14)$$

❖ Design of C_S

Designing the stabilizing PD controller in such a way that the control loop comprises $G(s) = P_1(s)P_2(s)$ and C_S attains an accepted value of maximum sensitivity [26]. Also, the characteristic polynomial $1 + P_1(s)P_2(s)C_S(s) = 0$ meets the RH stability condition. Replacing $C_S(s) = K_p(1 + T_d s)$ and $G(s) = (K_1 K_2 e^{-(\theta_1 + \theta_2)s}) / ((\tau_1 s - 1)(\tau_2 s + 1))$ in (5.3) and estimating the denominator's dead time term by $(1 - 0.5(\theta_1 + \theta_2)s) / (1 + 0.5(\theta_1 + \theta_2)s)$, we get

$$P_t(s) = \frac{K e^{-\theta_m s}}{(\tau_1 s - 1)(\tau_2 s + 1) + K_p K (1 + T_d s) \frac{(1 - 0.5\theta_m s)}{(1 + 0.5\theta_m s)}} \quad (5.15)$$

In the above equation, $\theta_m = \theta_1 + \theta_2$ and $K = K_1 K_2$. Selecting $T_d = 0.5\theta_m$, we get

$$P_t(s) = \frac{K e^{-\theta_m s}}{a_2 s^2 + a_1 s + a_0} \quad (5.16)$$

where $a_2 = \tau_1 \tau_2$, $a_1 = \tau_1 - \tau_2 - 0.5K_p K \theta_m$ and $a_0 = K K_p - 1$. According to RH criteria, P_t is stable within the desired range of K_p in $1/K < K_p < (\tau_1 - \tau_2) / (0.5K \theta_m)$. RH stability criteria are only applied to the above range of K_p . The graph of K_p vs maximum sensitivity as discussed in section 5.4 decides the appropriate value of K_p .

❖ Design of C_1

The controller G_C is developed without taking into account the delay term θ_m because the external loop of the suggested SCCS contains the dead-time compensator. C_1 is found utilizing P_m . It is already formulated that $G_C(s) = C_1(s) / (1 - P_m(s)C_1(s))$. P_m is evaluated from (5.16) as

$$P_m(s) = \frac{K}{a_2 s^2 + a_1 s + a_0} \quad (5.17)$$

where $a_2 = \tau_1 \tau_2$, $a_1 = \tau_1 - \tau_2 - 0.5K_p K \theta_m$ and $a_0 = K K_p - 1$. Therefore,

$$C_1(s) = \frac{a_2 s^2 + a_1 s + a_0}{K(1 + \lambda_1 s^\alpha)^2} \quad (5.18)$$

Where λ_1 and α are time constant and FO. As detailed in the following section, the application of the FOIMC strategy is now expanded to encompass the innovative strategies FOLY and FO-smith predictor schemes.

5.3 Fractional Order Dual-loop Strategy

This section proposes a series of FO based dual-loop control strategies: (1) A FOLY scheme of MRAC in the external loop and an optimal FOPID scheme in the internal loop (2) A FOLY scheme in the external loop and IMC based FOPID scheme in the internal loop, and (3) A FOIMC scheme in the external loop coupled with a Smith predictor, and a FOPD scheme in the inner loop. By looking into the superior performance of FOLY law on inverted pendulum in chapter-4, the significant application of dual-loop FOLY over stand-alone FOLY is explored in this chapter.

5.3.1 Dual-loop FOLY-FOPID strategy

In this control structure, FOLY strategy is used in the external-loop whereas an optimal FOPID scheme is employed in the internal-loop to attain enhanced control action than unity feedback method. The FOPID scheme is followed as

$$G_C(s) = K_p + \frac{K_I}{s^\lambda} + K_D s^\mu \quad (5.19)$$

FOLY control law is already discussed in 4.2.3.2. The layout of the dual-loop FOLY-FOPID scheme is established in Fig 5.2. The closed-loop transfer model of the internal-loop is presented by

$$G_1(s) = \frac{G_C(s)Y_P(s)}{1 + G_C(s)Y_P(s)} \quad (5.20)$$

The closed-loop model of dual-loop configuration as depicted in Fig 5.2 is

$$G_2(s) = \frac{U(s)G_C(s)Y_P(s)}{1 + G_C(s)Y_P(s) + U(s)G_C(s)Y_P(s)} \quad (5.21)$$

5.3.3 Dual-loop FOIMC-FOPD predictor

The proposed Dual-loop predictor is illustrated in Fig 5.4 has a FOIMC scheme (G_C) and a stabilizing FOPD controller $G_{PD}(s) = K_P + K_d s^\mu$. P_m represents the model of the following (without dead-time):

$$P_t(s) = \frac{y(s)}{r'(s)} = \frac{G_P(s)}{1 + G_P(s)G_{PD}(s)} \quad (5.31)$$

From Fig 5.4, the external model is provided by

$$\frac{y(s)}{r(s)} = \frac{G_C(s)P_t(s)}{1 + G_C(s)(P_m(s) + P_t(s) - P_m(s)e^{-\theta s})} \quad (5.32)$$

Taking into account ideal-model circumstances ($P_t(s) = P_m(s)e^{-\theta s}$), (5.32) reduces to

$$\frac{y(s)}{r(s)} = \frac{G_C(s)P_m(s)e^{-\theta s}}{1 + G_C(s)P_m(s)} \quad (5.33)$$

where $G_C(s) = C_{foimc}(s)/(1 - P_m(s)C_{foimc}(s))$ is the external-loop scheme. Since the denominator of (5.33) is independent on θ , the design C_{foimc} relies only on P_m . It is the benefit of this control strategy.

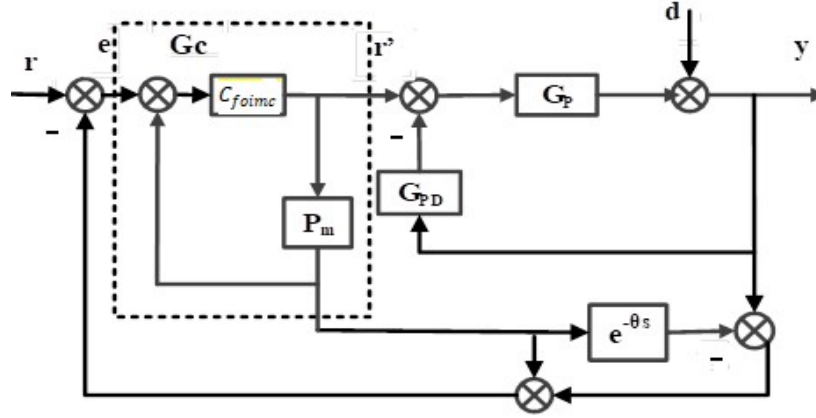


Fig. 5.4. Dual-loop FOPD-FOIMC smith predictor.

G_C and G_{PD} need to be designed for the suggested dual-loop FOIMC-FOPD predictor. G_C is computed by developing the FOIMC filter. The method for finding the control functions is demonstrated below:

❖ Design of G_{PD}

The FOPD scheme is developed for stabilizing the inner-loop involving $G_P(s)$ and $G_{PD}(s)$. Ideal values of K_p , K_d and μ are found applying the PSO demonstrated in Appendix C. Replacing $G_{PD}(s) = K_p + K_d s^\mu$ and $G_P(s) = (K e^{-\theta}) / (a_2 s^2 + a_1 s + a_0)$ in (4.110) and neglecting $e^{-\theta s}$ the denominator, we get

$$P_t(s) = \frac{K e^{-\theta s}}{a_2 s^2 + a_1 s + K K_d s^\mu + K_p K + a_0} \quad (5.34)$$

❖ Design of C_{FOIMC}

C_{FOIMC} is designed using P_m . Therefore, $G_C(s) = C_{FOIMC}(s) / (1 - P_m(s) C_{FOIMC}(s))$. P_m is obtained from (5.34) as

$$P_m(s) = \frac{K}{a_2 s^2 + a_1 s + K K_d s^\mu + K_p K + a_0} \quad (5.35)$$

Therefore,

$$C_{FOIMC}(s) = \frac{a_2 s^2 + a_1 s + K K_d s^\mu + K_p K + a_0}{K(1 + \tau s^\alpha)^2} \quad (5.36)$$

where τ and α are the variable tuning parameter and FO, accordingly. In this study, G_{PD} is obtained as a FOPD scheme rather than FOPID to ignore the integral term $(1/s)$ in (5.36). The aforementioned stand-alone and augmented fractional order topologies are employed to investigate the performance of inverted pendulum and CSTR in different scenarios from a real time perspective in the following case studies. Different optimization strategies are recommended in some case studies in order to attain the best outcomes for various fractional order control topologies. Different optimization methods such as ABC [27] and MPSO [28] methods are employed in this work. In order to create some meta heuristics, nature-inspired optimization method typically concentrates on insect behavior and imitate their problem-solving techniques. PSO and ABC are two often employed methods that imitate insect behavior. The ABC optimization makes an effort to imitate honey bee behavior when seeking out food. In order to select the best time constants (λ_1 and λ_2) FOs (α and β) of IMC filters for various processes in section 5.2, the ABC method is used. The flowchart of the ABC optimization is discussed in Appendix C. Closed-loop time constant ranges are set to 0 to 100 and fractional orders to 0 to 2, accordingly. In section 5.3, it is recommended to use PSO, another population-based evolutionary technique, to determine the best values for various controllers. The standard PSO is more popular because it is very simple to implement and does

not require the gradient of the problem being optimized. The PSO is an extremely resilient and versatile solution to optimization issues. Due to the fact that it essentially determines the PSO's convergence nature, inertia weight is crucial to obtaining the best settings when utilizing the PSO method. The particle swarm will not converge to produce an optimal solution if a big inertia weight value is applied. The inertia weight in this study has been constrained to fall inside a predetermined range known as random inertia weight. The pseudo code of this method is discussed in Appendix C. For both optimization techniques, the following multi-objective function encompassing IAE, ISE, and ITAE determines the required optimal parameters

$$J = W_1 \int_0^\infty t|e(t)|dt + W_2 \int_0^\infty |e(t)|dt + W_3 \int_0^\infty |e(t)|^2 dt \quad (5.37)$$

where, W_1 , W_2 and W_3 are the weights whose values are considered 0.5.

5.4 Investigation on Proposed Fractional Order Standalone and Augmented Control Schemes on Continuous Stirred Tank Reactor

To demonstrate the benefits of the proposed techniques in comparison to the state of the art, simulation tests are carried out using some reported benchmark models that have been adopted in the literature. Additionally, the proposed design's robust stability is examined, and different performance metrics are computed.

Case study I: Comprehensive study of Optimal FOIMC rule based SCCS with advanced dead time compensator

The following steps for applying the suggested method are proposed as

- I. In light of the parameters of $P_2(s)$, $C_2(s)$ is developed using (5.13) or (5.14).
- II. The entire model $G(s) = P_1(s)P_2(s)$ is obtained.
- III. $C_S(s)$ is developed assuming $T_d = 0.5\theta_m$ and selecting K_p in the range $1/K < K_p < (\tau_1 - \tau_2)/(0.5K\theta_m)$, a graph of K_p vs M_S ($M_S = \|1/1 + C_S(s)G(s)\|_\infty$) is evaluated.
- IV. The actual value of M_S is acquired from the graph generated in step-III. The most common recommendation for M_S is 1.6. However, for the majority of unstable processes, $M_S = 1.6$ is challenging to attain. In that situation, choosing the option that corresponds to the lowest value of M_S is advised to establish an acceptable trade-off between performance and stability.
- V. From (5.34), P_m is computed. Using P_m , $C_1(s)$ is obtained as shown in (5.36).

The actual plant model $G(s)$ is only approximated by the nominal plant ($G_{ov}(s) = P_{m1}(s)P_{m2}(s)$), which is utilized to calculate the controller functions. Therefore, it is crucial to build the closed-loop process in a way that makes it resistant to changes in the parameters of the plant model.

Robust Stability Analysis:

The following need [29], must be met in order to provide robust stability:

$$\|\Delta(s)T_d(s)\|_\infty < 1, \quad \forall \omega \in (-\infty, \infty) \quad (5.38)$$

where, $T_d(s)$ is denoted as complementary sensitivity function and $\Delta(s)$ is denoted as the multiplicative uncertainty in the plant model which is obtained as

$$\Delta(s) = \left| \frac{G(s) - G_{ov}(s)}{G_{ov}(s)} \right| \quad (5.39)$$

The system should be designed so that the following condition is met in the event that the process gain, delay time, and time constant of the primary and secondary models are disturbed:

$$\|T_d\|_\infty < \left| \frac{[(\tau_1 + \Delta\tau_1)s - 1][(\tau_2 + \Delta\tau_2)s + 1]}{(\tau_1 s - 1)(\tau_2 s + 1)e^{-\Delta\theta_m s} - [(\tau_1 + \Delta\tau_1)s - 1][(\tau_2 + \Delta\tau_2)s + 1]} \right| \quad (5.40)$$

where, ΔK_1 , $\Delta\theta_1$ and $\Delta\tau_1$ / ΔK_2 , $\Delta\theta_2$ and $\Delta\tau_2$ represent uncertainties in process gain, delay time, and time constant of primary/secondary models, respectively. To investigate the robustness, the magnitude graphs of $T_d(s)$ and $\Delta(s)$ are obtained as depicted in Fig. 5.5. It is noticeable that in all frequencies, the decibel magnitude of $T_d(s)$ is less than that of $\Delta(s)$.

Two benchmark instances examined by [7-8] are used in simulation research. A step input r_1 is considered at $t = 0$ that is detailed in this section in order to contrast the servo behavior. The controlled variable should oscillate and overshoot as less as possible to attain the set-point as rapidly as possible. By applying negative step load disruptions (d_1 and d_2) at different times, regulatory responses are contrasted. The controlled variable should begin following the desired set-point as soon as it deviates from it due to disturbances, with the least amount of overshoot or undershoot possible. To investigate the system stability, disturbances of +10% are applied in the gain and dead time of P_1 and P_2 . Additionally, τ_1 and τ_2 are altered by -10%. Computation of instantaneous error $e(t)$ involves by subtracting y_1 from r_1 at time 't'. Using $e(t)$, integral errors are obtained as $IAE = \int_0^\infty |e(t)|dt$ and $ISE = \int_0^\infty e(t)^2 dt$. By incorporating the settling time of servo and regulatory performances, the entire settling time

(t_{sov}) is evaluated as $t_{sov} = t_{s(y_1/r_1)} + t_{s(y_1/d_1)} + t_{s(y_1/d_2)}$. Reliability of control output $u_2(t)$ is computed by its overall variation ($TV = \sum_{i=1}^{\infty} |u_2(i+1) - u_2(i)|$). Lower readings of IAE, ISE, t_{sov} and TV measurements are preferable. In the simulation studies, the C_S is designed with a derivative filter as shown below:

$$C_S(s) = K_p \left(1 + \frac{T_d s}{0.1T_d s + 1} \right) \quad (5.41)$$

Example-1

The following primary and secondary models are used:

$$P_1(s) = \frac{e^{-0.339s}}{5s - 1}, P_2(s) = \frac{e^{-0.6s}}{2.07s + 1} \quad (5.42)$$

The secondary and primary controllers [7] are developed as:

$$G_{C2}(s) = (2.07s + 1)/(0.3s + 1), G_{C1}(s) = 0.478(1 + 1/(0.99s) + 0.213s)(6.821s + 1)/(0.567s + 1) \text{ whereas the transfer function of set point filter is } F_R(s) = 1/(6.821s + 1).$$

The controller settings [8] are used as:

$$G_{C2}(s) = (2.07s + 1)/(0.3s + 1), G_{CS}(s) = 4.646(1 + 1/(4.255s) + 0.28s)(0.47s + 1)/(0.23s + 1), G_{Cd}(s) = 4.646(1 + 1/(4.255s) + 0.28s)(0.47s + 1)/(0.023s + 1) \text{ and } F(s) = 1/(1.19s^2 + 4.255s + 1). \text{ Using the ABC optimization, } \lambda_1 = 0.439, \lambda_2 = 0.1 \text{ and } \alpha = 1.05 \text{ and } \beta = 1.15 \text{ are found for the proposed method. From Fig. 5.6, appropriate reading of } K_p \text{ can be chosen to attain a } M_S \text{ of 1.6. The fractional order sole approximations using phase modulated biquadratic equiripple approximation is presented in Table 5.1.}$$

The proposed strategy yields $C_2(s) = (2.07s + 1)(s + 1)/(0.1s^{1.15} + 1)^2, C_S(s) = 1.54(1 + 0.47s)$ and $C_1(s) = (10.35s^2 + 2.207s + 0.54)/(0.193s^{2.1} + 0.878s^{1.05} + 1)$. The proposed method's performances are contrasted to those of the reported ones using the aforementioned controller settings. Unit negative step disturbances are applied at the 30s and 60s, respectively, to evaluate the regulatory responses. Figs. 5.7 to 5.10 show the system behaviors and control efforts for the nominal and disturbed plants. A band-limited white noise block (noise strength 0.0001, sampling time 0.5, and seed 0) is introduced to the measured output to evaluate the impact of measurement noise. In Figs. 5.11 and 5.12, respectively, the closed-loop control efforts amid noise are illustrated. The IAE and ISE for the proposed technique are much lower in both the normal and perturbed circumstances, as can be found from the quantitative analysis presented in Table 5.2. The proposed method's entire settling time (for the nominal situation) is somewhat higher than that of existed ones. However, in practice, it cannot anticipate the hypothetical model to function smoothly. It is important to note

that if the plant model is disrupted, the technique [8] produces an unstable closed-loop response. Additionally, the TV readings of the suggested approach are higher than those that were published. Nevertheless, as shown in Fig. 10, the control signal of the suggested method is significantly smoother than the reported works amid measurement noise. Thus, it can be encapsulated that the following benefits of the proposed strategy have been reported: (1) a quicker servo response, as shown in Figures 5.9 and 5.11; (2) steady control action (amid measurement noise); and (3) a somewhat less oscillating outcome if the plant is upset. As per the proposed scheme, $G_c = C_1/(1 - P_m C_1)$ and for this case, $P_m = 1/(10.35s^2 + 2.207s + 0.54)$ and $P_t = P_m e^{-0.939s}$.

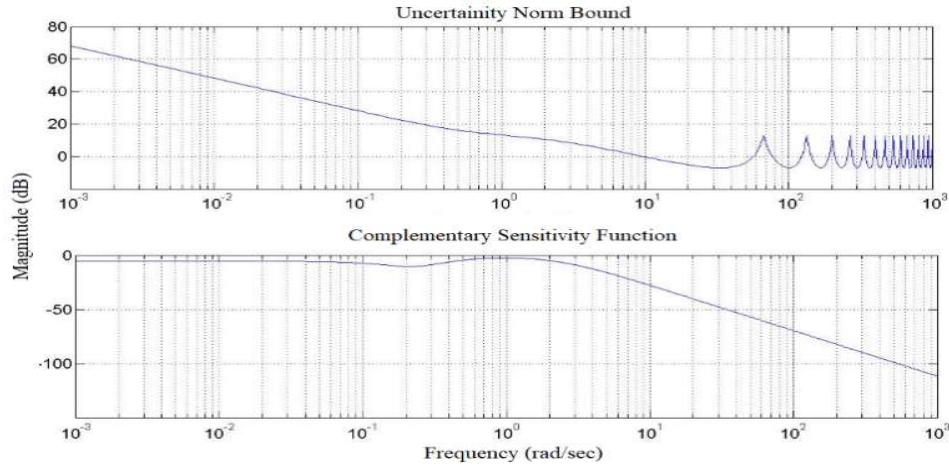


Fig. 5.5. Magnitude plots of stability for the proposed method.

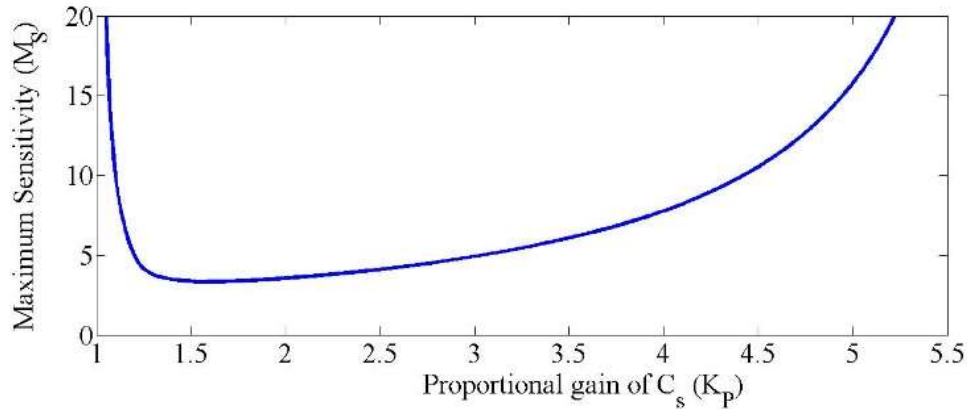


Fig. 5.6. Finding appropriate value of K_p .

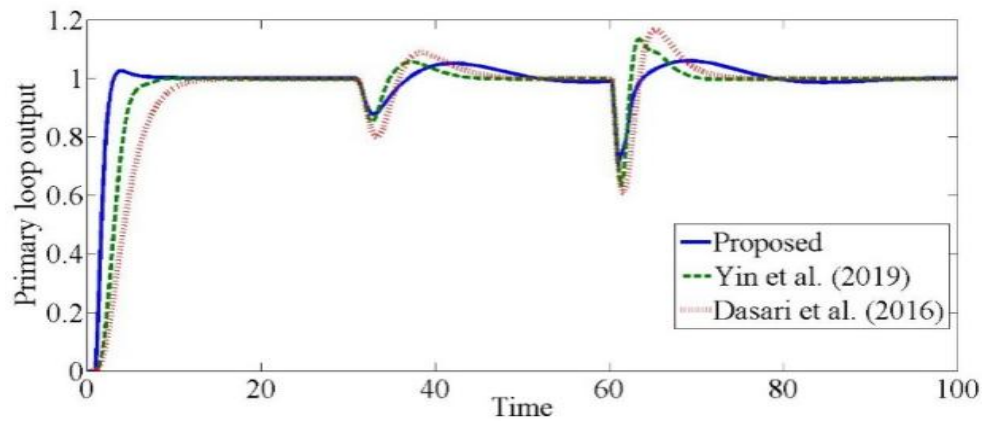


Fig. 5.7. Nominal outputs in presence of load disturbance.

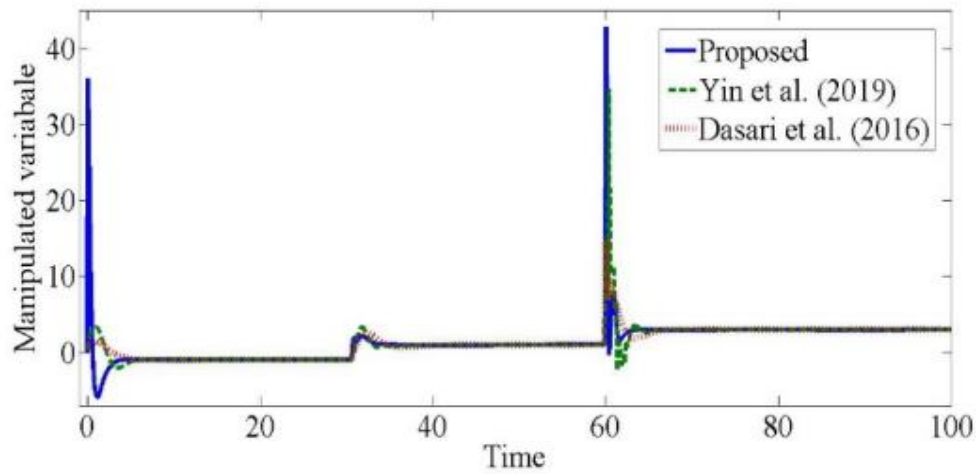


Fig. 5.8. Nominal control efforts.

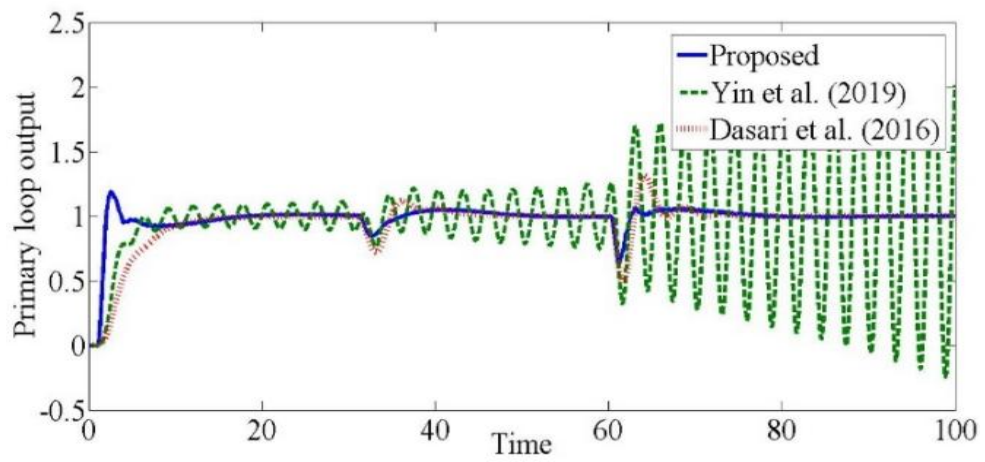


Fig. 5.9. Perturbed outputs.

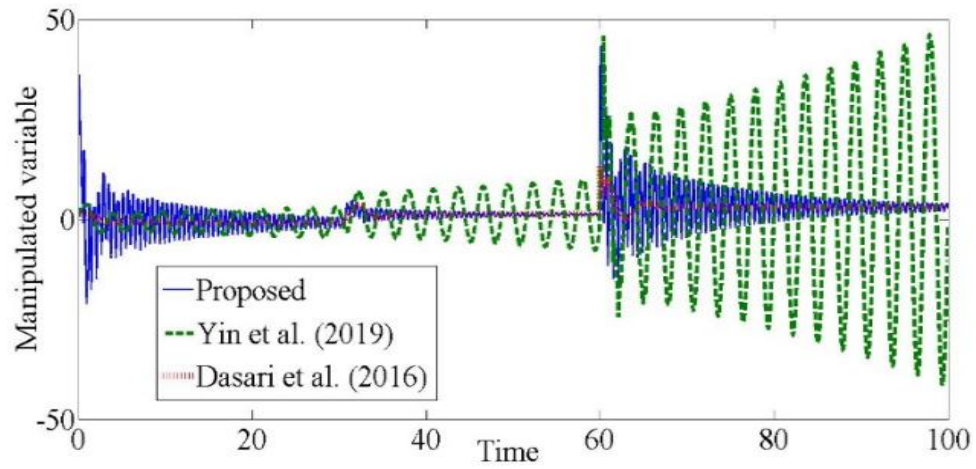


Fig. 5.10. Perturbed control actions.

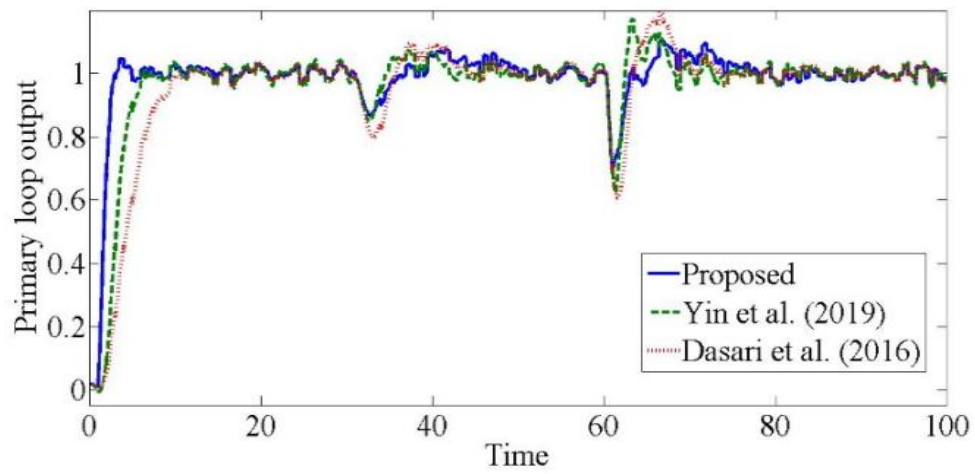


Fig. 5.11. Nominal outputs in presence of noise.

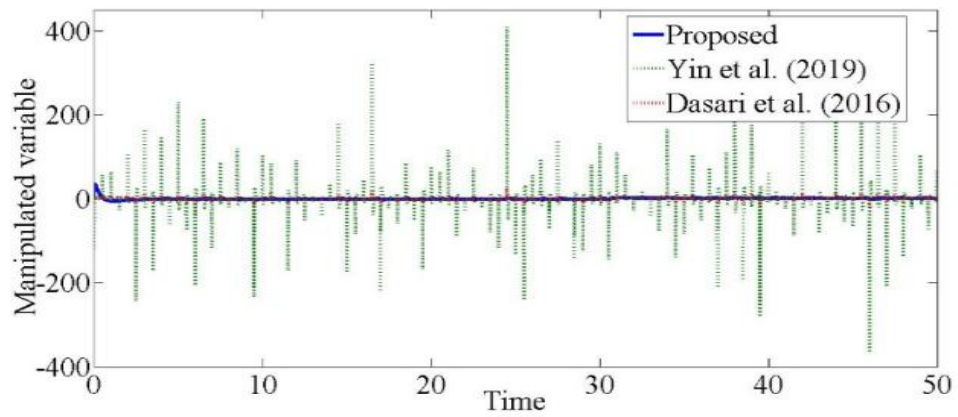


Fig. 5.12. Control efforts in presence of noise.

Example-2

In this case, the following primary and secondary models are adopted:

$$P_1(s) = \frac{e^{-3s}}{10s-1}, P_2(s) = \frac{2e^{-2s}}{s+1} \quad (5.43)$$

The following control settings [7] are employed as: $G_{C2}(s) = (s+1)/(6s+2)$, $G_{C1}(s) = 0.122(1+1/(5.5s)+1.728s)(72.25s+1)/(0.886s+1)$ and $F_R(s) = 1/(72.25s+1)$. The controller settings [8] are used as: $G_{C2}(s) = (s+1)/(3s+2)$, $G_{CS}(s) = 1.823(1+1/(46.522s)+1.465s)(2.5s+1)/(1.285s+1)$, $G_{Cd}(s) = 1.643(1+1/(63.873s)+1.502s)(2.5s+1)/(0.172s+1)$ and $F(s) = 1/(68.152s^2+46.522s+1)$. The time constants and FO parameters computed using ABC technique are as follows: $\lambda_1 = 9.85$, $\lambda_2 = 1.004$, $\alpha = 1.04$ and $\beta = 1.16$. Acceptable reading of K_p can be selected from Fig. 5.13. Taking into account the models in (5.43), $M_S = 1.6$ is not attainable. Therefore, the least value of M_S is determined to be $K_p = 0.75$. Accordingly, the proposed controller functions are computed as $C_2(s) = (s+1)^2/2(1.004s^{1.16}+1)^2$, $C_S(s) = 0.75(1+2.5s)$ and $C_1(s) = (10s^2+5.25s+0.5)/(194.05s^{2.08}+39.4s^{1.04}+2)$. The regulatory performance is investigated by combining negative disturbances (d_1 and d_2) at 150s and 300s, accordingly. Figs. 5.14–5.17 show closed-loop findings and control actions that match the nominal and perturbed models. The impact of measurement noise is investigated by combining a white noise source (noise strength = 0.0001, sampling time = 0.5 and seed = 0). Figs. 5.18–5.19, accordingly, show the system responses and control attempts amid noise.

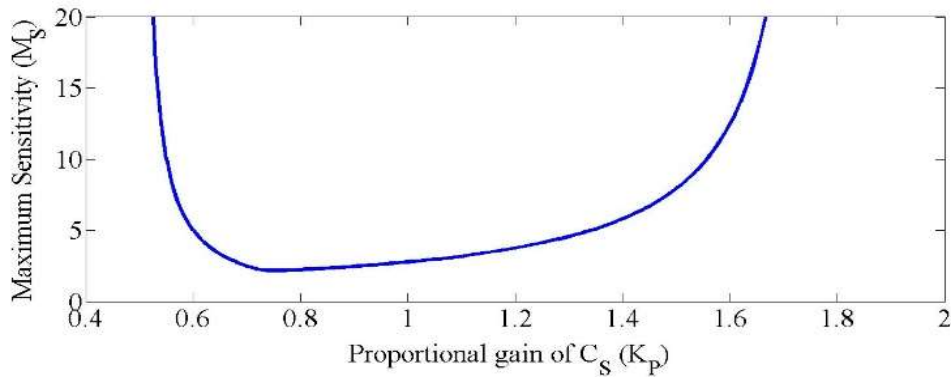


Fig. 5.13. Finding appropriate value of K_p .

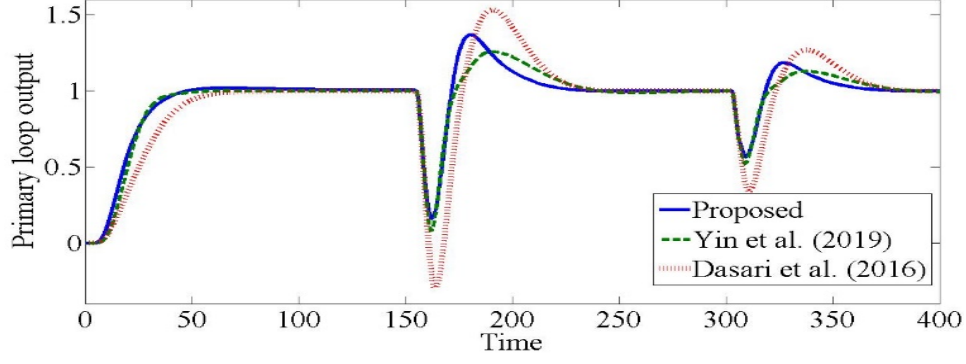


Fig. 5.14. Nominal outputs.

Table 1 shows that, in comparison to the reported methods (for both nominal and perturbed models), the closed-loop response of the suggested method has reduced IAE, ISE, and t_{sov} measures. Fig. 5.18 illustrates how the steady control action amid noise justifies the high TV measurements for the suggested approach. As opposed to the previous statement, the described works' control signal exhibits significant amplitude surges when noise is present. Actuator saturation could result from this, which is undesirable in real-world situations. Therefore, the proposed approach leads to a notable enhancement in closed-loop performance.

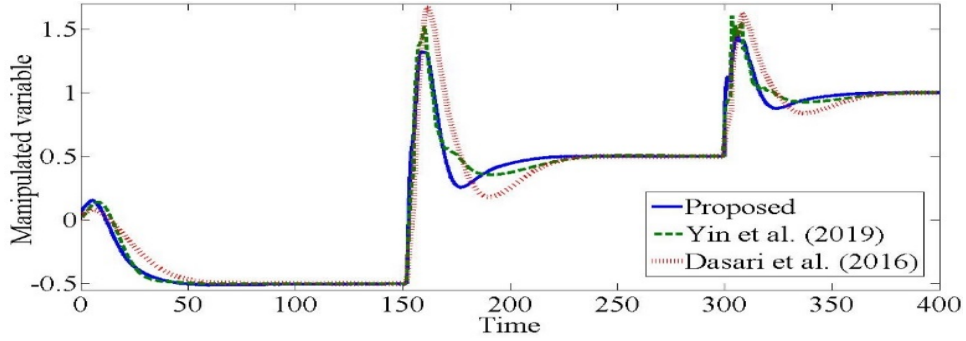


Fig. 5.15. Nominal control actions.

In this case study, $P_m = 2/(10s^2 + 5.25s + 0.5)$ and $P_t = P_m e^{-5s}$. The $T_d(s)$ can be found as $G_c P_t / (1 + G_c P_m)$, where $G_c = C_1 / (1 - P_m C_1)$. In this case study, $\Delta(s)$ is calculated with (5.41) for the perturbation values taken into consideration. Stability analysis is explored by showcasing the magnitude plots of $T_d(s)$ and $\Delta(s)$. At all frequencies, it is found that the complementary sensitivity function's decibel magnitude is smaller than the uncertainty norm bound. According to (5.40), it is the essential criteria for robustness.

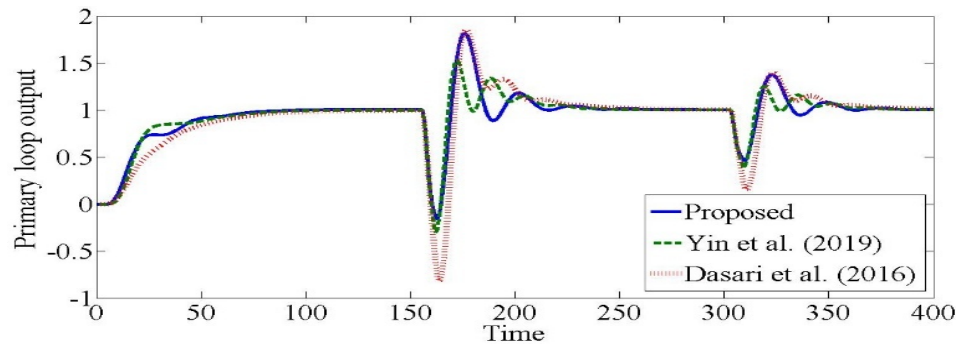


Fig. 5.16. Perturbed outputs.

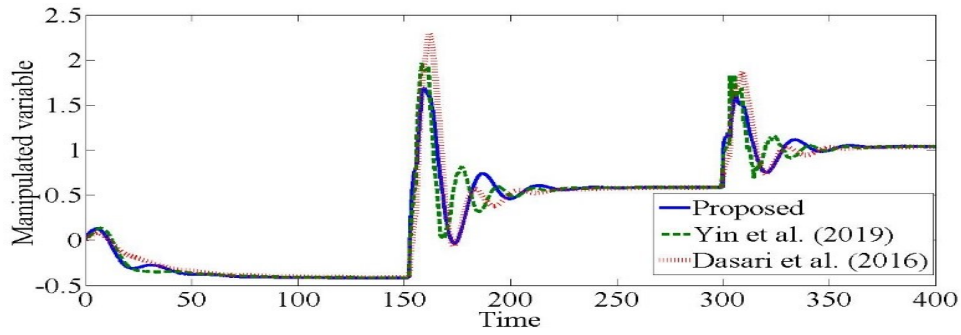


Fig. 5.17. Perturbed control actions.

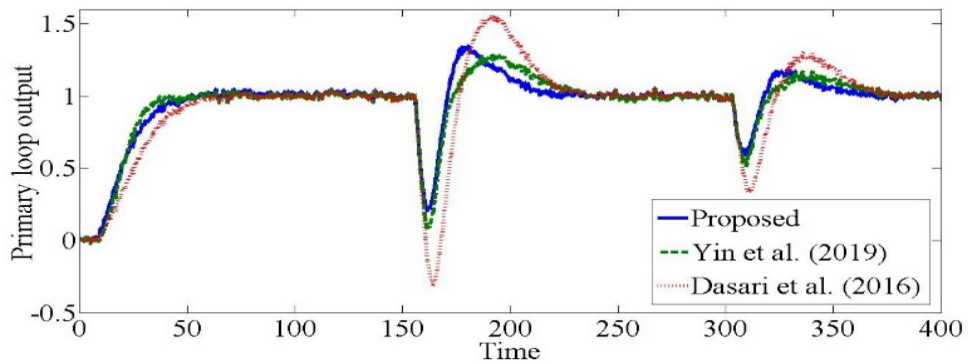


Fig. 5.18. System outputs amid noise.

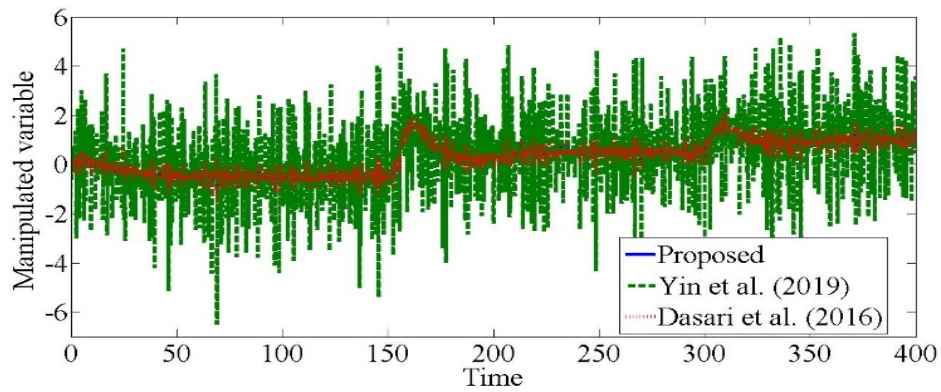


Fig. 5.19. Control efforts amid noise.

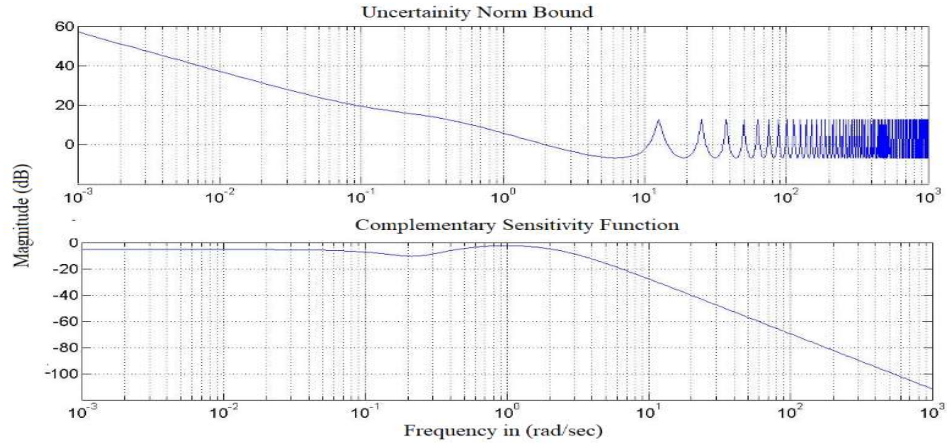


Fig. 5.20. Magnitude graphs of stability for the proposed method.

Example-3

The various steady state solutions that resulting from an isothermal chemical reactor are studied in terms of its dynamics [7] in order to investigate the effects of potential nonlinearities.

$$\frac{dC}{dt} = \frac{Q}{V}(C_f - C) - \frac{k_1}{(k_2 C + 1)^2} \quad (5.44)$$

Where, Q is the inlet flow rate and C_f is the inlet concentration. The parameter settings are $Q = 0.0333$ L/s, $V = 1$ L, $k_1 = 10$ L/s and $k_2 = 10$ L/mol. It is proposed that there is an unstable steady condition at $C = 1.316$ which is the nominal value of $C_f = 3.288$ mol/L. By linearizing around $C = 1.316$ and considering a delay time of 20 seconds, the following model is computed:

$$P_1(s) = \frac{3.433e^{-20s}}{103.1s - 1} \quad (5.45)$$

The disruptive element in this case is the inlet flow rate. As a result, the cascade control technique is put into practice. The secondary process model's dynamics are taken to be

$$P_2(s) = \frac{e^{-0.5s}}{3s + 1} \quad (5.46)$$

Choosing $T_d = 10.25$ and for several values of K_p in the range $0.291 < K_p < 2.845$, we compute $K_p = 0.891$ corresponding to $M_s = 1.6$. Using ABC optimization, $\lambda_1 = 4.86$, $\lambda_2 = 0.25$ and $\alpha = 1.08$ and $\beta = 1.12$ are computed. The fractional order sole approximations using phase modulated biquadratic equiripple approximation is presented in Table 5.1. Consequently, the estimated proposed control settings are

$C_2(s) = (3s + 1)(0.25s + 1)/(0.25s^{1.12} + 1)^2$, $C_S(s) = 0.891(1 + 10.25s)$ and $C_1(s) = (309.3s^2 + 68.736s + 2.06)/(3.433(25s^{2.16} + 10s^{1.08} + 1))$. Only (5.45) is utilized to get the aforementioned controller settings. In simulation, however, (5.44)'s nonlinear differential equation is applied rather than (5.44)'s. To analyze the servo operation, a set-point step change from 0 to 5 is used. Disturbances $d_1 = -10$ and $d_2 = -10$ are presented at 500s and 700s, respectively, to evaluate regulatory action. A +20% perturbation is taken into consideration in order to attain the suggested dead time compensator's resilience. Figs. 5.21- 5.22, which correspond to the nominal and disturbed plant models, respectively, exhibit plots of closed-loop outputs and control efforts. It is clear from Figs. 5.21 and 5.22 that the suggested system produces reliable closed-loop reactor control.

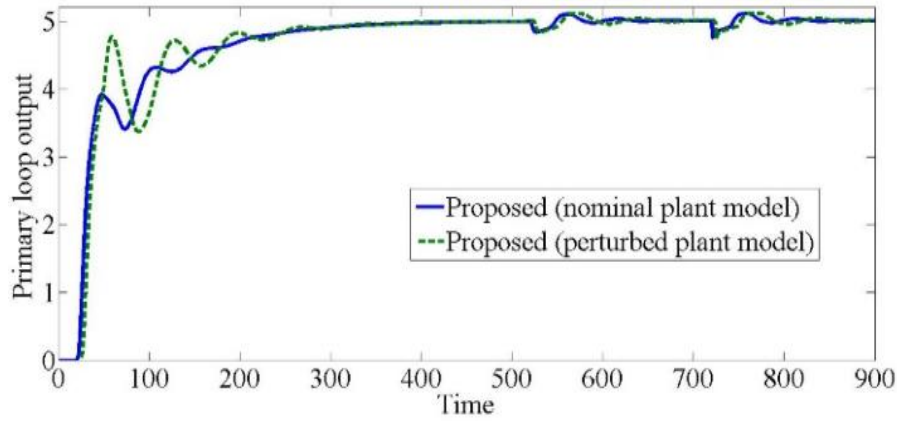


Fig. 5.21. Robustness of proposed method.

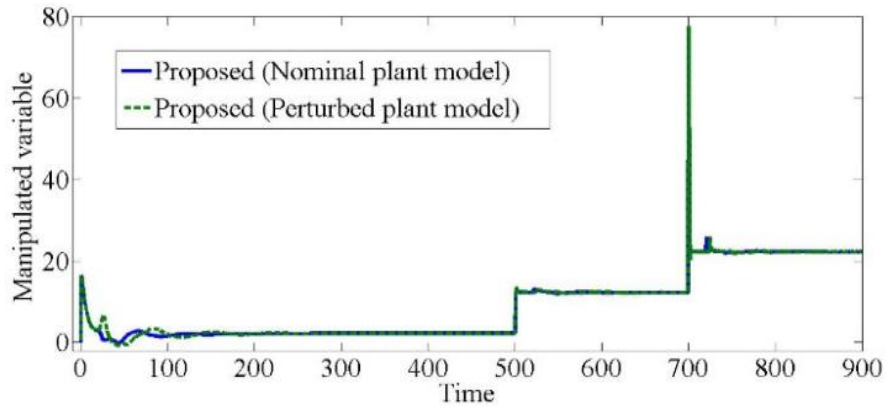


Fig. 5.22. Nominal and perturbed control actions.

Table 5.1
Approximated model of fractional order

| Fractional order | Approximated transfer functions $G(s)$ |
|------------------|---|
| $s^{1.05}$ | $\frac{0.85s^2 + 16.02s + 2.03}{2.03s^2 + 16.02s + 0.85}$ |
| $s^{1.15}$ | $\frac{2.24s^2 + 8.53s + 6.29}{6.29s^2 + 8.53s + 2.24}$ |
| $s^{1.08}$ | $\frac{2.25s^2 + 9.37s + 4.23}{4.23s^2 + 9.37s + 2.25}$ |
| $s^{1.12}$ | $\frac{5.84s^2 + 12.43s + 3.62}{3.62s^2 + 12.43s + 5.84}$ |

| Table 5.2 | | | | | |
|----------------------|-------------------|----------------|--------------|----------------------------|-----------------------|
| Performance measures | | | | | |
| Case | Tuning strategies | Nominal system | | | |
| | | IAE | ISE | TV | $t_{sov}(\text{sec})$ |
| Nominal case | | | | | |
| 1 | Proposed | 3.99 | 1.69 | 361.57 | 113.5 |
| | Yin et al. [8] | 4.89 | 2.91 | 126.15 | 111 |
| | Dasari et al. [7] | 7.32 | 3.93 | 43.47 | 118 |
| 2 | Proposed | 45.61 | 23.91 | 44.74 | 601 |
| | Yin et al. [8] | 47.27 | 25.88 | 6.60 | 624 |
| | Dasari et al. [7] | 72.62 | 45.63 | 6.72 | 641 |
| Perturbed case | | | | | |
| 1 | Proposed | 4.39 | 1.70 | 2.69x10³ | 109.2 |
| | Yin et al. [8] | -- | -- | -- | -- |
| | Dasari et al. [7] | 7.71 | 3.96 | 59.45 | 119.45 |
| 2 | Proposed | 53.12 | 30.81 | 50.44 | 627 |
| | Yin et al. [8] | 52.16 | 30.45 | 11.56 | 650 |
| | Dasari et al. [7] | 78.45 | 55.30 | 9.71 | 659 |

According to the aforementioned studies, the proposed optimal FOIMC-SCCS technique significantly outperforms certain recent research in terms of closed-loop servo and regulatory responses. Even if the overshoot during servo action is reduced, overshoots in regulatory action still occur and need to be addressed. But this proposed approach attains long-term stability with ease compared to existing conventional schemes.

After the significant application of an optimal FOIMC-SCCS scheme, the second novel investigation is carried out with FOMRAC augmented control schemes on another reported benchmark model. Only FOLY based standalone and augmented techniques are examined in this application for regulating process variables because FOLY is proven to be more efficient than FOMIT as discussed in chapter-4. Dual-loop techniques are implemented in a Simulink environment using Figs. 4.11, 4.14, and 4.15. The significant applications of the FOLY-based

dual-loop approach are explored in the subsequent research, and to assess the effectiveness of control. The performance of this proposed dual-loop strategies is further compared to another alternative proposed dual-loop scheme based on FOIMC-FOPD predictor for better improvement of control action.

Case study II: Comprehensive study of different FO-augmented strategies

Simulations are conducted using the different operating points of a benchmark plant models that are used in (5.47) and (5.52).

Example-4

Five linear operational regions comprise the linearized CSTR utilizing data shown in Table 5.3. In this work, the following linear operating points [30] are used: $C_A(t) = 0.1425 \text{ mol/l}$, $T_S = 460.12 \text{ K}$ and $q_c(t) = 113.25 \text{ l/min}$. The Eigen values of selected linear operating region are found as 3.478 and 1.356. This means that the resulting system is unstable with the following model:

$$Y_p(s) = \frac{0.1915}{s^2 - 5.948s + 22.69} \quad (5.47)$$

The parameters [30] of this CSTR are presented in Table 5.3.

| Table 5.3 Parameters of CSTR | |
|--|---------------------------------------|
| Parameters | Specifications |
| Concentration ($C_o(t)$) | 0.0885 mol/l |
| Reactor temperature ($T(t)$) | 441.14 K |
| Coolant flow rate ($q_c(t)$) | 100 l/min |
| Feed flow rate ($q_f(t)$) | 100 l/min |
| Feed concentration (C_f) | 1 mol/l |
| Feed temperature (T_f) | 350 K |
| Inlet coolant temperature (T_{cf}) | 350 K |
| CSTR volume (V) | 100 l |
| Reaction rate constant (k_0) | $7.2 \times 10^{10} \text{ min}^{-1}$ |
| Activation Energy (E/R) | $1 \times 10^4 \text{ K}$ |
| Heat of reaction ($-\Delta H$) | $-2 \times 10^3 \text{ cal/mol}$ |
| Liquid density (ρ) | $1 \times 10^3 \text{ g/l}$ |
| Heat transfer term (hA) | $7 \times 10^5 \text{ cal/(min K)}$ |

Now, choosing an ideal model (y_p) is crucial in MRAC based schemes. For the current procedure, the ideal parameters are peak overshoot (M_p) = 3% and settling time (T_s) = 3 seconds. For these specifications the damping ratio (ξ) = 0.59 and natural frequency (ω_n) = 2.259 are obtained using the following expressions:

$$M_p = e^{-\pi\xi/\sqrt{1-\xi^2}} \quad (5.48)$$

$$T_s = \frac{4}{\xi \omega_n} \quad (5.49)$$

So, the reference model is obtained as

$$Y_M(s) = \frac{5.103}{s^2 + 2.665s + 5.103} \quad (5.50)$$

In MRAC, the FOLY rule is always preferred over the MIT rule based on fractional orders. This is due to the fact that, as described in chapter 4, the adaptive gain of the Lyapunov stability rule is 1.5 times higher than the MIT rule. The FOLY rule includes γ and α as control law parameters which are frequently tuned to attain promising servo-regulatory behaviors. In general, system tracking performance enhances with increase in γ and reduction of α . It is discovered that increasing the value of adaptive gain and reducing extra degree of freedom makes the system responds quicker and minimizes the value of integral errors. All systems work satisfactorily within a certain range of adaptive gain and an additional degree of freedom. The closed-loop findings are examined for various γ values (between 0 to 50) and α values (between 0 to 1) for unstable plants.

Extensive research indicates that when $\gamma = 45$ and $\alpha = 0.75$ are used, the system provides adequate tracking performance (in terms of error values and response time). For the previously described gain levels, the FOLY rule yields more stable and enhanced closed-loop behavior when compared to the other gain values. The FOLY rule is added to the FOPID and FOIMC-FOPID controllers to further enhance performance. The modified PSO method is used to derive the parameters of the FOPID controller in (5.19). The suggested values for FOs in (5.25) are $\alpha = 0.492$ and $\beta = 0.246$ for unstable processes, respectively, based on extensive simulation research. Now, modified PSO is used to determine the best values of the filter time constant and fractional filter in (5.26). The MPSO method is also used to estimate the three tuning parameters (K_p , K_D and μ) of the FOPD scheme for the dual-loop FOIMC-FOPD predictor. K_p , K_I , K_D have ideal values between 0 and 100. In a manner similar to this, the ideal FO values (λ and μ) in the FOPID scheme are examined between 0 and 1. Likewise, a range of 0 to 100 is searched for the ideal filter time constant. The fractional filter is tuned for an order between 0 and 1. Next, the fractional-order tuning parameters of the FOPD prediction method are examined between 0 and 2, while the ideal values of the proportional and derivative tuning parameters are examined between 0 and 500. The optimization algorithm is discussed in Appendix-C. Table 5.4 depicts the proposed controller settings and Table 5.5 shows rational approximations of different computed fractional orders using exact phase modulated biquadratic approximation. To examine the servo response, a unit step change in set-point is taken into account at $t = 1$ second. Application of a unit-step disturbance at $t = 25$ seconds

allows for the study of regulatory responses. System outputs from all three of the multi-loop systems that have been suggested are compared to those of the FO-Lyapunov method. The system output is subtracted from the set-point at time 't' to produce the instantaneous error. ISE and ITAE are calculated using IAE. TV is determined by $\sum_{i=1}^{\infty} |u(i+1) - u(i)|$. To discover a workable balance between performance and robustness, the suggested predictor assumes that τ of the FOIMC controller is 0.5. Beyond 0.5 may result in a decline in closed-loop performance but enhance system robustness. On the other hand, performance is improved but robustness is sacrificed when the value is decreased below 0.5. The control actions and closed-loop outcomes for the three suggested control methods and the FOLY approach are plotted for the CSTR unstable process model in Figs. 5.23 and 5.24, respectively. At the plant's output, a 0.01 second delay is also taken into account. Gain of the process model is studied with a +10% perturbation to study the stability of the design. In Figs. 5.25 and 5.26, respectively, the system and controller outputs for the perturbed example are displayed. There is no doubt that the suggested methods produce more reliable closed-loop performance than the FO-Lyapunov stand-alone method.

The FOIMC-FOPD predictor, out of the three suggested control structures, produces a quicker servo action and noise rejection in both nominal and perturbed scenarios. Additionally, as shown in Table 5.6, the proposed FOIMC-FOPD predictor's IAE, ISE, ITAE, and TV measures are lower than those of the other three techniques.

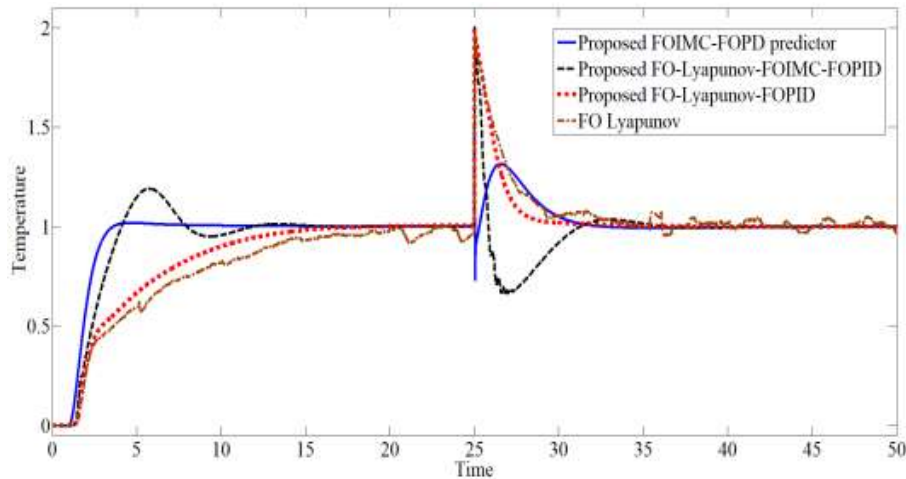


Fig. 5.23. Nominal outputs with stand-alone and augmented control topologies.

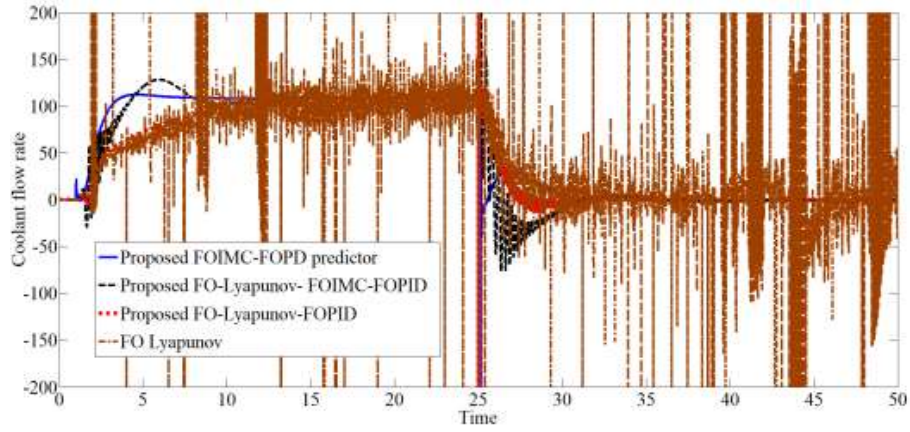


Fig. 5.24. Nominal control actions.

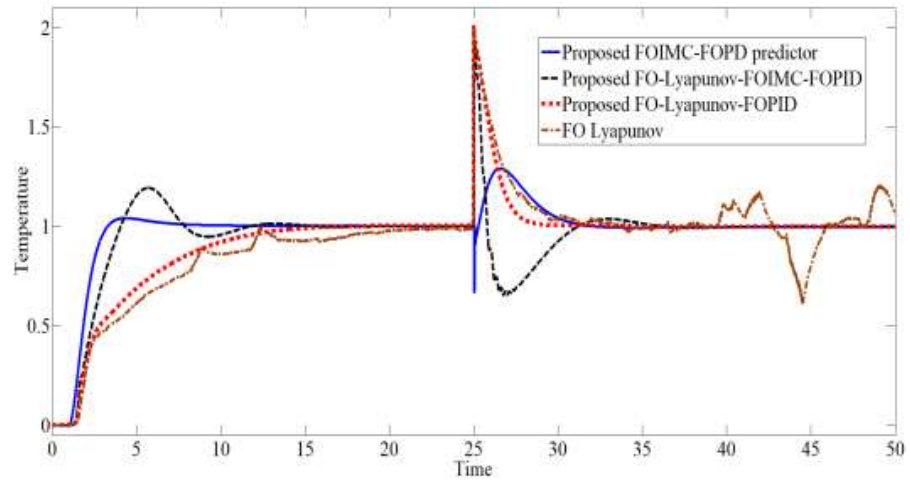


Fig. 5.25. Perturbed outputs with stand-alone and augmented control topologies.

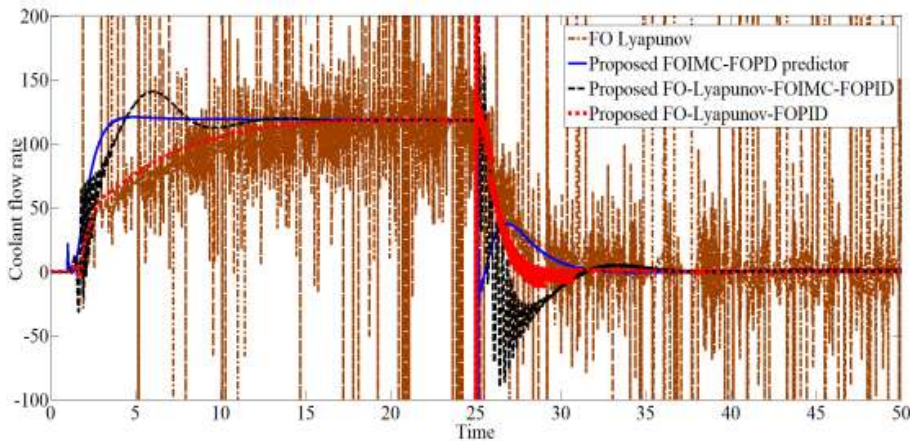


Fig. 5.26. Perturbed control actions.

A Gaussian noise source is introduced to the control actions for each of the four methods under consideration for comparison to evaluate the impact of measurement noise on system response

(mean = 0, variance = 0.001, seed = 41, and time = 1 second). In Fig. 5.27, the closed-loop servo and regulatory responses to noise are depicted. It is found that even amid the measurement noise, the proposed approaches follow the set-point and reject the disturbances. But, proposed FOMIC-FOPD predictor tackles the system more swiftly and gracefully.

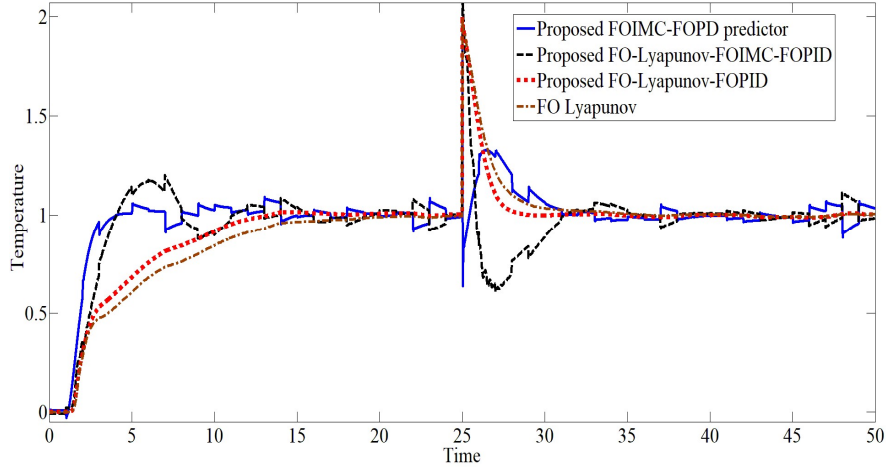


Fig. 5.27. Nominal outputs under noise.

Example-5

In this study, the following linear operating points [30] are used: $C_A(t) = 0.0885$ mol/l, $T_S = 441.14$ K, $q_c(t) = 100$ l/min. These settings are applied in (2.98) to define the matrix A as illustrated below:

$$A = \begin{bmatrix} -11.435 & -0.1436 \\ 3144.6 & 2.583 \end{bmatrix} \quad (5.51)$$

Since, the Eigen values of (5.51) are obtained as -2.3899, -1.0, it results stable state. The following stable state based model is found for the above operating zones as found below:

$$Y_P(s) = \frac{0.04327}{s^2 + 3.931s + 13.22} \quad (5.52)$$

In this instance, multiple adaptive gains (ranging from 0 to 200) and additional degrees of freedom (between 0 and 1) are examined for the closed-loop servo-regulatory responses. Extensive simulations reveal that, with $\gamma = 150$ and $\alpha = 0.5$, the system offers reasonable tracking performance in terms of error levels and speed. The fractional-orders are suggested as $\alpha = 0.304$ and $\beta = 0.152$ in (5.25). Table 5.4 depicts the proposed controller settings and Table 5.5 shows rational approximations of different computed fractional orders using exact phase modulated biquadratic approximation.

The system outputs and control efforts are shown as illustrated in Figs. 5.28 and 5.29, accordingly, taking into account the CSTR process model established. A dead time of 0.0001 second is taken into consideration along with the process model described in (5.51) in order to examine the system's robustness. Figs. 5.30 and 5.31, respectively, depict closed-loop outputs and control attempts of the perturbed model using the aforementioned delay. Table 5.6's IAE, ISE, ISTE, and TV metrics demonstrate that the suggested solutions produce improved closed-loop performance and significantly smoother control actions. Notably, Compared to other suggested control structures, the FOIMC-FOPD predictor performs better. The suggested FOIMC-FOPD control strategy's control signal is significantly smoother and smaller in amplitude than those of the other methods. It is hence ecologically friendly. It's also important to note that the FOIMC-FOPD control approach is simpler and takes less time 5 sec than the other three techniques. Similar to Example 3, same noise source is added to the system outputs for each of the strategies under consideration for comparison to evaluate the impact of measurement noise on system response. Fig. 5.32 illustrates servo-regulatory outputs with noise. It has been found that the suggested methods work well even when there is measurement noise since they can follow the set-point and reject disruptions.

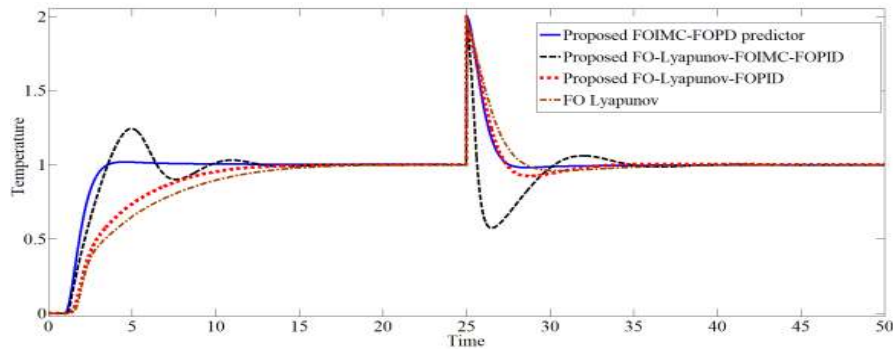


Fig. 5.28. Nominal outputs with stand-alone and augmented control topologies.

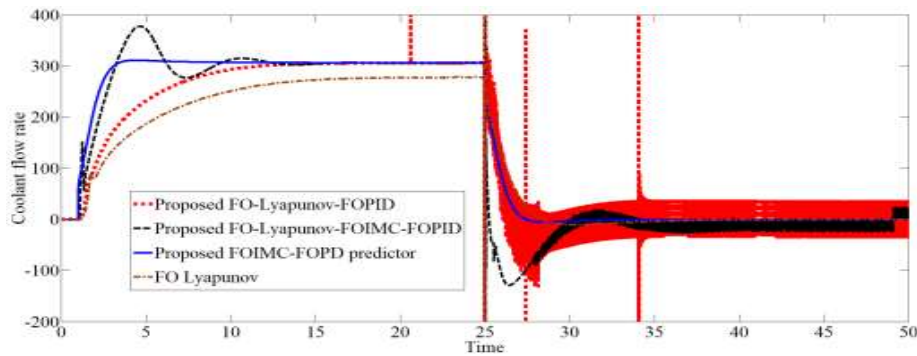


Fig. 5.29. Nominal control actions.

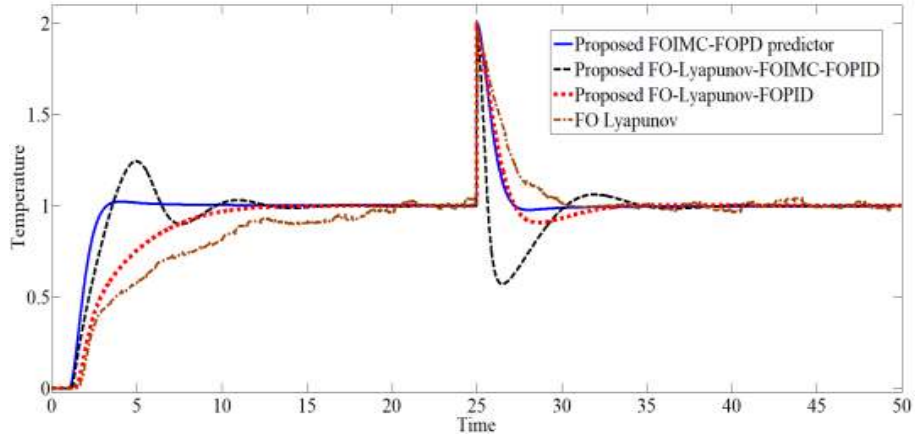


Fig. 5.30. Perturbed outputs with stand-alone and augmented control topologies.

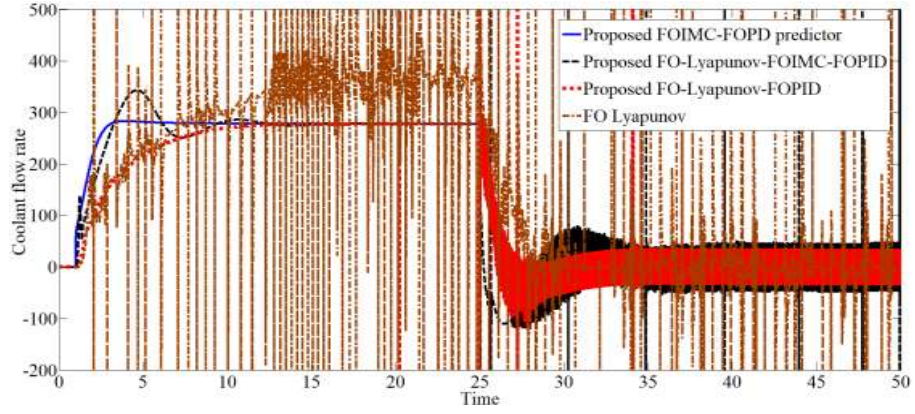


Fig. 5.31. Perturbed control actions.

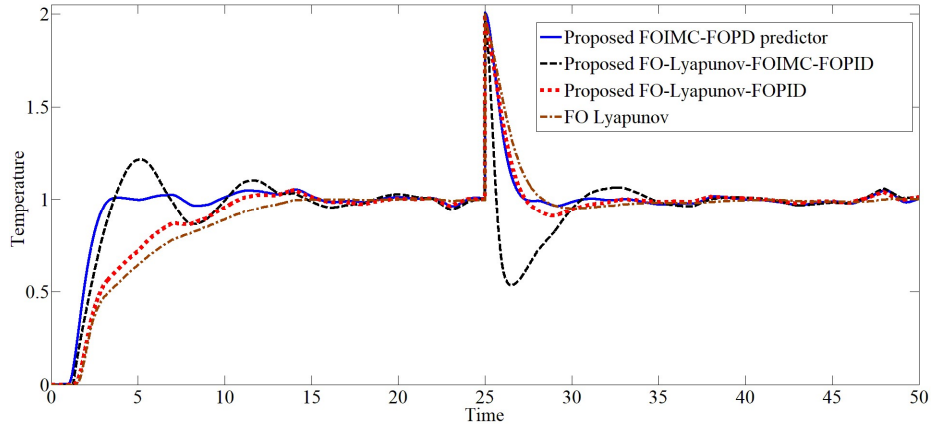


Fig. 5.32. Nominal outputs in the presence of noise.

Table 5.4
Controller settings

| | Method | Controller functions |
|------------------|--|---|
| Example-4 | Proposed FO-Lyapunov | $\theta_1 = 45e^{\frac{1}{s^{0.75}}u_c}, \theta_2 = -45e^{\frac{1}{s^{0.75}}\frac{0.1915}{s^2-5.948s+22.69}}$ $U(s) = 45e^{\frac{1}{s^{0.75}}u_c} - [-45e^{\frac{1}{s^{0.75}}\frac{0.1915}{s^2-5.948s+22.69}}]$ |
| | Proposed Multi-loop FOLY-FOPID | $C_{FOPID} = 0.984 + \frac{0.113}{s^{0.32}} + 0.376s^{.26}$ $U(s) = 45e^{\frac{1}{s^{0.75}}u_c} - [-45e^{\frac{1}{s^{0.75}}\frac{0.1915}{s^2-5.948s+22.69}}]$ |
| | Proposed multi-loop FOLY-FOIMC-FOPID | $C_{FOIMC-FOPID} = \left(-30 + \frac{118}{s^{0.246}} + 5s^{0.246}\right)\frac{1}{6.22s^{0.24}}$ $U(s) = 45e^{\frac{1}{s^{0.75}}u_c} - [-45e^{\frac{1}{s^{0.75}}\frac{0.1915}{s^2-5.948s+22.69}}]$ |
| | Proposed Multi-loop FOIMC-FOPD predictor | $G_{PD}(s) = 0.01 + 248.45s^{1.05}$ $C(s) = \frac{s^2 + 47.875s^{1.05} - 5.948s + 22.69}{0.048s^{2.1} + 0.192s^{1.05} + 0.192}$ |
| Example-5 | Proposed FO-Lyapunov | $\theta_1 = 150e^{\frac{1}{s^{0.5}}u_c}, \theta_2 = -150e^{\frac{1}{s^{0.5}}\frac{0.04327}{s^2+3.931s+13.22}}$ $U(s) = 150e^{\frac{1}{s^{0.5}}u_c} - [-150e^{\frac{1}{s^{0.5}}\frac{0.04327}{s^2+3.931s+13.22}}]$ |
| | Proposed Multi-loop FOLY-FOPID | $C_{FOPID} = 0.957 + \frac{0.0634}{s^{0.435}} + 0.835s^{.328}$ $U(s) = 150e^{\frac{1}{s^{0.5}}u_c} - [-150e^{\frac{1}{s^{0.5}}\frac{0.04327}{s^2+3.931s+13.22}}]$ |
| | Proposed multi-loop FOLY-FOIMC-FOPID | $C_{FOIMC-FOPID} = \left(90 + \frac{305.42}{s^{0.152}} + 23.11s^{.152}\right)\frac{1}{1.025s^{.34}}$ $U(s) = 150e^{\frac{1}{s^{0.5}}u_c} - [-150e^{\frac{1}{s^{0.5}}\frac{0.04327}{s^2+3.931s+13.22}}]$ |
| | Proposed Multi-loop FOIMC-FOPD predictor | $G_{PD}(s) = 0.92 + 1.15s^{1.02}$ $C(s) = \frac{s^2 + 0.05s^{1.02} + 3.931s + 13.263}{0.01s^{2.04} + 0.0433s^{1.02} + 0.0433}$ |

Table 5.5
Approximations of fractional order

| Fractional order | Approximated transfer functions $G(s)$ |
|------------------|---|
| $s^{0.75}$ | $\frac{8.026s^2 + 24.73s + 4.536}{4.536s^2 + 24.73s + 8.026}$ |
| $s^{.246}$ | $\frac{3.36s^2 + 12.53s + 4.03}{4.03s^2 + 12.53s + 3.36}$ |
| $s^{0.32}$ | $\frac{6.82s^2 + 3.47s + 2.36}{2.36s^2 + 3.47s + 6.82}$ |
| $s^{1.05}$ | $\frac{2.54s^2 + 6.38s + 4.82}{4.82s^2 + 6.38s + 2.54}$ |
| $s^{2.1}$ | $\frac{4.29s^2 + 11.23s + 2.57}{2.57s^2 + 11.23s + 4.29}$ |
| $s^{0.5}$ | $\frac{5.025s^2 + 36.88s + 6.525}{6.525s^2 + 36.88s + 5.025}$ |
| $s^{0.435}$ | $\frac{3.135s^2 + 10.43s + 0.652}{0.652s^2 + 10.43s + 3.135}$ |
| $s^{0.152}$ | $\frac{8.255s^2 + 2.62s + 3.623}{3.623s^2 + 2.62s + 8.255}$ |
| $s^{1.02}$ | $\frac{2.475s^2 + 5.63s + 1.525}{01.525 + 5.63s + 2.475}$ |
| $s^{2.04}$ | $\frac{3.525s^2 + 9.473s + 0.884}{0.844s^2 + 9.473s + 3.525}$ |

Table 5.6
Quantitative performance measures

| | Control Structure | Nominal plant | | | | Perturbed plant | | | |
|------------|--|---------------|-------------|--------------|--------------------------------------|-----------------|-------------|--------------|--------------------------------------|
| | | IAE | ISE | ITAE | TV | IAE | ISE | ITAE | TV |
| Example -4 | Proposed dual-loop FOLY-FOPID | 4.89 | 2.44 | 50.68 | 1.58×10^{15} | 4.51 | 2.31 | 44.79 | 1.45×10^{15} |
| | Proposed dual-loop FOLY-FOIMC-FOPID | 3.63 | 1.63 | 49.97 | 8.37×10^3 | 3.62 | 1.62 | 49.97 | 8.08×10^3 |
| | Proposed dual-loop FOIMC-FOPD predictor | 2.10 | 0.86 | 31.36 | 2.99×10^5 | 2.05 | 0.83 | 29.20 | 2.99×10^5 |
| | FO-Lyapunov | 6.88 | 3.02 | 90.35 | 6.75×10^{15} | 6.88 | 3.02 | 116.2 | 7.34×10^{15} |
| Example -5 | Proposed dual-loop FOLY-FOPID | 4.34 | 2.31 | 46.37 | 4.27×10^{15} | 4.15 | 2.23 | 45.16 | 4.27×10^{15} |
| | Proposed dual-loop FOLY-FOIMC-FOPID | 3.61 | 1.54 | 52.58 | 1.78×10^5 | 3.61 | 1.54 | 52.64 | 1.78×10^5 |
| | Proposed dual-loop FOIMC-FOPD predictor | 2.119 | 1.27 | 30.38 | 1.68×10^3 | 1.96 | 1.18 | 28.07 | 1.68×10^3 |
| | FO-Lyapunov | 5.338 | 2.79 | 58.21 | 5.77×10^{15} | 6.57 | 3.26 | 79.88 | 2.95×10^{16} |

According to the aforementioned findings, a dual-loop control scheme may be suggested as a more effective method than unity feedback for regulating unstable systems. Simulation tests reveal that the suggested dual-loop FOLY-FOIMC-FOPID technique improves servo and regulatory performance, but the proposed FOIMC-FOPD predictor performs particularly well when compared to other methods. Ongoing study is currently underway to investigate the FOLY rule's optimum gains. The use of two alternative optimization algorithms, such as ABC and MPSO, to the FOLY and FOMIT rules for searching for optimal gains is presented in the following case study III.

Case study III: Comprehensive study of optimal FOMRAC rules

Simulations are conducted using the different operating points of another benchmark plant models that are used in (5.53) and (5.54).

Example-6

Without jacket dynamics, the model equations for jacketed CSTR [31] are appeared as

$$\frac{dC}{dt} = \frac{F}{V} (C_{Af} - C_A) - K_0 \exp\left(-\frac{E_a}{RT}\right) C_A \quad (5.53)$$

$$\frac{dT}{dt} = \frac{F}{V} (T_f - T) - \frac{\Delta H K_0}{\rho C_p} \exp\left(\frac{-E_a}{RT}\right) C_A - \frac{UA}{V \rho C_p} (T - T_j) \quad (5.54)$$

Around unstable operating locations, the nonlinear model mentioned above is linearized [32]: $C_A=0.0644$ lb.mol/ft³, $T = 560.77$ °R, $T_j = 523.0122$ °R. The values of process parameters are shown in Table 5.7. The transfer function with a delay time of 0.0317 sec is computed with the following expression as

$$G(s) = \frac{.82055s + 6.5565}{.9416s^2 + 2.6977s - 1} e^{-0.0317s} \quad (5.55)$$

The optimal values of γ and α are found as 0.08 and 0.24653 using MPSO. Using the ABC optimization, $\gamma = 0.20034$ and $\alpha = 0.30456$ are obtained. Figs. 5.33 and 5.34 display the closed-loop actions and control initiatives corresponding to the nominal plant. The control settings for the proposed technique and the approaches under consideration for comparison are summarized in Table 5.8. The approximate results of various ideal fractional orders are shown using exact phase modulated biquadratic equiripple approximation in Table 5.9. Figs. 5.35 and 5.36 show the perturbed model's plant output and control signal graphs. It is clear that the recommended optimal FOLY strategy exceeds the competition in terms of rejecting disturbances and following set points.

A noise generator ($\sigma=0.01$, seed = 0.1, and time = 1 sec) is incorporated into the output to evaluate the impact of measurement noise on system response. Figs. 5.37 and 5.38, respectively, depict closed-loop results and control actions amid noise. It has been found that even with noise, the suggested methods track the set point and reject the disturbances.

Table 5.7
Specifications of Jacketed CSTR

| Parameters | value |
|---|---|
| Feed concentration (C_{Af}) | 0.132 lb.mol/ ft ³ |
| Feed Temperature (T_f) | 519.67°R |
| Nominal reactor volume | 668 ft ³ |
| Heat transfer area | 309 ft ² |
| Diameter | 7.5 ft |
| Operating volume | 500 ft ³ |
| Operating flow rate | 2000 ft ³ /hr |
| Overall heat transfer coefficient (U) | 75 Btu/hr ft ² °F |
| Activation energy (E_a) | 32400 Btu/lb.mol |
| Frequency factor (K_o) | 16.96x10 ¹² hr ⁻¹ |
| Heat of reaction ($-\Delta H$) | 39000 Btu/lb.mol |
| Product of density and specific heat (ρC_p) | 53.25 Btu/ft ³ °F |
| Ideal gas constant (R) | 1.987 Btu/lb.mol °R |

Table 5.8
Parameters of controller tuning

| Control scheme | Adaptive gain(γ) | Extra degree of freedom(α) |
|----------------|---------------------------|-------------------------------------|
| PSO FOLY | 0.12 | 0.24653 |
| ABC FOLY | 0.30051 | 0.30456 |
| PSO FOMIT | 0.08 | 0.24653 |
| ABC FOMIT | 0.20034 | 0.30456 |

Table 5.9
Approximations of fractional order

| Fractional order | Approximated transfer functions G(s) |
|------------------|---|
| $s^{0.30456}$ | $\frac{8.026s^2 + 24.73s + 4.536}{4.536s^2 + 24.73s + 8.026}$ |
| $s^{-2.4653}$ | $\frac{3.36s^2 + 12.53s + 4.03}{4.03s^2 + 12.53s + 3.36}$ |

Further evidence of the excellence of the proposed plan is explored by the lower values of the quantitative performance metrics provided in Table 5.10.

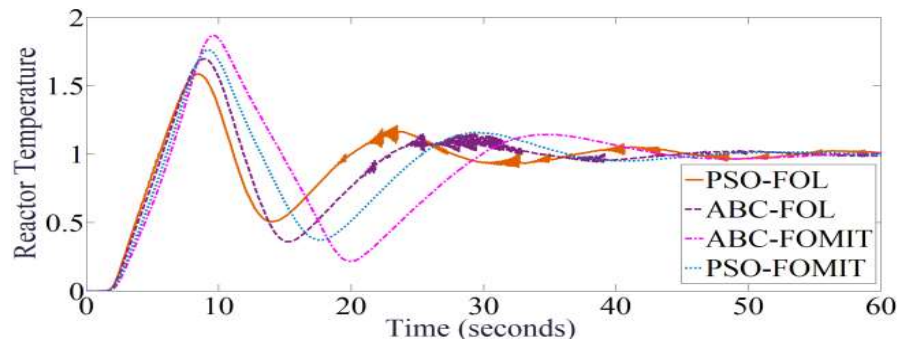


Fig. 5.33. System outputs using different optimal FOMRAC rules.

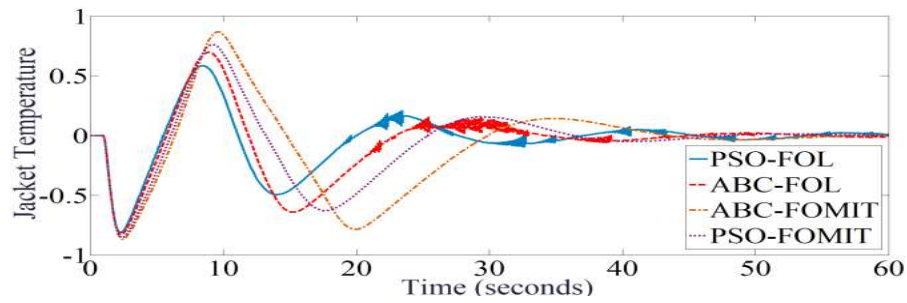


Fig. 5.34. Nominal Control actions.

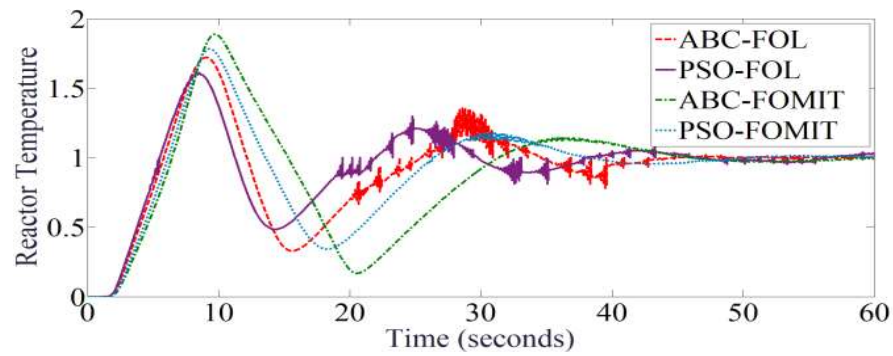


Fig. 5.35. Perturbed outputs using different optimal FOMRAC rules.

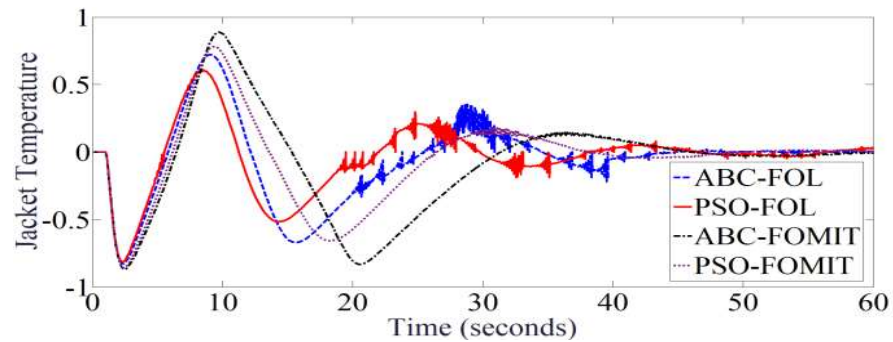


Fig. 5.36. Perturbed Control efforts.

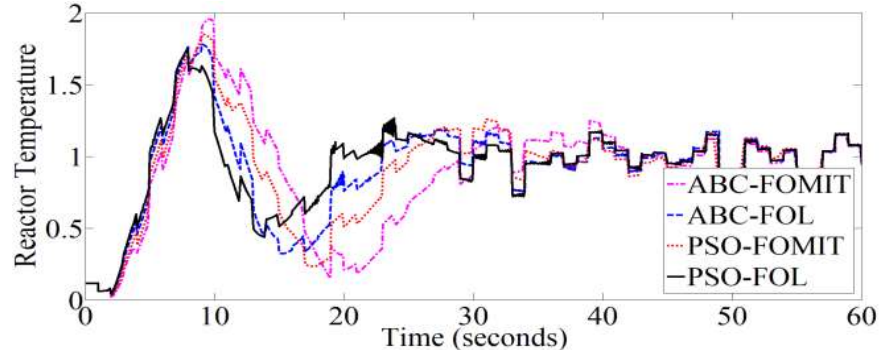


Fig. 5.37. Noise measurement of outputs.

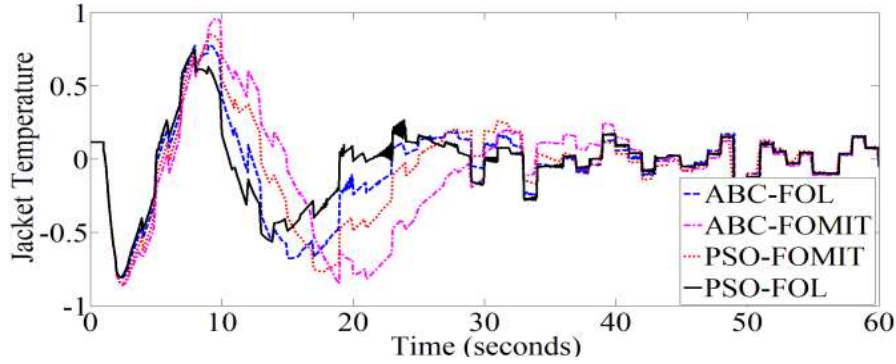


Fig. 5.38. Noise impact on control efforts.

Table 5.10
Quantitative analysis

| Control Structure | Nominal process | | | | Perturbed process | | | |
|--------------------|-----------------|-------|-------|-------|-------------------|-------|-------|-------|
| | IAE | ISE | ITAE | TV | IAE | ISE | ITAE | TV |
| Proposed PSO-FOLY | 9.029 | 4.102 | 126.3 | 167.8 | 9.963 | 4.462 | 147.8 | 168.2 |
| Proposed ABC-FOLY | 12.12 | 6.394 | 173.8 | 237.3 | 12.77 | 6.859 | 189.3 | 234.3 |
| Proposed PSO-FOMIT | 10.55 | 5.59 | 138.9 | 132.7 | 11.95 | 6.162 | 174.3 | 142.4 |
| Proposed ABC-FOMIT | 15.13 | 7.413 | 246.8 | 302.4 | 15.99 | 9.464 | 270.2 | 298.2 |

Based on a comparison of two optimization methods, MPSO-based FOMRAC schemes produce promising results than the ABC method, but MPSO-based FOLY outperforms the other optimal rules. As shown in Case Study II, a stand-alone FOLY produces a servo-regulatory response with minute oscillations. This issue might be resolved by adjusting the gain parameters to their ideal values using the MPSO optimization approach which is under investigation.

5.5 Summary

For different benchmark models of the continuous stirred tank reactor, fractional order standalone and augmented novel control topologies are proposed in this chapter. All proposed control methods' underlying mathematical presuppositions are thoroughly explained. Fractional orders are approximated by rational modified biquadratic exact phase approximation method. A combination of sophisticated simulation and optimization techniques are used to set the controller's parameters. In comparison to existing schemes, the significant effects of the proposed SCCS scheme with the optimal FOIMC controller are investigated in order to tackle the process variable with robust control effort. Additionally, the FOIMC rule's application is expanded to include the FOPD-Smith prediction method and the fractional order modified Lyapunov stability rule. To demonstrate the advantages of enhanced approaches over standalone method with regard to various error metrics and TV measurement from a real-time perspective, a thorough simulation analysis is presented. Instead of employing FOLY-FOPID or standalone FOLY rules, the FOIMC based FOPID controller aids in demonstrating more stable control action when augmented with FOLY rules. In the second investigation, the FOPD-FOIMC smith predictor outperforms due to its smoother control action. Even if the augmented FOLY-FOIMC-FOPID is well competent of handling noise, the FOPD-FOIMC predictor approach exhibits superior noise rejection action with significantly reduced overshoot for specific linearized operating points based on the current benchmark model employed in this chapter. Later, it is suggested to use both ABC and PSO optimization techniques to look for the FOLY rules' ideal gain values. Therefore, in a multi-loop method, ideal values might help to strengthen the control action. It is established that PSO looks for better gain parameter values than the ABC approach, and while this method significantly reduces the oscillation of the FOLY rule, PSO still results in higher overshoot. Research is still underway to offer zero overshoot at the intended level and enhance control action more swiftly in servo-regulatory performance.

References

- [1] Panda, A., Goswami, S. & Panda, R.C. Dual estimation and combination of state and output feedback based robust adaptive NMBC control scheme on non-linear process. *Int. J. Dynam. Control* 7, 725–743, 2019.
- [2] N. Kumar and N. Kahnduja, Mathematical modelling and simulation of CSTR using MIT rule, In: *Proceedings of IEEE India International Conference on Power Electronics (IICPE)*, Delhi, 2012, 1-5.

- [3] M. Ravari and M. Yaghoobi, Optimum design of fractional order PID controller using chaotic firefly algorithms for a control CSTR System, *Asian journal of control*, 21(2018), 2245-2255.
- [4] O. Alshammari, M.N. Mahyuddin and H. Jerbi, An advanced PID based control technique with adaptive parameter scheduling for a nonlinear CSTR plant, *IEEE Access*, 7(2019), 158085-158094.
- [5] F. Meng, S. Liu and K. Liu, "Design of an Optimal Fractional Order PID for Constant Tension Control System", in *IEEE Access*, vol. 8, pp. 58933-58939, 2022.
- [6] Çakıroğlu O, Güzelkaya M and Eksin I (2015) Improved cascade controller design methodology based on outer-loop decomposition. *Transactions of the Institute of Measurement and Control* 37: 623-635.
- [7] Dasari P.R, Alladi L, Rao A.S and Yoo C (2016) Enhanced design of cascade control systems for unstable processes with time delay. *Journal of Process Control* 45:43-54.
- [8] Yin, C. Q., Wang, H. T., Sun, Q., & Zhao, L. (2019) Improved cascade control system for a class of unstable processes with time delay. *International Journal of Control, Automation and Systems*, 17: 126-135.
- [9] Jeng J.C (2014) Simultaneous closed-loop tuning of cascade controllers based directly on set-point step-response data. *Journal of Process Control*, 24: 652-662.
- [10] Kaya I and Nalbantoğlu M (2016) Simultaneous tuning of cascaded controller design using genetic algorithm. *Electrical Engineering*, 98: 299-305.
- [11] Uma S, Chidambaram M, Rao A.S and Yoo C (2010) Enhanced control of integrating cascade processes with time delays using modified smith predictor. *Chemical Engineering Science*, 65: 1065-1075.
- [12] Veronesi M and Visioli A (2011) Simultaneous closed-loop automatic tuning method for cascade controllers. *IET Control Theory and Applications*, 5: 263-270.
- [13] Kaya I and Atherton D.P (2008) Use of smith predictor in the outer loop for cascaded Control of unstable and integrating processes. *Industrial & Engineering Chemistry Research* 47: 1981-1987.

- [14] Uma S, Chidambaram M and Rao (2009), Enhanced control of unstable cascade processes with time delays using a modified smith predictor. *Industrial & Engineering Chemistry Research* 48: 3098-3111.
- [15] García P, Santos T, Normey-Rico J.E and Albertos P (2010) Smith predictor-based control schemes for dead-time unstable cascade processes. *Industrial & Engineering Chemistry Research* 49: 11471-1181.
- [16] Efe M (2011) Fractional order systems in industrial automation: a survey. *IEEE Transactions on Industrial Informatics* 7: 582-591.
- [17] Pashaei S and Bagheri P (2020) Parallel cascade control of dead time processes via fractional order controllers based on Smith predictor. *ISA transactions* 98: 186-197.
- [18] S. Nema and P.K. Padhy, Identification and cuckoo PI-PD controller design for stable and unstable processes, *Transactions of the Institute of Measurement and Control*, 37(2015), 708–720.
- [19] B.A. Conway, A Survey of Methods Available for the Numerical Optimization of Continuous Dynamic Systems, *Journal of Optimization Theory and Applications*, 152(2012), 271–306.
- [20] B. Verma and P.K. Padhy, Optimal PID controller design with adjustable maximum sensitivity, *IET Control Theory and Applications*, 12(2018), 1156–1165.
- [21] N.S. Özbek and I. Eker, Design of an optimal fractional fuzzy gain-scheduled Smith Predictor for a time-delay process with experimental application, *ISA Transactions*, 97(2020), 14–35.
- [22] H. Goud and P. Swarnkar, Signal synthesis model reference adaptive controller with artificial intelligent technique for a control of continuous stirred tank reactor, *International Journal of Chemical Reactor Engineering*, 17 (2018), 1-11.
- [23] Y.G. Wang and W.J. Cai, Advanced proportional– integral– derivative tuning for integrating and unstable processes with gain and phase margin specifications, *Industrial & engineering chemistry research*, 41(2002), 2910-2914.
- [24] Daniel Martins Lima, Tito Luís Maia Santos, Julio Elias Normey-Rico, Robust nonlinear predictor for dead-time systems with input nonlinearities, *Journal of Process Control*, Vol. 27, 2015, pp. 1-14.

- [25] Liu T, Zhang W and Gu D (2005), IMC-based control strategy for open-loop unstable cascade processes. *Industrial & Engineering Chemistry Research*, 44: 900-909.
- [26] So, GB., Jin, GG. Fuzzy-based nonlinear PID controller and its application to CSTR. *Korean J. Chem. Eng.* 35, 819–825 (2018).
- [27] Karaboga, D., Basturk, B. (2007). Artificial Bee Colony (ABC) Optimization Algorithm for Solving Constrained Optimization Problems. In: Melin, P., Castillo, O., Aguilar, L.T., Kacprzyk, J., Pedrycz, W. (eds) Foundations of Fuzzy Logic and Soft Computing. IFSA 2007. Lecture Notes in Computer Science, vol 4529.
- [28] Chaturvedi, S., Kumar, N. & Kumar, R. A PSO-optimized novel PID neural network model for temperature control of jacketed CSTR: design, simulation, and a comparative study. *Soft Comput* 28, 4759–4773 (2024).
- [29] Morari M and Zafiriou E (1989) Robust process control. Prentice Hall: Englewood Cliffs, NJ.
- [30] Siddiqui, M. A., Anwar, M. N., & Laskar, S. H. (2021). Control of nonlinear jacketed continuous stirred tank reactor using different control structures. *Journal of Process Control*, 108, 112-124.
- [31] Rosy Pradhan, Santosh Kumar Majhi, Jatin Kumar Pradhan, Bibhuti Bhusan Pati, “Optimal fractional order PID controller design using Ant Lion Optimizer”, *Ain Shams Engineering Journal*, Vol.11 (2),2020, pp. 281-291.
- [32] D. Li, D. Wang, L. Liu and Y. Gao, "Adaptive Finite-Time Tracking Control for Continuous Stirred Tank Reactor With Time-Varying Output Constraint," in *IEEE Transactions on Systems, Man, and Cybernetics: Systems*, vol. 51, no. 9, pp. 5929-5934, Sept. 2021.

Publication

1. **D. Mukherjee**, G.L. Raja, P. Kundu, “Optimal Fractional Order IMC-Based Series Cascade Control Strategy with Dead-Time Compensator for Unstable Processes”, **Journal of Control Automation & Electrical System**, Vol. 32, pp. 30–41, 2021.

2. **D. Mukherjee**, G.L. Raja, P. Kundu, A. Ghosh, “Improved fractional augmented control strategies for continuously stirred tank reactors”, **Asian Journal of Control**, Vol. 25, pp. 2165–2182, 2023.
3. **D. Mukherjee** , G.L. Raja, P. Kundu, A. Ghosh, “Design of Optimal Fractional Order Lyapunov Based Model Reference Adaptive Control Scheme for CSTR”, **IFAC-PapersOnLine**, Vol. 55, pp. 436-441, 2022.
4. **D. Mukherjee**, G.L. Raja, P. Kundu, “A SYSTEM FOR ADVANCED DEAD-TIME COMPENSATOR-BASED SERIES CASCADE CONTROL STRUCTURE FOR UNSTABLE PROCESSES”, **PATENT No: 2021102343, Australian Innovation Patent**, 2021.
5. **D. Mukherjee**, P. Kundu, A. Ghosh, “Analysis of Conventional and Fractional-Order Controllers for Nonlinear CSTR System”, In: Sherpa, K.S., Bhoi, A.K., Kalam, A., Mishra, M.K. (eds) *Advances in Smart Grid and Renewable Energy. ETAEERE 2020. Lecture Notes in Electrical Engineering*, vol 691. **Springer**, Singapore, 2021.

CHAPTER 6

Fractional Order Standalone Backstepping Control Strategy for Unstable Processes

6.1 Introduction

A nonlinear control technique called backstepping control [1] is used to design stabilizing controllers for intricate systems. The process is decomposing the control problem into a number of more straightforward subsystems with a single input and single output, and designing a controller for each subsystem that guarantees the stability of the system as a whole. This method [2] is particularly useful for systems that are difficult to model or have complex dynamics. For a specific type of nonlinear dynamical systems, the method is especially helpful in building stabilizing controls. The subsystems that make up these systems [2] branch out from an irreducible subsystem that can be stabilized in another way. The backstepping technique [2] offers a recursive way to stabilize a system's origin in strict-feedback form. The design process begins with the system that is known to be stable, then new controllers are gradually "back out" [2] to stabilize each outer subsystem. The phrase "backstepping" refers to the process's termination when the final external control is reached. The augmented conventional adaptive and block backstepping methods received much of the attention in the literature [3–4], where it was found that they performed satisfactorily without overshoots. Nevertheless, no reports of noise and disturbance were found while using the previously indicated backstepping techniques. It is apparent that there is a dearth of information regarding the independent traditional backstepping approach that might be used for unstable systems. Based on previous discussions, in contrary to the current reported works on significant impact of various proposed fractional order based standalone and augmented topologies on inverted pendulum and continuous stirred tank reactor systems, It is worthwhile to investigate a fractional standalone backstepping rule since it is anticipated to provide promising result than the traditional backstepping method. Furthermore, there aren't enough research in the literature to support the backstepping method's advantages over other contemporary control techniques.

Even backstepping methods that are already in place are frequently enhanced with additional control rules, making their implementation more difficult [5–6]. For practical applications, simple control systems may be more advantageous in practice [16].

So, the significant impact of proposed standalone fractional order backstepping (FOB) rule is discussed as an efficient alternative to standalone CB scheme and its augmented version for reported benchmark inverted pendulum and continuous stirred tank reactor in this chapter. There is still a significant opportunity to enhance performance by offering the lowest integral errors, zero overshoot, and fastest rate of action, even though the currently reported proposed fractional order control schemes provide the expected performance robustness trade-off with lower integral errors and overshoot. Various novel case studies are conducted to investigate the performance of FOB. Like other schemes as discussed in the previous chapters, the same proposed modified biquadratic equiripple approximation method is employed to approximate FO in the fractional order backstepping law.

There are mainly two approaches [3] for designing Backstepping controller, which are stabilizing design and tracking design, are discussed in the next section.

6.2 Rule of Backstepping Scheme

The step by step procedure for designing backstepping controller using stabilizing and tracking methods [3] is discussed in this section.

6.2.1 Implementation of Stabilizing Design

The steps [3] to implement the backstepping controller is followed as

- I. Transfer function of the system is simplified as state equations with state variables.
- II. The appropriate Lyapunov function is selected and necessary substitutions are made followed by simplifications on each subsystem of the model.
- III. Finally, controller transfer function is evaluated and it is connected with the model using closed-loop feedback rule.

6.2.2 Implementation of Tracking Design

The steps [3] to implement the backstepping controller is followed as

- I. The transfer function of the system is simplified as state equations with state variables.

II. Virtual control input is selected to choose the first backstepping variable for the second subsystem.

III. The appropriate Lyapunov function is selected and necessary substitutions are made followed by simplifications on each subsystem of the model.

IV. Finally, controller transfer function is evaluated and it is connected with the model using closed-loop feedback rule.

In this chapter, the aforementioned methods are used to implement the fractional order rule to ensure global stability. Finally, using direct Lyapunov theory (with the proper Lyapunov functions) three distinct strategies are proposed with global stability considerations to stable the continuous stirred tank reactor and inverted pendulum. The steps below are involved in controller design:

- The required output variable for the state equation of the system is developed.
- Each subsystem is globally stabilized by applying the Lyapunov approach with the appropriate Lyapunov functions.
- The factors pertaining to global stability are considered. After that, the required simplifications and replacements are made in order to synthesize the controller.

A continuous scalar function locally or globally, $P(x)$ is referred to as positive definite [21–25] if

$$\begin{cases} P(0) = 0 \wedge (\forall x \neq 0 \wedge \|x\| < R) \Rightarrow P(x) > 0: \text{Local stability} \\ P(0) = 0 \wedge (\forall x \neq 0) \Rightarrow P(x) > 0: \text{Global stability} \end{cases}$$

A function $P(x)$ is considered the Lyapunov function for a system if it is positive definite, has continuous partial derivatives and has a negative semi-definite time derivative ($\dot{P}(x) \leq 0$) along the trajectory of the system $\dot{x} = f(x)$. Finding the Lyapunov function's time derivative yields $\dot{P}(x) = \nabla P(x)f(x) \leq 0, \nabla P(x) = (\frac{dP(x)}{dx_1} \dots \frac{dP(x)}{dx_n}) \in R^n$.

6.3 Design of Standalone Fractional Order Backstepping Strategy on Inverted Pendulum

The inverted pendulum [7] is an under-actuated SIMO process that uses force, position, and angle as inputs and outputs. A system's schematic with both vertical and horizontal directions are shown in Fig. 6.1.

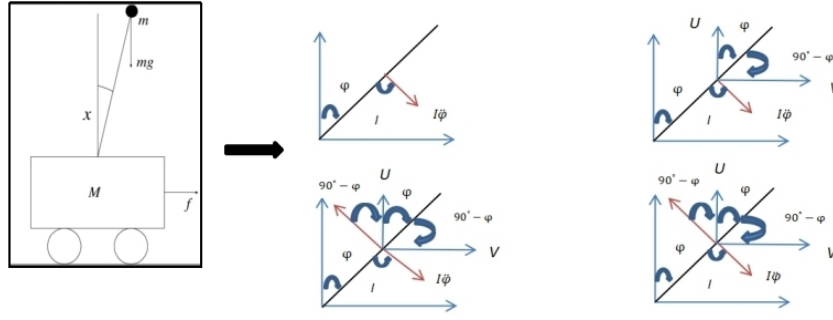


Fig. 6.1. Physical model representation of inverted pendulum.

Newton's law of motion estimates the cart's actual force in the horizontal direction.

$$M\ddot{x} = F - V \quad (6.1)$$

The following phrase can be used to assess force in a horizontal direction:

$$V = m\ddot{x} + ml\ddot{\phi} \cos \phi - ml\dot{\phi}^2 \sin \phi \quad (6.2)$$

The following expression is used to represent the equation of motion:

$$(M + m)\ddot{x} + ml\ddot{\phi} \cos \phi - ml\dot{\phi}^2 \sin \phi = F \quad (6.3)$$

The following expression can be used to examine the force in the vertical direction:

$$U - mg = m \frac{d^2}{dt^2} (l \cos \phi) \quad (6.4)$$

where the expression below illustrates the second equation of motion, $F = U - mg$:

$$(I + ml^2)\ddot{\phi} + mgl \sin \phi = -ml\ddot{x} \cos \phi \quad (6.5)$$

The following results are shown for the mathematical representation of the system:

$$\ddot{\phi} = \frac{(M + m)g \sin \phi - (F + ml\dot{\phi}^2 \sin \phi) \cos \phi}{\frac{4}{3}(M + m)l - ml \cos^2 \phi} \quad (6.6)$$

$$\ddot{x} = \frac{F + ml(\dot{\phi}^2 \sin \phi - \ddot{\phi} \cos \phi)}{(M + m)} \quad (6.7)$$

6.3.1 Proposed Fractional Order Backstepping (FOB) Rule

More flexibility in choosing controller parameters according to system requirements is provided by fractional calculus [8].

Definition 1. Cauchy's theorem [11–12] can be expressed as follows:

$$I^n f(t) = \frac{1}{(n-1)!} \int_0^t (t-h)^{n-1} f(h) dh, t > 0 \quad (6.8)$$

The gamma function can be used to expand the above equation to any positive real value. As $(n - 1)! = \Gamma(n)$, a random positive real number (α) is defined as follows:

$$I^\alpha f(t) = \frac{1}{\Gamma(\alpha)} \int_0^t (t - h)^{\alpha-1} f(h) dh \quad (6.9)$$

For the Laplace transform of a fractional integral, the following rule is defined:

$$I^\alpha f(t) \leftrightarrow f(s)s^{-\alpha} \quad (6.10)$$

(6.6) and (6.8) are now suggested with the help of the following expressions:

$$\ddot{\varphi}^{(\alpha)} = \frac{(M + m)g \sin \varphi - (F + ml\dot{\varphi}^2 \sin \varphi) \cos \varphi}{\frac{4}{3}(M + m)l - ml \cos^2 \varphi} \quad (6.11)$$

$$\begin{bmatrix} \dot{y}_1^{(\alpha)} \\ \dot{y}_2^{(\alpha)} \end{bmatrix} = \begin{bmatrix} y_2 \\ \frac{294.2 \sin y_1 - 1.5 y_2^2 \sin(2y_1)}{20 - 3 \cos^2 y_1} \end{bmatrix} - \begin{bmatrix} 0 \\ \frac{3 \cos y_1}{20 - 3 \cos^2 y_1} \end{bmatrix} u \quad (6.12)$$

where, $y_1 = \varphi, y_2 = \dot{\varphi}^{(\alpha)}$ and the control input, denoted as u , is intended to be integrated into the fractional order backstepping architecture. The following are the steps involved in stabilizing the first fractional order subsystem:

Step 1:

$$z_1 = y_1, \dot{z}_1^{(\alpha)} = y_2 \quad (6.13)$$

In order to construct the rule, each subsystem is now globally stabilized using the Lyapunov function. The following is an enhanced application of the Lyapunov function using the Caputo fractional derivative calculus [17-20]:

$${}_a^c D_t^\alpha f(t) = \frac{1}{\Gamma(n - \alpha)} \int_a^t \frac{f^n(w)}{(t - w)^{\alpha-n+1}} dw \quad (6.14)$$

The recently expanded Lyapunov function is given in Lemma 1.

Lemma 1. Let $q(t) \in \mathbb{R}$ is a derivable function and for any time instant

$$\frac{1}{2} {}_a^c D_t^\alpha q^2(t) \leq q(t) {}_a^c D_t^\alpha q(t) \quad (6.15)$$

Global Stability Analysis:

Step 2:

Firstly, Lyapunov function (v_1) is proposed to explore the global stability:

$$v_1 = \frac{1}{2} z_1^2 \quad (6.16)$$

$${}^c D_t^\alpha v_1(t) = z_1 \dot{z}_1^{(\alpha)} \quad (6.17)$$

Step 3:

To develop the updated control law, it is approached as

$${}^c D_t^\alpha z_1(t) = \rho(y_1) + e_2 \quad (6.18)$$

where, error function $(e_2) = y_2 - \rho(y_1)$.

$${}^c D_t^\alpha z_1(t) = \rho(y_1) + z_2 \quad (6.19)$$

Now, $\rho(y_1) = -p_1 z_1$ is selected to stabilize the aforementioned FO subsystem. As p_1 is constant, so we find

$${}^c D_t^\alpha z_1(t) = -p_1 z_1 + z_2 \quad (6.20)$$

So, replacing (6.20) into (6.17) the updated equation is established as follows:

$${}^c D_t^\alpha v_1(t) = z_1(-p_1 z_1 + z_2) = -p_1 z_1^2 + z_1 z_2 \leq 0 \quad (6.21)$$

Thus, the FO subsystem z_1 is stabilized globally.

Step 4:

Currently, the second order system's related mathematical equation is displayed by

$${}^c D_t^\alpha z_1(t) = -p_1 z_1 + z_2 \quad (6.22)$$

$${}^c D_t^\alpha z_2(t) = \frac{294.2 \sin y_1 - 1.5 y_2^2 \sin(2y_1)}{20 - 3 \cos^2 y_1} - \frac{3 \cos y_1}{20 - 3 \cos^2 y_1} u + p_1 y_2 \quad (6.23)$$

Step 5:

Now, second Lyapunov function (v_2) is defined as

$$v_2 = \frac{1}{2} z_1^2 + \frac{1}{2} z_2^2 \quad (6.24)$$

$${}^c D_t^\alpha v_2(t) = -p_1 z_1^2 + z_2(z_1 + \frac{294.2 \sin y_1 - 1.5 y_2^2 \sin(2y_1)}{20 - 3 \cos^2 y_1} - \frac{3 \cos y_1}{20 - 3 \cos^2 y_1} u + p_1 y_2) \quad (6.25)$$

Step 6:

Now, control input u is proposed as

$$u = \frac{20 - 3 \cos^2 y_1}{3 \cos y_1} (p_2 z_2 + z_1 + \frac{294.2 \sin y_1 - 1.5 y_2^2 \sin(2y_1)}{20 - 3 \cos^2 y_1} + p_1 y_2) \quad (6.26)$$

Now, replacing u into the (6.25), the expression of the Lyapunov function is found as

$${}^c D_t^\alpha v_2(t) = -p_1 z_1^2 - p_2 z_2^2 \leq 0 \quad (6.27)$$

Hence, the FO subsystem z_2 is also stabilized. The closed-loop basic standalone backstepping strategy is designed in Fig. 6.2 by linking the Simulink model of the inverted pendulum to the controller subsystem.

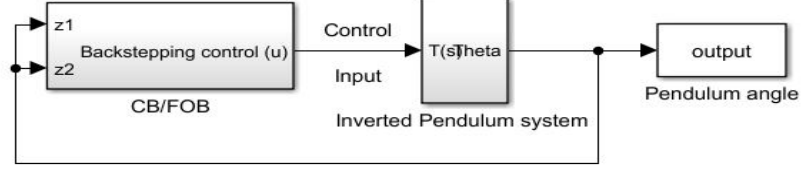


Fig. 6.2. Proposed standalone fractional order backstepping scheme.

6.4 Design of Standalone Fractional Order Backstepping Strategy on CSTR

The tri-state nonlinear CSTR process is adopted in this work where the level (h) of the tank, molar concentration (C), and reactor temperature (T) are adopted as state variables. The major goal is to smoothly regulate the molar concentration at the desired position while dealing with nonlinear factors. The mathematical expressions of the three state variables [9] are proposed with the following equations:

$$\dot{h}(t) = \frac{F' - F}{\pi r^2} \quad (6.28)$$

$$\dot{C}(t) = \frac{F'(C' - C)}{\pi r^2 h} - k' C e^{-\frac{E}{R T}} \quad (6.29)$$

$$\dot{T}(t) = \frac{F'(T' - T)}{\pi r^2 h} + \frac{-\Delta H}{\rho C''} k' C e^{-\frac{E}{R T}} + \frac{2U}{r \rho C''} (T'' - T) \quad (6.30)$$

In this work, output variable is chosen as

$$y(t) = [C(t)]^T \quad (6.31)$$

The state equations of required molar concentration in (6.29) is adopted by following the discussions in Chapter-2 under section 2.3.3.1.

For backstepping scheme, the state vector of the system is represented as follows:

$$x(t) = [h(t) \ C(t) \ T(t)]^T$$

where

$$x_1(t) = h(t) \quad (6.32)$$

$$x_2(t) = C(t) \quad (6.33)$$

$$x_3(t) = z_4 e^{-z_5/T(t)} \quad (6.34)$$

From (6.34), the first derivative of the third state variable is shown as

$$\dot{x}_3(t) = \frac{x_3 \ln^2(x_3/z_4)}{z_5} \dot{T}(t) \quad (6.35)$$

Now, nonlinear dynamics of (6.28) to (6.34) are transformed into a suitable for designing the backstepping rule as

$$\dot{x}_1(t) = z_0 + z_1 v_1(t) \quad (6.36)$$

$$\dot{x}_2(t) = z_2/x_1 + z_3 x_2/x_1 - x_2 x_3 \quad (6.37)$$

$$\dot{x}_3(t) = \tau(x) + \frac{z_9 x_3 \ln^2(x_3/z_4)}{z_5} v_2(t) \quad (6.38)$$

$$y(t) = [x_2(t)]^T \quad (6.39)$$

where $\tau(x) = \frac{x_3 \ln^2(x_3/z_4)}{z_5} \left(\frac{z_6}{x_1} - \frac{z_3 z_5}{x_1 \ln(x_3/z_4)} - z_7 x_2 x_3 - \frac{z_5 z_8}{\ln(x_3/z_4)} \right)$ and the parameters $z_0 \dots z_9$

are defined in Table 6.1. From the above nonlinear dynamics, (6.36) is treated as the first subsystem. (6.37) and (6.38) are treated as the second subsystem. In this work, the stabilization technique is applied to the second subsystem only for designing a backstepping controller.

Table 6.1
Parameters for newly transformed CSTR subsystems

| Parameters | Actual definition |
|------------|-----------------------------|
| z_0 | $\frac{F'}{\pi r^2}$ |
| z_1 | $\frac{-1}{\pi r^2}$ |
| z_2 | $\frac{F' C'}{\pi r^2}$ |
| z_3 | $-\frac{F'}{\pi r^2}$ |
| z_4 | $-k'$ |
| z_5 | E/R |
| z_6 | $\frac{F' T'}{\pi r^2}$ |
| z_7 | $\frac{\Delta H}{\rho C''}$ |
| z_8 | $\frac{-2U}{r \rho C''}$ |
| z_9 | $\frac{2U}{r \rho C''}$ |

6.4.1 Proposed Fractional Order Backstepping (FOB) Rule

Using (6.37) and (6.38), the following steps are proposed for designing a fractional order backstepping rule.

Step 1:

The following control variable $v_2(t)$ is selected to develop the back-stepping controller:

$$v_2(t) = -\frac{z_5}{z_9 x_3 \ln^2(x_3/z_4)} (\tau(x) - U_{FO-backste}(t)) \quad (6.40)$$

$U_{FO-backste}(t)$ is the FOB to be developed. Finally, the dynamics of the subsystem are shown with the following expressions:

$$\dot{x}_2(t) = z_2/x_1 + z_3 \dot{x}_2/x_1 - x_2 x_3 \quad (6.41)$$

$$\dot{x}_3(t) = U_{IO-backstep}(t) \quad (6.42)$$

Step 2:

Fractional order backstepping law is established by modifying (6.41) and (6.42) with an extra DOF (α) as follows:

$$D^\alpha x_2(t) = z_2/x_1 + z_3 \dot{x}_2/x_1 - x_2 x_3 \quad (6.43)$$

$$D^\alpha x_3(t) = U_{FO-backste}(t) \quad (6.44)$$

where x_3 is considered as a virtual input in (6.43).

Step 3:

The first error variable is defined as

$$e_1(t) = y_r(t) - x_2(t) \quad (6.45)$$

$$\dot{e}_1(t) = \dot{y}_r(t) - \dot{x}_2(t) \quad (6.46)$$

$$D^\alpha e_1(t) = D^\alpha y_r(t) - D^\alpha x_2(t) \quad (6.47)$$

Global Stability Analysis:**Step 4:**

To design the rule, each subsystem is stabilized globally using the Lyapunov function. We examine the need for the Lyapunov function using the Caputo fractional derivative calculus in the following ways:

$${}_a^c D_t^\alpha f(t) = \frac{1}{\Gamma(n-\alpha)} \int_a^t \frac{f^n(w)}{(t-w)^{\alpha-n+1}} dw \quad (6.48)$$

Lemma 1 defines the new expanded Lyapunov function.

Lemma 1. Let $q(t) \in \mathbb{R}$ is a derivable function and for any time instant

$$1/2 {}_a^c D_t^\alpha q^2(t) \leq q(t) {}_a^c D_t^\alpha q(t) \quad (6.49)$$

To stabilize globally the first subsystem, the first Lyapunov function is proposed as follows:

$$V_1(t) = \frac{1}{2} e_1^2(t) \quad (6.50)$$

$$D^\alpha V_1(t) = e_1 D^\alpha e_1(t) \quad (6.51)$$

$$D^\alpha V_1(t) = e_1(D^\alpha y_r(t) - D^\alpha x_2(t)) \quad (6.52)$$

$$D^\alpha V_1(t) = e_1(D^\alpha y_r(t) - \frac{z_2}{x_1} - z_3 \frac{x_2}{x_1} + x_2 x_3) \quad (6.53)$$

To make $D^\alpha V_1(t) \leq 0$, x_3 is chosen as

$$x_3 = \frac{1}{x_2} (\frac{z_2}{x_1} + z_3 \frac{x_2}{x_1} - \mu_1 e_1 - D^\alpha y_r) \quad (6.54)$$

$\dot{V}_1^\alpha(t) = -\mu_1 e_1^2 \leq 0$ shows global stability as $e_1 \rightarrow 0$.

Step 5:

Now, the second error function is defined to design fractional order backstepping law as stated in (6.55).

$$e_2(t) = x_3(t) - \varphi(x_2)(t) \quad (6.55)$$

Now, using (6.55) the modified expression is proposed by

$$D^\alpha x_2(t) = \frac{z_2}{x_1} + z_3 \frac{x_2}{x_1} - x_2 \varphi(x_2) - x_2 e_2 \quad (6.56)$$

$$D^\alpha e_2(t) = D^\alpha x_3(t) - D^\alpha \varphi(x_2)(t) \quad (6.57)$$

$$D^\alpha e_2(t) = U_{FO-backste}(t) - D^\alpha \varphi(x_2)(t) \quad (6.58)$$

$$D^\alpha e_2(t) = w \quad (6.59)$$

Where, $w = U_{FO-backstep}(t) - D^\alpha \varphi(x_2)$

Step 6:

The second Lyapunov function is proposed to show local stability with $e_2 \rightarrow 0$.

$$V_2(t) = \frac{1}{2} e_2^2(t) + V_1 \quad (6.60)$$

$$D^\alpha V_2(t) = D^\alpha V_1(t) + e_2 D^\alpha e_2(t) \quad (6.61)$$

$$D^\alpha V_2(t) = e_1 D^\alpha e_1(t) + e_2 w \quad (6.62)$$

$$D^\alpha V_2(t) = e_1(D^\alpha y_r(t) - \frac{z_2}{x_1} - z_3 \frac{x_2}{x_1} + x_2 \varphi(x_2)) + e_1 x_2 e_2 + e_2 w \quad (6.63)$$

$$D^\alpha V_2(t) = -\mu_1 e_1^2 + e_1 x_2 e_2 + e_2 w \quad (6.64)$$

Step 7:

The appropriate value w is chosen to satisfy the following stability criteria:

$$D^\alpha V_2(t) = -\mu_1 e_1^2 + e_1 x_2 e_2 + e_2(-e_1 x_2 - e_2 \mu_2) \quad (6.65)$$

$$D^\alpha V_2(t) = -\mu_1 e_1^2 - \mu_2 e_2^2 \leq 0 \quad (6.66)$$

Finally, the fractional order backstepping rule is established as

$$U_{FO-backstep}(t) = D^\alpha \varphi(x_2)(t) - e_1 x_2 - e_2 \mu_2 \quad (6.67)$$

As, $x_3 = \varphi(x_2) = 1/x_2 (z_2/x_1 + z_3 x_2/x_1 - \mu_1 e_1 - D^\alpha y_r)$, then

$$D^\alpha \varphi(x_2)(t) = \varepsilon(x_2) (z_2/x_1 + z_3 x_2/x_1 - x_2 x_3) - x_2 e_1 - \mu_2 (x_3 - \varphi(x_2)) \quad (6.68)$$

$$\varepsilon(x_2) = D^\alpha \varphi(x_2)(t) = D^\alpha \left(\frac{z_2}{x_1 x_2} - \frac{\mu_1 e_1}{x_2} - \frac{D^\alpha y_r(t)}{x_2} \right) \quad (6.69)$$

Now, substituting (6.69) into (6.67) the fractional order backstepping law is established as

$$U_{FO-backstep}(s) = D^\alpha \left(\frac{z_2}{x_1 x_2} - \frac{\mu_1 e_1}{x_2} - \frac{D^\alpha y_r(t)}{x_2} \right) - e_1 x_2 - e_2 \mu_2 \quad (6.70)$$

α is taken into account as 1 in (6.70) for conventional backstepping rule. In Fig.6.3, the simple standalone backstepping control architecture is proposed after the aforementioned formulations.

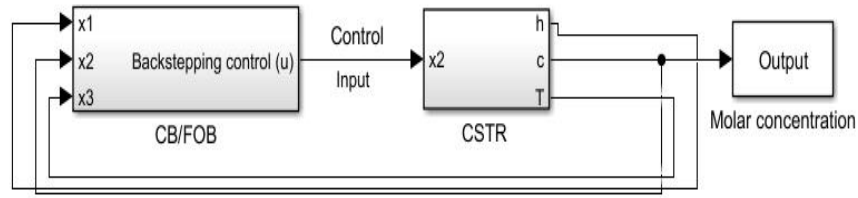


Fig. 6.3. Proposed standalone fractional order backstepping scheme.

6.5 Investigation into The Performance of FOB Rule on Inverted Pendulum

The investigation of various novel closed-loop servo and regulatory actions, as well as control actions, is conducted in the following simulation investigations. The parameters of inverted pendulum [7] is presented in Table 6.2.

Table 6.2
Parameter specifications of inverted pendulum

| Symbol | Quantity | Value |
|--------|-------------------|----------------------|
| M | mass of cart | 6.0 Kg |
| m | mass of pendulum | 10.0 Kg |
| l | length of rod | 0.5 m |
| g | gravity | 9.8 m/s ² |
| I | Moment of inertia | 0.833 |

Case I: Comparative study between CB and FOB rules

Fig. 6.4 illustrates how the system is controlled with varying initial angular positions at random, such as 0.4 and 0.167 radians, using CB and FOB to bring it upright. The FO (α) is found by extensive simulation techniques on frequency and time domain platforms. Fig. 6.6 depicts how the servo actions are also explored by varying FOs, such as 0.6 and 0.8, with a fixed initial location of 0.4 radians.

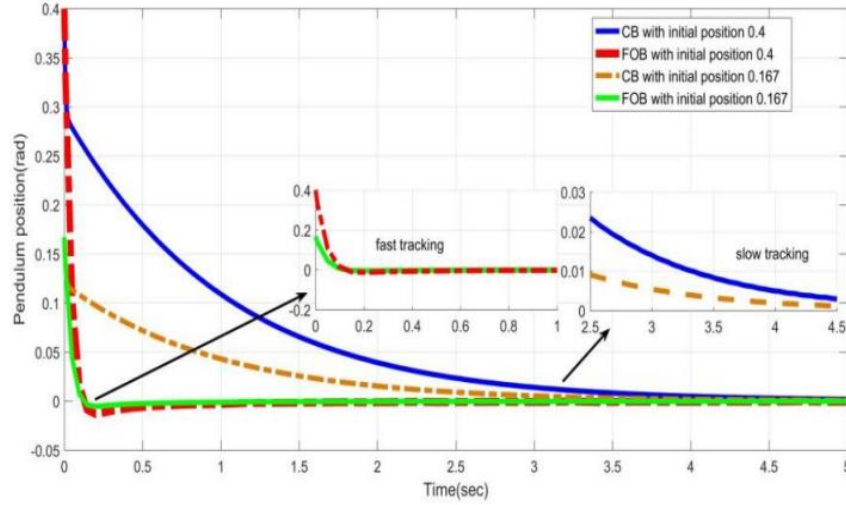


Fig. 6.4. Upright trajectory from different locations.

Fig. 6.4 illustrates how the system responds very slowly when utilizing CB, despite the fact that both backstepping topologies with different initial locations track the target position effectively. For FOB with selected FO 0.4, this issue is overcome swiftly in 1 to 2 seconds at the target position. Fig. 6.5 reveals that the FO 0.4 approximation shows a better stable gain and flatter response with a larger band gap than the 0.6 and 0.8 approximations.

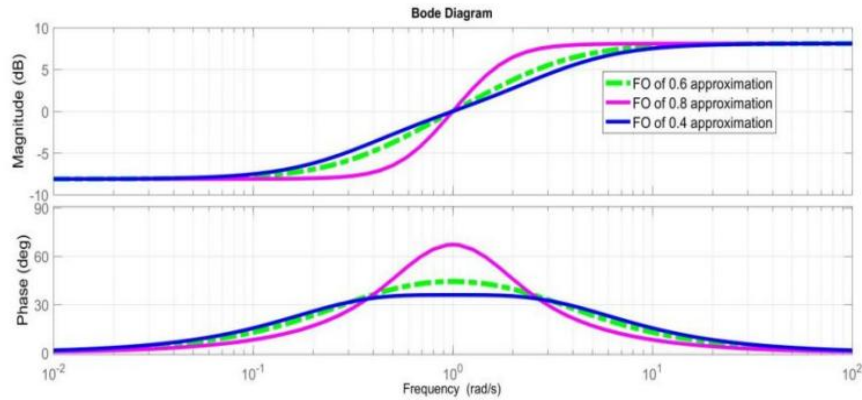


Fig. 6.5. Performance study between different fractional orders on Bode plots.

The importance of fractional order 0.4 is further explored on time domain platform, as shown in Fig. 6.6, compared to other fractional orders.

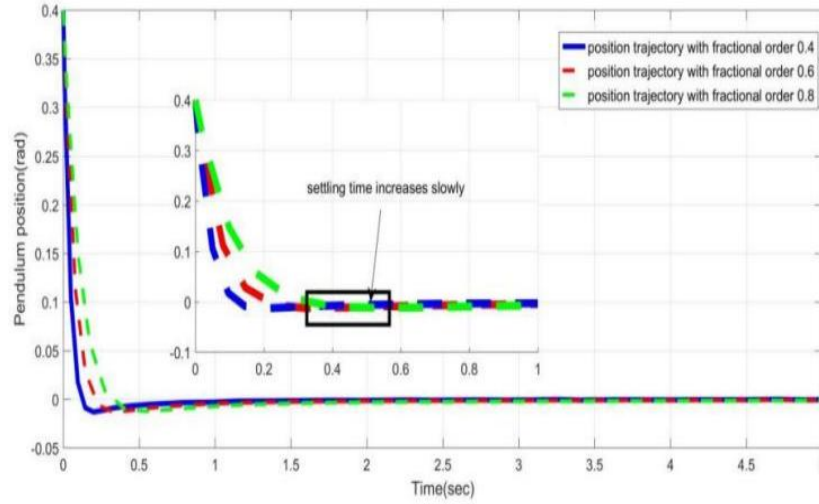


Fig. 6.6. Time responses of fractional orders.

The settling time towards the zero posture is depicted as progressively increasing by orders of 0.6 and 0.8. Therefore, the following case studies are conducted with fractional order 0.4 of FOB. As seen in (6.105), a load (d_1) is now induced on both the CB and the FOB in order to examine the resilience of the system.

$${}_a^c D_t^\alpha z_2(t) = \frac{294.2 \sin y_1 - 1.5 y_2^2 \sin(2y_1)}{20 - 3 \cos^2 y_1} - \frac{3 \cos y_1}{20 - 3 \cos^2 y_1} u + p_1 y_2 + d_1 \quad (6.71)$$

As demonstrated in Fig. 6.7, the trajectory unquestionably shows the durability of both of the backstepping systems with a load at $t=4$ seconds.

Both of methods correctly follow the target even after providing disturbance, and they keep doing so for 4 seconds. On the other hand, the regulatory performance makes it clear that the FOB is substantially quicker than the CB. With the FOB, the system effortlessly settles into zero level in 5.5 sec; however, the CB performs extremely slowly, with continuous, minute oscillations. Another important parameter to consider while analyzing the system's stability pragmatically is noise generation, as shown in Fig. 6.8.

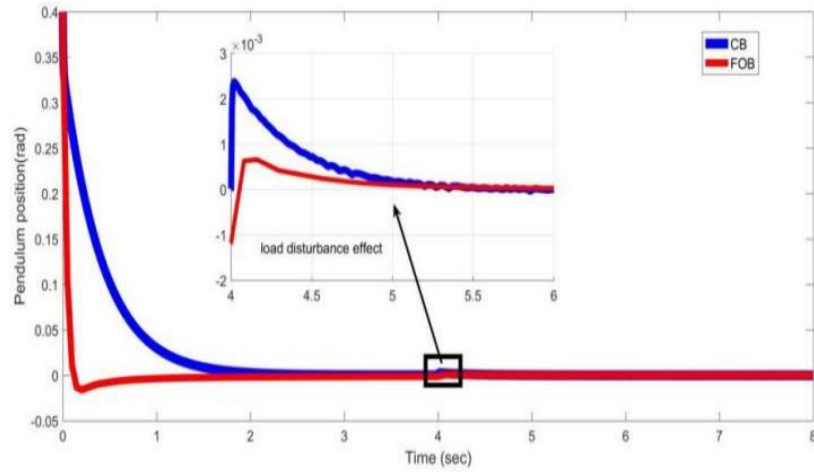


Fig. 6.7. Nominal system output in presence of load disturbance.

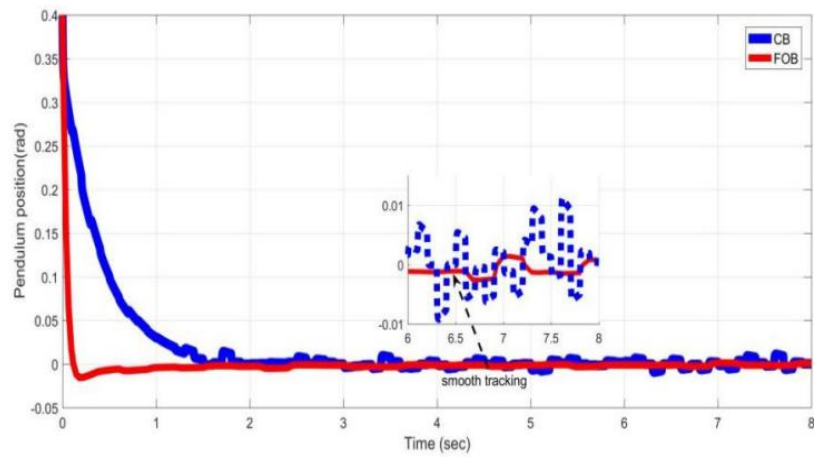


Fig. 6.8. Nominal responses under noise.

Furthermore, as previously noted Fig. 6.8 shows, despite applying noise using mean = 0, variance = 0.01, seed = 35, and time = 1 sec, FOB assists the plant smoothly towards zero position, in contrast to CB. Thus, even with the noise and disturbance shown in Fig. 6.9, FOB's control effort is far smoother than CB's, with a lower amplitude within the saturation bounds.

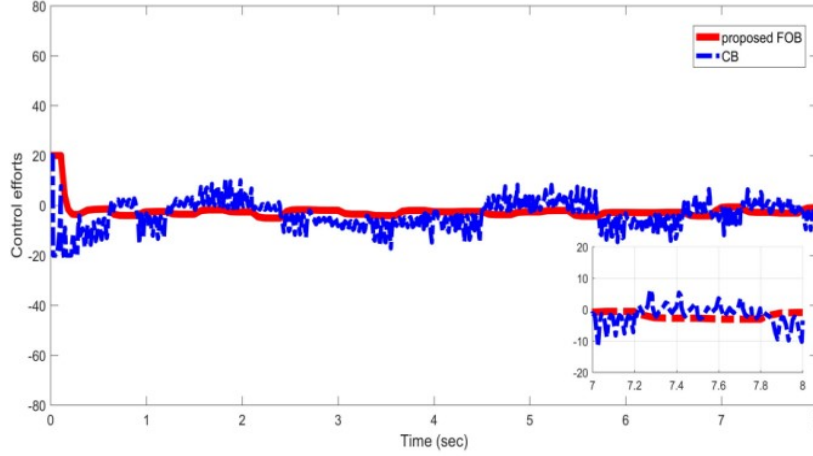


Fig. 6.9. Nominal control actions.

Case II: Stability of FOB strategy

By changing the plant parameter by $m=15$ kg, as depicted in Fig. 6.10 and 6.12, the stability of FOB is explored, and it is investigated that even when the parameter is changed, despite the noise, the proposed strategy consistently guides the plant to the intended level. However, the system acts a slightly slow because of the greater weight of the pendulum. As shown in Fig. 6.11, despite giving an active impulse of 0.3 rad, the system smoothly follows to the desired upright position in addition to parametric uncertainty and noise. Fig. 6.12 illustrates the control inputs of FOB with nominal and model uncertainties amid noise, within the saturation limits. The smoothness of the control signal with perturbed parameters is too investigated. So, it is vindicated that, FOB delivers robust solution on set-point tracking and noise rejection.

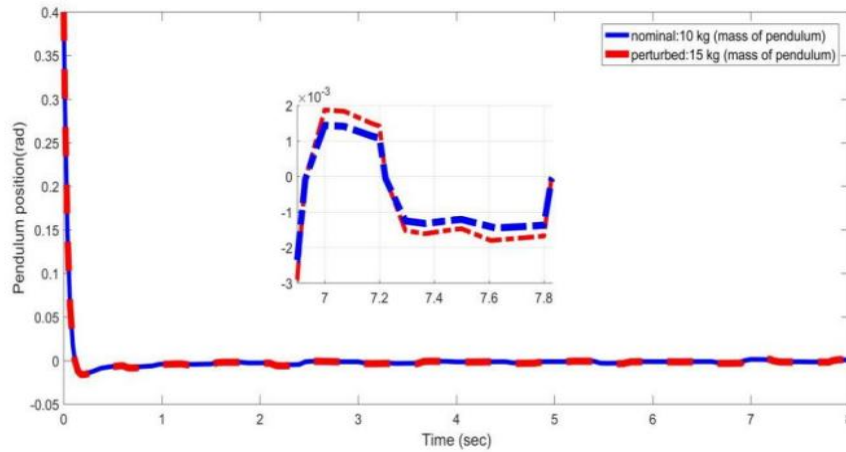


Fig. 6.10. Perturbed system outputs in presence of noise.

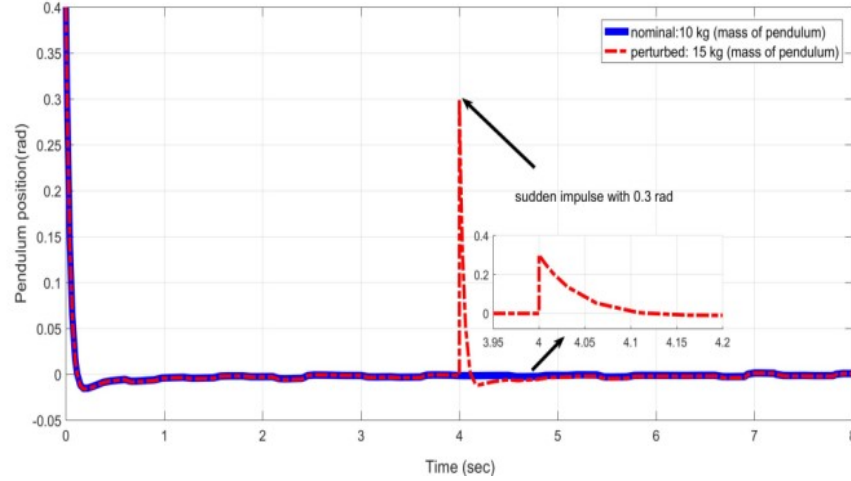


Fig. 6.11. Global stability analysis of FOB with impulse 0.3 rad under disturbance.

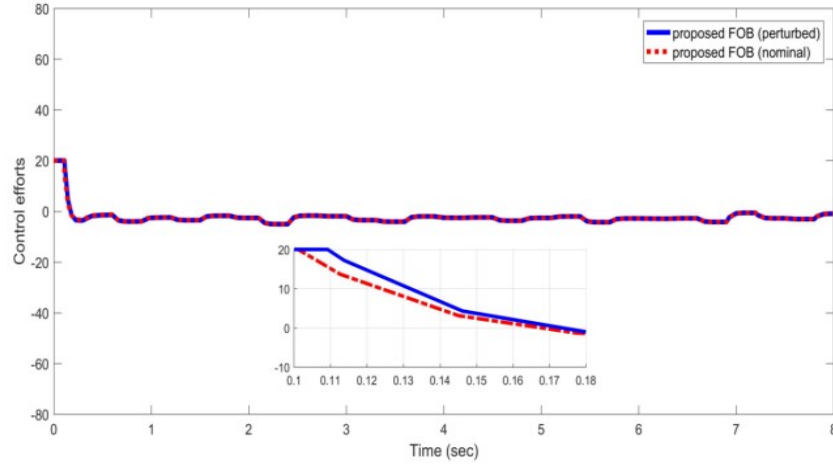


Fig. 6.12. Robustness of FOB in presence of noise.

Case III: Comparative analysis between FOB, FOLY and FOLY-2 DOF FOPI schemes

As illustrated in Figs. 6.13 and 6.14, the performance of a system with $m = 10$ kg is explored in the context of a practical scenario using FOB, FOLY, and FOLY- 2DOF FOPI controllers with load at $t = 15$ seconds and noise. Gain (γ) of FOLY is selected after extensive simulation techniques and it follows the intended position swiftly with minimum oscillations compared to FOLY-2 DOF FOPI [15]. Notably, FOB rule more swiftly and elegantly follows the intended location in an upright state. In the presence of noise, Fig. 6.15 compares the control efforts as well within the saturation limits. It is investigated that the proposed standalone FOB performs far superior to all control strategies without needless overshoot.

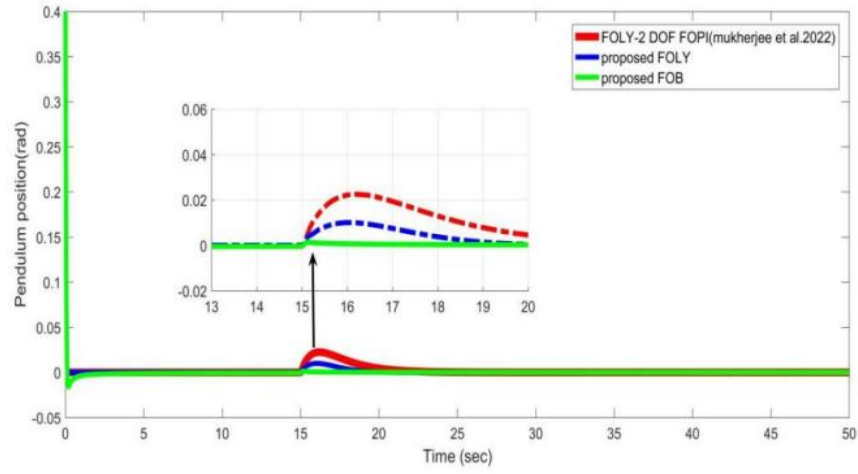


Fig. 6.13. Nominal outputs under load.

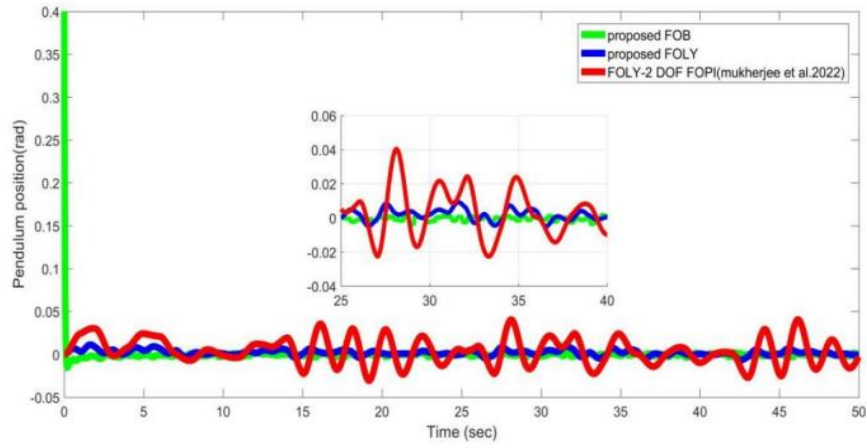


Fig. 6.14. Nominal performances under noise.

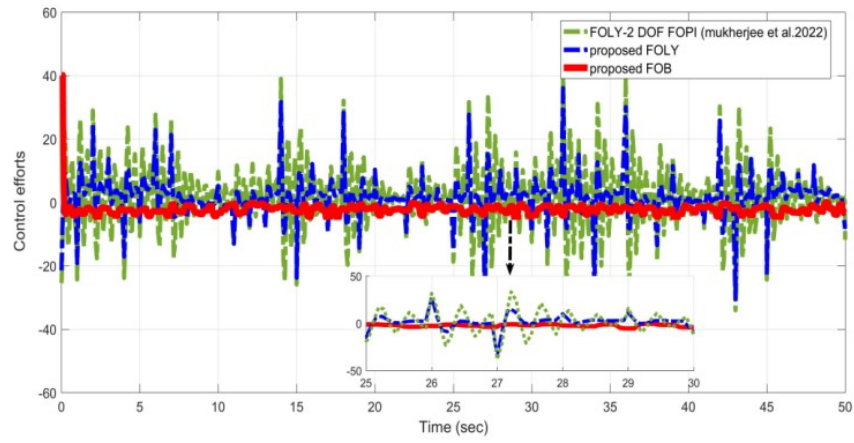


Fig. 6.15. Different control actions under noise.

Table 6.3 shows a controller functions. Employing Instantaneous error $e(t)$, IAE, ISE and ITAE are computed. As shown in Table 6.5, the proposed FOB offers lower error metrics and TV compared to other rules. The TV is determined as follows:

$$\mathbf{TV} = \sum_{i=1}^{\infty} |u(i+1) - u(i)| \quad (6.72)$$

From Table 6.5, it is evident that the proposed FOB rule has lower TV values, which suggests that the control operation is more smoothly executed.

Table 6.3
Controller Settings

| Case study | Techniques | Controller functions |
|------------|----------------------|--|
| I | CB | $p_1 + p_2 = 100, p_1 p_2 + 1 = 150$ |
| | FOB | $p_1 + p_2 = 100, p_1 p_2 + 1 = 150 \quad \alpha = 0.4, 0.6, 0.8$ |
| II | FOB | $p_1 + p_2 = 100, p_1 p_2 + 1 = 150 \quad \alpha = 0.4$ |
| III | FOB | $p_1 + p_2 = 100, p_1 p_2 + 1 = 150 \quad \alpha = 0.4$ |
| | FOLY | $\gamma = 25, \alpha = 0.4, K_p = 1, K_D = 0.5$ |
| | FOLY-2 DOF FOPI [15] | $K_{p1} = 11.24, K_{I1} = 2.67, K_{p2} = 18.54, K_{I2} = 2.67, \lambda = 0.45, b = 0.65, \gamma = 100, \alpha = 0.5$ |

Table 6.4
Approximations of fractional order

| Fractional order | Approximated transfer functions $G(s)$ |
|------------------|---|
| $s^{0.4}$ | $\frac{9.025s^2 + 16.88s + 3.545}{3.545s^2 + 16.88s + 3.545}$ |
| $s^{0.6}$ | $\frac{9.873s^2 + 14.93s + 2.776}{2.776s^2 + 14.93s + 9.873}$ |
| $s^{0.8}$ | $\frac{10.883s^2 + 17.53s + 1.176}{1.176s^2 + 17.53s + 10.883}$ |

Table 6.5
Quantitative measurement analysis

| Control Techniques | IAE | ITAE | ISE | TV |
|--|--------------|--------------|---------------|---|
| CB | 0.252 | 1.342 | 0.0062 | 8.73×10^{-2} |
| Proposed FOB | 0.103 | 1.259 | 0.0024 | 2.47×10^{-2} |
| Proposed FOB (Perturbed system) | 0.109 | 1.273 | 0.0047 | 2.68×10^{-2} |
| FOLY | 0.416 | 1.426 | 0.018 | 1.84×10^{-3} |
| FOLY-2 DOF FOPI [15] | 0.602 | 1.837 | 0.082 | 4.42×10^{-5} |

6.6 Investigation into The Performance of FOB Rule on CSTR

The investigation of various novel closed-loop servo and regulatory actions, as well as control actions, is conducted in the following simulation case studies. The values of all the parameters are presented by [9] as shown in Table 6.6.

Table 6.6
Actual parameters for CSTR

| Parameters | Actual value |
|------------|--|
| F' | 0.1 m ³ /sec |
| T' | 350 K |
| C' | 1 Kmole/m ³ |
| k' | 7.2x10 ¹⁰ min ⁻¹ |
| E/R | 8750 K |
| U | 54.92 W/m ² .K |
| ρ | 1000 kg/m ³ |
| C'' | 0.239 kJ/kg.K |
| ΔH | -5x10 ⁴ kJ/kmol |

Case I: Comparative analysis between CB and FOB

In this section, simulation studies are carried out for nominal and perturbed system scenarios with a desired concentration level of 0.877 kmol/m³ and 1 kmol/m³ respectively. The efficiency of the proposed FOB rule is investigated employing the selected fractional order (α) 0.4 by extensive simulation studies on frequency domain platform as discussed in section 6.5 and also on time domain platform as depicted in Fig. 6.16. As the fractional order expands, the system gets sluggish. The tuning parameters of all control schemes are summarized in Table 6.7. The plant's state variables in Equations (6.43-6.45) are used in simulation. Positive scalars [14] (μ_1, μ_2) of both FOB and CB are considered as 1 and 5 respectively. A comparative study is also carried out between CB and FOB with different positive scalars 5 and 15, towards a desired concentration level of 0.877 kmol/m³ and FOB outperforms CB as depicted in Fig 6.17. As shown in (6.106), the servo and regulatory performances are carried out with a disturbance at $t = 4$ seconds.

$$U_{FO-backste}(s) = D^\alpha \left(\frac{z_2}{x_1 x_2} - \frac{\mu_1 e_1}{x_2} - \frac{D^\alpha y_r(t)}{x_2} \right) - e_1 x_2 - e_2 \mu_2 + d \quad (6.73)$$

Despite applying disturbance, both of the schemes efficiently track the desired level, and keep tracking after 4 seconds, as depicted in Fig. 6.18. However, FOB keeps tracking the target more efficiently and reduces the error signal as presented in Table 6.8 respectively.

Molar concentration is controlled smoothly by FOB even under Gaussian noise with mean = 0, variance = 0.01, seed = 21, and time = 1 as depicted in Fig. 6.19. FOB also outperforms CB with different molar concentration 1 kmol/m³. Since it is impractical to obtain perfect models of reactors, the robustness of the process is studied by perturbing feed concentration by +20% to the desired positions 0.877 kmol/m³ and also 1 kmol/m³ as illustrated in Figs 6.21 and 6.23. FOB continues to follow the target consistently rejecting noise more smoothly than CB. Fig. 6.22 again shows the smooth control action.

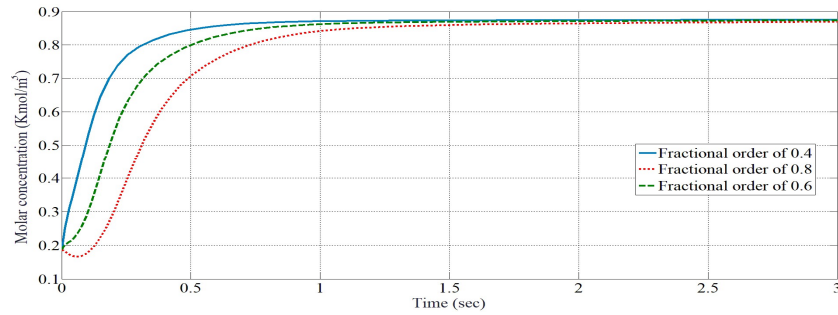


Fig. 6.16. System outputs using different fractional orders.

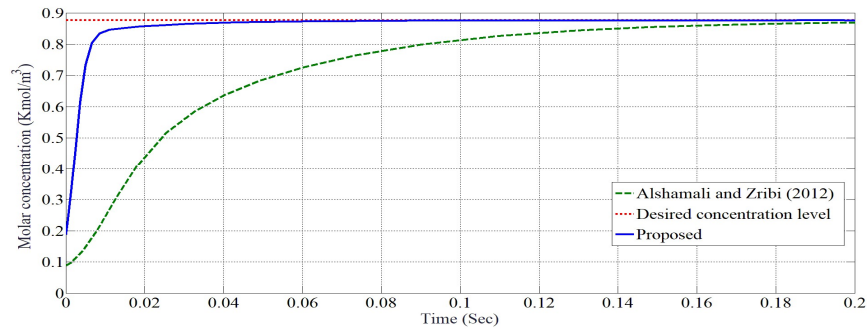


Fig. 6.17. Nominal outputs using positive scalars = 5 and 15.

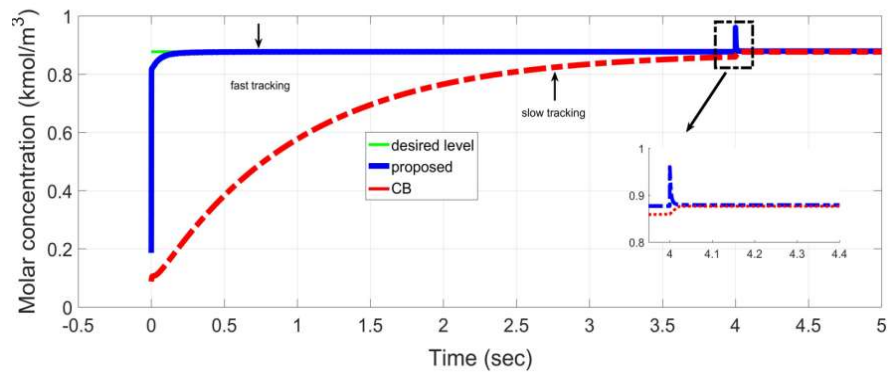


Fig. 6.18. Servo-regulatory outputs with load disturbance.

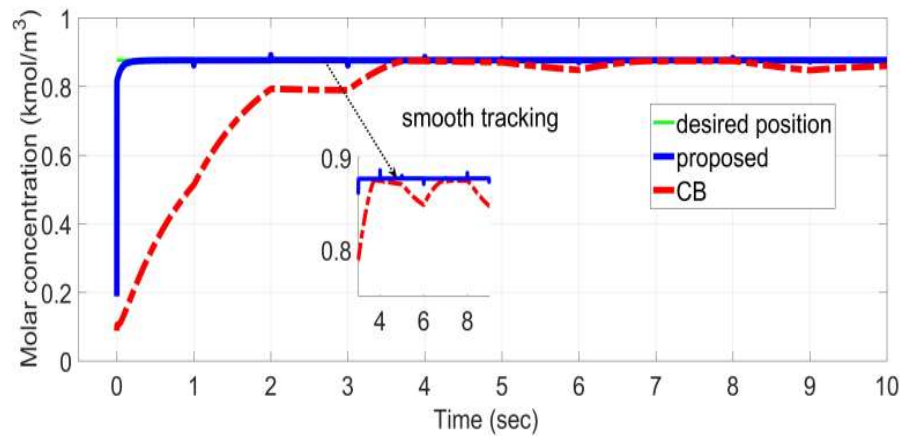


Fig. 6.19. Nominal outputs with noise.

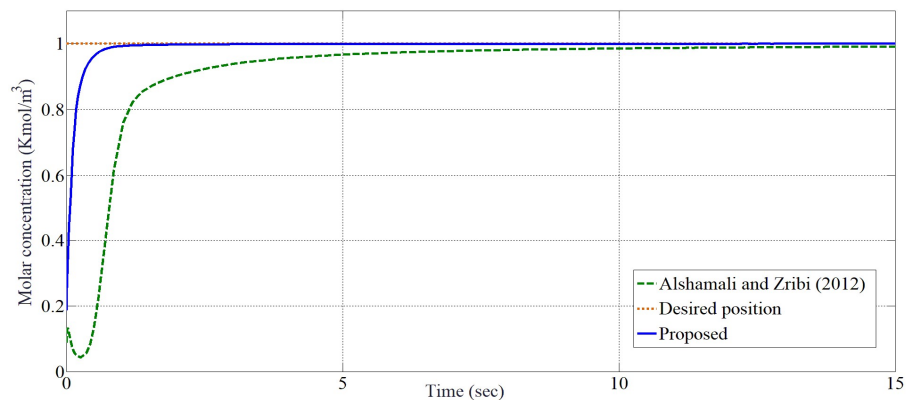


Fig. 6.20. Nominal outputs with different molar concentration 1 Kmol/m³.

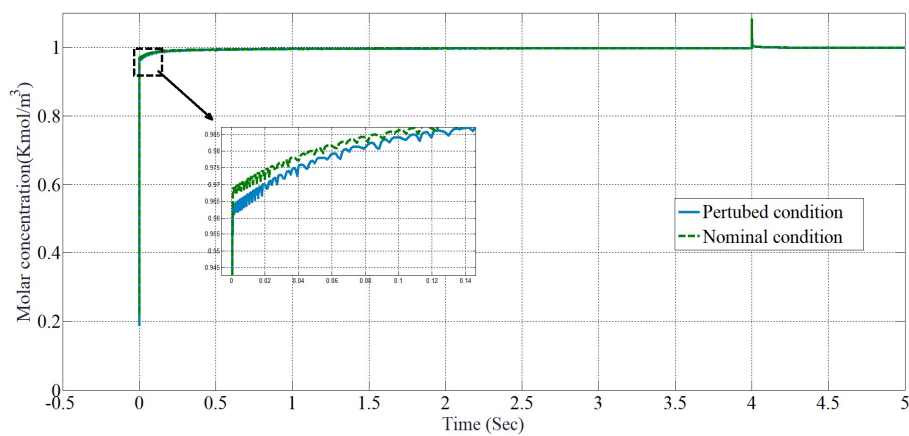


Fig. 6.21. Nominal and perturbed servo-regulatory outputs with FOB rule.

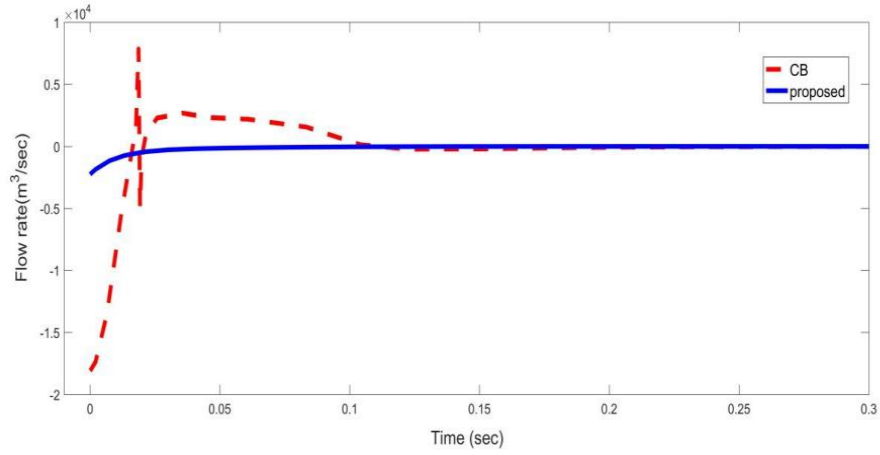


Fig. 6.22. Control efforts between CB and FOB.

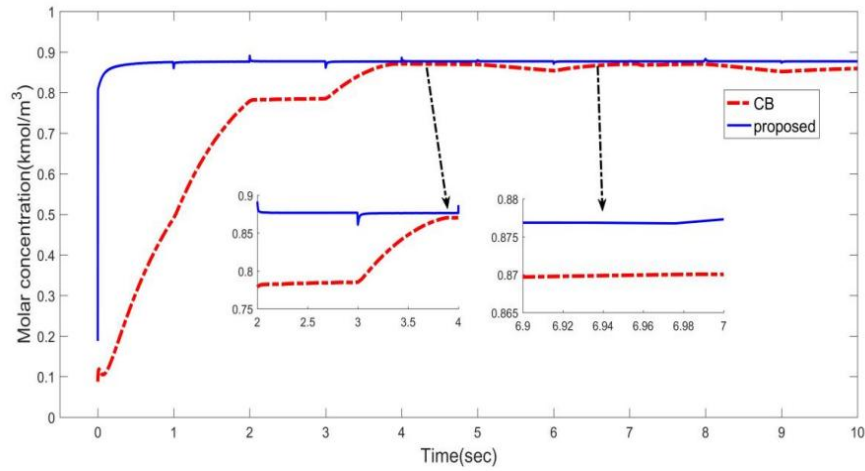


Fig. 6.23. Perturbed outputs with noise.

Case II: Comparative analysis between FOB, FOPID and FOLY-FOPID rules

The control efficiency of the proposed technique is investigated using the same control settings ($\mu_1 = 1$, $\mu_2 = 5$, $\alpha = 0.4$) compared to existing fractional modern control rules in both nominal and perturbed circumstances as illustrated in Figs. 6.24-6.28. In nominal settings, servo response is studied by applying step input at $t = 0$ second and regulatory performance is explored by applying disturbance at 10 seconds. The closed-loop performances and control efforts are contrasted by the following rules: optimal FOLY-FOPID [13], optimal FOPID [10], and the proposed structure, as illustrated in Figs. 6.24–6.26. As depicted in Fig. 6.24, optimal FOPID results in more computation time to attain the desired level 0.877 kmol/m^3 under load disturbance.

The performance is enhanced by the optimal FOLY-FOPID scheme with its improved control settings as presented in Table 6.7. However, prior to applying load, the proposed method more swiftly tracks the desired level within 6 seconds and, even after applying load, molar concentration is tackled more gracefully, as illustrated in Fig. 6.24. Proposed FOB yields also robust noise rejection as depicted in Fig. 6.25. As depicted in Fig. 6.26, the flow rate exhibits relatively steady control action using the proposed FOB amid noise.

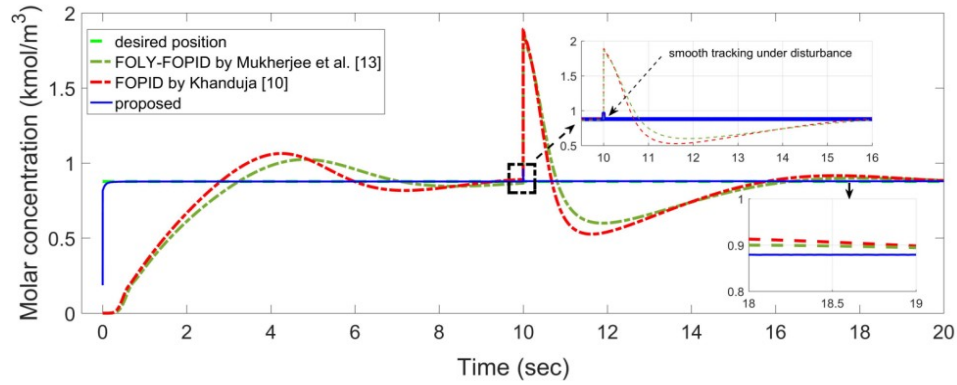


Fig. 6.24. Servo-regulatory nominal outputs with load disturbance.

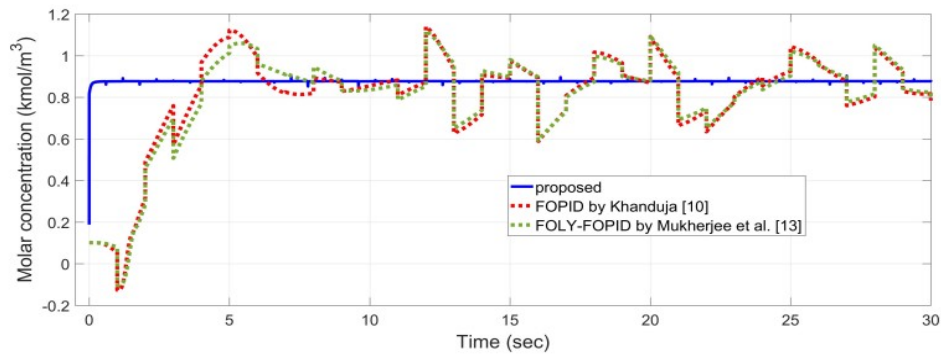


Fig. 6.25. Nominal outputs with noise.

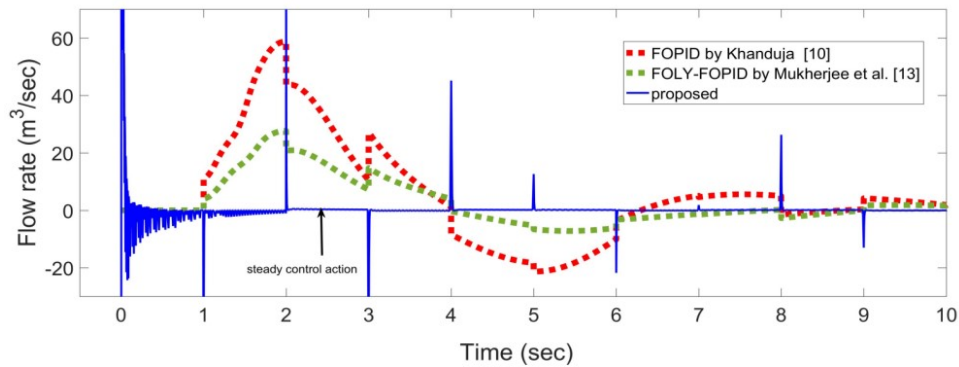


Fig. 6.26. Input control actions with disturbance.

Simulation studies are further carried out to compare the robustness of the existing and proposed control methods by perturbing feed concentration by +30%. As depicted in Figs. 6.27 and 6.28, the closed-loop performances are analyzed by applying two unit step disturbances at $t = 10$ seconds, 15 seconds, and noise. It is shown that optimal FOPID does not exhibit satisfactory result when subjected to noise. In contrast to FOPID, the disturbance is controlled by optimal FOLY-FOPID resulting in smooth tracking of the concentration and more efficient noise rejection. Enhanced performance is further evident from lesser error metrics of Table 6.8.

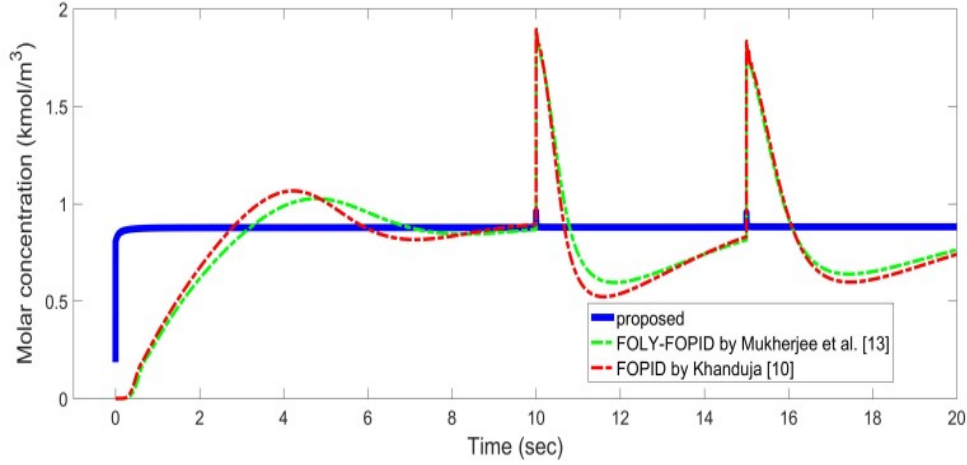


Fig. 6.27. Servo-regulatory perturbed outputs in presence of load disturbance.

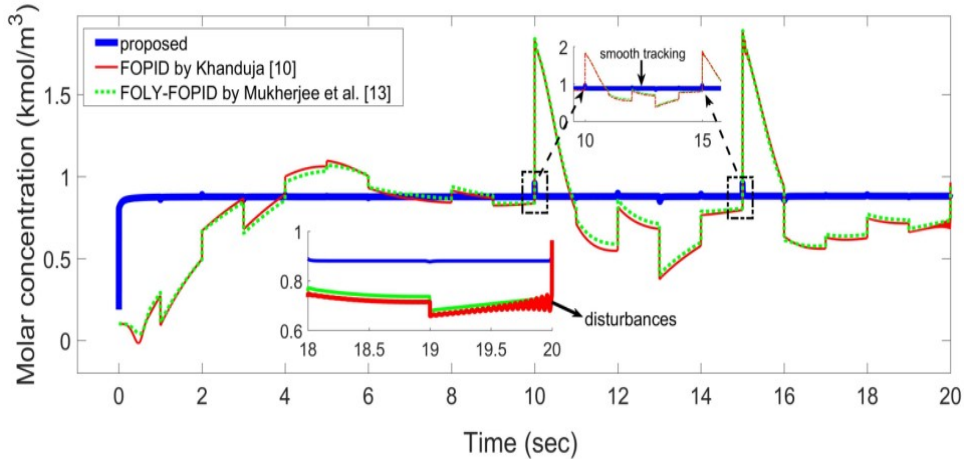


Fig. 6.28. Servo-regulatory perturbed outputs in presence of noise.

TV is also computed by $\sum_{i=1}^{\infty} |u(i+1) - u(i)|$. Table 6.8 vindicates the smoothest performance of control action resulting from the proposed scheme and proves it to be suitable for practical application.

Table 6.7
Summary of control functions

| Methods | Controller Settings |
|-----------------|---|
| CB [14] | $\mu_1 = 1, \mu_2 = 5, \alpha = 1$ |
| Proposed FOB | $\mu_1 = 1, \mu_2 = 5, \alpha = 0.4$ |
| FOLY-FOPID [13] | $\gamma = 45, \alpha = 0.75, K_p = 0.984, K_I = 0.113,$ $K_D = 0.376, \lambda = 0.32, \mu = 0.26$ $C_{FOPID} = 0.984 + \frac{0.113}{s^{0.32}} + 0.376s^{-26}$ $U(s) = 45e^{\frac{1}{s^{0.75}}}u_c - [-45e^{\frac{1}{s^{0.75}}} \frac{0.1915}{s^2 - 5.948s + 22.69}]$ |
| FOPID [10] | $K_p = 1.57, K_I = 0.83, K_D = 1.04, \lambda = 0.54, \mu = 0.72$ $C_{FOPID} = 1.57 + \frac{0.83}{s^{0.54}} + 1.04s^{-72}$ |

Table 6.8
Quantitative measurement with load disturbance

| Methods | Nominal Condition | | | |
|-----------------|---------------------|--------------|--------------|--------------------|
| | IAE | ISE | ITAE | TV |
| FOPID [10] | 2.614 | 1.243 | 25.64 | 6.62×10^5 |
| FOLY-FOPID [13] | 2.463 | 1.054 | 18.07 | 1.86×10^3 |
| CB [14] | 1.309 | 0.583 | 2.804 | 5.3 |
| Proposed | 0.163 | 0.021 | 1.204 | 3.8 |
| Methods | Perturbed Condition | | | |
| | IAE | ISE | ITAE | TV |
| FOPID [10] | 4.284 | 2.759 | 45.35 | 6.85×10^5 |
| FOLY-FOPID [13] | 2.832 | 1.308 | 27.74 | 2.46×10^3 |
| CB [14] | 1.402 | 0.748 | 3.046 | 5.8 |
| Proposed | 0.189 | 0.088 | 1.783 | 4.7 |

6.7 Summary

In this chapter, a novel FOB controller is developed independently of the nonlinear inverted pendulum and CSTR systems. By proposing an improved indirect biquadratic rational approximation technique, FOB delivers robust servo performance and disturbance rejection with the highest speed of action compared to CB, FOLY, and FOLY-2 DOF FOPI control strategies for inverted pendulum. In addition to this superior performance, the noteworthy results exhibit the benefits of the proposed rule in both nominal and perturbed circumstances of nonlinear CSTR system. In comparison to CB, FOPID, and FOLY-FOPID rules, proposed FOB delivers robust servo-regulatory performances and noise rejections. In the final analysis, the proposed FOB rule is investigated as the most trustworthy and feasible strategy since it provides the fastest speed of robust control action in comparison to other proposed fractional order schemes, as well as the lowest integral errors without needless overshoots in set-point tracking and noise rejection.

References

1. Witkowska and R. Śmierzchalski, "Nonlinear backstepping ship course controller," *Int. J. Autom. Comput.*, Vol. 6, pp. 277–284, Aug. 2009.
2. L-C. Guo and J-W. Liu, "Improved backstepping control for stochastic high-order nonlinear time delay system with a constructive mechanical system," *Transactions of the Institute of Measurement and Control*. Vol. 40, pp. 4115-4124, Jan. 2018.
3. Zhong-Ping Jiang and D. J. Hill, "A robust adaptive backstepping scheme for nonlinear systems with unmodeled dynamics," in *IEEE Transactions on Automatic Control*, vol. 44, no. 9, pp. 1705-1711, Sept. 1999.
4. Jin Young Choi and J. A. Farrell, "Adaptive observer backstepping control using neural networks," in *IEEE Transactions on Neural Networks*, vol. 12, no. 5, pp. 1103-1112, Sept. 2001.
5. Y. Liu, Q. Zhu and G. Wen, "Adaptive Tracking Control for Perturbed Strict-Feedback Nonlinear Systems Based on Optimized Backstepping Technique," in *IEEE Transactions on Neural Networks and Learning Systems*, vol. 33, no. 2, pp. 853-865, Feb. 2022.
6. G. Shao, X. Zhao, R. Wang and B. Yang, "Fuzzy Tracking Control for Switched Uncertain Nonlinear Systems With Unstable Inverse Dynamics," in *IEEE Transactions on Fuzzy Systems*, vol. 26, no. 2, pp. 1066-1072, April 2018.
7. Dong W, Farrell J.A, Polycarpou M.M, Djapic V and Sharma M 2012 Command filtered adaptive backstepping. *IEEE Transactions on Control Systems Technology*. 20 : 566-580.
8. Mondal R and Dey J 2022 A novel design methodology on cascaded fractional order (FO) PI-PD control and its real time implementation to cart -inverted pendulum system. *ISA Transactions*. 130 : 565-581.
9. Yin, C. Q., Wang, H. T., Sun, Q., & Zhao, L. (2019) Improved cascade control system for a class of unstable processes with time delay. *International Journal of Control, Automation and Systems* 17: 126-135.
10. N. Khanduja and B. Bhushan, "Optimal design of FOPID Controller for the control of CSTR by using a novel hybrid metaheuristic algorithm," *Sādhanā*, Vol. 46, pp. 1-12, 2021.

11. R. Almeida, "A caputo fractional derivative of a function with respect to another function," *Communications in Nonlinear Science and Numerical Simulation*, vol. 44, pp. 46-481, Mar. 2017.
12. T. Odziejewicz, A.B. Malinowska, and D.F.M. Torres, "Fractional variational calculus with classical and combined Caputo derivatives," *Nonlinear Analysis: Theory, Methods & Applications*, vol. 75, pp. 1507-1515, Feb. 2012.
13. D. Mukherjee, G.L. Raja, P. Kundu and A.Ghosh, "Improved fractional augmented control strategies for continuously stirred tank reactors," *Asian Journal of Control*, Vol. 25, pp. 2165-2182, 2022.
14. S. Alshamali and M. Zribi, "Backstepping control design on Continuous stirred tank", *IJICIC*, Vol.8, pp. 7747-7760, 2012.
15. Mukherjee D, Raja G.L, Kundu P and Ghosh A 2022 Modified augmented fractional order control schemes for cart inverted pendulum using constrained luus-jaakola optimisation. *International Journal of Modeling, Identification and Control*. 38: 67-79.
16. Grimble M.J and Majecki P 2020 Introduction to nonlinear systems modelling and control. In: *Nonlinear Industrial Control Systems*, London, pp. 3-63.
17. S. Ghasemi, A. Tabesh and J. Askari-Marnani, "Application of Fractional Calculus Theory to Robust Controller Design for Wind Turbine Generators," in *IEEE Transactions on Energy Conversion*, vol. 29, no. 3, pp. 780-787, Sept. 2014.
18. Ascione G 2021 Abstract cauchy problems for the generalized fractional calculus. *Nonlinear Analysis*. 209: 112339.
19. Shiwei Yu, T.-Z. Huang, Xiaoyun Liu, Wufan Chen, Information measures based on fractional calculus, *Information Processing Letters*, 112 (23), 2012, pp. 916-921.
20. S. Das, "Functional fractional calculus", Springer Science and Business Media, Technology and Engineering, 2011, pp. 1-612.
21. Shevitz D and Paden B 1994 Lyapunov stability theory of nonsmooth systems. *IEEE Transactions on Automatic Control*. 39: 1910-1914.
22. S. Deb and R. Srikant, "Global stability of congestion controllers for the Internet," in *IEEE Transactions on Automatic Control*, vol. 48, no. 6, pp. 1055-1060, June 2003.

23. J. Cao and Jun Wang, "Global asymptotic stability of a general class of recurrent neural networks with time-varying delays," in *IEEE Transactions on Circuits and Systems I: Fundamental Theory and Applications*, vol. 50, no. 1, pp. 34-44, Jan. 2003.
24. Jinde Cao, "Global stability conditions for delayed CNNs," in *IEEE Transactions on Circuits and Systems I: Fundamental Theory and Applications*, vol. 48, no. 11, pp. 1330-1333, Nov. 2001.
25. Anders Rantzer, A dual to Lyapunov's stability theorem, *Systems & Control Letters*, Vol.42(3), 2001, pp.161-168.

Publication

1. **D.Mukherjee**, G. L. Raja, P. Kundu, A. Ghosh, "Analysis of improved fractional backstepping and Lyapunov strategies for stabilization of inverted pendulum", *Sādhana*, Vol. 49, 2024.
2. **D.Mukherjee**, G. L. Raja, P. Kundu, and A. Ghosh, "Fractional Standalone Backstepping control approach for continuous stirred tank reactors", *International Journal of Robust and Nonlinear Control*, Under - Review.

CHAPTER 7

Conclusion & Future Work

7.1 Conclusion

This thesis considers two distinct benchmark nonlinear systems: the SIMO inverted pendulum (IP) and the continuous stirred tank reactor (CSTR) for an extensive analysis of their performances under different external conditions, including noise, perturbations, dead time, and load disturbance from a real-time viewpoint using different fractional order standalone and dual-loop control strategies. The main contributions of this dissertation are,

- (a) This work proposes a novel biquadratic equiripple approximation technique that outperforms the popular indirect Oustaloup and CFE approximation techniques by rejecting ripples. In order to attain smoothest and ripple-free approximation, the recommended method is further modified with exact phase approximation technique. In order to attain a fair level of accuracy, the fractional orders in the entire proposed control rules are solely approximated by the biquadratic exact phase approximation method to transform an estimated integer order model.
- (b) Standalone fractional order MIT (FOMIT) and fractional order Lyapunov (FOLY) stability rules of model reference adaptive control (MRAC) are proposed on linear inverted pendulum. Both techniques attempt to tackle the system with their efficient control actions in presence of noise and load disturbance. However, in terms of global stability, FOLY scheme is explored as a robust technique by tackling the system more swiftly and gracefully. FOLY rules also outperform other existing standalone and augmented traditional schemes with lower integral errors and overshoot. Following a fair investigation on standalone FOLY rule, the noteworthy benefits of the proposed augmented optimal FOLY-FOPID and FOLY-2 DOF FOPID rules are also explored. A combination of extensive simulation technique and optimization methods is addressed to tune FOMRAC rules. In comparison to the augmented FOMIT rules, both methods produce lower quantitative performance measurements (IAE, ISE, ITAE, and TV)

under unperturbed, perturbed, and nonlinear circumstances. In handling the noise, the noteworthy influence of FOLY-2 DOF FOPI is also addressed.

- (c) In addition to investigation on the inverted pendulum, the significant impact of the fractional order controller is also explored on industrial unstable processes. A novel FOIMC based series cascaded control structure (SCCS) with dead time compensator is proposed to reject disturbance in benchmark unstable processes and the proposed optimal fractional order based IMC filter assists in successfully rejecting the noise in controlling the industrial unstable plants. The stability of the proposed rule is also confirmed. The significant impact of this proposed scheme is also explored on benchmark CSTR. Following a robust servo action and noise rejection using the standalone FOIMC scheme, the rule is expanded by proposing an enhanced version with the optimal FOLY-FOPID and alternatively, the optimal FOPD-smith predictor techniques to investigate control efficiencies on controlling the process variables of various benchmark CSTR systems. In comparison to standalone FOLY topology, the proposed optimal dual-loop schemes show more satisfactory results. A combination of extensive simulation technique and optimization methods is addressed to tune FOMRAC rules. The robustness of all the proposed augmented schemes is also confirmed in presence of model uncertainties. However, the proposed FOIMC-FOPD smith predictor, which is a more straightforward and simpler representation, outperforms FOLY-IMC FOPID and FOLY-FOPID rules with smoother control actions and efficiently rejects noise, resulting in fewer integral errors and TV.
- (d) In last chapter to handle nonlinear systems (inverted pendulum and continuous stirred tank reactor) in the presence of nonlinear effects amid noise, a standalone linear fractional order backstepping (FOB) rule is proposed and found to be a more effective control strategy by stabilizing each subsystems of the nonlinear process recursively. This proposed rule improves the control action without needless overshoot and offers robust noise rejection with the fastest set-point tracking. FOB controls the inverted pendulum towards its desired upright position more swiftly and gracefully from any random locations. Similar to that, the proposed FOB tracks any desired level of process variable of the CSTR process without unnecessary overshoots or undershoots and offers steady control action amid noise and disturbances. The robustness and stability of the proposed FOB are explored for both of unstable systems. Compared to various fractional order control rules, this novel approach provides a robust closed loop servo-regulation performance and noise rejection with a notably reduced error measurement signal and TV of control efforts.

Thus, it is anticipated that the proposed standalone FOB rule will produce satisfactory closed-loop performance and control action even in practical scenarios since that our current research finally establishes it as the most effective control strategy when compared to the conventional method and other proposed fractional order schemes on nonlinear systems producing lowest integral errors and total control signal variance in presence of model uncertainties, noise within saturation limit, load disturbance, and nonlinear effect.

7.2 Future Works

In order to continue this current work, the following future works must be investigated as follows:

- (a) Higher order biquadratic exact phase approximation compared to the currently proposed lower order method in fractional order control rules must be explored using different corner frequencies to investigate for wider frequency band gap.
- (b) To discover optimum control settings of FOB rule, any appropriate optimization algorithm might also be attempted. Instead of using in-depth simulation methods, the performance of the system must be investigated using optimization strategies.
- (c) The proposed standalone FOB rule might also be augmented with other control topologies to study the effectiveness of the augmented FOB schemes compared to standalone FOB scheme on different benchmark models of inverted pendulum and CSTR processes.
- (d) Proposed various novel standalone, and augmented fractional order control strategies including FOMIT, FOLY, FOMIT-FOPI and 2 DOF FOPI, FOLY-FOPI and 2 DOF FOPI, FOIMC-SCCS with dead-time compensator, dual-loop FOLY-FOPID, FOLY-IMC FOPID, FOIMC-FOPD predictor strategies and fractional order backstepping (FOB) strategies have been successfully simulated on MATLAB and SIMULINK platform. The real time simulation and experimental validation of the results obtained in the present work could not be accommodated in the scope of the present thesis. Fractional order description and design of the aforesaid control algorithms needed meticulous combination of existing few fractional order systems engineering utility with indigenously constituted *s-functions* before closed loop simulation. A classic problem in control engineering and dynamics as well as some industrial problem performances are tested using those proposed control algorithms

and the results are validated with existing ones. This very parlance remains an open domain for future experimental endeavors.

Appendix -A

Chapter-3

MATLAB Codes:

3.3.1

```
clc
close all
alpha1=0.75; alpha2=0.5; alpha3=0.2; alpha4=1;
%alpha=input('Enter the value of alpha:')
m = 2; y=[];
funname='myfunc'
%x=1:1:100;
t=1:0.1:100 ; n=size(t);
for i=1:n(1,2)

y= [y;find_fraction_derivative(m,i,alpha1, funname) find_fraction_derivative(m,i,alpha2,
funname) find_fraction_derivative(m,i,alpha3, funname) find_fraction_derivative(m,i,alpha4,
funname)];

end

plot(t,y(:,1),'r',t,y(:,2),'b',t,y(:,3),'g',t,y(:,4),'y');

title('fractional order derivative for y=x^2');

xlabel('t') ; ylabel('y')

%User must declare the function

function z= myfunc(m,x,ALPHA)

z= (gamma(m+1)/gamma(m-ALPHA+1))*x^(m-ALPHA)
end

function t = find_fraction_derivative(m,x,alpha,funname)

func = str2func(funname);

t = func(m,x,alpha);

end
```

3.3.3.1

```
clc
close all

alpha1=-0.75; alpha2=-0.5; alpha3=-0.2; alpha4=-1;
```

```

%alpha=input('Enter the value of alpha:')

m = 2;

y=[];

funname='myfunc1'

%x=1:1:100;

t=1:0.1:100 ; n=size(t);

for i=1:n(1,2)

y= [y;find_fraction_integral(m,i,alpha1, funname) find_fraction_integral(m,i,alpha2,
funname) find_fraction_integral(m,i,alpha3, funname) find_fraction_integral(m,i,alpha4,
funname)];

end

plot(t,y(:,1),'r',t,y(:,2),'b',t,y(:,3),'g',t,y(:,4),'y');

title('fractional order derivative for y=x^2');

xlabel('t') ; ylabel('y')

%User must declare the function

function z= myfunc1(m,x,ALPHA)

z= (gamma(m+1)/gamma(m+ALPHA+1))*x^(m+ALPHA);

End

function t = find_fraction_integral(m,x,alpha,funname)

func = str2func(funname);

t = func(m,x,alpha);

end

3.4.1.3

clc
clear all

G = tf([22500 -27000 10800],[109042.0813664.41 28394.9 27258.2810801])

kp=input('enter kp')

kd=input('enter kd')

ki=input('enter ki')

```

```

lam=input('enter lam')
mu=input('enter mu')
fpid_G=fotf([1],[lam],[kd kp ki],[lam+mu lam 0])
sys1=fpid_G*G; sys2=feedback(sys1,1);

```

3.4.1.4

```

b = [3530.5,3400.92,2161.08]; nb = [0.96003,1.858,0];
a = [5252.2,256.28,10801,3530.5,3400.92,2161.08];
na = [2.96003,1.96003,.96003,.96003,1.858,0];
G=fotf(a,na,b,nb); [K,alpha]=isstable(G)

```

3.4.2

```

alpha = 0.5; a = 1; y0 = 1; h = 0.01; n = 1000;
t = linspace(0,20,n+1);
y = FODE(alpha,0,1,y0,h,n);
plot(t,y)
xlabel('t')
ylabel('y(t)')
title('Solution of Fractional Order Differential Equation')

%User must declare the function

function [y] = FODE(alpha,a,b,y0,h,n)

% alpha is the order of the derivative
% a,b are the interval endpoints
% y0 is the initial condition
% h is the step size
% n is the number of steps

t = linspace(a,b,n+1); y = zeros(1,n+1); y(1) = y0;

for i=1:n

y(i+1) = y(i) +
h^(alpha)/gamma(alpha+1)*(sum((t(i+1)-t(1:i)).^(alpha-1/2)).*y(1:i).*h.^(alpha)));

end
end

```

3.4.2.2

```
alpha = 0.5; beta=1;

a = 1;

f = @(t,y) mlf(alpha,beta,-a*t.^(0.5));

% Define the initial condition

y0 = 1;

% Define the time interval

tspan = [0 20];

% Solve the fractional differential equation

[t,y] = ode45(f,tspan,y0);

% Plot the solution

plot(t,y)

xlabel('t'), ylabel('y(t)')

function E = mlf(alpha,beta,z)

k = 0:100;

E = sum((z.^k)./gamma(alpha*k+beta));

End
```

3.4.3.1

```
function G=ousta_fod(alpha,N,wb,wh)

z=1:N; wu=sqrt(wh/wb); wkp=wb*wu.^((2*z-1-alpha)/N); wk=wb*wu.^((2*z-1+alpha)/N);

G=zpk(-wkp,-wk,wh^alpha);

G=tf(G);

G1=ousta_fod(0.4,5,1e-2,1e2); bode(G1)
```

Appendix –B

Chapter-4

Pseudo code of Luus-Jaakola (LJ) optimization:

Input: *Objective Function*, $lb \rightarrow$ Lower bounds, $ub \rightarrow$ Upper bounds, $N_T \rightarrow$ Number of iteration, $N_p \rightarrow$ Number of counts, $r^1 \rightarrow$ Size vector, $R \rightarrow$ Random points, $\phi \rightarrow$ Tolerance

% Begins %

$$M^{(0)} = 0.5(a_l + a_u).$$

$$M^* = M^{(0)}.$$

$$J_{old} = 10^{50}.$$

for $q = 1: 1: N_p$
 for $j = 1: 1: N_T$
 for $x = 1: 1: R$

$$M^j = M^* + D^* r^j,$$

Where M^* is best value and D^* is a diagonal matrix in the range $[-0.5, 0.5]$. Computation of the value of fitness function J using M^j .

if $J < J_{old}$

$$J_{old} = J$$

$$M_S^* = M^j$$

end if
 end for

$$r^{j+1} = r^j \eta$$

$$M^* = M_S^*$$

end for

for $k = 1: 1: n$

Evaluation of size vector

$$r_k^{q+1} = |M^{*q} - M^{*1}|$$

where M^{*q} and M^{*1} are the best values of x^{th} parameter obtained at the end and beginning of q^{th} pass

if $r_k^{q+1} < \phi$

$$r_k^{q+1} = \phi$$

end if
 end for

$$r^1 = [r_1^{q+1}, \dots, r_p^{q+1}]^T$$

if $q > 5$

if $J < \phi$

$$\phi = 0.5 * \phi$$

end if
 end if

if $\phi < 10^{-5}$

Algorithm stopped

end if

end for

% stops %

The parameters of LJ are $N_p = 50$, $N_T = 100$, $R = 30$, $\phi = 10^{-3}$, $\eta = 0.95$, $a_l = [0 \ 0 \ 0.001]$, $a_u = [10^4, 10^4, 1]$. For the sake of more clarity, the overall procedure is presented in the form of a flowchart in Fig. B.1.

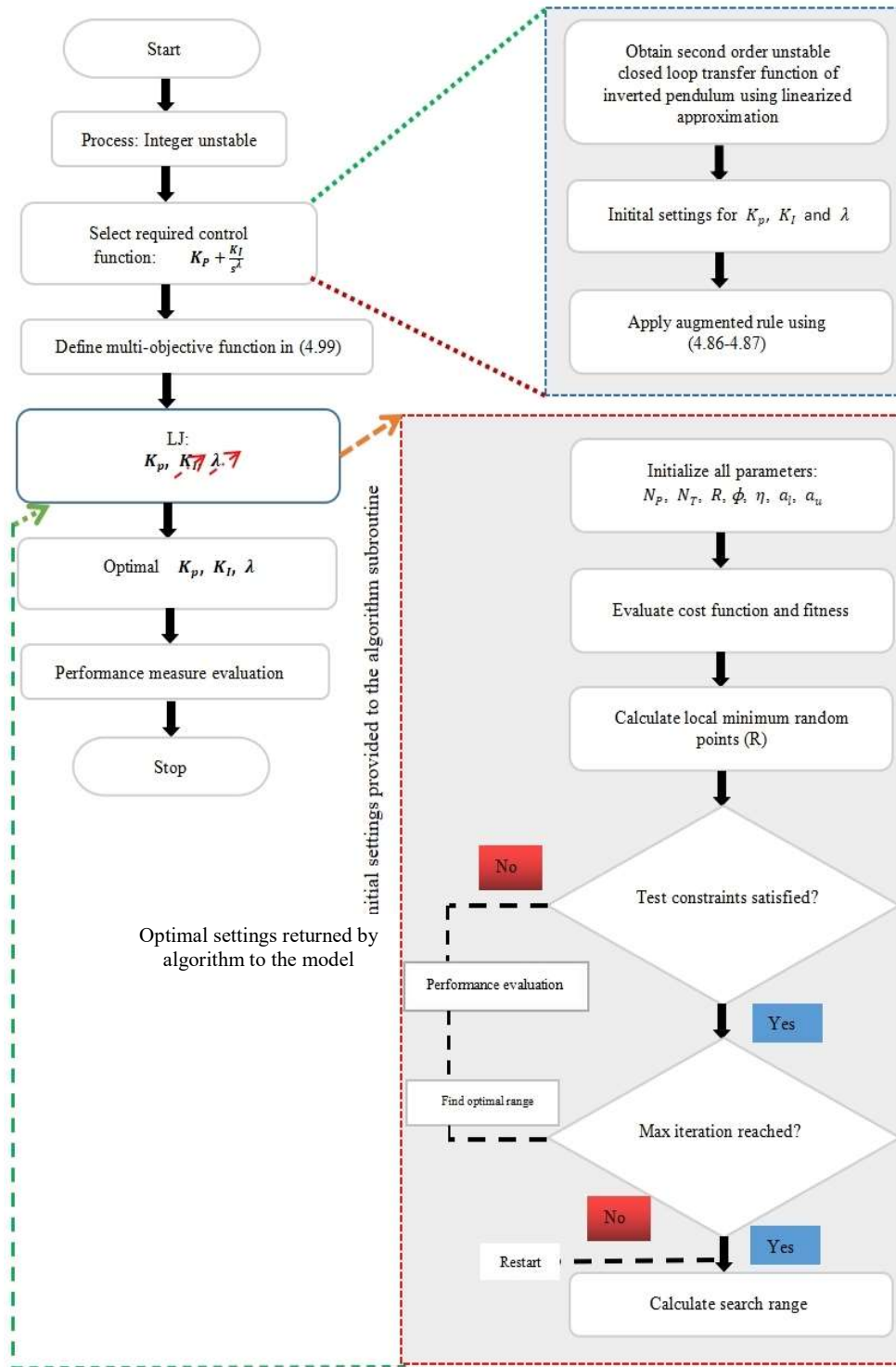


Fig. B.1 Steps of Luus-Jaakola optimization algorithm.

Code for TV (Total variation) Computation:

```
N=size(u);
M=size(u2);
P=size(u3);
Q=size(u4);
R=size(u5);
u=u';
u2=u2';
u3=u3';
u4=u4';
u5=u5';
sum=0;
sum1=0;
sum2=0;
sum4=0;
sum5=0;
for i=1:N-1
    TV(i)=abs(u(i+1)-u(i));
    sum=sum+TV(i);
end

for i=1:M-1
    TV1(i)=abs(u2(i+1)-u2(i));
    sum1=sum1+TV1(i);
end
for i=1:P-1
    TV2(i)=abs(u3(i+1)-u3(i));
    sum2=sum2+TV2(i);
end
for i=1:Q-1
    TV4(i)=abs(u4(i+1)-u4(i));
    sum4=sum4+TV4(i);
end
for i=1:R-1
    TV5(i)=abs(u5(i+1)-u5(i));
    sum5=sum5+TV5(i);
end

sum
sum1
sum2
sum4
sum5
```


Appendix C

Chapter-5

Steps of Artificial Bee Colony (ABC) optimization algorithm:

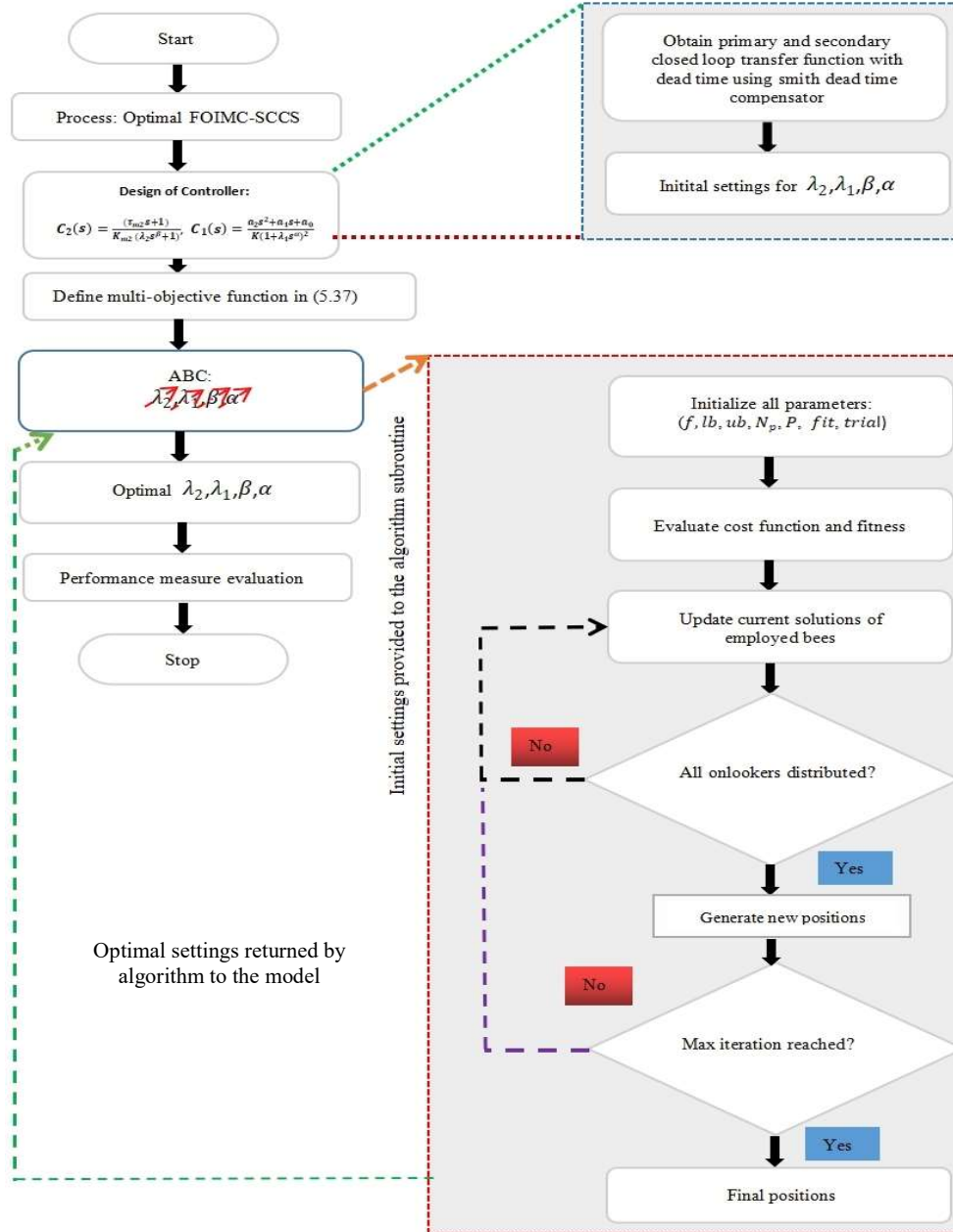


Fig. C.1 Optimization steps of Artificial Bee Colony (ABC) optimization method.

It is evident from the optimization methodology shown in Fig.C.1 that the method described below is mostly employed for the selection of new solutions:

- i. Assess the objectivity, suitability, and utility of newly developed solutions
- ii. To update the present solution, perform greedy selection.
- iii. A trial counter is used to keep track of how many times each solution has failed.
- iv. If the new solution is inferior, extend the trial of the existing one more time.
- v. If a better answer is produced, the trial should be reset to 0.

The parameters settings are followed as

N_p (Population size) = 10, MCN = 50, $limit$ (Permissible number of failures) =5, lb = [0 0], ub = [100 2].

Pseudo code of Modified Particle Swarm Optimization (MPSO) optimization:

The pseudo code of MPSO is shown below:

```

Initialize population
for  $t = 1$ : maximum generation
  for  $j = 1$ :population size
    if  $f(x_{j,d}(t)) < f(p_j(t))$  then  $p_j(t) = x_{j,d}(t)$ 
       $f(p_g(t)) = \min_t(f(p_j(t)))$ 
    end if
    for  $d = 1$ : dimension
       $v_{j,d}(t+1) = wv_{j,d}(t) + c_1r_1(p_j - x_{j,d}(t)) + c_2r_2(p_g - x_{j,d}(t))$ 
       $x_{j,d}(t+1) = x_{j,d}(t) + v_{j,d}(t+1)$ 
      if  $v_{j,d}(t+1) > v_{max}$  then  $v_{j,d}(t+1) = v_{max}$ 
      else if  $v_{j,d}(t+1) < v_{min}$  then  $v_{j,d}(t+1) = v_{min}$ 
      end if
      if  $x_{j,d}(t+1) > x_{max}$  then  $x_{j,d}(t+1) = x_{max}$ 
      else if  $x_{j,d}(t+1) < x_{min}$  then  $x_{j,d}(t+1) = x_{min}$ 
      end if
    end for
  end for
end for

```

In this method, modified inertia weight is proposed below:

$$w = 0.5 + \frac{r}{2} \quad (C.1)$$

The limit of r lies between 0 and 1 while the limit of w lies between 0.5 and 1. The optimization step is presented for different control schemes as shown in Fig. C.2.

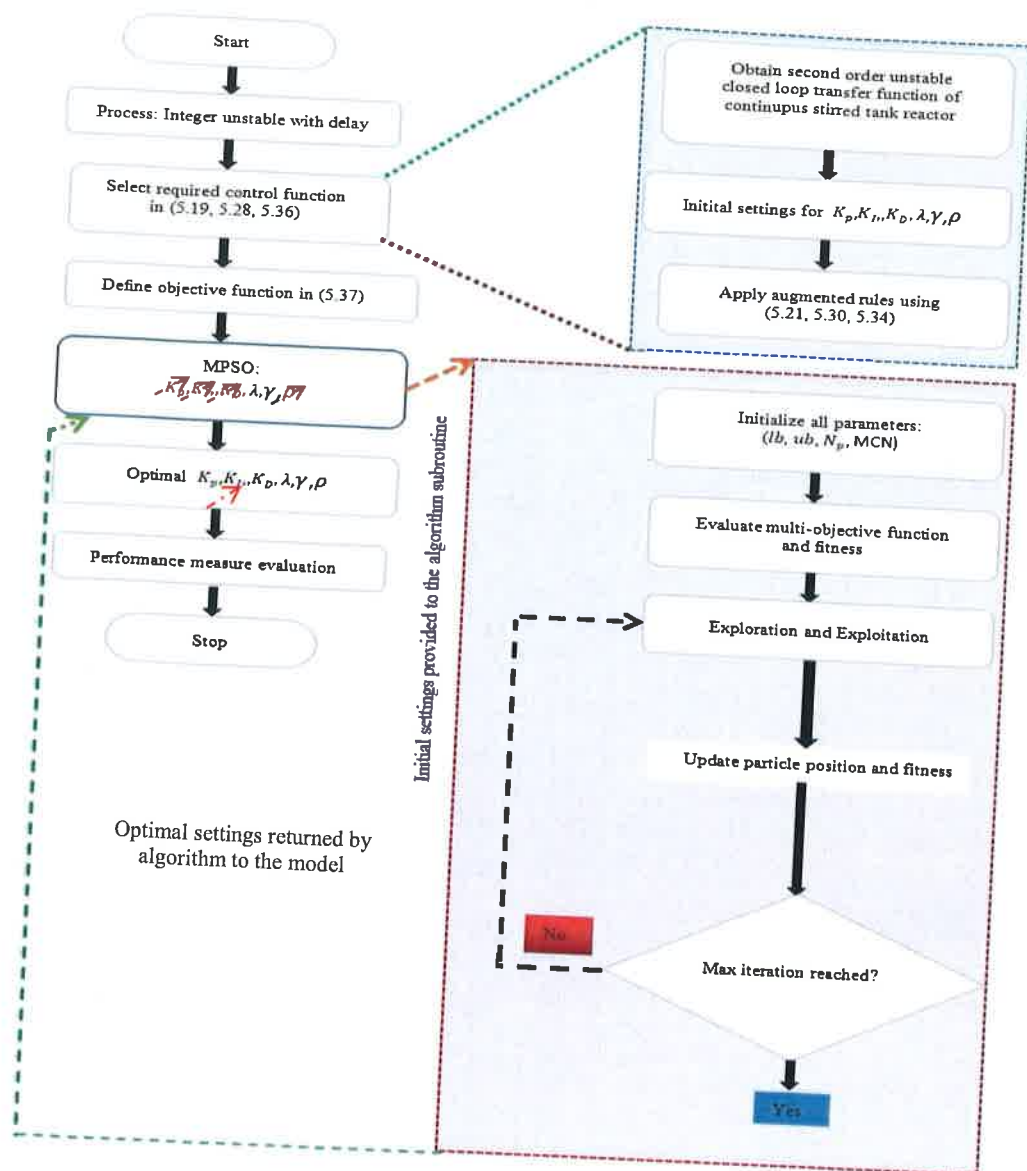


Fig. C.2 Optimization steps of modified particle swarm optimization (MPSO) method.

Deep Mukherjee
29/5/2024